Time-domain quantum dynamics: Optical properties from time-dependent electronic-structure theory

Benedicte Sverdrup Ofstad

Supervisors:
Simen Kvaal
Thomas Bondo Pedersen

The Hylleraas Centre for Quantum Molecular Sciences

The Faculty of Mathematics and Natural Sciences

Preface

I wish to express my deepest appreciation to my supervisors, Simen and Thomas, for their unwavering guidance and expertise, and for their patience and belief in my capabilities, even in moments where I might have doubted myself. I'm privileged to have been part of an incredibly supportive and harmonious research group. A special thanks to Håkon for his invaluable contributions. I would also like to extend my appreciation to Einar, Øyvind, and Eirill for their collaboration and shared insights.

To Stella and Petros in Mainz, and Andy and Meilani and Tom in Nottingham, I offer my sincere gratitude. Your perspectives and expertise have been invaluable to the broader scope of my research.

The Hylleraas Centre of Quantum Molecular Sciences at the University of Oslo provided a nurturing environment for my research. For that, and all the wonderful people I have gotten to know during my years here, I am thankful. I would be remiss if I didn't thank Christian, Simon, Margrethe, and Fredrik for their meticulous eyes and feedback on the mechanics of the manuscript.

Lastly, a heartfelt thanks to Tesla, my thirteen year old dog, whose idea it was to consider magnetic fields.

Preface

Abstract

While frequency-domain response theory is the conventional approach for computing nonlinear optical properties within time-dependent electronic-structure theory, time-domain methods offer an advantage by also accommodating non-perturbative responses. Furthermore, the time-domain approach significantly simplifies the implementation of highly nonlinear responses compared to the traditional response theory.

My research, contained in four papers and one review article, aims to contribute to the field of time-domain time-dependent electronic structure theory for the description of linear and nonlinear optical properties. These contributions include: Investigating the capability of dynamic orbitals to improve the description of linear and nonlinear optical properties, extending a hierarchy of time-domain time-dependent coupled-cluster methods with dynamic and static orbitals to accommodate strong magnetic fields, and developing an efficient approach for the extraction of higher-order response properties.

We have found that dynamic orbitals improve the accuracy of linear and nonlinear optical properties with minimal additional computational cost. By applying time-domain electronic-structure theory in strong magnetic fields, we have demonstrated that magnetic optical rotation, generally treated as linearly dependent on the magnetic field strength, deviates from linearity in strong magnetic fields. Finally, the finite-difference approach used for property extraction from time-domain simulations proved to be highly accurate, even for nonlinear optical properties up to fourth order. These contributions pave the way for further exploration of accurate, time-resolved nonlinear magneto-optic phenomena.

Preface

Sammendrag

Den konvensjonelle metoden for å beregne ikke-lineære optiske egenskaper innenfor tidsavhengig elektronstrukturteori er responsteori i frekvensdomenet. Alternativt kan man benytte tidsdomenemetoder, som har den fordel at også ikke-perturbative responser kan håndteres. Videre er utledningen og implementeringen av ikke-lineære responser av høyere orden svært mye enklere for tidsdomenemetoder sammenlignet med den tradisjonelle responsteorien.

Mitt mål i forskningen har vært å bidra til feltet for tidsavhengig elektronstrukturteori i tidsdomenet, for å beskrive lineære og ikke-lineære optiske egenskaper. Mine forskningsbidrag inkluderer følgende: Å undersøke potensialet til dynamiske orbitaler for å forbedre beskrivelsen av lineære og ikke-lineære optiske egenskaper. Å utvide et hierarki av tidsavhengige coupled-cluster tidsdomenemetoder med både dynamiske og statiske orbitaler, slik at de håndterer sterke magnetiske felt. Å utvikle en effektiv, nøyaktig metode for å utvinne responsegenskaper av høyere orden.

Arbeidet mitt har resultert i fire forskningsartikler og en oversiktsartikkel, der hovedresultatene er som følger. Observasjon av dynamiske orbitaler som forbedrer nøyaktigheten av lineære og ikke-lineære optiske egenskaper med minimal ekstra beregningskostnad. Demonstrasjon av at magnetisk optisk rotasjon, som generelt betraktes som lineært avhengig av magnetfeltstyrken, avviker fra linearitet i sterke magnetfelt. Differensmetodene som blir brukt for utvinning av egenskaper fra tidsdomenesimuleringer viser seg å være svært nøyaktig, selv for ikke-lineære optiske egenskaper opp til fjerde orden. Disse bidragene baner vei for videre forskning på nøyaktige, tidsoppløste ikke-lineære magneto-optiske fenomener.

Preface

Contents

Contents

Acronyms

CCSD coupled-cluster singles and doubles.

CCSD(T) coupled-cluster singles, doubles and perturbative triples.

CCSDT coupled-cluster singles, doubles, and triples.

CDFT current-dependent density-functional theory.

DFT density-functional theory.

EOM-CC equation-of-motion coupled-cluster.

FCI full configuration interaction.

FEDVR finite-element discrete variable representation.

LAOs London atomic orbitals.

MCTDHF multiconfigurational time-dependent Hartree–Fock.

mGGA meta-generalized gradient approximation.

NOCC non-orthogonal orbital-optimized coupled-cluster.

OATDCC orbital-adapted time-dependent coupled-cluster.

OCC orbital-optimized coupled-cluster.

PW pulsed wave.

RCW ramped continuous wave.

TDCC time-dependent coupled-cluster.

TDCC2 time-dependent second-order coupled-cluster.

TDCCSD time-dependent coupled-cluster singles and doubles.

TDCCSDT time-dependent coupled-cluster singles, doubles, and triples.

Acronyms

TDCDFT time-dependent current-dependent density-functional theory.

TDCIS time-dependent configuration interaction singles.

TDDFT time-dependent density-functional theory.

TDHF time-dependent Hartree–Fock.

TDNOCC time-dependent non-orthogonal orbital-optimized coupled-cluster.

TDNOCCD time-dependent non-orthogonal orbital-optimized coupled-cluster doubles.

TDOCC time-dependent orbital-optimized coupled-cluster.

TDOMP2 time-dependent second-order Møller–Plesset.

Chapter 1

Introduction

Within the field of nonlinear optics [1, 2], nonlinear optical properties are defined as frequency-dependent responses. This definition emerged in the frequency domain, as lasers used in these early experiments emitted monochromatic continuous waves [3]. This led to the development of time-dependent electronic-structure theory [4] predominantly in the frequency domain, using perturbation-theory-based response theory [5, 6]. However, in recent years, advances in computing power and the advent of ultrashort laser pulses [7] have sparked interest in the time-domain for both electronic-structure theory and nonlinear optics. Time-domain electronic-structure theory [8, 9] provides a time-resolved description of light-matter interaction, closely mimicking experiments. As an emerging field, many subjects within it remain to be explored. The goal of this thesis is to contribute to the development of time-dependent electronic-structure theory for describing nonlinear optical properties, with a focus on signal processing, electron correlation, and strong magnetic fields.

1.1   Setting

The goal of time-dependent electronic-structure theory is to find an approximate solution to the electronic non-relativistic time-dependent Schrödinger equation

$$i\frac{\partial}{\partial t}\Psi(t) = \hat{H}\Psi(t), \qquad (1.1)$$

where $\Psi(t)$ is the exact wavefunction governing the electronic system and Hamiltonian operator $\hat{H}$ represents the total energy of the system. The prevailing electronic-structure methods in the realm of quantum chemistry, namely Kohn–Sham density-functional theory (DFT) [10] and post-Hartree–Fock methods and their time-dependent variants, have demonstrated to be broadly applicable to the understanding and interpretation of experimental measurements of molecular properties. Among these, time-dependent density-functional theory (TDDFT) stands out as a method that strikes a favorable balance between efficiency and accuracy, thus garnering widespread adoption. However, despite its popularity, TDDFT suffers from inherent limitations; the theory lacks systematic improvability and therefore depends on higher level *ab initio* methods

or experimental data for benchmarking. It also exhibits notable failures including unphysical peak shifting of absorption spectra and an inability to capture Rabi oscillations due to the adiabatic approximation nearly always being invoked [9]. On the other hand, time-dependent post-Hartree–Fock methods, particularly time-dependent coupled-cluster (TDCC) theory, are comprehensively understood and deliver remarkable accuracy, albeit at a higher computational cost.

Time-domain TDDFT [11] has been under development since the 1990s, and although time-dependence was considered theoretically within coupled-cluster theory already in the 1970s, a practical implementation of time-domain TDCC [12] was not explored until 2011 [13]. Time-domain methods [8, 9] offer the advantage of being able to describe non-perturbative responses in addition to allowing for a time-resolved description of the electron dynamics. The ultimate goal of time-domain electronic-structure methods is to simulate experiments within the field of attochemistry. This could one day enable the investigation and control of chemical reactions at the most fundamental level [14]. Another area where time-domain methods show promising potential is for the computation of nonlinear properties. Linear optical properties, as well as nonlinear optical properties of second and third order, are efficiently computed with response theory; highly nonlinear properties (here defined as those above third order), however, require equations that are complicated to derive. These are more easily found in the time domain using finite-difference methods.

While the more mature field of frequency-domain methods closely resemble their time-domain counterparts, there are certain distinguishing factors between the two. Signal processing is required for the extraction of properties that can be directly compared to experimental nonlinear optical measurements. Furthermore, the interaction of electrons with explicit magnetic fields needed for simulations at non-perturbative magnetic field strengths have not yet been implemented for the time-domain TDCC methods.

1.2 Research objectives

With the goal of advancing the development of time-dependent electronic-structure theory for nonlinear optical properties, the following research objectives have been defined:

- To extend the time-domain methods implemented for use in strong magnetic fields to encompass the hierarchy of TDCC methods.

- To investigate whether dynamic orbitals provide an improved description of linear and nonlinear optical properties.

- To compare the performance of different current-dependent density-functional theory (CDFT) functionals with TDCC theory for describing optical properties in the presence of magnetic fields.

- To investigate whether magnetic optical rotation[1] remains a linear function of the magnetic field strength, even at very high field strengths.

- To explore the existing approaches for extracting non-linear response properties from time-domain signals and identify a reliable and efficient scheme that can be used for higher-order response properties.

Achieving these objectives will lead to an improved description of nonlinear optical properties with time-domain methods. Extending time-domain TDCC theory to accommodate finite magnetic fields will allow for the accurate exploration of other magnetic and magneto-optic phenomena, such as: magnetic circular dichroism, the Cotton–Mouton effect [16]; and at a later stage, the description of strong field and ionization dynamics in a magnetic field.

1.3 Scope

Time-dependent electronic-structure theory nearly always invokes the Born-Oppenheimer approximation [17, 18] where nuclei are treated as classical clamped point charges. This approximation is fully justified for the short simulation times that will be studied in this thesis. Secondly, the semiclassical approach will be taken, where electrons are treated quantum-mechanically, and electromagnetic fields are treated classically. Thirdly, we will assume the dipole approximation for the first three papers presented in this thesis: The electromagnetic field potential $\mathbf{A}$ is taken to be uniform over the entire molecule, $\mathbf{A}(\mathbf{r}, t) \approx \mathbf{A}(0, t) = \mathbf{A}(t)$. The interacting light in the 'optical' region has wavelengths longer than 1×10^4 a.u., which is much longer than the size of the small molecules considered here ($\sim 1 - 10$ a.u.); therefore, the electromagnetic field is approximately position-independent. Finally, the basis sets most commonly used within quantum chemistry are built from Gaussian atomic type orbitals. These are situated on the nuclei, and cannot be used to describe ionization. This limits the research within this thesis to dynamics of bound electrons and therefore to weak electric fields. Non-linear optical properties are weak-field phenomena by definition, and Gaussian atomic type orbitals are therefore appropriate for the small closed-shell molecules that will be considered here.

1.4 Outline

This dissertation is a collection of five papers: four research articles presented in chronological order of writing, and one review article titled *Time-dependent coupled-cluster theory*. In the four chapters preceding the papers, I will attempt to unify the research articles and set them into a broader context. After the introduction in Chapter 1, a review of the literature will be presented in Chapter 2.

---

[1]Although strictly speaking a magneto-optical response, Bloembergen's has defined magnetic optical rotation as a "nonlinear response in which the optical polarization is a bilinear function of the optical field amplitude and the applied magnetic field" [15]
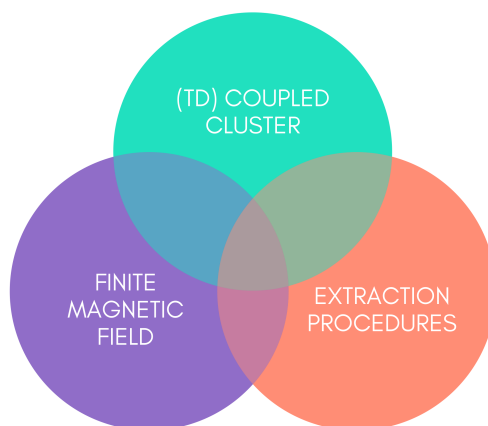
Figure 1.1: Research area

The research conducted within this thesis builds upon three more or less separable research fields illustrated in Figure 1.1. Firstly, I am furthering the development of TDCC theory, and this work naturally builds on all the prior development, primarily conducted in our research group. Secondly, approaches for extracting properties from real-time simulations have been a parallel research field, mainly dominated by researchers within TDDFT, with Dr. Xiaosong Li and coworkers having made notable contributions. Thirdly, implementing a finite magnetic field is made possible by researchers including Dr. Erik Tellgren, Prof. Trygve Helgaker, Prof. Stella Stopkowicz and Assoc. Prof. Andrew Teale. These three fields have all been highly relevant for the work in this thesis, and the literature of each will be presented. Chapter 3 introduces the papers and the main findings, with a focus on how they relate to the overarching theme of this dissertation, to each other, and to the research objectives. My contributions will also be explicitly highlighted. The fulfillment of the research objectives will be assessed in Chapter 4, in addition to discussions of future work.

Chapter 2

Literature and previous research

2.1 Coupled-cluster theory

Coupled-cluster theory, in conjunction with a suitable basis set, embodies almost all the characteristics of the exact wave function that *Molecular Electronic-Structure Theory* [4] defines as desirable. It provides an approximate wavefunction that is square-integrable, antisymmetric, size-extensive, it can be made gauge-invariant, and it is equivalent to the exact solution with the given basis set when the cluster operator is untruncated. Although the theory is not variational, it can be derived from bivariational principles. Consequently, the exact ground state is not the upper limit to the coupled cluster ground state, it does however allow for adding degrees of freedom to the bivariatoinal *ansätze* in the same manner as for variational methods.

This section will provide a streamlined account of the development of coupled-cluster theory, focusing only on contributions that directly relate to the time-domain TDCC methods developed and explored in this thesis. With that said, I would like to acknowledge the extensive development of alternative variants of coupled-cluster theory including coupled-cluster response-theory [5, 6] and equation-of-motion coupled-cluster (EOM-CC) theory [19–26].

2.1.1 Coupled-cluster equations

Coupled-cluster theory was originally developed in nuclear physics by Coester and Kümmel [27, 28] and was introduced to computational chemistry by Čížek and Paldus [29–31], among others. The wavefunction *ansatz* was constructed as the exponential of a linear combination of excitation operators acting on a reference determinant

$$|\Psi\rangle = e^{\hat{T}} |\Phi\rangle = e^{\hat{T}_1 + \hat{T}_2 + \hat{T}_3 + \cdots} |\Phi\rangle. \tag{2.1}$$

The cluster operator $\hat{T}_n$

$$\hat{T}_n = \sum_{\mu_n} \tau_{\mu_n} \hat{X}_{\mu_n}, \tag{2.2}$$

parameterized by the cluster amplitudes τ_{μ_n} was defined as the sum of all possible n-electron (n-rank) excitations from the reference Hartree–Fock determinant,

$$\hat{X}_{\mu_n} |\Phi\rangle = |\Phi_{\mu_n}\rangle. \tag{2.3}$$

The naming convention in coupled-cluster theory is based on the electron-ranks included in the approximation [32], —i.e. the coupled-cluster singles and doubles (CCSD) is obtained by truncating after double excitations $n = 2$, and the coupled-cluster singles, doubles, and triples (CCSDT) is obtained by truncating after triple excitations $n = 3$.

A major advantage of coupled-cluster theory is that the coupled-cluster *ansatz* leads to size-consistency being preserved even when the cluster operator is truncated. The power series expansion of the exponential *ansatz* $e^{\hat{T}} = \sum_{k=0}^{\infty} \frac{1}{k!} \hat{T}^k$, however, leads to the variational solution, constructed by minimizing the energy expression

$$E = \frac{\langle \Phi | (e^{\hat{T}})^\dagger \hat{H} (e^{\hat{T}}) | \Phi \rangle}{\langle \Phi | (e^{\hat{T}})^\dagger (e^{\hat{T}}) | \Phi \rangle} \tag{2.4}$$

not terminating until the N-electron limit has been reached. Instead, Coester and Kümmel used a projection technique for obtaining equations for the energy and amplitudes:

$$E = \langle \Phi | e^{-\hat{T}} \hat{H} e^{\hat{T}} | \Phi \rangle, \tag{2.5}$$

$$0 = \langle \Phi_{\mu_n} | e^{-\hat{T}} \hat{H} e^{\hat{T}} | \Phi \rangle. \tag{2.6}$$

When the cluster operator was truncated (after an excitation rank n), one equation was included per μ_n, giving a set of nonlinear amplitude equations that could then be solved iteratively.

2.1.2 Time-dependent coupled-cluster theory

A time-dependent coupled-cluster theory was introduced by Monkhorst [33], and Dalgaard and Monkhorst [34] for calculating dynamic first-order response properties. The TDCC theory was later developed for dynamics by Hoodbhoy and Negele [35, 36], and Schönhammer and Gunnarsson [37].

For variational methods, the Hellmann-Feynman theorem allows the calculation of first-order response properties with

$$\langle \hat{A} \rangle = \frac{d}{d\epsilon} \frac{\langle \Psi | \hat{H} + \epsilon \hat{A} | \Psi \rangle}{\langle \Psi | \Psi \rangle} \bigg|_{\epsilon=0} = \frac{\langle \Psi | \hat{A} | \Psi \rangle}{\langle \Psi | \Psi \rangle}. \tag{2.7}$$

However, in coupled-cluster theory, the ground state is not a stationary point of the energy functional, making Eq. (2.7) inapplicable.

To address this, Arponen [38] proposed a bivariational framework that by definition adhered to the Hellmann-Feynman theorem. In this framework, the bra and ket were treated as independent variables, parameterized with independent operators. The $|\Psi(t)\rangle$ was the standard Coester and Kümmel ket-state. The bra-state:

$$\langle \tilde{\Psi}(t) | = \langle \tilde{\Phi}(t) | e^{\hat{\Lambda}(t)} e^{-\hat{T}(t)}, \quad \hat{\Lambda}_n(t) = \sum_{\mu_n} \lambda_{\mu_n}(t) \hat{Y}_{\mu_n}, \tag{2.8}$$

was parametrized by both the bra cluster operator $\hat{\Lambda}(t)$ and the $-\hat{T}(t)$ cluster operator originating from the similarity transformation of the Schrödinger equation in Eq. (2.5).

Arponen demonstrated the feasibility of deriving both the time-independent and time-dependent equations using *bivariational principles*. The stationary points of the *bivariational expectation value functional*,

$$\mathcal{E}[\langle\tilde{\Psi}|,|\Psi\rangle] = \frac{\langle\tilde{\Psi}|\,\hat{H}\,|\Psi\rangle}{\langle\tilde{\Psi}|\Psi\rangle}, \tag{2.9}$$

were were shown to be equivalent to the left and right eigenvector equations

$$E\,|\Psi\rangle = \hat{H}\,|\Psi\rangle\,, \quad \langle\tilde{\Psi}|\,\hat{H} = E\,\langle\tilde{\Psi}|\,, \tag{2.10}$$

which are the time-independent Schrödinger equation and its dual, respectively. In a similar vein, Arponen determined that the stationary conditions of a bivariational action-functional,

$$\mathcal{S}[\tilde{\Psi}(t),\Psi(t)] = \int_0^T \mathcal{L}dt = \int_0^T \langle\tilde{\Psi}(t)|\,i\frac{d}{dt} - \hat{H}(t)\,|\Psi(t)\rangle\,dt, \tag{2.11}$$

yielded the time-dependent Schrödinger equation and its complex conjugate,

$$i\hbar\frac{\partial}{\partial t}\,|\Psi(t)\rangle = \hat{H}\,|\Psi(t)\rangle\,, \quad -i\hbar\frac{\partial}{\partial t}\,\langle\tilde{\Psi}(t)| = \langle\tilde{\Psi}(t)|\,\hat{H}. \tag{2.12}$$

These formulations satisfied the time-dependent Hellmann-Feynman theorem, and expectation values could thus be calculated with the usual formula,

$$\langle\hat{A}\rangle\,(t) = \langle\tilde{\Psi}(t)|\,\hat{A}\,|\Psi(t)\rangle\,. \tag{2.13}$$

Arponen and coworkers [39–41] went on to explore the connection between the bivariational action-functional (2.11) and classical Hamiltonian mechanics. Either the bra and ket states $\mathcal{S}[\tilde{\Psi}(t),\Psi(t)]$ or the cluster amplitudes $\mathcal{S}[\lambda,\tau]$ could be used as canonical variables: The bivariational action-functional in terms of the cluster amplitudes was given by

$$\mathcal{S}[\lambda,\tau] = \int_0^T \mathcal{L}dt = \int_0^T i\lambda\cdot\dot{\tau} - \langle\Psi(\tau,\lambda)|\hat{H}|\Psi(\tau)\rangle\,dt. \tag{2.14}$$

This form allowed the equations of motion to be found with the Euler-Lagrange equation,

$$\frac{\partial\mathcal{L}}{\partial z_{\mu_n}} = \frac{d}{dt}\frac{\partial\mathcal{L}}{\partial\dot{z}_{\mu_n}}, \tag{2.15}$$

with z_{μ_n} representing the collection of all independent variations of the wavefunction parameters: These equations are much simpler to evaluate than procedures employing projections techniques. Using $\mathcal{H}(\tau,\lambda) = \langle\Psi(\tau,\lambda)|\hat{H}|\Psi(\tau)\rangle$ as a short-hand, the equations of motion were evaluated to [42],

$$i\dot{\tau} = \frac{\partial\mathcal{H}}{\partial\lambda_{\nu_n}}, \quad -i\dot{\lambda} = \frac{\partial\mathcal{H}}{\partial\tau_{\nu_n}}. \tag{2.16}$$

Eqs (2.16) constitute classical (complex) Hamilton's equations of motions. Consequently, they evolve in time as symplectic transformations. This makes it possible to use symplectic integrators developed for exact quantum mechanics known for their capability to conserve physical properties with high precision.

The exponential $e^{\hat{\Lambda}(t)}$, referred to as extended coupled cluster [39, 43, 44], was not widely adapted in quantum chemistry, due to the complexity of its implementation: The working equations proved to be computationally expensive, without offering improvements in describing dynamic electron correlation. The form that prevailed was a linear parametrization $(1 + \Lambda)$, introduced by Helgaker and Jørgensen [45, 46], independently of Arponen's bivariational framework. Instead, they performed a constrained optimization of the coupled-cluster functional,

$$L(\tau, \lambda) = \langle \Phi | e^{-\hat{T}} \hat{H} e^{\hat{T}} | \Phi \rangle + \sum_{\mu_n} \lambda_{\mu_n} \langle \Phi_{\mu_n} | e^{-\hat{T}} \hat{H} e^{\hat{T}} | \Phi \rangle, \qquad (2.17)$$

giving a second set of parameters through the Lagrangian multipliers λ_{μ_n}.

With coupled-cluster *ansätze* that fulfilled the Hellmann-Feynman theorem established, Koch and Jørgensen [47, 48] derived equations of motion for the wavefunction parameters using projection techniques, albeit for the development of coupled-cluster response theory, where the time-dependence was solved order for order in the frequency-domain [49]

$$i\dot{\tau}_0(t) = \langle \tilde{\Phi}_0 | e^{-\hat{T}(t)} \hat{H}(t) e^{\hat{T}(t)} | \Phi_0 \rangle, \quad i\dot{\tau}_{\mu_n}(t) = \langle \tilde{\Phi}_{\mu_n} | e^{-\hat{T}(t)} \hat{H}(t) e^{\hat{T}(t)} | \Phi_0 \rangle,$$
$$i\dot{\lambda}_0(t) = 0, \qquad\qquad\qquad i\dot{\lambda}_{\mu_n}(t) = - \langle \tilde{\Psi}(t) | [\hat{H}(t), \hat{X}_{\mu_n}] | \Psi(t) \rangle. \quad (2.18)$$

The $\tau_0(t)$ amplitude is seen to be decoupled from the other amplitudes, and therefore acts as a phase factor. The λ_0 amplitude is time-independent and is fixed to $\langle \tilde{\Psi} | \Psi \rangle = 1$ in order to ensure normalization. These amplitudes can be formally eliminated but the phase carries additional information that may be useful.

Linear-response coupled-cluster theory was mostly successful, but observables where found to exhibit an unphysical gauge-origin dependence when magnetic fields where introduced into the Hamiltonian, even at the complete basis set limit. Pedersen and Koch [50] demonstrated that gauge-origin invariance was reinstated when the orbitals were fully optimized. Specifically, the orbital-optimized coupled-cluster (OCC) [51–53], where the single excitation operator was replaced by a Brueckner-type unitary rotation operator $e^{\hat{\kappa}}$,

$$\hat{\kappa} = -\hat{\kappa}^\dagger = \sum_{\mu_1} (\kappa_{\mu_1} \hat{X}_{\mu_1} - \hat{\kappa}_{\mu_1}^* \hat{X}_{\mu_1}^\dagger), \qquad (2.19)$$

was shown to be gauge-origin invariant.

The non-orthogonal orbital-optimized coupled-cluster (NOCC) [54] was also proposed and implemented in order reduce the dimension of the eigenvalue problem used for determining the excitation energies. The NOCC methods were identical to the OCC methods, apart from a loosening of the $\hat{\kappa} = -\hat{\kappa}^\dagger$ constraint. While the OCC method was later found to not converge to full configuration interaction (FCI) at the untruncated limit [55] for systems larger than 2 electrons, the NOCC method *was* found to have this property [56].

2.1.3 Time-domain time-dependent coupled-cluster theory

Up until 2011, TDCC theory had mainly been developed within response theory. It was again considered for studying time-resolved dynamics when Huber and Klamroth [13] presented an implementation of time-dependent coupled-cluster singles and doubles (TDCCSD) that propagated the equations of motion of the τ-amplitudes with the explicit fourth order Runge–Kutta (RK4) algorithm. The implementation, however, did not propagate the λ-amplitudes. Furthermore, it was found that simulations become numerically unstable in strong external fields.

A year later, Kvaal [57] presented a time-domain orbital-adapted time-dependent coupled-cluster (OATDCC) theory, based on Arponen's bivariational framework. The OATDCC theory encompassed time-varying bi-orthogonal orbitals $\Phi(t)$ and $\tilde{\Phi}(t)$ as additional degrees of freedom. The equations of motion were found by requiring an action functional to be stationary with respect to all variations of the wavefunction parameters. The Euler-Lagrange equations corresponding to amplitude variations alone read

$$i\dot{\tau}^{\mu_n}(t) = \langle\Phi_0|\hat{Y}^{\mu_n}e^{-\hat{T}(t)}(\hat{H}(t) - i\hat{D}_0)e^{\hat{T}(t)}|\Phi_0\rangle\,, \tag{2.20}$$

$$-i\dot{\lambda}_{\mu_n}(t) = \langle\Phi_0|\hat{\Lambda}(t)e^{-\hat{T}(t)}[\hat{H}(t) - i\hat{D}_0, \hat{X}_{\mu_n}]e^{\hat{T}(t)}|\Phi_0\rangle\,. \tag{2.21}$$

These were equivalent to the standard TDCC equations of motion, found by Koch and Jørgensen [47, 48], with an additional operator,

$$\hat{D}_0 = \sum_{pq}\langle\tilde{\phi}_p|\dot{\phi}_q\rangle a_p^\dagger \tilde{a}_q^\dagger, \tag{2.22}$$

emerging from the time-dependence of the orbitals. Hence, the standard TDCC method could be derived using the bivariational framework.

The OATDCC theory provided polynomially scaling methods when the coupled-cluster *ansätze* are nontrivially truncated. Within the bivariational framework [58], it was additionally possible to introduce active and frozen subspaces into the OATDCC theory. When the entire space is defined as active, the OATDCC methods became equivalent to time-dependent non-orthogonal orbital-optimized coupled-cluster (TDNOCC) [54]. Furthermore, the theory reduces to time-dependent Hartree–Fock (TDHF) at the highest level of truncation, and becomes identical to multiconfigurational time-dependent Hartree–Fock (MCTDHF) [59] at the untruncated limit.

Inspired by the OATDCC theory, Sato and coworkers [60–64] developed a time-domain time-dependent formulation of OCC theory [51–53]. As with the OATDCC framework, the time-dependent orbital-optimized coupled-cluster (TDOCC) implementation allowed for the utilization of frozen, dynamic, and active orbitals. Coupled with a finite-element discrete variable representation (FEDVR) basis, the TDOCC method was capable of describing the electron continuum. This enhancement facilitated the simulation of strong field and ionization dynamics. As illustrated by Sato et al. [60], TDOCC simulations could be employed to calculate both first and second ionization probabilities and high harmonic generation spectra. Despite the TDOCC model lacking formal

convergence, it was observed to be virtually indistinguishable from FCI for the cases studied.

The connection to classical Hamiltonian mechanics motivated Pedersen and Kvaal [65] to recommend using a symplectic integrator for integrating the equations of motion of the coupled-cluster amplitudes. This would facilitate proper conservation of physical properties, also for truncated cluster operators. An implementation of a time-domain TDCCSD method, evolved with the symplectic s-stage Gauss–Legendre integrator [66] demonstrated that energy was conserved, even after extended simulation periods. Furthermore, the intuition gleaned from the bivariational framework of two dual states being required to define a single coupled-cluster state, motivated the definition of a *two-component* state vector,

$$|S\rangle\rangle = \frac{1}{\sqrt{2}} \left(\begin{array}{c} |\Psi\rangle \\ |\tilde{\Psi}\rangle \end{array} \right). \tag{2.23}$$

An indefinite inner product, and an autocorrelation function were then defined for the state vector. The indefinite inner product was given as

$$\langle\langle S_1 | S_2 \rangle\rangle \equiv \frac{1}{2} \left(\langle \tilde{\Psi}_1 | \Psi_2 \rangle + \langle \Psi_1 | \tilde{\Psi}_2 \rangle \right). \tag{2.24}$$

This form of the state vector gave expectation values with the same expression that was proposed in Ref. [42] within response theory

$$\langle\langle S | \hat{P} | S \rangle\rangle = \frac{1}{2} \langle \tilde{\Psi} | \hat{P} | \Psi \rangle + \frac{1}{2} \langle \tilde{\Psi} | \hat{P}^\dagger | \Psi \rangle^*. \tag{2.25}$$

The autocorrelation function, giving the overlap between states at different times t' and t, was defined as

$$A(t', t) \equiv \langle\langle S(t') | S(t) \rangle\rangle. \tag{2.26}$$

The autocorrelation function was used for generating dipole spectra, by taking the Fourier transform of $A(t_1, t)$, where $t > t_1$ is the time after the system has interacted with a laser pulse. The autocorrelation function $A(0, t)$ quantifies the probability amplitude of a system staying in its ground state at a subsequent time $t > 0$. It was utilized to probe the source of the numerical instabilities reported in Ref. [13] during high intensity laser-driven dynamics. The instabilities were reproduced and were found to coincide with ground state depletion and a rapid increase in the τ-amplitudes. These findings supported the following mechanism for the numerical stabilities: As the reference determinant probability approaches zero, the amplitudes need to steeply increase in order to ensure the intermediate normalization $e^{-\tau_0(t)} \langle \tilde{\Phi} | \Psi(t) \rangle = 1$, imposed on the system holds. This, however, leads to challenging integrator conditions.

Typically, the laser pulse is handled semi-classically as a one-electron operator. Pedersen and Kvaal [65] therefore argued that dynamical orbital methods such as TDOCC, TDNOCC , and OATDCC should be capable of capturing the main effects of the laser pulse, and provide stable conditions for the integrator.

This led Kristiansen et al. to implement the time-domain TDNOCC method [67], an implementation that would later be part of the HYQD [68]

software suite. In order to quantify the dynamic orbitals' ability to capture the effects, the overlap between the reference state vector,

$$|R\rangle\rangle = \frac{1}{\sqrt{2}} \left(\begin{array}{c} |\Phi_0\rangle \\ |\tilde{\Phi}_0\rangle \end{array} \right), \qquad (2.27)$$

and the state vector was monitored using a reference weight

$$W = |\langle\langle S(t)|R(t)\rangle\rangle|^2. \qquad (2.28)$$

The large oscillation in the amplitudes, accompanied with W approaching zero, and subsequent failure of the simulation was reproduced when using the static TDCCSD method subject to a high-intensity laser pulse. The dynamic orbitals of time-dependent non-orthogonal orbital-optimized coupled-cluster doubles (TDNOCCD) were found to successfully capture the laser pulse effects, with a reference weight that remained close to one for laser fields with field strengths of 1 a.u. However, upon application of an adequately high field strength, the TDNOCCD method was destabilized, accompanied by an unphysical rise in the reference weight above one.

Electron dynamics in exact quantum mechanics is commonly analyzed by considering the populations of stationary states. Pedersen et al. defined the time-resolved populations p_n in terms of the expectation value of the indefinite inner product [69],

$$p_n(t) = \langle\langle S(t)|\hat{P}_n|S(t)\rangle\rangle. \qquad (2.29)$$

Where $\hat{P}_n$ is a projection operator, defined as

$$\hat{P}_n = |E_n\rangle\rangle\langle\langle E_n|, \qquad (2.30)$$

and E_n are a set of orthonormal excitation state-vectors. The process of defining excitation states for approximate wavefunctions carries inherent ambiguities. This is particularly relevant in the context of coupled-cluster theory, as two prevalent approaches can be used: equation-of-motion coupled-cluster theory and linear response coupled-cluster theory. Projection operators based on both approaches were derived, implemented, and shown to conserve the stationary state populations over time. The study of excited-state Rabi oscillation, chirped lasers, and the attribution of features within the transient spectra (computed by Skeidsvoll et al. [70]) has been conducted with the use of stationary-state populations. Despite the EOM-CC projection operator lacking formal size-intensity, the results obtained from the two methods were largely similar. However, minor spurious effects were observed with the LR-CC projection operator, leading to the recommendation of constructing the stationary-state projection operator from EOM-CC excited states.

Given the computationally intensive nature of coupled-cluster methods, it is natural to consider time-saving approximations. Sato and coworkers have implemented a range of TDOCC approximative methods. The cheapest method, the time-dependent second-order Møller–Plesset (TDOMP2) method [61, 71] scales as $\mathcal{O}(K^5)$ with respect to the number of basis functions K. This method is particularly efficient as the right and left hand amplitude coefficients are each

others complex conjugate $(\tau_{ij}^{ab} = \lambda_{ab}^{ij*})$, making it sufficient to only solve for the right-hand side. Despite being a perturbative method, explicit time-dependence is achieved through the time-dependent orbitals, granting stability even when simulating strong laser-electron interactions.

The favorable scaling of TDOMP2 makes it a particularly appealing method, but it has not yet been applied to the description of linear and nonlinear optical properties. Although the development of time-domain time-dependent coupled-cluster methods has primarily focused on dynamics outside of the perturbation region this far, there are clear advantages in using time-domain methods for simulating weak-field dynamics. These advantages are particularly relevant for the evaluation and extraction of nonlinear response properties which will be the topic of the next two sections.

2.2 Evaluating magnetic and electric properties

The incorporation of the electromagnetic field into the Hamiltonian for studying magneto-optical properties introduces a new layer of computational complexity. For both wavefunction methods and DFT methods, the Hamiltonian becomes complex. Additionally, efforts must be undertaken to ensure gauge invariance. Beyond these computational aspects, it is also necessary to expand DFT to include an additional basic variable, supplementing the charge density.

2.2.1 London orbitals

The time-dependent non-relativistic closed-shell electronic Hamiltonian $\hat{H}_0 = \frac{1}{2}\hat{\mathbf{p}} + W$, where $\hat{\mathbf{p}} = -i\nabla$ is the momentum operator and W represents all Coulomb interactions, may be coupled to a classical electromagnetic field through the interaction of a vector potential $\mathbf{A}(\mathbf{r}, t)$ and a scalar potential $\phi(\mathbf{r}, t)$ as

$$\hat{H}(t) = \frac{1}{2}(\hat{\mathbf{p}} + \mathbf{A}(\mathbf{r}, t))^2 + W - \phi(\mathbf{r}, t). \tag{2.31}$$

The gauge freedom of a classical electric and magnetic field allows for a Coulomb gauge fixing condition to be applied

$$\nabla \cdot \mathbf{A}(\mathbf{r}) = 0, \tag{2.32}$$

simplifying Eq. (2.31) to

$$\hat{H}(t) = \hat{H}_0 + \hat{\mathbf{p}} \cdot \mathbf{A}(\mathbf{r}, t) + \frac{1}{2}\mathbf{A}(\mathbf{r}, t)^2 - \phi(\mathbf{r}, t). \tag{2.33}$$

However, this still leaves residual gauge freedom that can be expressed with gauge transformations of the form

$$\mathbf{A}'(\mathbf{r}, t) = \mathbf{A}(\mathbf{r}, t) + \nabla f, \quad \nabla^2 f = 0. \tag{2.34}$$

For the action of the Lagrangian $\mathcal{L} \equiv \langle\tilde{\Psi}(t)|i\frac{\partial}{\partial t} - \hat{H}(t)|\Psi(t)\rangle$, and thereby all the observables to remain invariant,

$$\langle\tilde{\Psi}(t)|i\frac{\partial}{\partial t} - \hat{H}(t)|\Psi(t)\rangle = \langle\tilde{\Psi}'(t)|i\frac{\partial}{\partial t} - \hat{H}'(t)|\Psi'(t)\rangle, \tag{2.35}$$

the bivariational wavefunction undergoes a compensating unitary local phase transformation,

$$\Psi'(t) = e^{-if}\Psi(t), \quad \tilde{\Psi}'(t) = e^{if}\tilde{\Psi}(t), \tag{2.36}$$

that introduces rapid oscillations into the wavefunction.

In the context of approximate wavefunctions, the inability of basis set parameters to fully describe $e^{-if(\mathbf{r}, t)}$ may lead to an unphysical gauge variance. Epstein [72] demonstrated that to ensure gauge invariance when modeling a wavefunction within an electromagnetic field, it is essential to employ a variational

wavefunction method in conjunction with a basis set at the basis set limit. However, the oscillations introduced into the wavefunction by the magnetic field can cause slow basis set convergence when using conventional Gaussian type orbitals.

In the specific case of a static magnetic field, gauge *origin* invariance can be guaranteed through the use of a specific class of orbitals known as London atomic orbitals (LAOs) [73]. The static magnetic field can be described by an external vector-potential in a cylindrical gauge with the origin placed at $\mathbf{O}$,

$$\mathbf{A_O}(\mathbf{r}) = \frac{1}{2}\mathbf{B} \times (\mathbf{r} - \mathbf{O}). \tag{2.37}$$

Defining $\mathbf{r_O} = \mathbf{r} - \mathbf{O}$, the closed-shell Hamiltonian of Eq. (2.31) can be expressed in terms of the magnetic field $\mathbf{B}$,

$$\hat{H}(t) = \hat{H}_0 + \frac{1}{2}\hat{\mathbf{l}}_\mathbf{O} \cdot \mathbf{B} + \frac{1}{8}[B^2 r_\mathbf{O}^2 - (\mathbf{r_O} \cdot \mathbf{B})^2],$$

where

$$\hat{\mathbf{l}}_\mathbf{O} = i\mathbf{r_O} \times \nabla \tag{2.38}$$

is the canonical angular momentum about $\mathbf{O}$.

The origin of the magnetic vector potential depends on the choice of the coordinate system and a shift of the vector potential origin by $\mathbf{G}$ can be expressed as the gauge transformation

$$\mathbf{A_G}(\mathbf{r}) = \mathbf{A_O}(\mathbf{r}) + \nabla f, \quad f = -\mathbf{A_O}(\mathbf{G}) \cdot \mathbf{r}. \tag{2.39}$$

The exact wavefunction is therefore transformed as

$$\Psi' = e^{i\frac{1}{2}\mathbf{B}\times(\mathbf{G}-\mathbf{O})\cdot\mathbf{r}}\Psi. \tag{2.40}$$

The LAOs emulate this by including the phase factor into the definition of the atomic orbitals:

$$\omega(\mathbf{B}, \mathbf{G}, \mathbf{C}) = e^{i\frac{1}{2}\mathbf{B}\times(\mathbf{G}-\mathbf{C})\cdot\mathbf{r}}\chi(\mathbf{r_C}). \tag{2.41}$$

The $\chi(\mathbf{r_C})$ is the standard atomic orbital, usually taken as a spherical Gaussian type orbital, centered at $\mathbf{C}$, and the attached field-dependent plane wave $e^{i\frac{1}{2}\mathbf{B}\times(\mathbf{G}-\mathbf{C})\cdot\mathbf{r}}$ moves the global gauge-origin $\mathbf{O}$ to the center of each atomic orbital, giving local gauge-origins. In addition to guaranteeing gauge-origin invariance, this hybrid atomic orbital leads to rapid basis-set convergence compared to standard Gaussian type orbitals as the bulk of the effect of the magnetic field is incorporated at the basis set level [74].

LAOs were incorporated into the Hartree–Fock method for magnetic property calculation using perturbation theory in 1972 [75]. An implementation employing efficient analytical derivative techniques was introduced in 1990 [76], greatly contributing to the establishment of LAOs as the standard for *ab initio* methods [77] for the calculations of magnetic and magneto-optical properties within response theory [78].

2.2.2 Finite-field methods with London orbitals

For magnetic fields of field strengths beyond the perturbative regime, finite-field methods may be employed instead. In perturbation-based theories, it was not necessary to compute molecular integrals over LAOs since the analytical derivatives were evaluated at zero magnetic field, replacing the plane-wave gauge factors with multipoles. However, for finite-field methods, the computation of integrals over LAOs becomes necessary.

In 2008, Tellgren and coworkers developed the LONDON program [79], capable of evaluating integrals over LAOs using the McMurchie–Davidson scheme [80] for both uniform and non-uniform [81] magnetic fields. This advancement facilitated the description of all molecular orientations in a finite magnetic fields. Additionally, the derivatives of integrals over LAOs were implemented in the LONDON program, enabling exploration of geometric changes as a function of the magnetic field [82]. Initial implementations were presented for the Hartree–Fock [83] and full configuration interaction methods [84]. This advancement allowed the demonstration of closed-shell paramagnetic systems transitioning to a diamagnetic state at sufficiently high magnetic fields [85], and the discovery of a new 'strong' type of bond — the perpendicular paramagnetic bonding mechanism — alongside the well-known ionic and covalent bonds.

Both the standard DFT and a CDFT [86–88] implementation was introduced for the first time for finite fields in LONDON [89] using the vorticity-dependent exchange-correlation functionals on the form suggested by Vignale and Rasolt [86].

CDFT is formally more correct than standard DFT. Furthermore, benchmarking of magnetizabilities, rotational g-tensors, nuclear shielding constants, and spin-rotation constants [90, 91] yielded subpar results for DFT compared to Hartree–Fock and coupled-cluster theory. It was found that the neglected current-density contributions to magnetic properties with standard DFT were significant: Even with constraints applied to Kohn–Sham calculations to achieve the same density as a coupled-cluster benchmark, the description of magnetic properties was still deficient. However, a comparison of the implemented CDFT with FCI calculations indicated that the inclusion of paramagnetic current densities dependence didn't substantially improve upon DFT. The current-dependent functionals used were parameterizations of a uniform electron gas. Although these functionals were modified to yield an electron density that diminished with distance, more sophisticated functionals were deemed necessary.

Finding appropriate CDFT functionals requires benchmarks, and only Hartree–Fock method and the exponentially scaling FCI method were implemented with LAOs so far. This motivated the implementation of finite-field coupled-cluster theory at the CCSD and coupled-cluster singles, doubles and perturbative triples (CCSD(T)) levels [92, 93]. The implementation was complex throughout, and the operations on the two-electron integrals did not rely on permutation symmetries. The coupled-cluster implementation was utilized to explore the impact of electron-correlation effects in atoms and molecules in the presence of strong magnetic fields, which proved to be significant. It was discovered that strong magnetic fields required larger basis sets, particularly when states of high angular momentum were important for describing the properties of interest.

The implementation of finite-field coupled-cluster methods in the LONDON software allowed for the accurate description of dynamic electron correlation with polynomial scaling. However, systems that exhibited multireference character cannot be addressed using standard coupled-cluster methods. An implementation of equation-of-motion coupled-cluster theory was introduced with the QCUMBRE software [94] allowing for the description of *certain* multireference states within a single reference framework [95]. This software suite included the standard EOM-CC at both the CCSD [96] and CCSDT levels [97], enabling the computation of excitation spectra in magnetic fields with high precision. Additionally, variants were developed that had the capability to flip the spin of the excited electron [96], ionize an electron, and investigate electron attachment. The software was also expanded to facilitate the computation of properties using linear response at the CCSD level [98].

The finite-field coupled-cluster methods allowed Furness et al. [99] to benchmark CDFT functionals. The meta-generalized gradient approximation (mGGA) functionals B98 [100], and TPSS [101, 102] were altered to include current dependence utilizing the modification of the kinetic energy density suggested by Dobson [103] and later used by Becke [104] and Bates and Furche [105]

$$\tau(\mathbf{r}) \rightarrow \tilde{\tau}(\mathbf{r}) = \sum_i^{\text{occ}} [\nabla \varphi_i(\mathbf{r})]^* \cdot [\nabla \varphi_i(\mathbf{r})] - \frac{|\mathbf{j}_{\text{p}}(\mathbf{r})|^2}{\rho(\mathbf{r})}, \tag{2.42}$$

giving cB98 and cTPSS. Furness et al. implemented these functionals, along with the hybrid TPSSh functional [106], which was composed of 10% orbital-dependent exchange. They then conducted benchmarking against CCSD(T). The inclusion of current dependence was found to improve the description of ground state systems in strong magnetic fields, while offering only modest improvements for low to moderate magnetic fields. The cTPSS, cTPSSh, and a range-separated variant denoted cTPSSrsh [107] were also applied to nuclear shielding constants [108], where, as in Ref. [99], the cTPSS-based functionals yielded only modest improvements.

Beyond the development of CDFT, numerical advances for more efficient calculation were presented in the QUEST program [79]. While the integration over LAOs was originally done with the McMurchie-Davidson (MD) scheme, Irons et al. [109] investigated the efficiency of the most popular integral schemes for hybrid LAO-plane wave basis functions: McMurchie-Davidson, Head–Gordon–Pople [110], and Rys quadrature [111]. A procedure for improving the integral performance was implemented where the best algorithm was chosen based on the angular momentum of the basis functions. Additionally, the scheme for finding gradients for LAOs was also improved [112].

2.2.3 Time-domain finite-field methods

A time-dependent electromagnetic pulse can be introduced into the Hamiltonian given in Eq. (2.31), which already includes an interaction with a static magnetic field. The Hamiltonian can then separated into a time-independent and time-dependent part

$$\hat{H}(t) = \hat{H} + \hat{V}(t). \tag{2.43}$$

The time-independent Hamiltonian $\hat{H}$ describes the interaction with the static magnetic field described by the vector potential $\mathbf{A_O}(\mathbf{r})$

$$\hat{H} = \hat{H}_0 + \mathbf{A_O}(\mathbf{r}) \cdot \hat{\mathbf{p}} + \frac{1}{2} A_{\mathbf{O}}^2(r), \tag{2.44}$$

and the time-dependent interaction operator $\hat{V}(t)$

$$\hat{V}(t) = [\hat{\mathbf{p}} + \mathbf{A_O}(\mathbf{r})] \cdot \mathbf{A}(\mathbf{r}, t) + \frac{1}{2} A^2(r, t), \tag{2.45}$$

describes the interaction with the dynamic electromagnetic pulse $\mathbf{A}(\mathbf{r}, t)$, coupled to the vector potential of the static field.

Simplifications can be achieved by invoking the dipole approximation, $\mathbf{A}(\mathbf{r}, t) \approx \mathbf{A}(0, t) = \mathbf{A}(t)$. The interaction operator $\hat{V}(t)$ then becomes independent of the static magnetic field. This allows the static magnetic field to be treated with the procedure used to obtain the reference determinant. The interaction with the time-dependent laser is treated separately with, for example, a time-dependent wavefunction method.

Finite magnetic fields with LAOs were recently implemented for time-domain TDHF and time-domain TDDFT in the Chronus Quantum (CHRONUSQ) software package [113]. The time-domain TDDFT implementation was used in conjunction with LAOs to obtain magnetic circular dichroism spectra in Ref. [114]. The generalized gradient approximation of magnetic field DFT [115–117] was used, and although the exchange-correlation functional did not explicitly depend on the magnetic field, the density functional implicitly depends on the magnetic field, through the perturbation of the electron density and its derivatives. Strong magnetic fields were implemented for time-domain time-dependent current-dependent density-functional theory (TDCDFT) [118] in the QUEST program. This implementation included field-dependent terms in the mGGA exchange-correlation functionals: cTPSS, cTPSSh and cTPSSrsh.

The finite-field approach is mostly straightforward to implement for time-domain TDCC theory, for example the formal TDCC method is left unchanged. The practical considerations of such an implementation is described in section 3.3. The implementation would lead to more comprehensive capturing of electron correlation compared to the existing time-domain TDHF and TDDFT methods and could serve as a benchmark for these.

Additionally, while the dipole approximation is applicable in most scenarios, it might not be suitable for absorption spectra in the X-ray region, given the high frequencies of the external laser involved. Consequently, simulations predicated with the dipole approximation are unable to compute properties that are contingent on beyond-dipole effects, such as anisotropic circular dichroism.

2.3 Extraction of linear and nonlinear optical properties

Time-domain methods find application in the computation of both linear as well as nonlinear optical properties. The objective of this section is to provide an overview of the development in computing dynamic optical properties starting from the static optical properties, tracing its evolution chronologically through key papers.

2.3.1 Static optical properties

The approaches for computing dynamic properties within electronic response theory are mainly based on the groundwork laid for static properties. In the static case, the molecule's dipole moment can be expressed as a power series expansion in the electric field strength:

$$\mu_i = \mu_i^0 + \mu_{ij}^{(1)} E_j + \mu_{ijk}^{(2)} E_j E_k + \mu_{ijkl}^{(3)} E_j E_k E_l + \cdots . \tag{2.46}$$

Here, μ_i^0 represents the permanent dipole moment, and the subscripts i, j, k, and l represent Cartesian coordinates $i, j, k, l \in \{x, y, z\}$, with summation over terms with repeated subscripts implied. The first order response function in Eq. (2.46) is the *static polarizability tensor* (α), the second order response function is the *static first hyperpolarizability tensor* (β), the third order response is the *static second hyperpolarizability tensor* (γ), and so on. The computation of static nonlinear properties relies on two primary categories of methods: perturbation-theory methods, and the finite-field methods, with the latter initially introduced by Cohen and Roothan [119] for computing static polarizabilities with Hartree–Fock theory.

In the finite-field method, the electronic system interacts with a *finite* electric field of field strength E_j by means of an interaction operator, given in the length gauge as $\hat{V} = E_j \cdot \hat{\mu}_i$. The dipole moment, traditionally obtained from the energy with second-order perturbation theory, was expressed by Cohen and Roothan [119] as the expectation value of the dipole operator

$$\mu_i = \langle \psi | \hat{\mu}_i | \psi \rangle . \tag{2.47}$$

For the case where the system did not possess a permanent dipole moment, the polarizability was identified from Eq. (2.46) as

$$\alpha_{ij} = \frac{\mu_i}{E_j}. \tag{2.48}$$

where the higher order terms in Eq. 2.46 were considered negligible.

The finite-field method was extended to compute higher-order responses by Zyss [120]. In Zyss' work, higher-order responses were obtained by numerically differentiating the dipole moment with respect to the field strengths using finite differences. To eliminate the second and fourth order responses functions $\mu_{ijk}^{(2)}$ and $\mu_{ijklm}^{(4)}$, symmetric finite difference expressions, with error terms on the order $\mathcal{O}(E_j^2)$, were employed.

2.3.2 Dynamic linear optical properties

The direct application of the finite-field method to dynamic fields posed a challenge. Consequently, alternative approaches based on the the sum-over-states formalism [121, 122], were developed for computing frequency-dependent polarizabilities and hyperpolarizabilities. To avoid explicit summation over excited states, the modified Sternheimer method [123–125] or response theory, initially introduced by Olsen and Jorgensen [49], can be employed. Although response theory is a powerful tool for calculating response functions, it becomes increasingly complex as higher-order responses are considered. Moreover, these perturbation theory-based methods in the frequency domain may exhibit divergence near resonant frequencies of the system.

Yabana and Bertsch, who had backgrounds from nuclear physics, where time-domain methods were commonly used, proposed the combination of time-domain methods with the original finite-difference approach to determine the dynamic polarizability [126–129]. By employing an external electric field of sufficiently low strength to induce only linear responses, the time-dependent analogue of Eq. (2.46) can be truncated to contain a single dynamic term. The relation between the dipole moment $\mu_i(t)$ and the driving electric field $E_j(t)$ in its most general form for a purely linear response is then given by

$$\mu_i(t) = \mu_i^0 + \int_{-\infty}^{\infty} \mu_{ij}^{(1)}(t, t_1) E_j(t_1) dt_1. \tag{2.49}$$

By imposing time-invariance and causality this relation is simplified, leading the first order response function $\mu_{ij}^{(1)}$ to depend solely on the time difference between t and t_1

$$\mu_i(t) = \mu_i^0 + \int_{-\infty}^{\infty} \mu_{ij}^{(1)}(t - t_1) E_j(t_1) dt_1. \tag{2.50}$$

This results in a second term consisting of a convolution of the electric field and the response function. By performing a Fourier transom of Eq. 2.50,

$$\mathcal{F}\left[\mu_i(t) - \mu_i^0\right] = \alpha_{ij}(\omega) \tilde{E}_j(\omega). \tag{2.51}$$

the dynamic polarizabilities, defined as a *frequency*-dependent response function, can be extracted

$$\alpha_{ij}(\omega) = \mathcal{F}[(\mu_i(t) - \mu_i^{(0)}) e^{-\gamma t}] / \tilde{E}_j(\omega), , \tag{2.52}$$

where a small dampening factor $\exp(-\gamma t)$ was added to the signal in order to remove artifacts originating from the abrupt cut of the signal at the end of the simulation.

2.3.3 Dynamic nonlinear optical properties

Even though one of the advantages of time-domain methods is its ability to simulate all nonlinear responses of a system to electromagnetic radiation simultaneously, only the computation of the dynamic polarizability had so far

been considered. The advantage of obtaining all orders of response in one signal, comes with the challenge of how to separate them. The explicit time dependence of the electric field introduces complicated expressions for the nonlinear relations [1, 130]

$$\mu_i(t) = \mu_i^0 + \int_{-\infty}^{\infty} \mu_{ij}^{(1)}(t - t_1)E_j(t_1)dt_1 \tag{2.53}$$
$$+ \int\int_{-\infty}^{\infty} \mu_{ijk}^{(2)}(t - t_1, t - t_2)E_j(t_1)E_k(t_2)dt_1dt_2$$
$$+ \int\int\int_{-\infty}^{\infty} \mu_{ijkl}^{(3)}(t - t_1, t - t_2, t - t_3)E_j(t_1)E_k(t_2)E_l(t_3)dt_1dt_2dt_3$$
$$+ \cdots$$

This led to finite-difference methods long being considered inappropriate for computing dynamic properties. Furthermore, when directly converting the expression for the dynamic dipole moment from the time domain to the frequency domain, using notation adapted from response theory with $\omega^{(n)} = \omega_1 + \omega_2 + \cdots + \omega_n$,

$$\mu_i(\omega) = \delta(\mu_i^0) + \alpha_{ij}(\omega)\tilde{E}_j(\omega) \tag{2.54}$$
$$+ \frac{1}{2}\iint_{-\infty}^{\infty} \beta_{ijk}(-\omega^{(2)}; \omega_1, \omega_2)\tilde{E}_j(\omega_1)\tilde{E}_k(\omega_2)d\omega_1d\omega_2$$
$$+ \frac{1}{6}\iiint_{-\infty}^{\infty} \gamma_{ijkl}(-\omega^{(3)}; \omega_1, \omega_2, \omega_3)\tilde{E}_j(\omega_1)\tilde{E}_k(\omega_2)\tilde{E}_l(\omega_3)d\omega_1d\omega_2d\omega_3$$
$$+ \cdots,$$

the higher-order response functions are convoluted with external fields. Consequently, the frequency-dependent nonlinear optical properties cannot be obtained by a simple Fourier transform of their time-domain counterparts.

When the interacting electromagnetic field is monochromatic, the first hyperpolarizability tensor $\beta_{ijk}(-\omega^{(2)}; \omega_1, \omega_2)$ consists of a contribution at a frequency twice the carrier frequency $\beta_{ijk}(-2\omega; \omega, \omega)$ and a contribution at zero frequency $\beta_{ijk}(0; \omega, -\omega)$. The prior describes the physical process of second harmonic generation and will be denoted $\beta_{ijk}^{\mathrm{SHG}}$ for short, the latter describes the process of optical rectification and will be denoted $\beta_{ijk}^{\mathrm{OR}}$. The second hyperpolarizability $\gamma_{ijkl}(-\omega^{(3)}; \omega_1, \omega_2, \omega_3)$ consists of a contribution at a frequency three times the carrier frequency $\gamma_{ijkl}(-3\omega; \omega, \omega, \omega)$ and a contribution at the same frequency as the carrier frequency $\gamma_{ijkl}(-\omega; \omega, \omega, -\omega)$. The $\gamma_{ijkl}(-3\omega; \omega, \omega, \omega)$ describes third harmonic generation, and will be denoted $\gamma_{ijkl}^{\mathrm{THG}}$, the $\gamma_{ijkl}(-\omega; \omega, \omega, -\omega)$ describes a degenerate four wave mixing, and will be denoted $\gamma_{ijkl}^{\mathrm{DFWM}}$.

In 2002, Tsolakidis et al. [131] made the initial attempt to develop a method for computing nonlinear properties using time-domain simulations, focusing specifically on the second hyperpolarizability. Their method was applicable to electric fields on the form of a step function and for molecules not possessing a first hyperpolarizability. Care had to be taken to ensure that the external field was sufficiently strong so as to excite the polarizability and second hyperpolarizability, but not so strong as to significantly excite higher-order responses. With a

similar sentiment, Wang et al. [132] presented a method for extracting the first hyperpolarizability. Their approach involved choosing an electric field that selectively excited the first-order and second-order responses, corresponding to the polarizability and first hyperpolarizability. The frequency-domain response functions; $\alpha(\omega)$, $\beta(-2\omega;\omega,\omega)$, and $\beta(0;\omega,-\omega)$ occur at unique frequencies, enabling their separation in the frequency domain. Both these methods, however, rely on a careful choice of the electric field strength and are limited to the specific hyperpolarizabilities for which they were developed.

A general approach for extracting higher perturbation was presented by Takimoto et al. [133, 134]. They demonstrated that by decomposing the dynamic electric field $E(t)$ into a time-dependent part and the time-independent field strength, $E_j(t) = E_j F(t)$, the finite-field method originally used for static electric fields could be used also for separating dynamic nonlinear responses by taking finite differences with respect to field strengths,

$$\mu_i = \mu_i^0 + E_j \int_{-\infty}^{\infty} \mu_{ij}^{(1)}(t - t_1)F(t_1)dt_1 \tag{2.55}$$

$$+ E_j E_k \iint_{-\infty}^{\infty} \mu_{ijk}^{(2)}(t - t_1, t - t_2)F(t_1)F(t_2)dt_1 dt_2$$

$$+ E_j E_k E_l \iiint_{-\infty}^{\infty} \mu_{ijkl}^{(3)}(t - t_1, t - t_2, t - t_3)F(t_1)F(t_2)F(t_3)dt_1 dt_2 dt_3 + \cdots .$$

The polarizability and the SHG components of the first hyperpolarizability were then computed using the quasi-monochromatic approximation. A monochromatic wave with the carrier frequency ω, enveloped by a Gaussian function of bandwidth δ, was chosen as the external field,

$$E_j(t) = E_j \exp[-(t - t_c)^2\delta^2/2]\sin(\omega t). \tag{2.56}$$

As the bandwidth approaches zero ($\delta \to 0$), the Fourier transform of the time-domain signal becomes a Dirac delta function in frequency space. Using the fact that nonlinear response functions vary slowly in the frequency domain, these can be extracted from the integrals in Eq. (2.54). The first hyperpolarizability components can thus be computed in a similar way as the polarizability, by Fourier transforming both the signal and the electric field.

Although performing a Fourier transform is the obvious method for converting the response functions from the time to frequency domain, it is computationally expensive to propagate the Schrödinger equation for the length of time required for adequate resolution, even when acceleration techniques such as filter-diagonlization, used by Wang et al., is employed.

Ding et al. [135] proposed an alternative ramped continuous wave (RCW) approach, that completely eliminates the need for Fourier transforms. By using an envelope-free monochromatic electric field

$$E_j(t) = E_j \cos(\omega t), \tag{2.57}$$

the Fourier transformations of the time-dependent response functions yield

analytic solutions

$$\mu_{ij}^{(1)}(t) = \alpha_{ij}(-\omega;\omega)\cos(\omega t), \tag{2.58a}$$

$$\mu_{ijk}^{(2)}(t) = \frac{1}{4}[\beta_{ijk}^{\text{SHG}}(\omega)\cos(2\omega t) + \beta_{ijk}^{\text{OR}}(\omega)], \tag{2.58b}$$

$$\mu_{ijkl}^{(3)}(t) = \frac{1}{24}[\gamma_{ijkl}^{\text{THG}}(\omega)\cos(3\omega t) + 3\gamma_{ijkl}^{\text{DFWM}}(\omega)\cos(\omega t)], \tag{2.58c}$$

and the frequency-dependent response functions can be found by fitting the analytic solution of Eqs. (2.58) to the time-domain response signal, typically with a least-squares fitting procedure.

The relations in Eqs. (2.58) are only exact in the limit where the field has been switched on for an infinite amount of time. If switched on abruptly, the system will perturb too far from the ground state resulting in a superposition of ground and excited states, the extracted polarizability and hyperpolarizabilities will then correspond to a system of significant excited-state character. The Gaussian envelope used by Takimoto et al. [133] to model an incoming pulse finite in time had the dual function of ensuring a slow switching-on of the field. Ding et al. instead suggested using a ramping phase to fill this requirement

$$F(t) = \begin{cases} \frac{t}{t_r}\cos(\omega t) & 0 \leq t < t_r \\ \cos(\omega t) & t_r \leq t \leq t_{\text{tot}}. \end{cases} \tag{2.59}$$

The ramping factor $\frac{t}{t_r}$ delivers a linear increase in the field strength from 0 to t_r, where t_r denotes the time duration of the ramping phase. The method was demonstrated by extracting nonlinear optical properties up to third order in response. The polarizability and first hyperpolarizabilities were predicted with a high degree of accuracy, the second hyperpolarizabilities, however, displayed a high frequency noise that was attributed to higher order effects [9]. In addition to the fitting scheme, the RCW approach introduced a finite-difference formula for the diagonal components with an error term in the fourth order given by

$$\mu_{ij}^{(1)} = \frac{8\Delta_i^-(t,E_j) - \Delta_i^-(t,2E_j)}{12E_j} + \mathcal{O}(E_j^4), \tag{2.60a}$$

$$\mu_{ijj}^{(2)} = \frac{16\Delta_i^+(t,E_j) - \Delta_i^+(t,2E_j) - 30\mu_i^0}{24E_j^2} + \mathcal{O}(E_j^4), \tag{2.60b}$$

$$\mu_{ijjj}^{(3)} = \frac{-13\Delta_i^-(t,E_j) + 8\Delta_i^-(t,2E_j) - \Delta_i^-(t,3E_j)}{48E_j^3} + \mathcal{O}(E_j^4), \tag{2.60c}$$

where we have used the short hand

$$\Delta_i^{\pm}(t,E_j) \equiv \mu_i(t,E_j) \pm \mu_i(t,-E_j), \tag{2.61}$$

for the sum/difference of the time-dependent dipole moments computed with opposite polarization directions and same field strength E_j.

The RCW approach was later applied to configuration interaction theory by Lestrange et al. [136]. In this work, the ramping time was increased from one to five optical cycles, followed by four optical cycles of propagation, improving

the accuracy of the computed second hyperpolarizabilities. The approach has also been extended to allow for relativistic corrections in Ref. [137]. In the same paper, the effect of the error term on the accuracy of the extracted first and second hyperpolarizability was investigated. Computations using finite-difference formulas with error of orders $\mathcal{O}(E_j^2)$, $\mathcal{O}(E_j^4)$, and $\mathcal{O}(E_j^6)$ were compared and it was found that the accuracy of the second hyperpolarizability, which had the highest sensitivity to the error term, had only a $\approx 0.3\%$ improvement for the pNA molecule by going from the $\mathcal{O}(E_j^4)$ to the $\mathcal{O}(E_j^6)$ finite-field equations.

Recently, Uemoto et al. [138] introduced an alternative finite-field based method specifically designed for ultrashort pulsed light that uses an enveloped monochromatic pulse

$$F(t) = \sin^2\left(\frac{\pi t}{t_{\text{tot}}}\right)\cos(\omega t), \qquad 0 \leq t \leq t_{\text{tot}}, \tag{2.62}$$

where the shape of the envelope, in theory, can be freely chosen. The frequency-dependent hyperpolarizability is assumed to slowly vary in frequency space, and can therefore be taken out of the integrals of Eq. (2.54). So far the approach is almost identical to the one presented by Takimoto et al. [133]. From here, Uemoto et al. [138] suggests separating the individual frequencies constituting the hyperpolarizabilities using Fourier filtration. Taking the first hyperpolarizability as an example, the zero-frequency component can be isolated by eliminating the 2ω peak from the Fourier spectrum. Generally, the Fourier filter is defined to exclude all frequencies outside of a $\pm\omega$ range centered around the frequency component of interest $k\omega$. Subsequently, the signal is transformed back to the time domain using an inverse Fourier transform.

$$\mu^{(n)}(t; k\omega) = \int_{-(k+1)\omega}^{-(k-1)\omega} \tilde{\mu}^{(n)}(\omega')e^{-i\omega' t}d\omega'$$
$$+ \int_{(k-1)\omega}^{(k+1)\omega} \tilde{\mu}^{(n)}(\omega')e^{-i\omega' t}d\omega'. \tag{2.63}$$

The same Fourier filtration is then applied to the electric field

$$F(t; k\omega) = \int_{-(k+1)\omega}^{-(k-1)\omega} \tilde{F}(\omega')e^{-i\omega' t}d\omega'$$
$$+ \int_{(k-1)\omega}^{(k+1)\omega} \tilde{F}(\omega')e^{-i\omega' t}d\omega', \tag{2.64}$$

and the frequency-dependent response functions can then be obtained by finding

the fraction of the Fourier-filtered field in the Fourier-filtered signal

$$\beta_{ijj}^{\text{OR}}(\omega) = \frac{4\mu_{ijj}^{(2)}(t;0)}{[F(t;0)]^2}, \tag{2.65a}$$

$$\beta_{ijj}^{\text{SHG}}(\omega) = \frac{4\mu_{ijj}^{(2)}(t;2\omega)}{[F(t;2\omega)]^2}, \tag{2.65b}$$

$$\gamma_{ijjj}^{\text{DFWM}}(\omega) = \frac{8\mu_{ijjj}^{(3)}(t;\omega)}{[F(t;\omega)]^3}, \tag{2.65c}$$

$$\gamma_{ijjj}^{\text{THG}}(\omega) = \frac{24\mu_{ijjj}^{(3)}(t;3\omega)}{[F(t;3\omega)]^3}. \tag{2.65d}$$

In practice, the fraction of the Fourier-filtered signal in the Fourier-filtered field is found by curve-fitting. This process ensures retrieval of the frequency-dependent information embedded in the monochromatic pulse and thus hinges on a similar argument as Ding et al.'s RCW approach.

Despite Uemoto et al. reintroducing the Fourier transform, which contradicts Ding et al.'s initial aim of avoiding it, their procedure does not demand a significantly high resolution. It is important to note that the purpose of the Fourier transform in their method is solely for filtering purposes, not for obtaining the frequency-dependent response function itself. Moreover, Uemoto et al.'s approach offers the advantage of closely resembling ultrashort pulsed laser experiments, aligning more closely with the objectives of time-domain methods to model experimental parameters.

The extraction of nonlinear optical properties in the time domain is gaining popularity [139–146]. However, it is important to acknowledge that response theory methods offer significantly faster computations. While a linear response calculations requires 10–100 evaluations of terms scaling as $\mathcal{O}(N^6)$ at the CCSD level, time-domain methods typically require over 50 000 evaluations of these $\mathcal{O}(N^6)$ terms. Efforts should therefore be made to reduce the propagation time required for extracting nonlinear properties. Furthermore, it is worth noting that none of the existing methods have successfully been applied to properties beyond the second hyperpolarizability. Already at the second hyperpolarizability, the finite-field methods encounter challenges, in particular for small molecules, with noticeable noise present in the time-domain signal.

Chapter 3

Research and papers

In addition to the research papers that will be presented in the chapter, my work has contributed to software development within the HYQD software suite [68]. HYQD is an open-access software hosted on GitHub and has been well-documented by Schøyen [147], Winter-Larsen [148], Sutterud [149] and Kristiansen [150].

In this chapter, an introduction to the attached papers will be presented, where the motivation behind their conception will be discussed, and their individual contributions towards the research objectives will be highlighted.

3.1 Paper I

Kristiansen, H. E., **Ofstad, B. S.**, Hauge, E., Aurbakken, E., Schøyen, Ø. S., Kvaal, S., & Pedersen, T. B. (2022). Linear and Nonlinear Optical Properties from TDOMP2 Theory. *Journal of Chemical Theory and Computation, 18*(6), 3687–3702. https://doi.org/10.1021/acs.jctc.1c01309

Motivated by the favorable $\mathcal{O}(K^5)$, scaling and performance of TDOMP2 for strong field dynamics reported by Pathak et al. [61], the TDOMP2 method was implemented in HYQD in order to evaluate its performance for weak-field dynamics. A unified derivation of the TDOMP2 and TDNOMP2 methods was also presented. The time-dependent second-order coupled-cluster (TDCC2) theory [151], which is the static-orbital equivalent to TDOMP2 theory, was implemented so that the effect of the dynamic orbitals could be isolated. The TDCCSD method was already available, and could be used as a benchmark.

Core excitations, as evaluated with linear response calculations, have been found to deviate more from experimental spectra than those of valence excitation character. This observation led us to investigate the impact of dynamic orbitals for this case. Additionally, previous studies have noted that orbital relaxation affects the computation of static polarizabilities and hyperpolarizabilities [152]. Consequently, we decided to further examine how dynamic orbitals influence *dynamic* polarizabilities and hyperpolarizabilities for the same ten electron systems: Ne, HF, H_2O, NH_3, and CH_4.

We compared the TDOMP2 and the TDCC2 methods by overlaying absorption spectra up to core excitations for the same systems as used for computing the
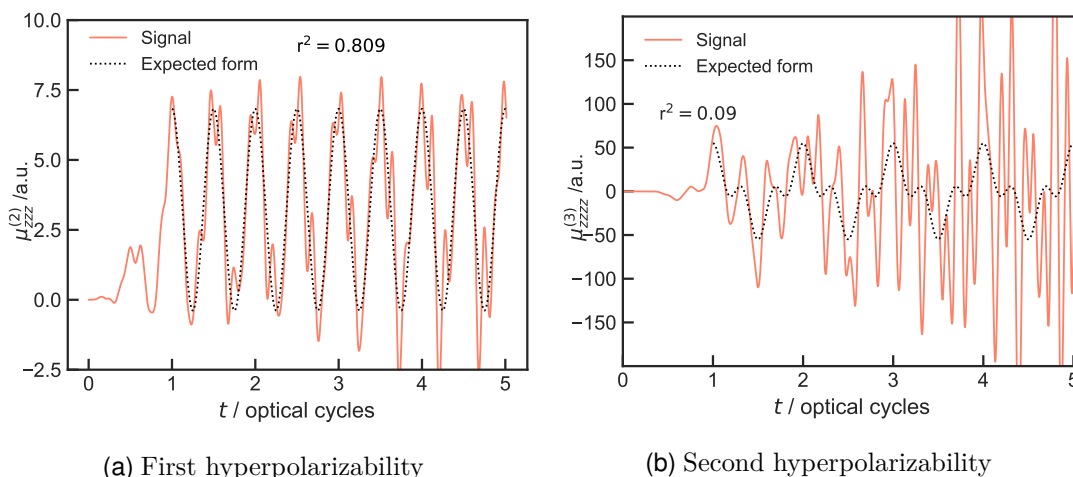
(a) First hyperpolarizability

(b) Second hyperpolarizability

Figure 3.2: Comparison of the induced dipole moments extracted from TDCCSD simulations of the HF molecule with a least-squares fitting to the form expected from response theory.

polarizabilities and hyperpolarizabilities. Except for minor differences in intensity and peak positions, the TDOMP2 and TDCC2 methods produced qualitatively similar absorption spectra. Furthermore, the differences between the excitations computed with TDOMP2 and TDCC2 were found to be consistent across both the valence and core regions. This led us to conclude that dynamic orbitals do not have a major impact on the description of the core region, and the previous difficulties in describing this region do not seem to stem from a lack of orbital relaxation.

The dynamic polarizabilities and first hyperpolarizabilities were computed with the linear RCW approach [135]. We used a one cycle ramp, followed by three optical cycles of propagation, in line with the recommendation in Ref. [135]. The second order hyperpolarizabilities were not evaluated however, due to difficulties with the curve fitting procedure. As discussed in Section 2.3, the extraction method is based on response theory, where the form of the time-dependent responses is assumed to follow specific sinusoidal functions. As seen in Figure 3.2b there are clear deviations from this presupposed form.

We compared the polarizability and hyperpolarizability computed with the TDCC2 and TDOMP2 methods to those calculated with the TDCCSD method. Additionally, we calculated the properties with the TDCC2-b variant introduced by Kats et al. [153]. This variant is less computationally effective than the standard TDCC2 method, but it includes a higher amount of orbital relaxation. In comparison to the TDCC2 method, the TDOMP2 method was found to produce polarizabilities and first hyperpolarizabilities that were closer to those of TDCCSD .

The dynamic polarizability and first hyperpolarizability for TDCCSD and TDCC2 were also compared to their linear and quadratic response counterparts, using DALTON [154]. In this way, the accuracy of the RCW approach could be monitored. The first hyperpolarizabilities extracted with the RCW approach

were found to differ more from those computed with quadratic-response coupled-cluster than the extracted polarizability differed from the linear-response coupled-cluster. This was accompanied by the time-dependent second-order response deviating more from its expected sinusoidal form than the time-dependent first-order response. As an aside, there is currently no implementation of linear- or quadratic-response TDOMP2 available, but its favorable scaling and strong performance for computing optical properties motivates such an implementation.

This paper was the first to consider nonlinear dynamic properties with time-domain TDCC. Specifically, the research objective of describing nonlinear optical properties with dynamic orbitals was addressed, with the observation that dynamic orbitals do in fact appear to improve the description.

Contributions   My largest contributions to this paper was the implementation of the time-domain TDCC2 and TDCC2-b methods. I was a supporting contributor to the writing of the original draft with Håkon Emil Kristiansen being the lead author. My writing contributions were mostly confined to the writing of Section 2.2: TDCC2 Approximation, and also to reviewing and editing the overall manuscript. I contributed to visualization, by aiding in the production of the absorption spectra figures.

3.2   Paper II

Ofstad, B. S., Kristiansen, H. E., Aurbakken, E., Schøyen, Ø. S., Kvaal, S., & Pedersen, T. B. (2023). Adiabatic extraction of nonlinear optical properties from real-time time-dependent electronic-structure theory. *The Journal of Chemical Physics*, *158*(15), 154102. https://doi.org/10.1063/5.0145521

Although the linear-response coupled-cluster and TDCC gave quite similar results for the polarizabilities and hyperpolarizabilities in Paper I, larger deviations between the time-dependent second order response (which is the time domain equivalence of the frequency-domain first hyperpolarizability) and the sinusoidal function that relates them in response theory were observed. These deviations were even more significant for the non-diagonal terms that were needed for the research objective of computing magnetic optical rotations. Ding et al. [135] had suggested that the high-frequency noise polluting the time-dependent second order response was a result of higher order perturbations remaining in the signal even after the separation using central finite differences. The finite difference formula has an error term of fourth order in the electric field strength $\mathcal{O}(E_j^4)$, and the time-dependent response functions cannot be expected to be error free.

It was found in Ref. [137], however, that only an approximate 0.3% error reduction between time-domain and response theory for the pNA molecule second hyperpolarizability calculations could be attained by using a central finite difference formula with $\mathcal{O}(E_j^6)$ instead of $\mathcal{O}(E_j^4)$. This indicates that the higher order terms are not the main source of error for the extraction of second
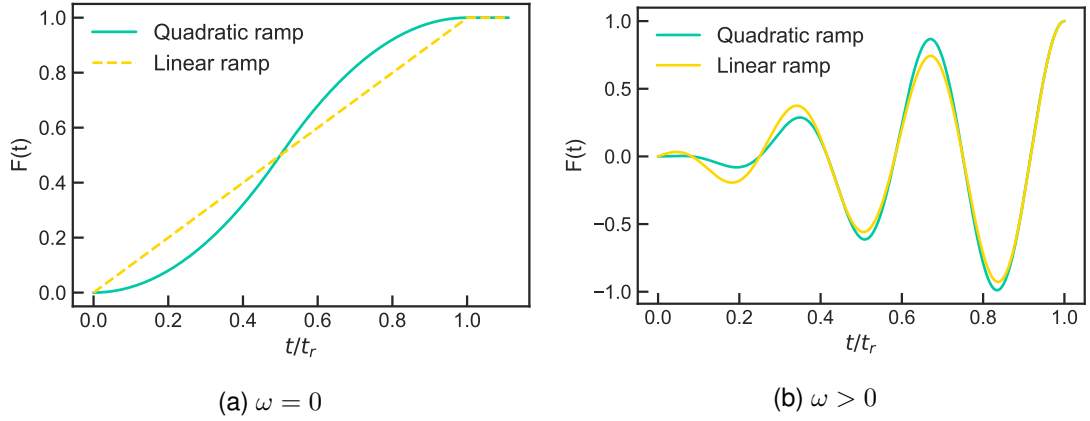
(a) $\omega = 0$ (b) $\omega > 0$

Figure 3.3: The time profiles of linear and quadratic ramps

hyperpolarizabilities. We sought to investigate whether these effects were instead due to an insufficiently adiabatic in the ramping phase.

A quadratic ramp, meant to give a more gentle ramping

$$F^{\mathrm{QRCW}}(t) = \begin{cases} \frac{2t^2}{t_r^2}\cos(\omega t) & 0 \leq t < \frac{t_r}{2} \\ \frac{t_r^2 - 2(t-t_r)^2}{t_r^2}\cos(\omega t) & \frac{t_r}{2} \leq t < t_r \\ \cos(\omega t) & t_r \leq t \leq t_{\mathrm{tot}} \end{cases} \qquad (3.1)$$

was therefore constructed. The linear ramp of the RCW approach was replaced by the quadratic ramp giving the linear RCW and quadratic RCW approaches, respectively. The form of the two ramping pulses can be compared Figure 3.3.

It was quickly uncovered that the quadratic ramp produced a signal that corresponded better to the expected form. In fact, the propagation phase was so regular that one might imagine that a whole three or four cycles of propagation after the ramping phase might be unnecessary. As stressed previously, the main advantage of response theory over time-domain methods lies in the former's superior computational efficiency. It would therefore be advantageous to explore *where* to attribute computational time when simulating with time-domain methods, in the ramping phase, or in the propagation phase. For completeness, the recent pulsed wave (PW) approach by Uemoto et al. [138], reviewed in Section 2.3, was also included in the comparison.

The three approaches were compared for computing polarizabilities, as well as first, second, and third-order hyperpolarizabilities with the time-dependent configuration interaction singles (TDCIS), TDCC2, and TDCCSD methods. It was demonstrated that the discrepancies between the signal and response equations are indeed a result of nonadiabatic effects that emerge due to the finite-time increase from zero to maximum intensity of the external laser field.

In fact, with a long enough ramping phase, the first hyperpolarizabilities could be extracted with the same accuracy as the polarizabilities. The error of the first hyperpolarizability was improved from approximately 0.4% with the standard one cycle of propagation followed by four cycles of propagation with linear RCW to below 0.0001% with a seven-cycle quadratic ramping, where six of the optical

cycles were dedicated to the ramping phase. This strongly suggests that the errors do not come from the finite-difference step, but rather from the ramping phase. The second hyperpolarizability was improved from having errors on the magnetude of 20% with the standard five-cycle linear RCW approach to errors below 0.8% with a seven-cycle quadratic RCW approach. This is a significant error reduction. The remaining error after the full adiabatic treatment could most likely be further reduced by considering a finite-difference equation with an error of $\mathcal{O}(E_j^6)$. This would, however, require running additional simulations at $4E_j$ and $-4E_j$.

The PW approach is fundamentally different from the linear and quadratic RCW approaches, in that the adiabatic effect of the ramping phase is instead provided by an envelope. The PW approach showed a consistent progression towards the correct value as a function of longer simulation time, but required longer simulation time overall to achieve accuracies comparable to the RCW approaches. This very consistent progression could make it possible to extrapolate a fully accurate answer with maybe a single, or two points, and if this is the case, the PW approach could be computationally competitive. The PW approach also differs from the RCW approach in what it aims to achieve. Uemoto et al. [138] were mostly interested in simulating short pulses. One can argue that if these short pulses excite wavefunctions into excited states, it is not appropriate to describe the response using response theory, which is fundamentally based on the ramping being fully adiabatic.

The successful extraction of the second hyperpolarizabilities encouraged the attempt to extend the quadratic RCW approach to also extract third and fourth order hyperpolarizabilities. The central finite-difference method of Ding et al. was extended to the next two orders,

$$\mu_{ijjjj}^{(4)}(t) = \frac{-39\Delta_i^+(t, E_j) + 12\Delta_i^+(t, 2E_j) - \Delta_i^+(t, 3E_j) + 56\mu^0}{144E_j^4} + \mathcal{O}(E_j^4), \quad (3.2)$$

$$\mu_{ijjjjj}^{(5)}(t) = \frac{29\Delta_i^-(t, E_j) - 26\Delta_i^-(t, 2E_j) + 9\Delta_i^-(t, 3E_j) - \Delta_i^-(t; 4E_j)}{720E_j^5} + \mathcal{O}(E_j^4),$$

$$(3.3)$$

with the third hyperpolarizabilities being accessible without needing to run any more simulations than those already run in order to acquire the second hyperpolarizabilities.

There are no available response theory implementations for the third and fourth hyperpolarizabilities, so we cannot quantify their accuracy. However, we did observe that the coefficient of determination, r^2, acquired through curve fitting of the time-dependent response function and the function that relates it to the frequency-dependent response function, was found to be a strong indicator of accuracy. The third order hyperpolarizabilities were fitted with r^2 in the range of $0.97 - 0.96$, and the main component of the fourth hyperpolarizabilities, the fifth order generation coefficient, could similarly be fit with an r^2 of 0.90. These fittings are of the same quality as what the standard linear RCW achieved for the first hyperpolarizabilities. Higher accuracy is probably achievable for these highly nonlinear responses if the simulation was ramped for longer than the six cycles, and also by using a finite-difference equation with an error of $\mathcal{O}(E_j^6)$.

The second paper further developed and improved upon the extraction approaches used in Paper I, and thus built on the foundational work presented in the first body of work. The work presented in Paper II acts as a utility that allows for a faster and more accurate approach for extracting optical properties from time-dependent simulations, needed for the research in Paper III. It was shown that only three cycles of simulations were needed to extract second hyperpolarizabilities, and we have thus achieved the research objective of identifying a reliable and efficient scheme that can be used for extracting higher-order response properties. While the approaches explored in the paper were applied to coupled-cluster and configuration-interaction theory, it is likely that the conclusions also apply to TDDFT.

Contributions As the main author, I was the lead contributor to the writing of the original draft. I was also the lead contributor to the review and editing process, the single contributor to the data collection and the lead contributor to the mathematical analysis of the data. I was the lead contributor to the visualization of the results. I contributed to the conceptualization of the research along with Thomas Bondo Pedersen and Håkon Emil Kristiansen.

3.3 Paper III

Ofstad, B. S., Wibowo-Teale, M., Kristiansen, H. E., Aurbakken, E., Kitsaras, P., Schøyen, Ø. S., Irons, T., Kvaal, S., Stopkowicz, S., Wibowo-Teale, A., & Pedersen, T. B. (2023). Magnetic Optical Activity from Real-Time Simulations. *The Journal of Chemical Physics*, (in press). https://doi.org/10.1063/5.0171927

In Paper III, the hierarchy of TDCC approaches was extended to be applicable for simulations in the finite-field framework with LAOs. The time-domain time-dependent coupled-cluster methods in HYQD were used in conjunction with integrals from the QUEST software and were successfully validated. This was achieved by comparing absorption spectra obtained from time-domain TDCC2 and TDCCSD with those determined using time-dependent EOM-CC2 and time-dependent EOM-CCSD as implemented in QCUMBRE [94].

The TDCC approaches were then used to explore the magnetic optical rotations of the H_2, HF, and CO molecules. The magnetic optical rotation, also referred to as the Faraday effect [155], was originally found to be linearly related to the magnetic field strength B and the length of the sample l in experiments conducted by Verdet [156, 157]. This relationship is expressed as

$$\theta = V(\omega)Bl, \tag{3.4}$$

with V being the Verdet constant.

Magnetic optical rotations have previously been computed with response theory according to [158–160]

$$\frac{\theta_r}{\ell} = \frac{1}{3} C \omega \sum_{ijk} \epsilon_{ijk} \text{Im} \left[\alpha_{ij}^{(k)}(-\omega; \omega) \right], \tag{3.5}$$

where C is a constant, ℓ is the path length, ω is the angular frequency of the incoming laser, $\alpha_{ij}^{(k)}(-\omega; \omega)$ is the Cartesian ij component of the molecular polarizability tensor in the presence of the magnetic field along axis k, and ϵ_{ijk} denotes the Levi–Civita tensor.

The dynamic polarizability $\alpha_{ij}(-\omega; \omega)$ has been successfully computed using LAOs and coupled-cluster methods in response theory, as demonstrated by Coriani et al. [161], in order to compute Verdet constants. While response theory is confined to the perturbative regime, the finite-field framework allows for computing magnetic optical rotation for magnetic field strengths that surpass those currently achievable in laboratories.

In the time domain, the complex polarizability was extracted from the time-domain TDCC and TDDFT methods using the method developed in Paper II. The magnetic optical rotation was computed for magnetic fields ranging from 1 T to 55 000 T, and it was demonstrated that the magnetic optical rotation no longer adheres to linearity at high magnetic fields, with a departure from linearity occurring at around 10 000 T, as depicted in Figure 3.4. This shift is observed at such a high magnetic field strength that perturbation theory remains sufficiently accurate for magnetic fields found on Earth, yet a finite-field approach might be necessary in more extreme (stellar) scenarios. Moreover, it was found that coupled-cluster methods with dynamic orbitals, specifically TDOMP2 and TDNOCC, yielded different values than their static method counterparts, TDCC2 and TDCCSD. Echoing the findings of Paper I, the TDOMP2 method produced magnetic optical rotations that more closely resembled those of TDCCSD than of TDCC2.

In computing magnetic optical rotations with the hierarchy of available TDCC methods in HYQD, this work contributes to the further assessment of dynamic orbitals. The observation that dynamic orbitals yield different results than static orbitals underscores the importance of accounting for orbital relaxation in magnetic optical properties. Moreover, the study found that the cTPSSh functional within the TDCDFT method modelled magnetic optical rotation more accurately, while the range-separated cTPSSrsh functional gave results with larger errors than the TDHF method. Overall, these findings advance our understanding of the behavior of magnetic optical rotations at high magnetic fields and shed light on the significance of orbital relaxation in magnetic optical properties.

The third paper extends the time-domain time-dependent coupled-cluster methods presented in Paper I and the extraction method recommended in Paper II to optical properties in finite magnetic fields. As such, the third paper can be seen as building upon the work done in both Paper I and Paper II. It showcases the main theme of optical properties from time-dependent electronic-structure theory with both the recent implementation of finite-field TDCDFT and the hierarchy of dynamic and static time-dependent coupled-cluster methods.
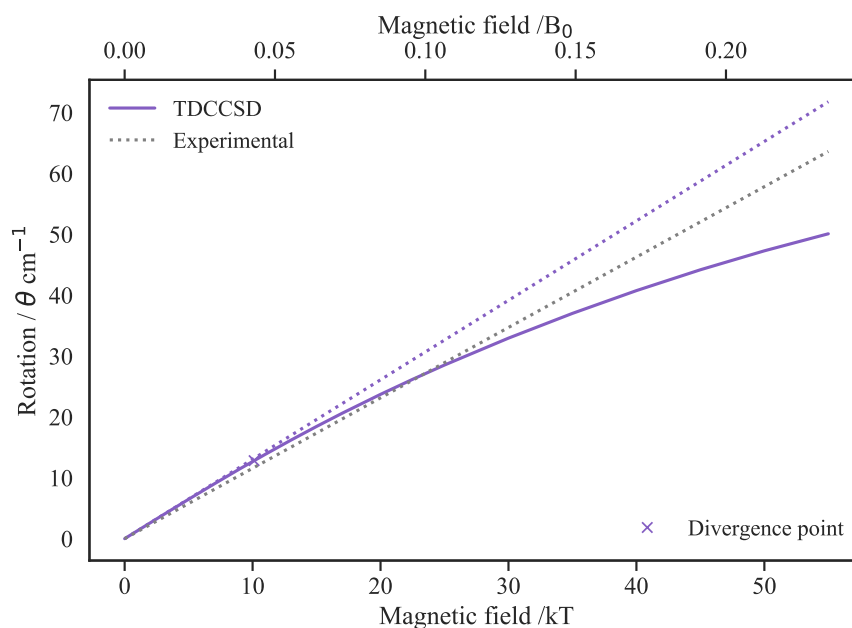
Figure 3.4: The magnetic optical activity of H_2 diverges from a straight line by 3% at the magnetic field strength of 10 000 Tesla. Basis set: aug-cc-pVDZ. Bond length: 1.4 Bohr.

Contributions I was the lead contributor to the writing of the original draft and to the review and editing process. I was the lead contributor to the data collection along with Meilani Wibowo who collected the TDCDFT data and Petros Kitsaras who generated the time-dependent EOM-CC data. I was the single contributor to the mathematical analysis of the data and visualization of the results. I was a supporting contributor to the conceptualization of the research with Thomas Bondo Pedersen as lead contributor. I was an equal contributor to the software development, along with the other authors of the paper.

3.4 Paper IV

Aurbakken, E., **Ofstad, B. S.**, Kristiansen, H. E., Schøyen, Ø. S., Kvaal, S., Sørensen, L. K., Lindh, R., & Pedersen, T. B. (2023). *Transient spectroscopy from time-dependent electronic-structure theory without multipole expansions* [Manuscript submitted for publication]. https://doi.org/10.48550/arXiv.2307.02519

The external electromagnetic fields used for simulating linear and nonlinear optical properties have so far been assumed to be spatially uniform. When considering shorter wavelength, the spatial component of the external electromagnetic field must be explicitly treated. The spatially dependent vector potential of an
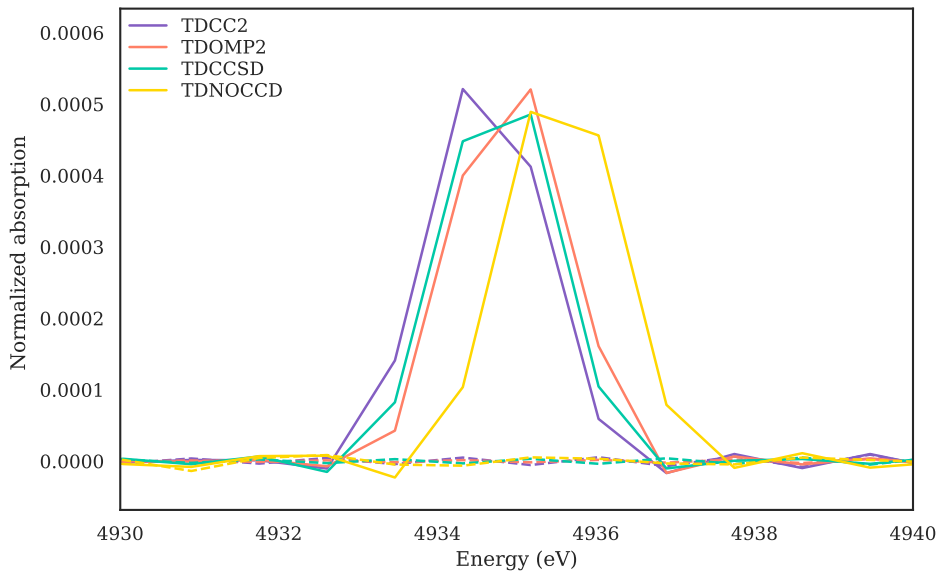
Figure 3.5: The quadrupole-allowed 1s → 3d transition of Ti^{+4} simulated with the electric-dipole approximation (dashed line) and the full plane-wave potential (solid line). Basis set: ANO-RCC-VDZ [163].

electromagnetic pulse is given by a sum of m plane waves,

$$\mathbf{A}(\mathbf{r}, t) = \sum_m A_m \text{Re}\{\mathbf{u}_m e^{i(\mathbf{k}_m \cdot \mathbf{r} - \omega_m t - \gamma_m)}\} G_m(t), \qquad (3.6)$$

where a Gaussian $G_m(t)$ controls the shape of the pulse, $\mathbf{k}_m$ is the wave vector, $\mathbf{u}_m$ the polarization vector, and γ_m the carrier envelope phase. A procedure for computing integrals over the full plane-wave vector potential has recently been implemented by Sørensen et al. [162]. This inspired the derivation and implementation of a general theory for transient absorption spectroscopy using the full plane-wave vector potential, presented in Paper IV. The implementation was validated against Ref. [70] for the computation of the core-level pump-probe spectrum of LiH, where the dipole approximation is valid.

The dipole and quadrupole allowed transitions for a titanium, both in ionic form Ti^{4+} and molecular form $TiCl_4$, has recently been investigated with EOM-CCSD level of theory in Ref. [164] using a multipole expansion. We therefore chose to explore these systems using the full plane-wave implementation of the vector field, using TDCC2, TDOMP2, TDCCSD, and TDNOCCD. A quadrupole allowed transition for the Ti^{4+} ion is displayed in Figure 3.5, where it can be seen that the quadrupole-allowed transition is, as expected, not captured when employing the dipole approximation. The observation from Papers I and III that TDOMP2 generally computes properties closer to the higher accuracy TDCCSD and TDNOCCD than TDCC2 appears to prevail, in this example. Lastly, the anisotropic circular dichroism of the chiral hydrogen peroxide molecule was computed using the hierarchy of TDCC methods.

Contributions My contributions to this paper was through the implemented time-domain TDCC2 method. I was a supporting contributor to the writing of the original draft with Einar Aurbakken being the lead author. I also contributed to the visualization, by formatting the figures, and creating Figure 7 in Blender.

3.5 Paper V

Ofstad, B. S., Aurbakken, E., Sigmundson, Ø. S., Kristiansen, H. E., Kvaal, S., & Pedersen, T. B. (2023). Time-dependent coupled-cluster theory. *WIREs Computational Molecular Science*, *13*(5) e1666. [ht-tps://doi.org/10.1002/wcms.1666](https://doi.org/10.1002/wcms.1666)

Paper V provides a comprehensive summary of time-dependent coupled-cluster theory, including the first work presented in this thesis. Although it does not directly contribute to the main theme in the same way as the other three papers do, in the form of new research findings, it is an essential resource for contextualizing and understanding the field to which the research in this thesis belongs. The review paper also aids in providing a direction for future research that can contribute to the advancement of the main theme of the dissertation, including the extension to strong field phenomena.

Contributions I was the lead contributor to the Section *Electronic dynamics with bivariational coupled-cluster theories*, with Thomas Bondo Pedersen as lead contributor overall. I was a supporting contributor to the review and editing process along with the other co-authors.

Chapter 4

Conclusion

In the preceding chapters and associated research articles, I have explored linear and nonlinear optical properties using time-domain methods. The achievements related to the research goals outlined in the introduction, along with suggestions for future work, will be summarized in this final chapter.

- A hierarchy of time-domain time-dependent coupled-cluster methods has been successfully applied to evaluate magneto-optical properties in strong magnetic fields.

- By computing polarizabilities, hyperpolarizabilities, magnetic optical rotation and X-ray absorption spectra with both static and dynamic orbitals, we have found indications that dynamic orbitals can enhance the description of nonlinear optical and magneto-optical properties.

- We have found that of the three correlation-exchange functionals explored for the TDCDFT method (cTPSS, cTPSSh, cTPSSrsh), the hybrid cTPSSh functional provided the strongest performance for describing optical properties in the presence of magnetic fields, while the range separated cTPSSrsh performed worse than the time-dependent Hartree-Fock method.

- A deviation from linearity in the relationship between magnetic optical rotation and magnetic field strength was observed at strengths of around 10 000 T.

- An efficient approach for extracting nonlinear properties of up to the fourth response order has been introduced.

The enhanced performance of the dynamic orbitals in describing nonlinear optical properties suggests that further work within methods employing dynamic orbitals could be fruitful. Our implementation of the time-domain TDCCSD method has led us to conclude that TDOMP2 may provide a more accurate description of nonlinear optical properties than the TDCC2 method. A time-domain implementation of time-dependent coupled-cluster singles, doubles, and triples (TDCCSDT) could reveal whether this observation extends to the TDNOCCD and TDCCSD methods, which we have identified as deviating in their representation of magnetic optical rotation and X-ray absorption spectra.

A more comprehensive assessment of the accuracy of both the wavefunction methods and the TDCDFT exchange-correlation functionals could be achieved by including vibrational effects and evaluating nonlinear optical properties at the basis set limit. This would enable a comparison of the computed properties with experimental results, which is more rigorous than only benchmarking against the higher accuracy TDCC methods. Additionally, further investigations of the extraction approach developed as part of this thesis might enable the extracting of even higher orders of response than presented here. This could be achieved through a combination of longer ramping time, increased electric field strength, and a finite-difference method with a smaller error term.

My studies of nonlinear properties for time-domain methods contribute to the cumulative understanding of these methods. The research presented within this thesis may aid not only in the advancement of computing nonlinear properties but also in the continued development of time-domain methods for describing electron dynamics.

Bibliography

[1] Paul N. Butcher and David Cotter. *The Elements of Nonlinear Optics.* Cambridge Studies in Modern Optics. Cambridge: Cambridge University Press, 1990. DOI: 10.1017/CBO9781139167994.

[2] Robert W. Boyd. *Nonlinear Optics.* London: Academic Press, 2003. ISBN: 978-0-12-1221682-5.

[3] P. A. Franken, A. E. Hill, C. W. Peters and G. Weinreich. 'Generation of Optical Harmonics'. In: *Physical Review Letters* 7.4 (Aug. 1961), pp. 118–119. DOI: 10.1103/PhysRevLett.7.118.

[4] Trygve Helgaker, Poul Jørgensen and Jeppe Olsen. *Molecular Electronic-Structure Theory.* London: John Wiley & Sons, Ltd, 2003. DOI: 10.1002/9781119019572.

[5] Jeppe Olsen and Poul Jørgensen. 'Time-dependent response theory with applications to self-consistent field and multiconfigurational self-consistent field wave functions'. In: *Modern Electronic Structure Theory.* Advanced Series in Physical Chemistry. World Scientific Publishing Company, Sept. 1995, pp. 857–990. ISBN: 978-981-02-1960-4. DOI: 10.1142/9789812832115_0002.

[6] Trygve Helgaker, Sonia Coriani, Poul Jørgensen, Kasper Kristensen, Jeppe Olsen and Kenneth Ruud. 'Recent Advances in Wave Function-Based Methods of Molecular-Property Calculations'. In: *Chemical Reviews* 112.1 (Jan. 2012), pp. 543–631. ISSN: 0009-2665. DOI: 10.1021/cr2002239.

[7] Ferenc Krausz and Misha Ivanov. 'Attosecond physics'. In: *Reviews of Modern Physics* 81.1 (Feb. 2009), pp. 163–234. DOI: 10.1103/RevModPhys.81.163.

[8] Joshua J. Goings, Patrick J. Lestrange and Xiaosong Li. 'Real-time time-dependent electronic structure theory'. In: *WIREs Computational Molecular Science* 8.1 (2018), e1341. ISSN: 1759-0884. DOI: 10.1002/wcms.1341.

[9] Xiaosong Li, Niranjan Govind, Christine Isborn, A. Eugene DePrince and Kenneth Lopata. 'Real-Time Time-Dependent Electronic Structure Theory'. In: *Chemical Reviews* 120.18 (Sept. 2020), pp. 9951–9993. ISSN: 0009-2665, 1520-6890. DOI: 10.1021/acs.chemrev.0c00223.

[10] Andrew M. Teale, Trygve Helgaker, Andreas Savin, Carlo Adamo, Bálint Aradi, Alexei V. Arbuznikov, Paul W. Ayers, Evert Jan Baerends, Vincenzo Barone, Patrizia Calaminici, Eric Cancès, Emily A. Carter, Pratim Kumar Chattaraj, Henry Chermette, Ilaria Ciofini, T. Daniel Crawford, Frank De Proft, John F. Dobson, Claudia Draxl, Thomas Frauenheim, Emmanuel Fromager, Patricio Fuentealba, Laura Gagliardi, Giulia Galli, Jiali Gao, Paul Geerlings, Nikitas Gidopoulos, Peter M. W. Gill, Paola Gori-Giorgi, Andreas Görling, Tim Gould, Stefan Grimme, Oleg Gritsenko, Hans Jørgen Aagaard Jensen, Erin R. Johnson, Robert O. Jones, Martin Kaupp, Andreas M. Köster, Leeor Kronik, Anna I. Krylov, Simen Kvaal, Andre Laestadius, Mel Levy, Mathieu Lewin, Shubin Liu, Pierre-François Loos, Neepa T. Maitra, Frank Neese, John P. Perdew, Katarzyna Pernal, Pascal Pernot, Piotr Piecuch, Elisa Rebolini, Lucia Reining, Pina Romaniello, Adrienn Ruzsinszky, Dennis R. Salahub, Matthias Scheffler, Peter Schwerdtfeger, Viktor N. Staroverov, Jianwei Sun, Erik Tellgren, David J. Tozer, Samuel B. Trickey, Carsten A. Ullrich, Alberto Vela, Giovanni Vignale, Tomasz A. Wesolowski, Xin Xu and Weitao Yang. 'DFT exchange: sharing perspectives on the workhorse of quantum chemistry and materials science'. In: *Phys. Chem. Chem. Phys.* 24.47 (2022), pp. 28700–28781. DOI: 10.1039/D2CP02827A.

[11] Makenzie R. Provorse and Christine M. Isborn. 'Electron dynamics with real-time time-dependent density functional theory'. In: *International Journal of Quantum Chemistry* 116.10 (2016), pp. 739–749. ISSN: 1097-461X. DOI: 10.1002/qua.25096.

[12] Benedicte Sverdrup Ofstad, Einar Aurbakken, Øyvind Sigmundson Schøyen, Håkon Emil Kristiansen, Simen Kvaal and Thomas Bondo Pedersen. 'Time-dependent coupled-cluster theory'. In: *WIREs Computational Molecular Science* n/a (), e1666. ISSN: 1759-0884. DOI: 10.1002/wcms.1666.

[13] Christian Huber and Tillmann Klamroth. 'Explicitly time-dependent coupled cluster singles doubles calculations of laser-driven many-electron dynamics'. In: *The Journal of Chemical Physics* 134.5 (Feb. 2011), p. 054113. ISSN: 0021-9606. DOI: 10.1063/1.3530807.

[14] Mauro Nisoli, Piero Decleva, Francesca Calegari, Alicia Palacios and Fernando Martín. 'Attosecond Electron Dynamics in Molecules'. In: *Chemical Reviews* 117.16 (Aug. 2017), pp. 10760–10825. ISSN: 0009-2665. DOI: 10.1021/acs.chemrev.6b00453.

[15] N. Bloembergen. 'Nonlinear optics: past, present, and future'. In: *IEEE Journal of Selected Topics in Quantum Electronics* 6.6 (Nov. 2000), pp. 876–880. ISSN: 1558-4542. DOI: 10.1109/2944.902137.

[16] Carlo Rizzo, Antonio Rizzo and David M. Bishop. 'The Cotton-Mouton effect in gases: Experiment and theory'. In: *International Reviews in Physical Chemistry* 16.1 (Jan. 1997), pp. 81–111. ISSN: 0144-235X. DOI: 10.1080/014423597230316.

[17] M. Born and R. Oppenheimer. 'Zur Quantentheorie der Molekeln'. In: *Annalen der Physik* 389.20 (1927), pp. 457–484. ISSN: 1521-3889. DOI: 10.1002/andp.19273892002.

[18] Max Born, Kun Huang and M. Lax. 'Dynamical Theory of Crystal Lattices'. In: *American Journal of Physics* 23.7 (Oct. 1955), p. 474. ISSN: 0002-9505. DOI: 10.1119/1.1934059.

[19] K. Emrich. 'An extension of the coupled cluster formalism to excited states: (II). Approximations and tests'. In: *Nuclear Physics A* 351.3 (Jan. 1981), pp. 397–438. ISSN: 0375-9474. DOI: 10.1016/0375-9474(81)90180-9.

[20] Hideo Sekino and Rodney J. Bartlett. 'A linear response, coupled-cluster theory for excitation energy'. In: *International Journal of Quantum Chemistry* 26.S18 (1984), pp. 255–265. ISSN: 1097-461X. DOI: 10.1002/qua.560260826.

[21] Jason A. Sonk, Marco Caricato and H. Bernhard Schlegel. 'TD-CI Simulation of the Electronic Optical Response of Molecules in Intense Fields: Comparison of RPA, CIS, CIS(D), and EOM-CCSD'. In: *The Journal of Physical Chemistry A* 115.18 (May 2011), pp. 4678–4690. ISSN: 1089-5639. DOI: 10.1021/jp107384p.

[22] Daniel R. Nascimento and A. Eugene III DePrince. 'Linear Absorption Spectra from Explicitly Time-Dependent Equation-of-Motion Coupled-Cluster Theory'. In: *Journal of Chemical Theory and Computation* 12.12 (Dec. 2016), pp. 5834–5840. ISSN: 1549-9618. DOI: 10.1021/acs.jctc.6b00796.

[23] Daniel R. Nascimento and A. Eugene III DePrince. 'Simulation of Near-Edge X-ray Absorption Fine Structure with Time-Dependent Equation-of-Motion Coupled-Cluster Theory'. In: *The Journal of Physical Chemistry Letters* 8.13 (July 2017), pp. 2951–2957. DOI: 10.1021/acs.jpclett.7b01206.

[24] Daniel R. Nascimento and A. Eugene DePrince. 'A general time-domain formulation of equation-of-motion coupled-cluster theory for linear spectroscopy'. In: *The Journal of Chemical Physics* 151.20 (Nov. 2019), p. 204107. ISSN: 0021-9606. DOI: 10.1063/1.5125494.

[25] Brandon C. Cooper, Lauren N. Koulias, Daniel R. Nascimento, Xiaosong Li and A. Eugene III DePrince. 'Short Iterative Lanczos Integration in Time-Dependent Equation-of-Motion Coupled-Cluster Theory'. In: *The Journal of Physical Chemistry A* 125.24 (June 2021), pp. 5438–5447. ISSN: 1089-5639. DOI: 10.1021/acs.jpca.1c01102.

[26] Andreas S. Skeidsvoll, Torsha Moitra, Alice Balbi, Alexander C. Paul, Sonia Coriani and Henrik Koch. 'Simulating weak-field attosecond processes with a Lanczos reduced basis approach to time-dependent equation-of-motion coupled-cluster theory'. In: *Physical Review A* 105.2 (Feb. 2022), p. 023103. DOI: 10.1103/PhysRevA.105.023103.

[27]   F. Coester and H. Kümmel. 'Short-range correlations in nuclear wave functions'. In: *Nuclear Physics* 17 (June 1960), pp. 477–485. ISSN: 0029-5582. DOI: 10.1016/0029-5582(60)90140-1.

[28]   F. Coester. 'Bound states of a many-particle system'. In: *Nuclear Physics* 7 (June 1958), pp. 421–424. ISSN: 0029-5582. DOI: 10.1016/0029-5582(58)90280-3.

[29]   Jiří Čížek. 'On the Correlation Problem in Atomic and Molecular Systems. Calculation of Wavefunction Components in Ursell-Type Expansion Using Quantum-Field Theoretical Methods'. In: *Journal of Chemical Physics* 45 (Dec. 1966), pp. 4256–4266. ISSN: 0021-96060301-0104. DOI: 10.1063/1.1727484.

[30]   Jiří Čížek. 'On the Use of the Cluster Expansion and the Technique of Diagrams in Calculations of Correlation Effects in Atoms and Molecules'. In: *Advances in Chemical Physics*. John Wiley & Sons, Ltd, 1969, pp. 35–89. ISBN: 978-0-470-14359-9. DOI: 10.1002/9780470143599.ch2.

[31]   J. Čižek and J. Paldus. 'Correlation problems in atomic and molecular systems III. Rederivation of the coupled-pair many-electron theory using the traditional quantum chemical methodst'. In: *International Journal of Quantum Chemistry* 5.4 (1971), pp. 359–379. ISSN: 1097-461X. DOI: 10.1002/qua.560050402.

[32]   R J Bartlett. 'Many-Body Perturbation Theory and Coupled Cluster Theory for Electron Correlation in Molecules'. In: *Annual Review of Physical Chemistry* 32.1 (1981), pp. 359–401. DOI: 10.1146/annurev.pc.32.100181.002043.

[33]   Hendrik J. Monkhorst. 'Calculation of properties with the coupled-cluster method'. In: *International Journal of Quantum Chemistry* 12.S11 (1977), pp. 421–432. ISSN: 1097-461X. DOI: 10.1002/qua.560120850.

[34]   Esper Dalgaard and Hendrik J. Monkhorst. 'Some aspects of the time-dependent coupled-cluster approach to dynamic response functions'. In: *Physical Review A* 28.3 (Sept. 1983), pp. 1217–1222. DOI: 10.1103/PhysRevA.28.1217.

[35]   P. Hoodbhoy and J. W. Negele. 'Time-dependent coupled-cluster approximation to nuclear dynamics. I. Application to a solvable model'. In: *Physical Review C* 18.5 (Nov. 1978), pp. 2380–2394. DOI: 10.1103/PhysRevC.18.2380.

[36]   P. Hoodbhoy and J. W. Negele. 'Time-dependent coupled-cluster approximation to nuclear dynamics. II. General formulation'. In: *Physical Review C* 19.5 (Apr. 1979), pp. 1971–1982. DOI: 10.1103/PhysRevC.19.1971.

[37]   K. Schönhammer and O. Gunnarsson. 'Time-dependent approach to the calculation of spectral functions'. In: *Physical Review B* 18.12 (Dec. 1978), pp. 6606–6614. DOI: 10.1103/PhysRevB.18.6606.

[38] Jouko Arponen. 'Variational principles and linked-cluster exp S expansions for static and dynamic many-body problems'. In: *Annals of Physics* 151.2 (Dec. 1983), pp. 311–382. ISSN: 0003-4916. DOI: 10.1016/0003-4916(83)90284-1.

[39] J. S. Arponen, R. F. Bishop and E. Pajanne. 'Extended coupled-cluster method. I. Generalized coherent bosonization as a mapping of quantum theory into classical Hamiltonian mechanics'. In: *Physical Review A* 36.6 (Sept. 1987), pp. 2519–2538. DOI: 10.1103/PhysRevA.36.2519.

[40] Jouko S. Arponen. 'Independent-cluster methods as mappings of quantum theory into classical mechanics'. In: *Theoretica chimica acta* 80.2 (Mar. 1991), pp. 149–179. ISSN: 1432-2234. DOI: 10.1007/BF01119618.

[41] Jouko Arponen. 'Constrained Hamiltonian approach to the phase space of the coupled cluster method'. In: *Physical Review A* 55.4 (Apr. 1997), pp. 2686–2700. DOI: 10.1103/PhysRevA.55.2686.

[42] Thomas Bondo Pedersen and Henrik Koch. 'On the time-dependent Lagrangian approach in quantum chemistry'. In: *The Journal of Chemical Physics* 108.13 (Apr. 1998), pp. 5194–5204. ISSN: 0021-9606. DOI: 10.1063/1.475956.

[43] Bridgette Cooper and Peter J. Knowles. 'Benchmark studies of variational, unitary and extended coupled cluster methods'. In: *The Journal of Chemical Physics* 133.23 (Dec. 2010), p. 234102. ISSN: 0021-9606. DOI: 10.1063/1.3520564. URL: https://doi.org/10.1063/1.3520564 (visited on 28/10/2023).

[44] Simen Kvaal, Andre Laestadius and Tilmann Bodenstein. 'Guaranteed convergence for a class of coupled-cluster methods based on Arponen's extended theory'. In: *Molecular Physics* 118.19-20 (Oct. 2020), e1810349. ISSN: 0026-8976. DOI: 10.1080/00268976.2020.1810349. URL: https://doi.org/10.1080/00268976.2020.1810349.

[45] Trygve Helgaker and Poul Jørgensen. 'Analytical Calculation of Geometrical Derivatives in Molecular Electronic Structure Theory'. In: *Advances in Quantum Chemistry*. Ed. by Per-Olov Löwdin. Vol. 19. Academic Press, Jan. 1988, pp. 183–245. DOI: 10.1016/S0065-3276(08)60616-4.

[46] Trygve Helgaker and Poul Jørgensen. 'Configuration-interaction energy derivatives in a fully variational formulation'. In: *Theoretica chimica acta* 75.2 (Mar. 1989), pp. 111–127. ISSN: 1432-2234. DOI: 10.1007/BF00527713.

[47] Henrik Koch and Poul Jørgensen. 'Coupled cluster response functions'. In: *The Journal of Chemical Physics* 93.5 (Sept. 1990), pp. 3333–3344. ISSN: 0021-9606. DOI: 10.1063/1.458814.

[48] Henrik Koch, Hans Jørgen Jensen, Poul Jørgensen and Trygve Helgaker. 'Excitation energies from the coupled cluster singles and doubles linear response function (CCSDLR). Applications to Be, CH+, CO, and H2O'. In: *The Journal of Chemical Physics* 93.5 (Sept. 1990), pp. 3345–3350. ISSN: 0021-9606. DOI: 10.1063/1.458815.

[49]   Jeppe Olsen and Poul Jørgensen. 'Linear and nonlinear response functions for an exact state and for an MCSCF state'. In: *The Journal of Chemical Physics* 82.7 (Apr. 1985), pp. 3235–3264. ISSN: 0021-9606. DOI: 10.1063/1.448223.

[50]   Thomas Bondo Pedersen and Henrik Koch. 'Coupled cluster response functions revisited'. In: *The Journal of Chemical Physics* 106.19 (May 1997), pp. 8059–8072. ISSN: 0021-9606. DOI: 10.1063/1.473814.

[51]   C. David Sherrill, Anna I. Krylov, Edward F. C. Byrd and Martin Head-Gordon. 'Energies and analytic gradients for a coupled-cluster doubles model using variational Brueckner orbitals: Application to symmetry breaking in O4+'. In: *The Journal of Chemical Physics* 109.11 (Sept. 1998), pp. 4171–4181. ISSN: 0021-9606. DOI: 10.1063/1.477023.

[52]   Anna I. Krylov, C. David Sherrill, Edward F. C. Byrd and Martin Head-Gordon. 'Size-consistent wave functions for nondynamical correlation energy: The valence active space optimized orbital coupled-cluster doubles model'. In: *The Journal of Chemical Physics* 109.24 (Dec. 1998), pp. 10669–10678. ISSN: 0021-9606. DOI: 10.1063/1.477764.

[53]   Thomas Bondo Pedersen, Henrik Koch and Christof Hättig. 'Gauge invariant coupled cluster response theory'. In: *The Journal of Chemical Physics* 110.17 (May 1999), pp. 8318–8327. ISSN: 0021-9606. DOI: 10.1063/1.478742.

[54]   Thomas Bondo Pedersen, Berta Fernández and Henrik Koch. 'Gauge invariant coupled cluster response theory using optimized nonorthogonal orbitals'. In: *The Journal of Chemical Physics* 114.16 (Apr. 2001), pp. 6983–6993. ISSN: 0021-9606. DOI: 10.1063/1.1358866.

[55]   Andreas Köhn and Jeppe Olsen. 'Orbital-optimized coupled-cluster theory does not reproduce the full configuration-interaction limit'. In: *The Journal of Chemical Physics* 122.8 (Feb. 2005), p. 084116. ISSN: 0021-9606. DOI: 10.1063/1.1850918.

[56]   Rolf H. Myhre. 'Demonstrating that the nonorthogonal orbital optimized coupled cluster model converges to full configuration interaction'. In: *The Journal of Chemical Physics* 148.9 (Mar. 2018), p. 094110. ISSN: 0021-9606. DOI: 10.1063/1.5006160.

[57]   Simen Kvaal. 'Ab initio quantum dynamics using coupled-cluster'. In: *The Journal of Chemical Physics* 136.19 (May 2012), p. 194109. ISSN: 0021-9606. DOI: 10.1063/1.4718427.

[58]   Simen Kvaal. 'Variational formulations of the coupled-cluster method in quantum chemistry'. In: *Molecular Physics* 111.9-11 (July 2013), pp. 1100–1108. ISSN: 0026-8976. DOI: 10.1080/00268976.2013.812254.

[59]   Graham A. Worth Hans-Dieter Meyer Fabien Gatti, ed. *Multidimensional Quantum Dynamics: MCTDH Theory and Applications*. Weinheim: Wiley-VCH, 2009. DOI: 10.1002/9783527627400.

[60] Takeshi Sato, Himadri Pathak, Yuki Orimo and Kenichi L. Ishikawa. 'Communication: Time-dependent optimized coupled-cluster method for multielectron dynamics'. In: *The Journal of Chemical Physics* 148.5 (Feb. 2018), p. 051101. ISSN: 0021-9606. DOI: 10.1063/1.5020633.

[61] Himadri Pathak, Takeshi Sato and Kenichi L. Ishikawa. 'Time-dependent optimized coupled-cluster method for multielectron dynamics. III. A second-order many-body perturbation approximation'. In: *The Journal of Chemical Physics* 153.3 (July 2020), p. 034110. ISSN: 0021-9606. DOI: 10.1063/5.0008789.

[62] Himadri Pathak, Takeshi Sato and Kenichi L. Ishikawa. 'Time-dependent optimized coupled-cluster method for multielectron dynamics. II. A coupled electron-pair approximation'. In: *The Journal of Chemical Physics* 152.12 (Mar. 2020), p. 124115. ISSN: 0021-9606. DOI: 10.1063/1.5143747.

[63] Himadri Pathak, Takeshi Sato and Kenichi L. Ishikawa. 'Time-dependent optimized coupled-cluster method for multielectron dynamics. IV. Approximate consideration of the triple excitation amplitudes'. In: *The Journal of Chemical Physics* 154.23 (June 2021), p. 234104. ISSN: 0021-9606. DOI: 10.1063/5.0054743.

[64] Takeshi Sato, Himadri Pathak, Yuki Orimo and Kenichi L. Ishikawa. 'Time-dependent multiconfiguration self-consistent-field and time-dependent optimized coupled-cluster methods for intense laser-driven multielectron dynamics'. In: *Canadian Journal of Chemistry* (Mar. 2023). ISSN: 0008-4042. DOI: 10.1139/cjc-2022-0297.

[65] Thomas Bondo Pedersen and Simen Kvaal. 'Symplectic integration and physical interpretation of time-dependent coupled-cluster theory'. In: *The Journal of Chemical Physics* 150.14 (Apr. 2019), p. 144106. ISSN: 0021-9606. DOI: 10.1063/1.5085390.

[66] Ernst Hairer, Christian Lubich and Gerhard Wanner. *Geometric numerical integration*. Second. Vol. 31. Springer Series in Computational Mathematics. Springer-Verlag, Berlin, 2006. ISBN: 3-540-30663-3; 978-3-540-30663-4.

[67] Håkon Emil Kristiansen, Øyvind Sigmundson Schøyen, Simen Kvaal and Thomas Bondo Pedersen. 'Numerical stability of time-dependent coupled-cluster methods for many-electron dynamics in intense laser pulses'. In: *The Journal of Chemical Physics* 152.7 (Feb. 2020), p. 071102. ISSN: 0021-9606. DOI: 10.1063/1.5142276.

[68] Aurbakken, E. and Fredly, K. H. and Kristiansen, H. E. and Kvaal, S. and Myhre, R. H. and Ofstad, B. S. and Pedersen, T. B. and Schøyen, Ø. S. and Sutterud, H. and Winther-Larsen, S. G. *HyQD: Hylleraas Quantum Dynamics*. URL: https://github.com/HyQD. 2023-02-04. URL: https://github.com/HyQD.

[69] Thomas Bondo Pedersen, Håkon Emil Kristiansen, Tilmann Bodenstein, Simen Kvaal and Øyvind Sigmundson Schøyen. 'Interpretation of Coupled-Cluster Many-Electron Dynamics in Terms of Stationary States'. In: *Journal of Chemical Theory and Computation* 17.1 (Jan. 2021), pp. 388–404. ISSN: 1549-9618. DOI: 10.1021/acs.jctc.0c00977.

[70] Andreas S. Skeidsvoll, Alice Balbi and Henrik Koch. 'Time-dependent coupled-cluster theory for ultrafast transient-absorption spectroscopy'. In: *Physical Review A* 102.2 (Aug. 2020), p. 023115. DOI: 10.1103/PhysRevA.102.023115. URL: https://link.aps.org/doi/10.1103/PhysRevA.102.023115 (visited on 28/09/2022).

[71] Uğur Bozkaya, Justin M. Turney, Yukio Yamaguchi, Henry F. Schaefer and C. David Sherrill. 'Quadratically convergent algorithm for orbital optimization in the orbital-optimized coupled-cluster doubles method and in orbital-optimized second-order Møller-Plesset perturbation theory'. In: *The Journal of Chemical Physics* 135.10 (Sept. 2011), p. 104103. ISSN: 1089-7690. DOI: 10.1063/1.3631129.

[72] Saul T. Epstein. 'Gauge Invariance of the Hartree-Fock Approximation'. In: *The Journal of Chemical Physics* 42.8 (July 1965), pp. 2897–2898. ISSN: 0021-9606. DOI: 10.1063/1.1703259.

[73] F. London. 'Théorie quantique des courants interatomiques dans les combinaisons aromatiques'. In: *Journal de Physique et le Radium* 8.10 (Oct. 1937), pp. 397–409. ISSN: 0368-3842, 2777-3442. DOI: 10.1051/jphysrad:01937008010039700.

[74] Esper Dalgaard. 'Comments on the use of London's field dependent orbitals'. In: *Chemical Physics Letters* 47.2 (Apr. 1977), pp. 279–282. ISSN: 0009-2614. DOI: 10.1016/0009-2614(77)80017-1.

[75] R. Ditchfield. 'Molecular Orbital Theory of Magnetic Shielding and Magnetic Susceptibility'. In: *The Journal of Chemical Physics* 56.11 (1972), pp. 5688–5691. ISSN: 0021-9606. DOI: 10.1063/1.1677088.

[76] Krzysztof Wolinski, James F. Hinton and Peter Pulay. 'Efficient implementation of the gauge-independent atomic orbital method for NMR chemical shift calculations'. In: *Journal of the American Chemical Society* 112.23 (Nov. 1990), pp. 8251–8260. ISSN: 0002-7863. DOI: 10.1021/ja00179a005.

[77] Trygve Helgaker and Poul Jørgensen. 'An electronic Hamiltonian for origin independent calculations of magnetic properties'. In: *The Journal of Chemical Physics* 95.4 (Aug. 1991), pp. 2595–2601. ISSN: 0021-9606. DOI: 10.1063/1.460912.

[78] Trygve Helgaker, Michał Jaszuński and Kenneth Ruud. 'Ab Initio Methods for the Calculation of NMR Shielding and Indirect Spin-Spin Coupling Constants'. In: *Chemical Reviews* 99.1 (Jan. 1999), pp. 293–352. ISSN: 0009-2665. DOI: 10.1021/cr960017t.

[79]   E. Tellgren, T. Helgaker, A. Soncini, K. K. Lange, A. M. Teale, U. Ekström, S. Stopkowicz, J. H. Austad and S. Sen. *LONDON, a quantum-chemistry program for plane-wave/GTO hybrid basis sets and finite magnetic field calculations.*

[80]   Larry E McMurchie and Ernest R Davidson. 'One- and two-electron integrals over cartesian gaussian functions'. In: *Journal of Computational Physics* 26.2 (Feb. 1978), pp. 218–231. ISSN: 0021-9991. DOI: 10.1016/0021-9991(78)90092-X.

[81]   Erik I. Tellgren and Heike Fliegl. 'Non-perturbative treatment of molecules in linear magnetic fields: calculation of anapole susceptibilities'. In: *The Journal of Chemical Physics* 139.16 (Oct. 2013), p. 164118. ISSN: 1089-7690. DOI: 10.1063/1.4826578.

[82]   Erik I. Tellgren, Simen S. Reine and Trygve Helgaker. 'Analytical GIAO and hybrid-basis integral derivatives: application to geometry optimization of molecules in strong magnetic fields'. In: *Physical Chemistry Chemical Physics* 14.26 (June 2012), pp. 9492–9499. ISSN: 1463-9084. DOI: 10.1039/C2CP40965H.

[83]   Erik I. Tellgren, Alessandro Soncini and Trygve Helgaker. 'Nonperturbative ab initio calculations in strong magnetic fields using London orbitals'. In: *The Journal of Chemical Physics* 129.15 (Oct. 2008), p. 154114. ISSN: 1089-7690. DOI: 10.1063/1.2996525.

[84]   Kai K. Lange, E. I. Tellgren, M. R. Hoffmann and T. Helgaker. 'A Paramagnetic Bonding Mechanism for Diatomics in Strong Magnetic Fields'. In: *Science* 337.6092 (July 2012), pp. 327–331. DOI: 10.1126/science.1219703.

[85]   Erik I. Tellgren, Trygve Helgaker and Alessandro Soncini. 'Non-perturbative magnetic phenomena in closed-shell paramagnetic molecules'. In: *Physical Chemistry Chemical Physics* 11.26 (June 2009), pp. 5489–5498. ISSN: 1463-9084. DOI: 10.1039/B822262B.

[86]   G. Vignale and Mark Rasolt. 'Density-functional theory in strong magnetic fields'. In: *Physical Review Letters* 59.20 (Nov. 1987), pp. 2360–2363. DOI: 10.1103/PhysRevLett.59.2360. (Visited on 09/05/2023).

[87]   G. Vignale and Mark Rasolt. 'Current- and spin-density-functional theory for inhomogeneous electronic systems in strong magnetic fields'. In: *Physical Review B* 37.18 (June 1988), pp. 10685–10696. DOI: 10.1103/PhysRevB.37.10685.

[88]   Erik I. Tellgren, Simen Kvaal, Espen Sagvolden, Ulf Ekström, Andrew M. Teale and Trygve Helgaker. 'Choice of basic variables in current-density-functional theory'. In: *Physical Review A* 86.6 (Dec. 2012), p. 062506. DOI: 10.1103/PhysRevA.86.062506.

[89]   E. I. Tellgren, A. M. Teale, J. W. Furness, K. K. Lange, U. Ekström and T. Helgaker. 'Non-perturbative calculation of molecular magnetic properties within current-density functional theory'. In: *The Journal of Chemical Physics* 140.3 (Jan. 2014), p. 034101. ISSN: 0021-9606. DOI: 10.1063/1.4861427.

[90]   Andrew M. Teale, Ola B. Lutnæs, Trygve Helgaker, David J. Tozer and Jürgen Gauss. 'Benchmarking density-functional theory calculations of NMR shielding constants and spin–rotation constants using accurate coupled-cluster calculations'. In: *The Journal of Chemical Physics* 138.2 (Jan. 2013), p. 024111. ISSN: 0021-9606. DOI: 10.1063/1.4773016. (Visited on 01/07/2023).

[91]   Ola B. Lutnæs, Andrew M. Teale, Trygve Helgaker, David J. Tozer, Kenneth Ruud and Jürgen Gauss. 'Benchmarking density-functional-theory calculations of rotational g tensors and magnetizabilities using accurate coupled-cluster calculations'. In: *The Journal of Chemical Physics* 131.14 (Oct. 2009), p. 144104. ISSN: 0021-9606. DOI: 10.1063/1.3242081.

[92]   Stella Stopkowicz, Jürgen Gauss, Kai K. Lange, Erik I. Tellgren and Trygve Helgaker. 'Coupled-cluster theory for atoms and molecules in strong magnetic fields'. In: *The Journal of Chemical Physics* 143.7 (Aug. 2015), p. 074110. ISSN: 0021-9606. DOI: 10.1063/1.4928056.

[93]   Stella Stopkowicz. 'Perspective: Coupled cluster theory for atoms and molecules in strong magnetic fields'. In: *International Journal of Quantum Chemistry* 118.1 (2018), e25391. ISSN: 1097-461X. DOI: 10.1002/qua.25391.

[94]   Hampe F., Stopkowicz S., Gross N., Kitsaras M.-P., Grazioli L. and Blaschke S. *QCUMBRE, quantum chemical utility en- abling magnetic-field dependent investigations benefitting from rigorous electron-correlation treatment.* 2023.

[95]   Anna I. Krylov. 'Equation-of-motion coupled-cluster methods for open-shell and electronically excited species: the Hitchhiker's guide to Fock space'. In: *Annual Review of Physical Chemistry* 59 (2008), pp. 433–462. ISSN: 0066-426X. DOI: 10.1146/annurev.physchem.59.032607.093602.

[96]   F. Hampe and S. Stopkowicz. 'Equation-of-motion coupled-cluster methods for atoms and molecules in strong magnetic fields'. In: *J. Chem. Phys.* 146 (2017), p. 154105. ISSN: 0021-9606. DOI: 10.1063/1.4979624.

[97]   F. Hampe, N. Gross and S. Stopkowicz. 'Full triples contribution in coupled-cluster and equation-of-motion coupled-cluster methods for atoms and molecules in strong magnetic fields'. In: *Phys. Chem. Chem. Phys.* 22 (2020), pp. 23522–23529. ISSN: 1463-9084. DOI: 10.1039/D0CP04169F.

[98]   Florian Hampe and Stella Stopkowicz. 'Transition-Dipole Moments for Electronic Excitations in Strong Magnetic Fields Using Equation-of-Motion and Linear Response Coupled-Cluster Theory'. In: *Journal of Chemical Theory and Computation* 15.7 (July 2019), pp. 4036–4043. ISSN: 1549-9618. DOI: 10.1021/acs.jctc.9b00242.

[99]   James W. Furness, Joachim Verbeke, Erik I. Tellgren, Stella Stopkowicz, Ulf Ekström, Trygve Helgaker and Andrew M. Teale. 'Current Density Functional Theory Using Meta-Generalized Gradient Exchange-Correlation Functionals'. In: *Journal of Chemical Theory and Computation* 11.9 (Sept. 2015), pp. 4169–4181. ISSN: 1549-9618. DOI: 10.1021/acs.jctc.5b00535.

[100]   Axel D. Becke. 'A new inhomogeneity parameter in density-functional theory'. In: *The Journal of Chemical Physics* 109.6 (Aug. 1998), pp. 2092–2098. ISSN: 0021-9606. DOI: 10.1063/1.476722.

[101]   Jianmin Tao, John P. Perdew, Viktor N. Staroverov and Gustavo E. Scuseria. 'Climbing the Density Functional Ladder: Nonempirical Meta–Generalized Gradient Approximation Designed for Molecules and Solids'. In: *Physical Review Letters* 91.14 (Sept. 2003), p. 146401. DOI: 10.1103/PhysRevLett.91.146401.

[102]   Jianmin Tao. 'Explicit inclusion of paramagnetic current density in the exchange-correlation functionals of current-density functional theory'. In: *Physical Review B* 71.20 (May 2005), p. 205107. DOI: 10.1103/PhysRevB.71.205107.

[103]   J. F. Dobson. 'Alternative expressions for the Fermi hole curvature'. In: *J. Chem. Phys.* 98 (1993), pp. 8870–8872. DOI: 10.1063/1.464444.

[104]   A. D. Becke. 'Current-density dependent exchange-correlation functionals'. In: *Can. J. Chem.* 74 (1996), pp. 995–997. DOI: 10.1139/v96-110.

[105]   J. E. Bates and F. Furche. 'Harnessing the meta-generalized gradient approximation for time-dependent density functional theory'. In: *J. Chem. Phys.* 137 (2012), p. 164105. DOI: 10.1063/1.4759080.

[106]   Viktor N. Staroverov, Gustavo E. Scuseria, Jianmin Tao and John P. Perdew. 'Comparative assessment of a new nonempirical density functional: Molecules and hydrogen-bonded complexes'. In: *The Journal of Chemical Physics* 119.23 (Dec. 2003), pp. 12129–12137. ISSN: 0021-9606, 1089-7690. DOI: 10.1063/1.1626543. (Visited on 17/07/2023).

[107]   Erich Goll, Matthias Ernst, Franzeska Moegle-Hofacker and Hermann Stoll. 'Development and assessment of a short-range meta-GGA functional'. In: *The Journal of Chemical Physics* 130.23 (June 2009), p. 234112. ISSN: 0021-9606. DOI: 10.1063/1.3152221. (Visited on 31/07/2023).

[108]   Tom J. P. Irons, Lucy Spence, Grégoire David, Benjamin T. Speake, Trygve Helgaker and Andrew M. Teale. 'Analyzing Magnetically Induced Currents in Molecular Systems Using Current-Density-Functional Theory'. In: *The Journal of Physical Chemistry A* 124.7 (Feb. 2020), pp. 1321–1333. ISSN: 1089-5639. DOI: 10.1021/acs.jpca.9b10833.

[109]   Tom J. P. Irons, Jan Zemen and Andrew M. Teale. 'Efficient Calculation of Molecular Integrals over London Atomic Orbitals'. In: *Journal of Chemical Theory and Computation* 13.8 (Aug. 2017), pp. 3636–3649. ISSN: 1549-9618. DOI: 10.1021/acs.jctc.7b00540.

[110] Peter M. W. Gill, Martin Head-Gordon and John A. Pople. 'An efficient algorithm for the generation of two-electron repulsion integrals over gaussian basis functions'. In: *International Journal of Quantum Chemistry* 36.S23 (1989), pp. 269–280. ISSN: 1097-461X. DOI: 10.1002/qua.560360831.

[111] Petr Čársky and Martin Polášek. 'Evaluation of Molecular Integrals in a Mixed Gaussian and Plane-Wave Basis by Rys Quadrature'. In: *Journal of Computational Physics* 143.1 (June 1998), pp. 266–277. ISSN: 0021-9991. DOI: 10.1006/jcph.1998.5976.

[112] Tom J. P. Irons, Grégoire David and Andrew M. Teale. 'Optimizing Molecular Geometries in Strong Magnetic Fields'. In: *Journal of Chemical Theory and Computation* 17.4 (Apr. 2021), pp. 2166–2185. ISSN: 1549-9618. DOI: 10.1021/acs.jctc.0c01297.

[113] David B. Williams-Young, Alessio Petrone, Shichao Sun, Torin F. Stetina, Patrick Lestrange, Chad E. Hoyer, Daniel R. Nascimento, Lauren Koulias, Andrew Wildman, Joseph Kasper, Joshua J. Goings, Feizhi Ding, A. Eugene DePrince III, Edward F. Valeev and Xiaosong Li. 'The Chronus Quantum software package'. In: *WIREs Computational Molecular Science* 10.2 (2020), e1436. ISSN: 1759-0884. DOI: 10.1002/wcms.1436.

[114] Shichao Sun, Ryan A. Beck, David Williams-Young and Xiaosong Li. 'Simulating Magnetic Circular Dichroism Spectra with Real-Time Time-Dependent Density Functional Theory in Gauge Including Atomic Orbitals'. In: *Journal of Chemical Theory and Computation* 15.12 (Dec. 2019), pp. 6824–6831. ISSN: 1549-9618. DOI: 10.1021/acs.jctc.9b00632.

[115] Christopher J. Grayce and Robert A. Harris. 'Magnetic-field density-functional theory'. In: *Physical Review A* 50.4 (Oct. 1994), pp. 3089–3095. DOI: 10.1103/PhysRevA.50.3089.

[116] Sarah Reimann, Alex Borgoo, Erik I. Tellgren, Andrew M. Teale and Trygve Helgaker. 'Magnetic-Field Density-Functional Theory (BDFT): Lessons from the Adiabatic Connection'. In: *Journal of Chemical Theory and Computation* 13.9 (Sept. 2017), pp. 4089–4100. ISSN: 1549-9618. DOI: 10.1021/acs.jctc.7b00295.

[117] Sarah Reimann, Alex Borgoo, Jon Austad, Erik I. Tellgren, Andrew M. Teale, Trygve Helgaker and Stella Stopkowicz. 'Kohn-Sham energy decomposition for molecules in a magnetic field'. In: *Molecular Physics* 117.1 (Jan. 2019), pp. 97–109. ISSN: 0026-8976. DOI: 10.1080/00268976.2018.1495849.

[118] M. Wibowo, T. J. P. Irons and A. M. Teale. 'Modeling Ultrafast Electron Dynamics in Strong Magnetic Fields Using Real-Time Time-Dependent Electronic Structure Methods'. In: *J. Chem. Theory Comput.* 17 (2021), pp. 2137–2165. DOI: 10.1021/acs.jctc.0c01269.

[119] Howard D. Cohen and C. C. J. Roothaan. 'Electric Dipole Polarizability of Atoms by the Hartree—Fock Method. I. Theory for Closed-Shell Systems'. In: *The Journal of Chemical Physics* 43.10 (May 1965), S34–S39. ISSN: 0021-9606. DOI: 10.1063/1.1701512.

[120] J. Zyss. 'Hyperpolarizabilities of substituted conjugated molecules. I. Perturbated INDO approach to monosubstituted benzene'. In: *The Journal of Chemical Physics* 70.7 (1979), pp. 3333–3340. ISSN: 0021-9606. DOI: 10.1063/1.437918.

[121] James A. Morrell and A. C. Albrecht. 'Second-order hyperpolarizability of p-nitroaniline calculated from perturbation theory based expression using CNDO/S generated electronic states'. In: *Chemical Physics Letters* 64.1 (1979), pp. 46–50. ISSN: 0009-2614. DOI: 10.1016/0009-2614(79)87272-3.

[122] Salvatore J. Lalama and Anthony F. Garito. 'Origin of the nonlinear second-order optical susceptibilities of organic systems'. In: *Physical Review A* 20.3 (Sept. 1979), pp. 1179–1194. DOI: 10.1103/PhysRevA.20.1179.

[123] G. D. Mahan. 'Modified Sternheimer equation for polarizability'. In: *Physical Review A* 22.5 (Nov. 1980), pp. 1780–1785. DOI: 10.1103/PhysRevA.22.1780.

[124] K. Yabana, T. Nakatsukasa, J. I. Iwata and G. F. Bertsch. 'Real-time, real-space implementation of the linear response time-dependent density-functional theory'. In: *physica status solidi (b)* 243.5 (2006), pp. 1121–1138. ISSN: 1521-3951. DOI: 10.1002/pssb.200642005.

[125] Xavier Andrade, Silvana Botti, Miguel A. L. Marques and Angel Rubio. 'Time-dependent density functional theory scheme for efficient calculations of dynamic (hyper)polarizabilities'. In: *The Journal of Chemical Physics* 126.18 (May 2007), p. 184106. ISSN: 0021-9606. DOI: 10.1063/1.2733666.

[126] K. Yabana and G. F. Bertsch. 'Time-dependent local-density approximation in real time'. In: *Physical Review B* 54.7 (Aug. 1996), pp. 4484–4487. DOI: 10.1103/PhysRevB.54.4484.

[127] K. Yabana and G.F. Bertsch. 'Optical response of small carbon clusters'. In: *Zeitschrift für Physik D Atoms, Molecules and Clusters* 42.3 (Sept. 1997), pp. 219–225. ISSN: 1431-5866. DOI: 10.1007/s004600050357.

[128] K. Yabana and G. F. Bertsch. 'Oscillator strengths with pseudopotentials'. In: *Physical Review A* 58.3 (Sept. 1998), pp. 2604–2607. DOI: 10.1103/PhysRevA.58.2604.

[129] K. Yabana and G. F. Bertsch. 'Time-dependent local-density approximation in real time: Application to conjugated molecules'. In: *International Journal of Quantum Chemistry* 75.1 (1999), pp. 55–66. ISSN: 1097-461X. DOI: 10.1002/(SICI)1097-461X(1999)75:1<55::AID-QUA6>3.0.CO;2-K.

[130] C. Flytzanis. 'Theory of Nonlinear Optical Susceptibilities'. In: *Quantum Electronics*. Ed. by H. Rabin and C.L. Tang. New York: Academic Press, 1975, pp. 9–199.

[131] Argyrios Tsolakidis, Daniel Sánchez-Portal and Richard M. Martin. 'Calculation of the optical response of atomic clusters using time-dependent density functional theory and local orbitals'. In: *Physical Review B* 66.23 (Dec. 2002), p. 235416. DOI: 10.1103/PhysRevB.66.235416.

[132] Fan Wang, Chi Yung Yam and GuanHua Chen. 'Time-dependent density-functional theory/localized density matrix method for dynamic hyperpolarizability'. In: *The Journal of Chemical Physics* 126.24 (2007), p. 244102. ISSN: 0021-9606. DOI: 10.1063/1.2746034.

[133] Y. Takimoto, F. D. Vila and J. J. Rehr. 'Real-time time-dependent density functional theory approach for frequency-dependent nonlinear optical response in photonic molecules'. In: *The Journal of Chemical Physics* 127.15 (2007), p. 154114. ISSN: 0021-9606. DOI: 10.1063/1.2790014.

[134] Y. Takimoto, C. M. Isborn, B. E. Eichinger, J. J. Rehr and B. H. Robinson. 'Frequency and Solvent Dependence of Nonlinear Optical Properties of Molecules'. In: *The Journal of Physical Chemistry C* 112.21 (2008), pp. 8016–8021. ISSN: 1932-7447. DOI: 10.1021/jp800444j.

[135] Feizhi Ding, Benjamin E. Van Kuiken, Bruce E. Eichinger and Xiaosong Li. 'An efficient method for calculating dynamical hyperpolarizabilities using real-time time-dependent density functional theory'. In: *The Journal of Chemical Physics* 138.6 (Feb. 2013), p. 064104. ISSN: 0021-9606, 1089-7690. DOI: 10.1063/1.4790583.

[136] Patrick J. Lestrange, Mark R. Hoffmann and Xiaosong Li. 'Chapter Seventeen - Time-Dependent Configuration Interaction Using the Graphical Unitary Group Approach: Nonlinear Electric Properties'. In: *Advances in Quantum Chemistry*. Ed. by Philip E. Hoggan. Vol. 76. Novel Electronic Structure Theory: General Innovations and Strongly Correlated Systems. Academic Press, Jan. 2018, pp. 295–313. DOI: 10.1016/bs.aiq.2017.06.003.

[137] Lukas Konecny, Marius Kadek, Stanislav Komorovsky, Olga L. Malkina, Kenneth Ruud and Michal Repisky. 'Acceleration of Relativistic Electron Dynamics by Means of X2C Transformation: Application to the Calculation of Nonlinear Optical Properties'. In: *Journal of Chemical Theory and Computation* 12.12 (Dec. 2016), pp. 5823–5833. ISSN: 1549-9618. DOI: 10.1021/acs.jctc.6b00740.

[138] Mitsuharu Uemoto, Yuki Kuwabara, Shunsuke A. Sato and Kazuhiro Yabana. 'Nonlinear polarization evolution using time-dependent density functional theory'. In: *The Journal of Chemical Physics* 150.9 (Mar. 2019), p. 094101. ISSN: 0021-9606, 1089-7690. DOI: 10.1063/1.5068711.

[139] Pascal Krause, Tillmann Klamroth and Peter Saalfrank. 'Molecular response properties from explicitly time-dependent configuration interaction methods'. In: *The Journal of Chemical Physics* 127.3 (2007), p. 034107. ISSN: 0021-9606. DOI: 10.1063/1.2749503.

[140] Vladimir A. Goncharov and Kalman Varga. 'Real-space, real-time calculation of dynamic hyperpolarizabilities'. In: *The Journal of Chemical Physics* 137.9 (Sept. 2012), p. 094111. ISSN: 0021-9606. DOI: 10.1063/1.4749793.

[141] Yu Zhang, Weijie Hua, Kochise Bennett and Shaul Mukamel. 'Nonlinear Spectroscopy of Core and Valence Excitations Using Short X-Ray Pulses: Simulation Challenges'. In: *Density-Functional Methods for Excited States*. Ed. by Nicolas Ferré, Michael Filatov and Miquel Huix-Rotllant. Springer International Publishing, 2016, pp. 273–345. ISBN: 978-3-319-22081-9. DOI: 10.1007/128_2014_618.

[142] Takashi Yatsui, Maiku Yamaguchi and Katsuyuki Nobusada. 'Nano-scale chemical reactions based on non-uniform optical near-fields and their applications'. In: *Progress in Quantum Electronics* 55 (Sept. 2017), pp. 166–194. ISSN: 0079-6727. DOI: 10.1016/j.pquantelec.2017.06.001.

[143] Maiku Yamaguchi and Katsuyuki Nobusada. 'Large Hyperpolarizabilities of the Second Harmonic Generation Induced by Nonuniform Optical Near Fields'. In: *The Journal of Physical Chemistry C* 120.41 (Oct. 2016), pp. 23748–23755. ISSN: 1932-7447. DOI: 10.1021/acs.jpcc.6b08507.

[144] Alberto Baiardi. 'Electron Dynamics with the Time-Dependent Density Matrix Renormalization Group'. In: *Journal of Chemical Theory and Computation* 17.6 (June 2021), pp. 3320–3334. ISSN: 1549-9618. DOI: 10.1021/acs.jctc.0c01048.

[145] Håkon Emil Kristiansen, Benedicte Sverdrup Ofstad, Eirill Hauge, Einar Aurbakken, Øyvind Sigmundsen Schøyen, Simen Kvaal and Thomas Bondo Pedersen. 'Linear and Nonlinear Optical Properties from TDOMP2 Theory'. In: *Journal of Chemical Theory and Computation* 18.6 (June 2022), pp. 3687–3702. ISSN: 1549-9618. DOI: 10.1021/acs.jctc.1c01309.

[146] Davis M. Welakuh and Prineha Narang. 'Tunable Nonlinearity and Efficient Harmonic Generation from a Strongly Coupled Light–Matter System'. In: *ACS Photonics* 10.2 (Feb. 2023), pp. 383–393. DOI: 10.1021/acsphotonics.2c00966.

[147] Øyvind Sigmundson Schøyen. 'Real-time quantum many-body dynamics'. MA thesis. University of Oslo, 2019.

[148] Sebastian Gregorius Winther-Larsen. 'AQUADUCT Ab Initio Quantum Dynamics Using Coupled Cluster in Time'. MA thesis. University of Oslo, 2019.

[149] Halvard Sutterud. 'Many-body methods and basis sets'. MA thesis. University of Oslo, 2020.

[150] Håkon Emil Kristiansen. 'Coupled cluster theory for electron dynamics'. PhD thesis. University of Oslo, 2022.

[151] Ove Christiansen, Henrik Koch and Poul Jørgensen. 'The second-order approximate coupled cluster singles and doubles model CC2'. In: *Chemical Physics Letters* 243.5 (Sept. 1995), pp. 409–418. ISSN: 0009-2614. DOI: 10.1016/0009-2614(95)00841-Q.

[152] Helena Larsen, Jeppe Olsen, Christof Hättig, Poul Jo/rgensen, Ove Christiansen and Jürgen Gauss. 'Polarizabilities and first hyperpolarizabilities of HF, Ne, and BH from full configuration interaction and coupled cluster calculations'. In: *The Journal of Chemical Physics* 111.5 (Aug. 1999), pp. 1917–1925. ISSN: 0021-9606. DOI: 10.1063/1.479460.

[153] Danylo Kats, Tatiana Korona and Martin Schütz. 'Local CC2 electronic excitation energies for large molecules with density fitting'. In: *The Journal of Chemical Physics* 125.10 (Sept. 2006), p. 104106. ISSN: 0021-9606. DOI: 10.1063/1.2339021.

[154] Kestutis Aidas, Celestino Angeli, Keld L. Bak, Vebjørn Bakken, Radovan Bast, Linus Boman, Ove Christiansen, Renzo Cimiraglia, Sonia Coriani, Pål Dahle, Erik K. Dalskov, Ulf Ekström, Thomas Enevoldsen, Janus J. Eriksen, Patrick Ettenhuber, Berta Fernández, Lara Ferrighi, Heike Fliegl, Luca Frediani, Kasper Hald, Asger Halkier, Christof Hättig, Hanne Heiberg, Trygve Helgaker, Alf Christian Hennum, Hinne Hettema, Eirik Hjertenæs, Stinne Høst, Ida-Marie Høyvik, Maria Francesca Iozzi, Branislav Jansík, Hans Jørgen Aa. Jensen, Dan Jonsson, Poul Jørgensen, Joanna Kauczor, Sheela Kirpekar, Thomas Kjærgaard, Wim Klopper, Stefan Knecht, Rika Kobayashi, Henrik Koch, Jacob Kongsted, Andreas Krapp, Kasper Kristensen, Andrea Ligabue, Ola B. Lutnæs, Juan I. Melo, Kurt V. Mikkelsen, Rolf H. Myhre, Christian Neiss, Christian B. Nielsen, Patrick Norman, Jeppe Olsen, Jógvan Magnus H. Olsen, Anders Osted, Martin J. Packer, Filip Pawlowski, Thomas B. Pedersen, Patricio F. Provasi, Simen Reine, Zilvinas Rinkevicius, Torgeir A. Ruden, Kenneth Ruud, Vladimir V. Rybkin, Pawel Sałek, Claire C. M. Samson, Alfredo Sánchez de Merás, Trond Saue, Stephan P. A. Sauer, Bernd Schimmelpfennig, Kristian Sneskov, Arnfinn H. Steindal, Kristian O. Sylvester-Hvid, Peter R. Taylor, Andrew M. Teale, Erik I. Tellgren, David P. Tew, Andreas J. Thorvaldsen, Lea Thøgersen, Olav Vahtras, Mark A. Watson, David J. D. Wilson, Marcin Ziolkowski and Hans Ågren. 'The Dalton quantum chemistry program system'. In: *WIREs Computational Molecular Science* 4.3 (2014), pp. 269–284. ISSN: 1759-0884. DOI: 10.1002/wcms.1172.

[155] M. Faraday. 'I. Experimental researches in electricity.—Nineteenth series'. In: *Philos. Trans. R. Soc. London* 136 (1846), pp. 1–20. DOI: 10.1098/rstl.1846.0001.

[156] E. Verdet. 'Recherches sur les propriétés optiques développées dans les corps transparents par l'action du magnétisme'. In: *Ann. Chim. Phys. 3e Sér.* 41 (1854), pp. 370–412.

[157] E. Verdet. 'Recherches sur les propriétés optiques développées dans les corps transparents par l'action du magnétisme'. In: *Ann. Chim. Phys. 3e Sér.* 43 (1855), pp. 37–44.

[158] R. Serber. 'The Theory of the Faraday Effect in Molecules'. In: *Phys. Rev.* 41 (1932), pp. 489–506. DOI: 10.1103/PhysRev.41.489.

[159]   A. D. Buckingham and P. J. Stephens. 'Magnetic Optical Activity'. In: *Ann. Rev. Phys. Chem.* 17 (1966), pp. 399–432. DOI: 10.1146/annurev.pc.17.100166.002151. URL: https://doi.org/10.1146/annurev.pc.17.100166.002151 (visited on 23/11/2021).

[160]   L. D. Barron. *Molecular Light Scattering and Optical Activity*. 2nd ed. Cambridge: Cambridge University Press, 2004. DOI: 10.1017/CBO9780511535468.

[161]   Sonia Coriani, Christof Hättig, Poul Jørgensen and Trygve Helgaker. 'Gauge-origin independent magneto-optical activity within coupled cluster response theory'. In: *The Journal of Chemical Physics* 113.9 (Sept. 2000), pp. 3561–3572. ISSN: 0021-9606. DOI: 10.1063/1.1287833.

[162]   Lasse Kragh Sørensen, Emil Kieri, Shruti Srivastav, Marcus Lundberg and Roland Lindh. 'Implementation of a semiclassical light-matter interaction using the Gauss-Hermite quadrature: A simple alternative to the multipole expansion'. In: *Physical Review A* 99.1 (Jan. 2019), p. 013419. DOI: 10.1103/PhysRevA.99.013419.

[163]   Björn O. Roos, Roland Lindh, Per-Ake Malmqvist, Valera Veryazov and Per-Olof Widmark. 'New relativistic ANO basis sets for transition metal atoms'. In: *The Journal of Physical Chemistry. A* 109.29 (July 2005), pp. 6575–6579. ISSN: 1089-5639. DOI: 10.1021/jp0581126.

[164]   Young Choon Park, Ajith Perera and Rodney J. Bartlett. 'Equation of motion coupled-cluster study of core excitation spectra II: Beyond the dipole approximation'. eng. In: *The Journal of Chemical Physics* 155.9 (Sept. 2021), p. 094103. ISSN: 1089-7690. DOI: 10.1063/5.0059276.

Bibliography

56

Paper I

Linear and nonlinear optical properties from TDOMP2 theory

Linear and Nonlinear Optical Properties from TDOMP2 Theory

Håkon Emil Kristiansen,* Benedicte Sverdrup Ofstad, Eirill Hauge, Einar Aurbakken,
Øyvind Sigmundson Schøyen, Simen Kvaal, and Thomas Bondo Pedersen*

Read Online

ACCESS | Metrics & More | Article Recommendations | Supporting Information

ABSTRACT: We present a derivation of real-time (RT) time-dependent orbital-optimized Møller−Plesset (TDOMP2) theory and its biorthogonal companion, time-dependent non-orthogonal OMP2 theory, starting from the time-dependent bivariational principle and a parametrization based on the exponential orbital-rotation operator formulation commonly used in the time-independent molecular electronic structure theory. We apply the TDOMP2 method to extract absorption spectra and frequency-dependent polarizabilities and first hyperpolarizabilities from RT simulations, comparing the results with those obtained from conventional time-dependent coupled-cluster singles and doubles (TDCCSD) simulations and from its second-order approximation, TDCC2. We also compare our results with those from CCSD and CC2 linear and quadratic response theories. Our results indicate that while TDOMP2 absorption spectra are of the same quality as TDCC2 spectra, including core excitations where optimized orbitals might be particularly important, frequency-dependent polarizabilities and hyperpolarizabilities from TDOMP2 simulations are significantly closer to TDCCSD results than those from TDCC2 simulations.
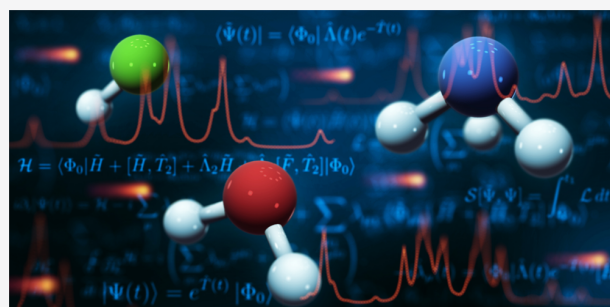
1. INTRODUCTION

The correct semiclassical description of interactions between matter and temporally oscillating electromagnetic fields must start from time-dependent quantum mechanics. Historically, the most often used approach within molecular electronic structure theory has been time-dependent perturbation theory, where the time-dependent Schrödinger equation is solved order by order in the external field strength, leading to a response theory of molecular properties in the frequency domain through the application of a series of Fourier transforms.[1] Response theory has the advantage that it directly addresses the quantities that are used for the interpretation of experimental measurements, such as one- and two-photon transition moments and frequency-dependent electric-dipole polarizabilities and hyperpolarizabilities, which may be expressed in terms of transition energies and stationary-state wave functions that can, at least in principle, be obtained from the time-independent Schrödinger equation for the particle system alone. A major disadvantage is that time resolution is lost when going from the time domain to the frequency domain. The obvious solution would be to skip the Fourier transforms and instead work directly in the time domain. This, however, implies that the time-dependent Schrödinger equation must be solved order by order in a discretized time series, making the approach much too computationally demanding for higher-order properties. Instead, so-called *real-time* (RT) methods have received increasing attention in recent years—see, for example, the review of RT time-dependent electronic structure theory by Li et al.[2]

RT methods approximate the solution of the time-dependent Schrödinger equation without perturbation expansions and, thus, contain information about the response of the atomic or molecular electrons to external electromagnetic fields to all orders in perturbation theory. Even extremely nonlinear processes that are practically out of reach within response theory, such as high harmonic generation and time-resolved one- and many-electron ionization probability amplitudes, are accessible with RT methods, see ref 2 and references therein. Moreover, because RT methods include the field explicitly in the simulation, it becomes possible to investigate the detailed dependence on laser parameters such as intensity, frequency distribution, pulse shape, and delay between pump and probe pulses without making explicit assumptions about the perturbation order of the electronic processes involved.

Although RT methods are usually much simpler to implement than response theory (typically, the same code is needed as for ground-state calculations, only generalized to complex parameters), a major downside of RT methods is the increased computational cost arising from the discretization of time. Thousands or even hundreds of thousands of time steps are
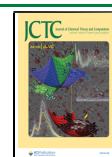
needed, each associated with a cost comparable to one (or a few) iterations of a ground-state optimization with the same (time-independent) method. In addition, the basis set requirements are generally more demanding because, in principle, all the excited states and even continuum states may be involved in the dynamics, and acceleration techniques commonly used for the ground-state and response calculations may not be generally applicable for RT simulations with all possible external electromagnetic fields.

It is no surprise, therefore, that the most widely used RT electronic structure method is RT time-dependent density-functional theory (RT-TDDFT).[2−5] Highly accurate wave function-based RT methods have also been developed, including multiconfigurational time-dependent Hartree−Fock (MCTDHF)[6−9] theory and related complete, restricted, and generalized active space formulations.[10−12] Avoiding the factorial computational scaling caused by the full configuration interaction (FCI) treatment at the heart of these approaches, time-dependent extensions of single-reference coupled-cluster (CC) theory[13] and equation-of-motion CC (EOM-CC) theory[14,15] have been increasingly often used to simulate laser-driven many-electron dynamics in the time domain in recent years.[16−33] The two approaches, time-dependent CC (TDCC) and time-dependent EOM-CC (TD-EOM-CC) theories, differ in their parametrization of the time-dependent left and right wave functions. While TDCC theory propagates the well-known exponential *Ansätze* for the wave functions, TD-EOM-CC theory expresses them as the linear combinations of EOM-CC left and right eigenstates. While both approaches are expected to give similar results (and, indeed, appear to do so, see ref 33) for weak-field processes, only the TDCC theory (albeit with dynamical orbitals) has been successfully applied to strong-field phenomena such as ionization dynamics and high harmonic generation[20] to date.

Although the original formulation of TDCC theory in nuclear physics was based on time-dependent Hartree−Fock (HF) orbitals,[34] conventional TDCC theory is formulated with a static reference determinant, the HF ground state, which is kept fixed during the dynamics in agreement with the conventional formulation of CC response (LRCC) theory.[35,36] The fixed orbital space has some unwanted side effects, however. Gauge invariance is lost in truncated TDCC theory (but recovered in the FCI limit),[37,38] severe numerical challenges arise as the CC ground state is depleted during the dynamics (e.g., in ground-excited state Rabi oscillations),[21,29] and it becomes impossible to reduce the computational effort while maintaining accuracy by splitting the orbital space into active and inactive orbitals for the correlated treatment, as required to efficiently describe ionization dynamics.[17] These deficiencies can, at least partially, be circumvented by allowing the orbitals to move in concert with the electron correlation. In practice, this is done by replacing the single excitations (and de-excitations) of conventional CC theory with full orbital rotations. This, in turn, can be done in two ways. Within orbital-optimized CC (OCC) theory,[37,39,40] the orbitals are required to remain orthonormal, whereas within nonorthogonal OCC (NOCC) theory[17,38] they are only required to be biorthonormal. The orthonormality constraint has an unfortunate side effect in the sense that the OCC theory does not converge to the FCI solution in the limit of full rank cluster operators for three or more electrons, as pointed out by Köhn and Olsen.[41] On the other hand, Myhre[42] recently showed that the NOCC theory may converge to the correct FCI limit for any number of electrons. In practice, however, time-dependent

OCC (TDOCC) theory does not appear to deviate from the FCI limit by any significant amount.[20]

The computational scaling with respect to the size of the basis set and with respect to the number of electrons in TDOCC and time-dependent NOCC (TDNOCC) theory is essentially identical to that of conventional TDCC theory with identical truncation of the cluster operators. The lowest-level truncation, after double excitations, yields the TDOCCD and TDNOCCD methods that both scale as $O(N^6)$, which is significantly more expensive than the formal $O(N^4)$ scaling of RT-TDDFT. In order to bring down the computational cost to a more tractable level, Pathak et al.[26,27] generalized the orbital-optimized second-order Møller−Plesset (OMP2)[43] method to the time domain and demonstrated that the resulting TDOMP2 method provides a reasonably accurate and gauge invariant description of highly nonlinear optical processes.

In this work, we assess the description of linear and quadratic optical properties within the TDOMP2 approximation. First, we review the TDCC theory and its second-order approximation TDCC2. Second, we review TDCC theories with dynamic orbitals—TDNOCC and TDOCC theory—as obtained from the time-dependent bivariational principle, and introduce the second-order approximations TDNOMP2 and TDOMP2. Finally, we compute linear (one-photon) absorption spectra and frequency-dependent polarizabilities and first hyperpolarizabilities with the TDOMP2, TDCCSD, and TDCC2 methods and compare them with results from CC2 and CCSD linear and quadratic response theory.

2. THEORY

2.1. Notation. We consider a system of N interacting electrons described by the second-quantized Hamiltonian

$$
\begin{aligned}
\hat{H} &= \sum_{pq} h_q^p \hat{a}_p^\dagger \hat{a}_q + \frac{1}{2} \sum_{pqrs} u_{rs}^{pq} \hat{a}_p^\dagger \hat{a}_q^\dagger \hat{a}_s \hat{a}_r \\
&= \sum_{pq} h_q^p \hat{a}_p^\dagger \hat{a}_q + \frac{1}{4} \sum_{pqrs} v_{rs}^{pq} \hat{a}_p^\dagger \hat{a}_q^\dagger \hat{a}_s \hat{a}_r
\end{aligned}
\tag{1}
$$

where $\hat{a}_p^\dagger$ ($\hat{a}_p$) are creation (annihilation) operators associated with a finite set of L orthonormal spin orbitals $\{\phi_p\}_{p=1}^L$. The one- and two-body matrix elements h_q^p and u_{rs}^{pq}, respectively, are defined as

$$
h_q^p = \langle \phi_p | \hat{h} | \phi_q \rangle = \int \phi_p^*(\mathbf{x}_1) \hat{h}(1) \phi_q(\mathbf{x}_1) d\mathbf{x}_1
\tag{2}
$$

$$
\begin{aligned}
u_{rs}^{pq} &= \langle \phi_p \phi_q | \hat{u} | \phi_r \phi_s \rangle \\
&= \iint \phi_p^*(\mathbf{x}_1) \phi_q^*(\mathbf{x}_2) \hat{u}(1,2) \phi_r(\mathbf{x}_1) \phi_s(\mathbf{x}_2) d\mathbf{x}_1 d\mathbf{x}_2
\end{aligned}
\tag{3}
$$

where $\mathbf{x}_i = (\mathbf{r}_i, \sigma_i)$ refers to the combined spatial-spin coordinate of electron i. The anti-symmetrized two-body matrix elements v_{rs}^{pq} are given by

$$
v_{rs}^{pq} = u_{rs}^{pq} - u_{sr}^{pq}
\tag{4}
$$

2.2. TDCC2 Approximation. The TDCC *Ansätze* for the left and right CC wave functions are defined by

$$
|\Psi(t)\rangle = e^{\hat{T}(t)} |\Phi_0\rangle, \qquad \langle \tilde{\Psi}(t)| = \langle \Phi_0 | \hat{\Lambda}(t) e^{-\hat{T}(t)}
\tag{5}
$$

where $|\Phi_0\rangle$ is a reference determinant built from orthonormal spin orbitals, typically taken as the HF ground-state determinant. The chosen reference determinant splits the orbital set into

occupied orbitals denoted by subscripts i, j, k, l and virtual orbitals denoted by subscripts a, b, c, d. Subscripts p, q, r, s are used to denote general orbitals. The cluster operators $T(t)$ and $\hat{\Lambda}(t)$ are given by

$$\hat{T}(t) = \sum_{\mu} \tau^{\mu}(t) \hat{X}_{\mu} = \hat{T}_0 + \hat{T}_1 + \hat{T}_2 + \hat{T}_3 + \dots + \hat{T}_N \tag{6}$$

$$\hat{\Lambda}(t) = \sum_{\mu} \lambda_{\mu}(t) \hat{Y}^{\mu} = \hat{\Lambda}_0 + \hat{\Lambda}_1 + \hat{\Lambda}_2 + \hat{\Lambda}_3 + \dots + \hat{\Lambda}_N \tag{7}$$

where μ denotes the excitations of rank 0, 1, 2, 3, ..., N, and the excitation and de-excitation operators $\hat{X}_{\mu}$ and $\hat{Y}^{\mu}$, respectively, are defined by

$$\hat{X}_0 \equiv 1, \qquad \hat{X}_{\mu} |\Phi_0\rangle \equiv |\Phi_{\mu}\rangle \tag{8}$$

$$\hat{Y}^0 \equiv 1, \qquad \langle\Phi_0|\hat{Y}^{\mu} \equiv \langle\tilde{\Phi}_{\mu}| \tag{9}$$

such that $\langle\tilde{\Phi}_{\mu}|\Phi_{\nu}\rangle = \delta_{\mu\nu}$. The rank-0 cluster operators are included to describe the phase and (intermediate) normalization of the CC state.[21]

The equations of motion for the wave function parameters are obtained from the bivariational action functional used by Arponen[44]

$$\mathcal{S}[\tilde{\Psi}, \Psi] = \int_{t_0}^{t_1} \mathcal{L}\, \mathrm{d}t \tag{10}$$

where the CC Lagrangian is given by

$$\mathcal{L} = \langle\tilde{\Psi}(t)|\hat{H}(t) - \mathrm{i}\partial_t|\Psi(t)\rangle = \mathcal{H} - \mathrm{i}\sum_{\mu} \lambda_{\mu} \dot{\tau}^{\mu} \tag{11}$$

and the Hamilton function $\mathcal{H}$ is given by

$$\mathcal{H} = \langle\tilde{\Psi}(t)|\hat{H}(t)|\Psi(t)\rangle \tag{12}$$

The requirement that $\mathcal{S}[\tilde{\Psi}, \Psi]$ be stationary with respect to variations of the complex parameters $z_{\mu} \in \{\tau^{\mu}, \lambda_{\mu}\}$ leads to the Euler–Lagrange equations

$$\frac{\partial\mathcal{L}}{\partial z_{\mu}} = \frac{\mathrm{d}}{\mathrm{d}t}\frac{\partial\mathcal{L}}{\partial\dot{z}_{\mu}} \tag{13}$$

Taking the required derivatives yields the equations of motion for the amplitudes,

$$\mathrm{i}\dot{\tau}^{\mu}(t) = \langle\Phi_0|\hat{Y}^{\mu} \mathrm{e}^{-\hat{T}(t)} \hat{H}(t) \mathrm{e}^{\hat{T}(t)}|\Phi_0\rangle \tag{14}$$

$$-\mathrm{i}\dot{\lambda}_{\mu}(t) = \langle\Phi_0|\hat{\Lambda}(t) \mathrm{e}^{-\hat{T}(t)}[\hat{H}(t), \hat{X}_{\mu}] \mathrm{e}^{\hat{T}(t)}|\Phi_0\rangle \tag{15}$$

Note that $\lambda_0(t)$ is a constant, which we choose such that the intermediate normalization condition $\langle\tilde{\Psi}(t)|\Psi(t)\rangle = 1$ is satisfied, whereas the phase amplitude τ_0 generally depends nontrivially on time.[21] The phase amplitude may, however, be ignored as long as we are only interested in the time evolution of expectation values.[35] For other quantities, such as the autocorrelation of the CC state[21] or certain stationary-state populations,[30] the phase amplitude is needed. In the present work, we will only consider expectation values.

Truncation of the cluster operators after single and double excitations defines the TDCCSD method, which has an asymptotic scaling of $O(N^6)$. Defined as a second-order approximation to the TDCCSD method within many-body perturbation theory, the TDCC2 method[45] reduces the

asymptotic scaling to $O(N^5)$. In order to derive the TDCC2 equations, we partition the time-dependent Hamiltonian

$$\hat{H}(t) = \hat{H}^{(0)}(t) + \hat{U} \tag{16}$$

into a zeroth-order term, $\hat{H}^{(0)}(t) = \hat{f} + \hat{V}(t)$, where $\hat{f}$ is the Fock operator, and

$$\hat{V}(t) = \sum_{pq} (V)_q^p(t) \hat{a}_p^{\dagger} \hat{a}_q \tag{17}$$

is a time-dependent one-electron operator representing the interaction with an external field. The first-order term (the fluctuation potential) is defined as,

$$\hat{U} = \hat{H}(t) - \hat{f} - \hat{V}(t) \tag{18}$$

In the many-body perturbation analysis of the TDCCSD equations, the singles and doubles amplitudes are considered zeroth-order and first-order quantities, respectively. For notational convenience, the time dependence of the amplitudes and operators will be understood implicitly in the following.

The equations of motion are obtained by making the action given by eq 10 stationary with respect to variations of the amplitudes. The TDCC2 Lagrangian is obtained from the TDCCSD Lagrangian by retaining terms up to quadratic in the doubles amplitudes and the fluctuation potential

$$\mathcal{L} = \mathcal{H} - \mathrm{i}\left(\sum_{\mu_1} \lambda_{\mu_1} \dot{\tau}^{\mu_1} + \sum_{\mu_2} \lambda_{\mu_2} \dot{\tau}^{\mu_2}\right) \tag{19}$$

Introducing $\hat{T}_1$-transformed operators as

$$\tilde{\Omega} = \mathrm{e}^{-\hat{T}_1} \hat{\Omega} \mathrm{e}^{\hat{T}_1} \tag{20}$$

the TDCC2 approximation to the TDCCSD Hamilton function becomes

$$\mathcal{H} = \langle\Phi_0|\mathrm{e}^{-\hat{T}_2}\tilde{H}\mathrm{e}^{\hat{T}_2}|\Phi_0\rangle + \sum_{\mu_1} \lambda_{\mu_1}\langle\tilde{\Phi}_{\mu_1}|\tilde{H} + [\tilde{H}, \hat{T}_2]|\Phi_0\rangle$$
$$+ \sum_{\mu_2} \lambda_{\mu_2}\langle\tilde{\Phi}_{\mu_2}|[\hat{f} + \tilde{V}, \hat{T}_2] + \tilde{U}|\Phi_0\rangle \tag{21}$$

Note that the Fock operator appearing in the commutator in the last term is *not* $\hat{T}_1$ transformed. The Euler–Lagrange equations then yield equations of motion for the singles amplitudes

$$\mathrm{i}\dot{\lambda}_a^i = (f_1)_a^i + \sum_b (f_1)_b^a \lambda_b^i - \sum_j (f_1)_j^i \lambda_a^j + \sum_{bj} \lambda_b^j \tilde{v}_{aj}^{ib}$$
$$+ \frac{1}{2}\sum_c \lambda_{bc}^{ij}\tilde{v}_{aj}^{bc} - \frac{1}{2}\sum_k \lambda_{ab}^{jk}\tilde{v}_{jk}^{ib}$$
$$+ \sum_{ck}\left(\lambda_b^j \tau_{jk}^{bc}\tilde{v}_{ac}^{ik} - \frac{1}{2}\lambda_b^i \tau_{jk}^{bc}\tilde{v}_{ac}^{jk} - \frac{1}{2}\lambda_a^j \tau_{jk}^{bc}\tilde{v}_{bc}^{ik}\right) \tag{22}$$

$$\mathrm{i}\dot{\tau}_i^a = (f_1)_i^a + \sum_{jb} (f_1)_b^j \tau_{ji}^{ba} + \frac{1}{2}\sum_{jbc} \tau_{ik}^{bc}\tilde{v}_{bc}^{aj} + \frac{1}{2}\sum_{jkc} \tau_{jk}^{ac}\tilde{v}_{bi}^{jk} \tag{23}$$

and for the doubles amplitudes,

$$\mathrm{i}\dot{\tau}_{ij}^{ab} = \tilde{v}_{ab}^{ij} + P(ab)\sum_c (f_2)_c^a \tau_{ij}^{cb} + P(ij)\sum_k (f_2)_j^k \tau_{ki}^{ab} \tag{24}$$

$$i\dot{\lambda}_{ab}^{ij} = \tilde{v}_{ab}^{ij} + \hat{P}(ab)\hat{P}(ij)(f_1)_a^i \lambda_b^j - \sum_c (\hat{P}(ab)(f_2)_a^c \lambda_{bc}^{ij}$$

$$+ \hat{P}(ij)\lambda_c^i \tilde{v}_{ab}^{jc}) + \sum_k (\hat{P}(ij)(f_2)_k^i \lambda_{ab}^{jk} + \hat{P}(ab)\lambda_a^k \tilde{v}_{bk}^{ij})$$

(25)

Here, we have defined the fully and partially T_1-transformed Fock matrices

$$(f_1)_q^p \equiv \tilde{f}_q^p + (\tilde{V})_q^p, \qquad (f_2)_q^p \equiv f_q^p + (\tilde{V})_q^p$$

(26)

and the operator $\hat{P}(pq)$ is an anti-symmetrizer defined by its action on the elements of an arbitrary tensor M: $\hat{P}(pq)M_{pq} = M_{pq} - M_{qp}$.

The presence of the untransformed Fock operator in eq 21 has a number of simplifying consequences. For example, the ground-state doubles amplitudes become explicit functions of the singles amplitudes, and the double excitation block of the EOM-CC Hamiltonian matrix (the CC Jacobian) becomes diagonal. In TDCC2 theory, however, it implies that the doubles amplitudes are not fully adjusted to the approximate orbital relaxation captured by the (zeroth-order) singles amplitudes. In order to test the consequences of this, we have implemented the TDCC2-b method of Kats et al.,[46] where the fully T_1-transformed Fock operator is used in eq 21.

2.3. Review of Time-dependent Coupled-Cluster Theories with Dynamic Orbitals.
The TDOCC and TDNOCC *Ansätze* replace the singles amplitudes of conventional TDCC theory with unitary and non-unitary orbital rotations, respectively. For both types of orbital rotations, the left and right CC wave functions can be written on the form

$$|\Psi(t)\rangle = e^{\hat{\kappa}(t)}e^{\hat{T}(t)}|\Phi_0\rangle, \qquad \langle\tilde{\Psi}(t)| = \langle\Phi_0|\hat{\Lambda}(t)e^{-\hat{T}(t)}e^{-\hat{\kappa}(t)}$$

(27)

where $|\Phi_0\rangle$ is a static reference determinant built from orthonormal spin orbitals, typically taken as the HF ground-state determinant in analogy with conventional TDCC theory. The terminology of occupied and virtual orbitals thus refers to this reference determinant, although both subsets are changed by the time-dependent orbital rotations. Excluding singles amplitudes, the cluster operators $\hat{T}(t)$ and $\hat{\Lambda}(t)$ are given by

$$\hat{T}(t) = \sum_\mu \tau^\mu(t)\hat{X}_\mu = \hat{T}_0 + \hat{T}_2 + \hat{T}_3 + \ldots + \hat{T}_N$$

(28)

$$\hat{\Lambda}(t) = \sum_\mu \lambda_\mu(t)\hat{Y}^\mu = \hat{\Lambda}_0 + \hat{\Lambda}_2 + \hat{\Lambda}_3 + \ldots + \hat{\Lambda}_N$$

(29)

where μ denotes excitations of ranks 0, 2, 3, ..., N, and the excitation and de-excitation operators $\hat{X}_\mu$ and $\hat{Y}^\mu$ are defined the same way as in conventional TDCC theory [eqs 8 and 9], respectively. The exclusion of singles amplitudes is rigorously justified, as they become redundant when the orbitals are properly relaxed by the orbital-rotation operator $\exp(\hat{\kappa})$.[17,37,38]

In TDNOCC theory, the orbital rotations are non-unitary, that is, $\hat{\kappa}^\dagger \neq -\hat{\kappa}$. If $\hat{\kappa}$ is restricted to be anti-Hermitian, we obtain TDOCC theory where the orbital rotations are unitary. However, this leads to the parametrization formally not converging to the FCI limit (for $N > 2$), as pointed out by Köhn and Olsen.[41] On the other hand, Myhre[42] showed that the proper FCI limit may be restored by non-unitary orbital rotations. Furthermore, it can be shown that occupied−occupied and virtual−virtual rotations are redundant,[17,37] and that it is sufficient to consider $\hat{\kappa}(t)$ on the form

$$\hat{\kappa}(t) = \sum_{ai} (\kappa_i^a(t)\hat{X}_i^a + \kappa_a^i(t)\hat{Y}_a^i)$$

(30)

Using the Baker−Campbell−Hausdorff expansion, one can show that the similarity transforms of the creation and annihilation operators with $\exp(\hat{\kappa})$ are given by

$$e^{-\hat{\kappa}(t)}\hat{a}_p^\dagger e^{\hat{\kappa}(t)} = \sum_q \hat{a}_q^\dagger [e^{-\kappa(t)}]_p^q$$

(31)

$$e^{-\hat{\kappa}(t)}\hat{a}_p e^{\hat{\kappa}(t)} = \sum_q \hat{a}_q [e^{\kappa(t)}]_q^p$$

(32)

Recalling that explicit time dependence only appears in the interaction operator and in the wave function parameters, we will suppress the dependence on time in the notation. For a general one- and two-body operator $\hat{\Omega}$, the TDNOCC and TDOCC expectation value functionals can be written as

$$\langle\tilde{\Psi}(t)|\hat{\Omega}|\Psi(t)\rangle = \sum_{pq} \tilde{\Omega}_q^p \gamma_p^q + \frac{1}{4}\sum_{pqrs} \tilde{\Omega}_{rs}^{pq} \Gamma_{pq}^{rs}$$

(33)

where

$$\tilde{\Omega}_q^p = \sum_{rs} [e^{-\kappa}]_r^p \Omega_s^r [e^\kappa]_q^s$$

(34)

$$\tilde{\Omega}_{rs}^{pq} = \sum_{tuvw} [e^{-\kappa}]_t^p [e^{-\kappa}]_u^q \Omega_{vw}^{tu} [e^\kappa]_r^v [e^\kappa]_s^w$$

(35)

and γ, Γ are the effective one- and two-body density matrices, respectively, given by

$$\gamma_p^q = \langle\Phi_0|\hat{\Lambda}(t)e^{-\hat{T}(t)}\hat{a}_p^\dagger \hat{a}_q e^{\hat{T}(t)}|\Phi_0\rangle$$

(36)

$$\Gamma_{pq}^{rs} = \langle\Phi_0|\hat{\Lambda}(t)e^{-\hat{T}(t)}\hat{a}_p^\dagger \hat{a}_q^\dagger \hat{a}_s \hat{a}_r e^{\hat{T}(t)}|\Phi_0\rangle$$

(37)

The equations of motion for the wave function parameters are, again, obtained from the Euler−Lagrange eq 13 for the full parameter set $z_\mu \in \{\tau^\mu, \lambda_\mu, \kappa_i^a, \kappa_a^i\}$ with the Lagrangian given by

$$\mathcal{L} = \langle\tilde{\Psi}|\hat{H} - i\partial_t|\Psi\rangle = \mathcal{H} - i\langle\tilde{\Psi}|\hat{Q}_1|\Psi\rangle - i\sum_\mu \lambda_\mu \dot{\tau}^\mu$$

(38)

where the Hamiltonian is given by eq 1. Here, the interaction with the external field (17) is absorbed into the one-body part of the Hamiltonian such that

$$h_q^p \leftarrow h_q^p + (V)_q^p(t)$$

(39)

The operator $\hat{Q}_1$ is defined as

$$\hat{Q}_1 \equiv \frac{\partial e^{\hat{\kappa}}}{\partial t} e^{-\hat{\kappa}}$$

(40)

and $\mathcal{H} = \langle\tilde{\Psi}|\hat{H}(t)|\Psi\rangle$.

The detailed derivation of the equations of motion is greatly simplified by absorbing the orbital rotation in the Hamiltonian at each point in time, $\hat{H} \leftarrow \exp(-\hat{\kappa})\hat{H}\exp(\hat{\kappa})$, which amounts to temporally local updates of the Hamiltonian integrals according to eqs 34 and 35. This allows us to compute the temporally local derivatives of the Lagrangian with respect to the parameters at the point $\hat{\kappa} = 0$, such that, for example, the rather complicated operator $\hat{Q}_1$ becomes the much simpler operator $\dot{\hat{\kappa}}$. We thus find that the equations of motion for the cluster amplitudes are given by

$$i\dot{\tau}^\mu = \langle \Phi_0 | \hat{Y}^\mu e^{-\hat{T}} (\hat{H} - i\hat{\kappa}) e^{\hat{T}} | \Phi_0 \rangle \tag{41}$$

$$-i\dot{\lambda}_\mu = \langle \Phi_0 | \hat{\Lambda} e^{-\hat{T}} [(\hat{H} - i\hat{\kappa}), \hat{X}_\mu] e^{\hat{T}} | \Phi_0 \rangle \tag{42}$$

where the right-hand sides are essentially identical to the usual amplitude equations of CC theory, with additional terms arising from the one-body operator $\hat{\kappa}$. As in conventional TDCC theory, λ_0 is constant and may be chosen such that intermediate normalization is preserved.[21] In the same manner, we may derive the equations of motion for the orbital-rotation parameters as

$$i \sum_{bj} \dot{\kappa}_b^j A_{aj}^{ib} = R_a^i \tag{43}$$

$$-i \sum_{bj} \dot{\kappa}_j^b A_{bi}^{ja} = R_i^a \tag{44}$$

where the right-hand sides are given by eqs 30a and 30b in ref 17, and

$$A_{aj}^{ib} = \langle \tilde{\Psi} | [\hat{a}_j^\dagger \hat{a}_b, \hat{a}_a^\dagger \hat{a}_i] | \Psi \rangle = \delta_a^b \gamma_j^i - \delta_j^i \gamma_a^b \tag{45}$$

Equations 43 and 44 are linear systems of algebraic equations that require the matrix $A = [A_{aj}^{ib}]$ to be nonsingular in order to have a unique solution. We remark that this matrix becomes singular whenever an eigenvalue of the occupied density block is equal to an eigenvalue of the virtual density block. Although this would prevent straightforward integration of the orbital equations of motion, we have not encountered the singularity in actual simulations thus far.

The abovementioned derivation does not require unitary orbital rotations and is, therefore, applicable to TDNOCC theory. Specialization to TDOCC theory is most conveniently done by starting from the inherently real action functional[20,37]

$$\mathcal{S} = \Re \int_{t_0}^{t_1} \mathcal{L} \, dt = \int_{t_0}^{t_1} \frac{1}{2} (\mathcal{L} + \mathcal{L}^*) dt \tag{46}$$

which is required to be stationary with respect to variations of all the parameters. The expression for the Lagrangian $\mathcal{L}$ is identical to eq 38 with $\hat{\kappa}$ anti-Hermitian. The Euler–Lagrange equations then take the form

$$0 = \frac{1}{2} \left(\frac{\partial \mathcal{L}}{\partial z_\mu} - \frac{d}{dt} \frac{\partial \mathcal{L}}{\partial \dot{z}_\mu} \right) + \frac{1}{2} \left(\frac{\partial \mathcal{L}}{\partial z_\mu^*} - \frac{d}{dt} \frac{\partial \mathcal{L}}{\partial \dot{z}_\mu^*} \right)^* \tag{47}$$

for $z_\mu \in \{ \kappa_a^i, \lambda_\mu, \tau^\mu \}$. The derivatives of $\mathcal{L}$ with respect to the complex-conjugated parameters vanish for the amplitudes λ_μ and τ^μ and, therefore, the resulting equations of motion for the amplitudes are identical to eqs 41 and 42.

Taking the derivative of $\mathcal{L}$ with respect to κ_i^a and using eqs 43–45, we obtain the equations of motion for the orbital-rotation parameters

$$i \sum_{bj} \dot{\kappa}_b^j B_{aj}^{ib} = \sum_p h_a^p D_p^i - \sum_q h_q^i D_a^q$$
$$+ \frac{1}{2} \left(\sum_{pqr} v_{ra}^{pq} P_{pq}^{ri} - \sum_{qrs} v_{rs}^{iq} P_{aq}^{rs} \right) + i\dot{D}_a^i \tag{48}$$

where we have defined the hermitized one- and two-body density matrices

$$D_q^p = \frac{1}{2} (\gamma_q^p + \gamma_p^{q*}) \tag{49}$$

$$P_{rs}^{pq} = \frac{1}{2} (\Gamma_{rs}^{pq} + \Gamma_{pq}^{rs*}) \tag{50}$$

and the matrix

$$B_{aj}^{ib} = \delta_a^b D_j^i - \delta_j^i D_a^b \tag{51}$$

Here, too, we face a potential singularity that we have never encountered in practical simulations thus far.

2.4. TDOMP2 Theory. In the spirit of the TDCC2 approximation to TDCCSD theory, we may introduce second-order approximations to TDNOCCD and TDOCCD theories, which we will designate TDNOMP2 and TDOMP2 theories, respectively, in accordance with the naming convention used in time-independent theory.[43] The TDOMP2[26,27] method has previously been formulated as a second-order approximation to the TDOCCD method[20,37] by Pathak et al.[26,27] The definition of perturbation order is analogous to that of the TDCC2 approximation to the TDCCSD method,[45] as outlined above. Thus, the Hamiltonian is split into a zeroth-order term, $\hat{H}^{(0)}(t) = \hat{f} + \hat{V}(t)$, and a first-order term, the fluctuation potential $\hat{U} = \hat{H}(t) - \hat{f} - \hat{V}(t)$ such that the HF reference determinant is the ground state of the zeroth-order Hamiltonian for $\hat{V}(t) \to 0$. The doubles amplitudes enter at the first-order level, whereas the orbital-rotation parameters are considered zeroth order in analogy with the singles amplitudes of TDCC2 theory.[45]

We start by considering non-unitary orbital rotations and introduce the $\hat{\kappa}$-transformed operators

$$\tilde{\Omega} = e^{-\hat{\kappa}} \hat{\Omega} e^{\hat{\kappa}} \tag{52}$$

The TDNOMP2 Lagrangian is defined by truncating the cluster operators at the doubles level and retaining terms up to quadratic in (λ, τ, u) in the TDNOCC Lagrangian 38

$$\mathcal{L} = \mathcal{H} - i \sum_{abij} \lambda_{ab}^{ij} \dot{\tau}_{ij}^{ab} - i \langle \Phi_0 | (1 + \hat{\Lambda}_2)(\tilde{Q}_1 + [\tilde{Q}_1, \hat{T}_2]) | \Phi_0 \rangle \tag{53}$$

The TDNOMP2 Hamilton function $\mathcal{H}$ becomes

$$\mathcal{H} = \langle \Phi_0 | \tilde{H} + [\tilde{H}, \hat{T}_2] + \hat{\Lambda}_2 \tilde{H} + \hat{\Lambda}_2 [\tilde{F}, \hat{T}_2] | \Phi_0 \rangle$$
$$= \sum_{pq} \tilde{h}_q^p \gamma_p^q + \frac{1}{4} \sum_{pqrs} \tilde{v}_{rs}^{pq} \Gamma_{pq}^{rs} \tag{54}$$

where $\tilde{h}_q^p, \tilde{v}_{rs}^{pq}$ are matrix elements transformed according to eqs 34 and 35. The operator $\tilde{F}$ is given by

$$\tilde{F} = \sum_{pq} \tilde{f}_q^p \hat{a}_p^\dagger \hat{a}_q \tag{55}$$

where

$$\tilde{f}_q^p = \langle \Phi_0 | [\hat{a}_q^\dagger, [\hat{a}_p, \tilde{H}]]_+ | \Phi_0 \rangle = \tilde{h}_q^p + \sum_j \tilde{v}_{qj}^{pj} \tag{56}$$

The non-zero matrix elements of the TDNOMP2 one- and two-body density matrices γ, Γ are given by

$$\gamma_i^j = \delta_i^j + (\gamma_c)_i^j, \quad (\gamma_c)_i^j = -\frac{1}{2} \sum_k \lambda_{ab}^{jk} \tau_{ik}^{ab}, \quad \gamma_a^b = \frac{1}{2} \sum_c \lambda_{ac}^{ij} \tau_{ij}^{bc} \tag{57}$$

$$\Gamma_{ij}^{kl} = \delta_i^k \delta_j^l - \delta_j^k \delta_i^l + \hat{P}(kl)\hat{P}(ij)\delta_i^k (\gamma_c)_j^l \tag{58}$$

$$\Gamma_{ij}^{ab} = \tau_{ij}^{ab}, \quad \Gamma_{ab}^{ij} = \lambda_{ab}^{ij} \tag{59}$$

$$\Gamma_{ak}^{bj} = -\Gamma_{ak}^{jb} = -\Gamma_{ka}^{bj} = \Gamma_{ka}^{jb} = \delta_k^j \gamma_a^b \tag{60}$$

The equations of motion now follow from the Euler−Lagrange equations, with the Lagrangian given by eq 53. Taking the required derivatives and the $\hat{\kappa} \to 0$ limit we find the equations of motion for the amplitudes

$$i\dot{\tau}_{ij}^{ab} = v_{ij}^{ab} - \hat{P}(ij) \sum_k f_j^k \tau_{ik}^{ab} + \hat{P}(ab) \sum_c f_c^a \tau_{ij}^{cb} \tag{61}$$

$$-i\dot{\lambda}_{ab}^{ij} = v_{ab}^{ij} - \hat{P}(ij) \sum_k f_k^i \lambda_{ab}^{kj} + \hat{P}(ab) \sum_c f_a^c \lambda_{cb}^{ij} \tag{62}$$

The time dependence of the orbital-rotation parameters in the $\hat{\kappa} \to 0$ limit takes the same form as eqs 43 and 44, with density matrices given by eqs 57−60. The explicit insertion of non-zero matrix elements yields

$$i\sum_{bj} \dot{\kappa}_b^j A_{aj}^{ib} = \sum_j f_a^j \gamma_j^i - \sum_b f_b^i \gamma_a^b + \sum_{jl} v_{aj}^{il} (\gamma_c)_l^j + \sum_{bc} v_{ac}^{ib} \gamma_b^c$$
$$+ \frac{1}{2} \left(\sum_{jbc} v_{aj}^{bc} \lambda_{bc}^{ij} - \sum_{klc} v_{kl}^{ic} \lambda_{ac}^{kl} \right) \tag{63}$$

$$i\sum_{bj} \dot{\kappa}_j^b A_{ib}^{aj} = \sum_b f_i^b \gamma_b^a - \sum_j f_j^a \gamma_i^j - \sum_{jl} v_{il}^{aj} (\gamma_c)_j^l - \sum_{bc} v_{ib}^{ac} \gamma_c^b$$
$$+ \frac{1}{2} \left(\sum_{klc} v_{ic}^{kl} \tau_{kl}^{ac} - \sum_{jbc} v_{bc}^{aj} \tau_{ij}^{bc} \right) \tag{64}$$

We can now obtain the TDOMP2 equations from the TDNOMP2 equations. The action functional takes the form of eq 46, which $\mathcal{L}$ is equivalent to the expression given by eq 53 with $\hat{\kappa} = -\hat{\kappa}^\dagger$ and the equations of motion are obtained from the Euler-Lagrange eq 47. Because the derivatives of the Lagrangian with respect to the complex-conjugated amplitudes are zero, the equations of motion for the amplitudes are equivalent to eqs 61 and 62. However, because the orbital transformation is orthonormal, h, u, and f are Hermitian, and it follows that the equation for λ_{ab}^{ij} is just the complex conjugate of that for τ_{ij}^{ab} such that

$$\lambda_{ab}^{ij} = \tau_{ij}^{ab*} \tag{65}$$

and, thus, it is sufficient to solve only one of the two sets of amplitude equations. This simplification arises from the unitarity of the orbital rotations and is not obtained within neither TDCC2 nor TDNOMP2 theory. In addition, it follows that the one- and two-body density matrices given by eqs 57−60 are Hermitian, that is,

$$\gamma_q^p = \gamma_p^{q*}, \qquad \Gamma_{rs}^{pq} = \Gamma_{pq}^{rs*} \tag{66}$$

From the Euler-Lagrange equation, we then find that the equation of motion for κ_a^i is given by

$$i\sum_{bj} \dot{\kappa}_b^j A_{aj}^{ib} = \sum_j f_a^j \gamma_j^i - \sum_b f_b^i \gamma_a^b + \sum_{jl} v_{aj}^{il} (\gamma_c)_l^j + \sum_{bc} v_{ac}^{ib} \gamma_b^c$$
$$+ \frac{1}{2} \left(\sum_{jbc} v_{aj}^{bc} (\tau_{ij}^{bc})^* - \sum_{klc} v_{kl}^{ic} (\tau_{kl}^{ac})^* \right) \tag{67}$$

Note that in contrast to the TDOCC equations, there is no need to explicitly hermitize the density matrices, as they are already Hermitian within TDOMP2 theory.

2.5. Optical Properties from RT Simulations.

In order to extract linear and nonlinear optical properties from RT time-dependent simulations, we subject an atom or molecule, initially in its (electronic) ground state, to a time-dependent electric field $E(t)$. The semiclassical interaction operator in the electric-dipole approximation in the length gauge is given by

$$\hat{V}(t) = - \sum_{i \in \{x,y,z\}} \mu_i E_i(t) \tag{68}$$

where μ_i is the ith Cartesian component of the electric dipole moment operator. The shape, frequency, and strength of the electric field determine which properties may be extracted from time-dependent simulations.

Linear (one-photon) absorption spectra can be computed by using a weak electric field impulse to induce transitions from the electronic ground state to all electric-dipole allowed excited states of the system,[47,48] including core excitations and valence excitations. Such an electric field kick is represented by the delta pulse $E(t) = E_{max}\delta(t)$, which we discretize by means of the box function

$$E_i(t) = \begin{cases} E_{max} n_i & 0 \le t < \Delta t \\ 0 & \text{else} \end{cases} \tag{69}$$

where E_{max} is the strength of the field, n_i is the ith Cartesian component of the real unit polarization vector $\vec{n}$, and Δt is the time step of the simulation.

The absorption spectrum is computed from the relationship

$$S(\omega) = \frac{4\pi\omega}{3c} \text{ImTr}[\alpha(\omega)] \tag{70}$$

where the frequency-dependent dipole polarizability tensor $\boldsymbol{\alpha}(\omega)$ is obtained from the Fourier transform of the induced dipole moment

$$\mu_{ij}^{ind}(t) = \mu_{ij}(t) - \mu_i^0 \tag{71}$$

Here, $\mu_{ij}^{ind}(t)$ is the ith component of the induced dipole moment with the field polarized in the direction $j \in \{x, y, z\}$, μ_i^0 is the ith component of the permanent dipole moment, and $\mu_{ij}(t)$ is computed as the trace of the dipole matrix in the orbital basis and the effective one-body density matrix (in the same basis). In practice, we only compute finite signals at discrete points in time, forcing us to use the fast Fourier transform (FFT) algorithm. In order to avoid artifacts arising from the periodicity of the FFT algorithm, we premultiply the dipole signal with the exponential damping factor $\exp(-\gamma t)$

$$\alpha_{ij}(\omega) = \text{FFT}(\mu_{ij}^{ind}(t) e^{-\gamma t}) / E_{max} \tag{72}$$

where $\gamma > 0$ is chosen such that the induced dipole moment vanishes at the end of the simulation. This choice of the damping factor artificially broadens the excited energy levels, producing Lorentzian line shapes in the computed spectra.

Also, dynamic polarizabilities and hyperpolarizabilities can be extracted from RT time-dependent simulations using the method described by Ding et al.[49] Suppose that the system under consideration interacts with a weak, adiabatically switched-on monochromatic electric field

$$E(t) = E_0 \cos(\omega t) \tag{73}$$

64
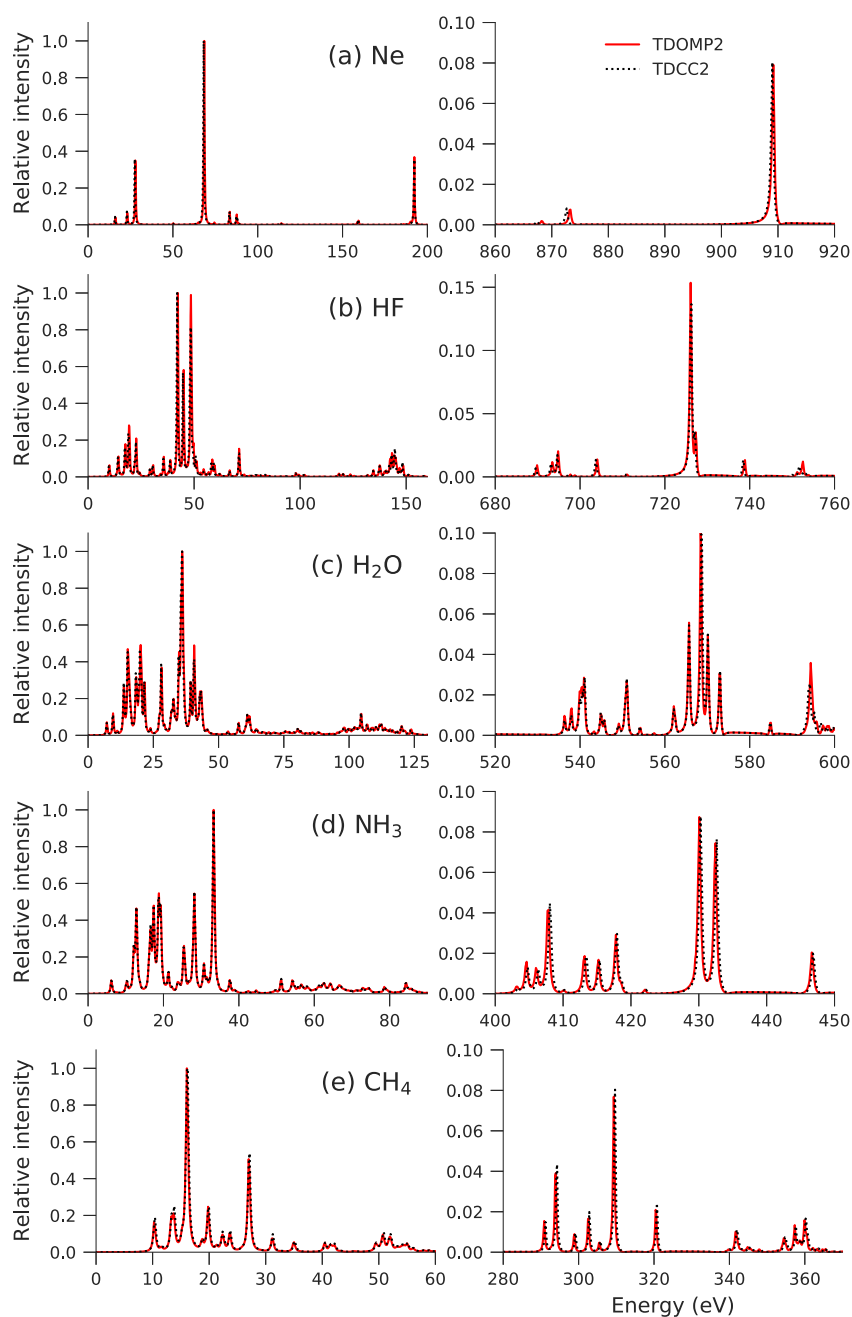
Figure 1. Absorption spectra computed with TDOMP2 and TDCC2 for Ne, HF, H_2O, NH_3, and CH_4.

where ω is the frequency and E_0 is the amplitude of the field. The dipole moment can then be written as a series expansion in the electric field strength,

$$\mu_i(t) = \mu_i^0 + \sum_{j \in \{x,y,z\}} \mu_{ij}^{(1)}(t)E_j + \sum_{j,k \in \{x,y,z\}} \mu_{ijk}^{(2)}(t)E_jE_k$$

$$+ \, ... \tag{74}$$

provided that E_0 is sufficiently small and ω belongs to a transparent spectral region of the system at hand. The time-dependent dipole response functions $\mu_{ij}^{(1)}(t)$ and $\mu_{ijk}^{(2)}(t)$ can be expressed as

$$\mu_{ij}^{(1)}(t) = \alpha_{ij}(-\omega; \omega)\cos(\omega t) \tag{75}$$

$$\mu_{ijk}^{(2)}(t) = \frac{1}{4}[\beta_{ijk}(-2\omega; \omega, \omega)\cos(2\omega t) + \beta_{ijk}(0; \omega, -\omega)] \tag{76}$$

where α_{ij}, β_{ijk} are Cartesian components of the polarizability and first hyperpolarizability tensors, respectively. The "diagonal" elements $\mu_{ij}^{(1)}$, $\mu_{ijj}^{(2)}$ of the dipole response functions can be calculated from the time-dependent signal using the four-point central difference formulas

$$\mu_{ij}^{(1)} \approx \frac{8[\mu_i(t, E_j) - \mu_i(t, -E_j)] - [\mu_i(t, 2E_j) - \mu_i(t, -2E_j)]}{12E_j} \tag{77}$$

Table 1. Dipole-Allowed Excitation Energies (in eV) below 30 eV Extracted from TDOMP2 and TDCC2 Simulations

	TDOMP2	TDCC2		TDOMP2	TDCC2		TDOMP2	TDCC2
H_2O	7.17	7.17	NH_3	6.15	6.15	CH_4	10.25	10.42
	9.56	9.56		7.52	7.69		11.61	11.61
	11.10	11.10		10.25	10.25		13.32	13.49
	13.66	13.66		12.13	12.13		13.66	13.83
	15.20	15.20		12.81	12.81		16.06	16.23
	18.45	18.28		16.57	16.57		18.79	18.79
	20.15	19.81		17.42	17.42		19.81	19.81
	21.69	21.52		18.79	18.79		21.35	21.35
	23.91	23.74		19.30	19.13		22.38	22.38
	27.33	27.33		21.35	21.35		23.57	23.74
	28.18	28.01		22.20	22.20		26.99	27.16
Ne	16.06	15.88		23.91	23.91	HF	10.08	9.91
	23.06	22.89		25.45	25.28		14.35	14.18
	27.84	27.50		26.82	26.82		19.30	18.96
				28.18	28.18		22.72	22.54
				29.21	29.21		24.25	24.08
							29.21	29.04

$$\mu_{ijj}^{(2)} \approx \frac{16[\mu_i(t, E_j) + \mu_i(t, -E_j)] - [\mu_i(t, 2E_j) + \mu_i(t, -2E_j)] - 30\mu_i^0}{24E_j^2}$$

(78)

with $\mu_i(t, E_j)$ being the ith component of the time-dependent dipole moment when a cosine field with a strength of E_j in the $\pm j$th direction is applied. Finally, the polarizabilities and first hyperpolarizabilities are determined by performing a curve fit of the dipole response functions computed with finite differences to the analytical forms given by eqs 75 and 76.

In practice, it is infeasible to adiabatically switch on the electric field. This is circumvented by Ding et al.[49] by turning on the field with a linear ramping envelope lasting for one optical cycle

$$t_c = \frac{2\pi}{\omega}$$

(79)

The electric field is then given by

$$E(t) = \begin{cases} \frac{t}{t_c} E_0 \cos(\omega t) & 0 \leq t < t_c \\ E_0 \cos(\omega t) & t \geq t_c \end{cases}$$

(80)

and the curve fit is performed only on the part of the signal computed after the ramp. Furthermore, Ding et al. suggest a total simulation time of three to four optical cycles after the ramp and that field strengths in the range $E_0 \in [0.0005, 0.005]$a.u. are used.

3. RESULTS AND DISCUSSION

In order to assess optical properties extracted from the RT TDOMP2 method, we compute absorption spectra, polarizabilities, and first hyperpolarizabilities for the 10-electron systems Ne, HF, H_2O, NH_3, and CH_4. To the best of our knowledge, response theory has neither been derived nor implemented for the OMP2 method and, therefore, we compare results from TDOMP2 simulations with those extracted from RT TDCCSD and TDCC2 simulations and with results from CCSD and CC2 response theory (LRCCSD/LRCC2).[35,45] We only compute polarizabilities and hyperpolarizabilities using the TDCC2-b method because Kats et al.[46] found that the effect of

the fully T_1-transformed Fock operator on excitation energies is negligible.

For Ne, we use the d-aug-cc-pVDZ basis set in order to compare with Larsen et al.,[50] while for the remaining molecules, we use the aug-cc-pVDZ basis set.[51−53] Basis set specifications were downloaded from the Basis Set Exchange,[54] and the molecular geometries used are given in the Supporting Information.

The RT simulations and correlated ground-state optimizations are carried out with a locally developed code described in previous publications[21,29,30] using Hamiltonian matrix elements and HF orbitals computed with the PySCF package.[55] The CCSD and CC2 ground states are computed with the direct inversion in the iterative subspace (DIIS)[56] procedure, and the OMP2 ground state with the algorithm described by Bozkaya et al.[43] with the diagonal approximation of the Hessian. The convergence threshold for the residual norms is set to 10^{-10}. The ground-state energies and non-zero permanent dipole moments for the systems considered are given in the Supporting Information. The CCSD and CC2 linear and quadratic response calculations are performed with the Dalton quantum chemistry package.[57,58]

The TDOMP2, TDCCSD, TDCC2, and TDCC2-b equations of motion are integrated using the symplectic Gauss-Legendre integrator.[21,59] For all cases, the integration is performed with a time step $\Delta t = 0.01$ a.u. using the sixth-order ($s = 3$) Gauss−Legendre integrator and a convergence threshold of 10^{-10} (residual norm) for the fixed-point iterations. In all the RT simulations, the ground state is taken as the initial state of the system, and we use a closed-shell spin-restricted implementation of the equations. Also, the response calculations are performed in the closed-shell spin-restricted formulation.

3.1. Absorption Spectra. Absorption spectra are computed as described in Section 2.5 with the electric-field impulse of eq 69. The field strength is $E_0 = 0.001$ a.u., which is small enough to ensure that only transitions from the ground state to dipole-allowed excited states occur, while strong enough to induce numerically significant oscillations. The induced dipole moment is recorded at each of 100 000 time steps after the application of the impulse, yielding a spectral resolution of about 0.006 a.u. (0.163 eV) in the FFT of eq 72. The damping parameter is $\gamma = 0.00921$ a.u. (0.251 eV), which implies that the full width at half

66

Table 2. Polarizabilities (a.u.) of Ne, HF, H_2O, NH_3, and CH_4 Extracted from TDCCSD, TDOMP2, TDCC2, and TDCC2-b Simulations[a]

Ne	ω (a.u.)	0.1	0.2	0.3	0.4	0.5
	LRCCSD	2.74	2.83	3.01	3.38	4.23
	TDCCSD	2.74	2.83	3.03	3.49	4.76
	TDOMP2	2.77	2.87	3.07	3.58	4.99
	LRCC2	2.86	2.96	3.18	3.59	4.74
	TDCC2	2.87	2.98	3.19	3.75	5.29
	TDCC2-b	2.86	2.97	3.18	3.73	5.26

HF	ω (a.u.)	0.1		0.2		0.3	
		α_{yy}	α_{zz}	α_{yy}	α_{zz}	α_{yy}	α_{zz}
	LRCCSD	4.44	6.41	4.83	6.83	6.19	7.73
	TDCCSD	4.45	6.41	4.84	6.83	6.72	7.84
	TDOMP2	4.56	6.49	5.03	6.94	7.71	7.96
	LRCC2	4.70	6.78	5.20	7.25	7.24	8.29
	TDCC2	4.75	6.85	5.28	7.36	8.54	8.45
	TDCC2-b	4.72	6.79	5.24	7.28	8.42	8.36

H_2O	ω (a.u.)	0.0428			0.0656			0.1		
		α_{xx}	α_{yy}	α_{zz}	α_{xx}	α_{yy}	α_{zz}	α_{xx}	α_{yy}	α_{zz}
	LRCCSD	8.78	9.93	9.11	8.89	9.99	9.19	9.18	10.14	9.37
	TDCCSD	8.78	9.93	9.11	8.90	10.00	9.19	9.19	10.14	9.37
	TDOMP2	9.16	10.06	9.34	9.29	10.13	9.42	9.62	10.27	9.63
	LRCC2	9.41	10.43	9.63	9.55	10.50	9.71	9.91	10.66	9.92
	TDCC2	9.51	10.56	9.74	9.65	10.63	9.83	10.01	10.79	10.06
	TDCC2-b	9.44	10.47	9.66	9.58	10.54	9.74	9.94	10.71	9.97

NH_3	ω (a.u.)	0.0428		0.0656		0.1	
		α_{yy}	α_{zz}	α_{yy}	α_{zz}	α_{yy}	α_{zz}
	LRCCSD	13.10	15.04	13.20	15.35	13.44	16.15
	TDCCSD	13.10	15.05	13.20	15.36	13.45	16.15
	TDOMP2	13.23	15.60	13.34	15.98	13.59	16.95
	LRCC2	13.56	15.86	13.67	16.21	13.92	17.15
	TDCC2	13.72	16.03	13.83	16.43	14.10	17.40
	TDCC2-b	13.64	15.93	13.75	16.32	14.01	17.28

CH_4	ω (a.u.)	0.0656	0.1	0.2
	LRCCSD	17.05	17.39	19.55
	TDCCSD	17.05	17.39	19.58
	TDOMP2	17.18	17.53	19.79
	LRCC2	17.49	17.84	20.08
	TDCC2	17.69	18.05	20.34
	TDCC2-b	17.61	17.96	20.25

[a]The LRCCSD and LRCC2 results for Ne and HF are from ref 50., and the remaining LRCCSD and LRCC2 results are computed with the Dalton quantum chemistry program (ref 57.).

maximum of the Lorentzian absorption lines is roughly 50% greater than the spectral resolution. Hence, very close-lying resonances will appear as a single broader absorption line, possibly with "shoulders".

The quality of TDOMP2 absorption spectra can be assessed by comparison with the well-known and highly similar TDCC2 theory (see Supporting Information for a validation of the TDCC2 spectra by comparison with LRCC2 spectra in the range from 0 to 930 eV), the essential difference between the two methods being how orbital relaxation is treated. In general, the LRCC2 theory provides excellent valence excitation energies, often better than those of LRCCSD theory, for states with predominant single-excitation character; see, for example, the benchmark study by Schreiber et al.[60] Preliminary and rather limited tests of excitation energies computed with NOCC theory revealed virtually no effect of the different orbital relaxation treatments[38] and, therefore, one might expect only minor deviations between TDOMP2 and TDCC2 absorption

spectra, at least in the valence regions. For a full comparison of the two methods, we will not limit ourselves to selected valence-excited states but rather compare the complete spectra up to core excitations, which are also activated by the broad-band electric-field impulse. This implies that we also compare unphysical spectral lines above the ionization threshold, which arise artificially from the use of an incomplete basis set that ignores the electronic continuum. Furthermore, we do not use proper core-correlated basis sets for describing core excitations, nor do we make any attempt at properly separating the core excitations from high-lying artificial valence excitations. Hence, no direct comparison with experimental data will be performed in this work. We instead refer to refs 24 and 61, where experimental near-edge X-ray absorption spectra are compared with those computed with a range of LRCC and EOM-CC methods and large basis sets for systems studied in this work. Importantly, the direct comparison of TDCC2 and TDOMP2 absorption spectra will indicate the effects of fully bivariational,
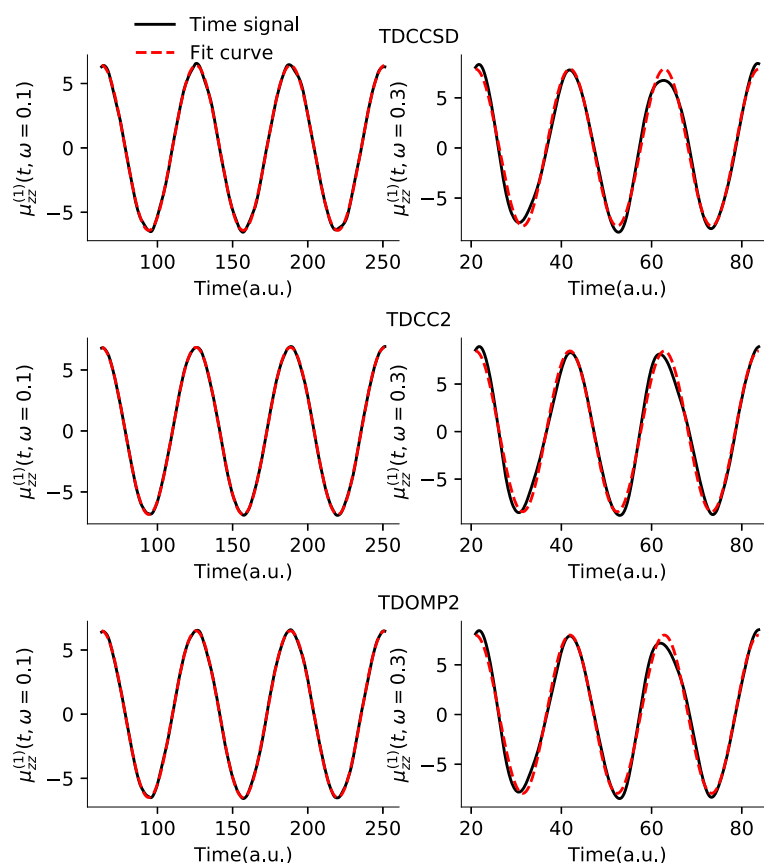
Figure 2. zz-component of the first-order dipole responses for HF at $\omega = 0.1$ a.u. and $\omega = 0.3$ a.u. from TDCCSD, TDCC2, and TDOMP2 simulations.

time-dependent orbitals on core excitations where orbital relaxation is expected to play a key role—see, for example, the discussion by Park et al.[24] for systems also considered in the present work.

In Figure 1 we have plotted the TDOMP2 and TDCC2 electronic absorption spectra up to and including the core region.

Although deviations between the TDOMP2 and TDCC2 spectra are visible, the two methods yield very similar results both in the valence region and in the core region. The excitation energies identified from the simulated spectra by automated peak detection are reported in Table 1 for the dipole-allowed states below 30 eV and confirm the close agreement between TDOMP2 and TDCC2 theories.

The greatest deviations are found for the HF molecule, especially for the intensities. Some intensity deviations are expected, as the TDOMP2 method is gauge invariant (in the complete basis set limit), while the TDCC2 theory is not,[37,38] which is bound to influence transition moments but not necessarily excitation energies. In the core regions, we note that the spectra of H_2O, NH_3, and CH_4 agree qualitatively with the core spectra obtained by Park et al.[24] from the TD-EOM-CCSD theory. Keeping in mind that the large deviations between LRCC2/LRCCSD and experimental core excitation energies are ascribed to missing orbital-relaxation effects, it is intriguing to observe that the fully bivariational orbital evolution included in the TDOMP2 theory hardly affects the core spectra relative to TDCC2 theory. Using automated peak detection, we find that the differences in excitation energies in the core region between the TDOMP2 and TDCC2 spectra are within 1−2 times the

spectral resolution. Because the error of LRCC2 core excitation energies is typically several eV, we conclude that the orbital relaxation provided by TDOMP2 theory is not sufficient to significantly improve the agreement with experimental results. This observation calls for further investigations with larger basis sets, higher resolution (longer simulation times), and full inclusion of double excitations (the TDOCCD and TDNOCCD methods).

3.2. Polarizabilities and First Hyperpolarizabilities. Polarizabilities and first hyperpolarizabilities are computed using an electric field given by eq 80. After the initial one-cycle ramp, we propagate for three optical cycles. The first- and second-order time-dependent dipole response functions are computed by finite differences according to eqs 77 and 78, with the first optical cycle of the time evolution discarded because of the ramping. We then perform least-squares fitting[62] of the time-domain dipole response functions to the form of eqs 75 and 76, obtaining frequency-dependent polarizabilities and hyperpolarizabilities. For all the systems, we use the field strengths $E_0 = \pm 0.0001, \pm 0.0002$ a. u. to compute the dipole derivatives using finite differences.

The diagonal elements of the frequency-dependent polarizability tensor extracted from TDCCSD, TDOMP2, TDCC2, and TDCC2-b simulations for Ne, HF, H_2O, NH_3, and CH_4 are listed in Table 2 along with results from LRCCSD and LRCC2 theories.

All the three diagonal elements are identical by symmetry for Ne and CH_4, $\alpha_{xx} = \alpha_{yy}$ for HF and NH_3, and off-diagonal elements vanish for all the systems considered here. The
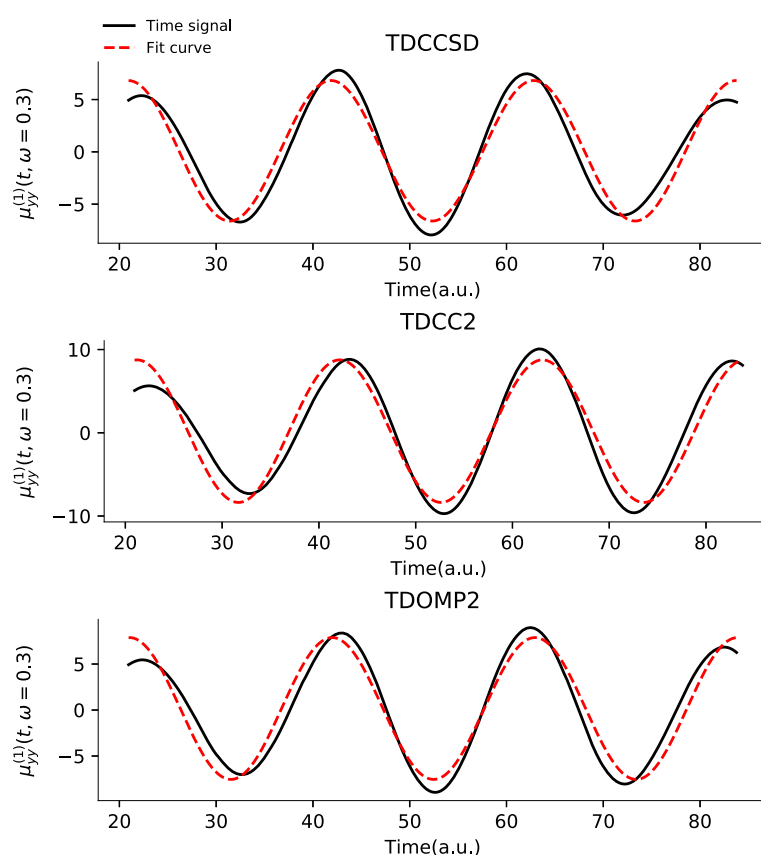
Figure 3. yy-component of the first-order dipole responses for HF at $\omega = 0.3$ a.u. from TDCCSD, TDCC2, and TDOMP2 simulations.

polarizability diverges at the (dipole-allowed) excitation energies and, therefore, we select frequencies below the first dipole-allowed transition in Table 1 (roughly 0.6 a.u. for Ne, 0.4 a.u. for HF, 0.3 a.u. for H_2O, 0.2 a.u. for NH_3, and 0.4 a.u. for CH_4).

The benchmark study by Larsen et al.[50] indicated that the LRCCSD theory yields accurate static and dynamic polarizabilities, although triple excitations are needed to obtain results very close to the FCI theory, whereas results from the LRCC2 theory are significantly less accurate. Our results in Table 2 confirm this finding in the sense that TDCC2 (and LRCC2) results are quite far from the corresponding TDCCSD (and LRCCSD) results. We also note that TDCCSD and LRCCSD results agree to a much greater extent than the results from TDCC2 and LRCC2 theories.

Unfortunately, we have not been able to identify the source of this behavior in the TDCC2 model. The agreement between the results from simulations and from response theory generally worsens as the frequency approaches the lowest-lying dipole-allowed transition. In this "semitransparent" regime, the assumptions of linear response theory are violated and the first-order time-dependent induced dipole moment cannot be described as the simple function in eq 75.

This is confirmed by the plots of simulated time signals and the least-squares fits in Figure 2 where the former clearly can only be accurately described by eq 75 at sufficiently low (transparent) frequencies. The TDCC2 least-squares fits, however, do not appear worse than those of TDCCSD or TDOMP2 theory. Hence, larger deviations from the form in eq

75 cannot explain the discrepancies between TDCC2 and LRCC2 results.

Furthermore, we note the relatively large discrepancy between the LRCCSD and TDCCSD results for the HF molecule at $\omega = 0.3$ a.u. and the Ne atom at $\omega = 0.4$ a.u. and $\omega = 0.5$ a.u. In these cases, the first-order response function extracted from the time-dependent simulations (77) for all the methods considered does not agree with the assumption of a pure cosine wave (75), as shown in Figure 3 for the HF molecule. The source of deviation is a combined effect of proximity to a pole, nonadiabatic effects arising from ramping up the field over a single cycle, and the absence of higher-order corrections in the finite-difference expressions for the response functions.[49] This is also likely to be the source of the irregular behavior of α_{yy} computed with the TDCC2 and TDCC2-b methods.

Interestingly, we observe that polarizabilities from the TDOMP2 theory are generally in better agreement with the TDCCSD values than those from TDCC2 (and LRCC2) theory. This trend is particularly evident from Figure 4 where we have plotted the dispersion of the isotropic polarizability, $\alpha_{\mathrm{iso}} = (\alpha_{xx} + \alpha_{yy} + \alpha_{zz})/3$.

Keeping in mind the similarity between the TDOMP2 and TDCC2 spectra, the pronounced difference between TDOMP2 and TDCC2 polarizabilities is somewhat surprising. It is, however, in agreement with the observation by Larsen et al.[50] that orbital relaxation has a sizeable impact on polarizabilities within CC theory, albeit not always improving the results relative to FCI calculations. Only static polarizabilities were considered by Larsen et al.[50] because the orbital relaxation—formulated as a variational HF constraint within conventional
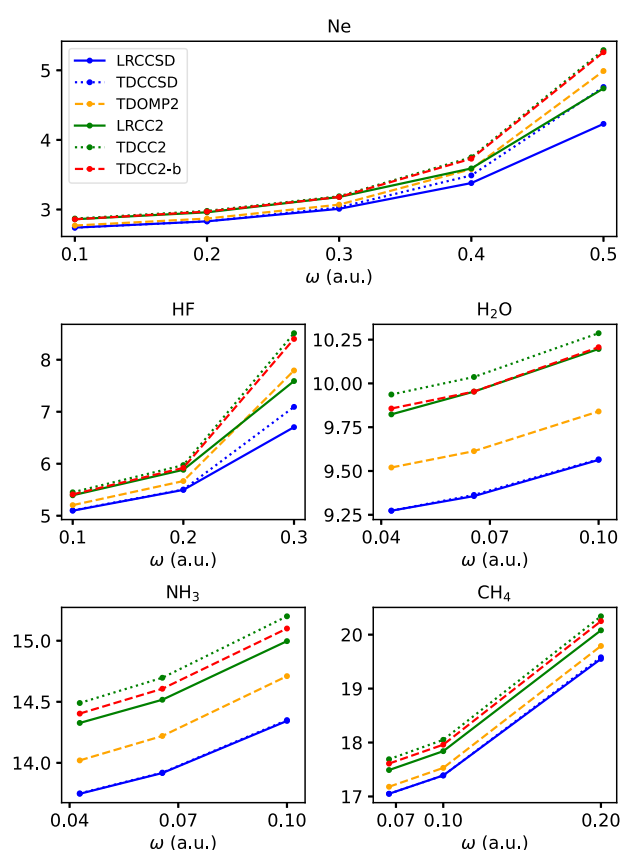
Figure 4. Isotropic polarizabilities extracted from TDCC2, TDCC2-b, TDOMP2, and TDCCSD simulations, and from LRCC2 and LRCCSD calculations.

CC response theory—leads to spurious uncorrelated poles in the response functions, making it useless for dynamic polarizabilities. The orbitals are treated as fully bivariational variables within the TDOMP2 theory and, consequently, spurious poles are avoided.[37] Our results, therefore, seem to indicate that a fully bivariational treatment of orbital relaxation is beneficial for polarizability predictions. The partial orbital relaxation included in the TDCC2-b method does not yield equally good polarizabilities. In most cases, the results are nearly identical to the TDCC2 ones, except for the H_2O and NH_3 molecules, where the TDCC2-b polarizabilities are closer to the LRCC2 results, see Figure 4.

In Table 3 we list frequency-dependent first hyperpolarizabilities for HF, H_2O, and NH_3. Only the nonvanishing diagonal components of the practically most important response tensors corresponding to optical rectification (OR), $\beta_{iii}^{OR} = \beta_{iii}(0, \omega, -\omega)$, and second harmonic generation (SHG), $\beta_{iii}^{SHG} = \beta_{iii}(-2\omega, \omega, \omega)$, are computed. Formally expressible as a double summation over all the excited states, the first hyperpolarizability generally requires a high-level description of electron correlation effects for accurate calculations.[63] This is reflected in our results by the relatively large difference between the TDCC2 and TDCCSD methods.

While β_{iii}^{OR} is singular when the magnitude of the radiation frequency ω equals the excitation energy of the molecule, β_{iii}^{SHG} has an additional set of poles at half the excitation energies. The β_{zzz}^{SHG} results at $\omega = 0.3$ a.u. for the HF molecule in Table 3 are past the first pole and, hence, the sign has changed compared with the SHG results at lower frequencies. The large negative value of β_{zzz}^{SHG} at $\omega = 0.3$ a.u. obtained with the LRCCSD method for the HF molecule is due to proximity to two dipole-allowed, z-polarized excitations at 0.598 a.u. (oscillator strength 0.005) and at 0.532 a.u. (oscillator strength 0.157).

Table 3. First Hyperpolarizabilities (a.u.) of HF, H_2O, and NH_3 from TDCCSD, TDOMP2, TDCC2, and TDCC2-b Simulations[a]

HF	ω (a.u.)	0.1		0.2		0.3	
		β_{zzz}^{OR}	β_{zzz}^{SHG}	β_{zzz}^{OR}	β_{zzz}^{SHG}	β_{zzz}^{OR}	β_{zzz}^{SHG}
	LRCCSD	12.81	14.38	15.28	29.40	21.86	−229.70
	TDCCSD	12.89	14.45	15.63	29.32	25.11	−73.94
	TDOMP2	13.05	14.66	15.21	28.16	24.98	−65.73
	LRCC2	15.52	17.52	18.69	37.67	27.35	−51.78
	TDCC2	16.53	18.63	19.40	36.39	32.11	−61.17
	TDCC2-b	15.32	17.26	17.95	33.56	29.76	−64.95
H_2O	ω (a.u.)	0.0428		0.0656		0.1	
		β_{zzz}^{OR}	β_{zzz}^{SHG}	β_{zzz}^{OR}	β_{zzz}^{SHG}	β_{zzz}^{OR}	β_{zzz}^{SHG}
	LRCCSD	−9.11	−9.59	−9.43	−10.72	−10.25	−14.52
	TDCCSD	−9.14	−9.62	−9.50	−10.78	−10.47	−14.69
	TDOMP2	−9.92	−10.49	−10.33	−11.80	−11.57	−17.63
	LRCC2	−12.39	−13.12	−12.87	−14.83	−14.11	−20.76
	TDCC2	−13.63	−14.42	−14.17	−16.18	−15.75	−23.70
	TDCC2-b	−11.89	−12.58	−12.38	−14.15	−13.84	−21.01

NH$_3$	ω (a.u.)	0.0428				0.0656			
		β_{yyy}^{OR}	β_{yyy}^{SHG}	β_{zzz}^{OR}	β_{zzz}^{SHG}	β_{yyy}^{OR}	β_{yyy}^{SHG}	β_{zzz}^{OR}	β_{zzz}^{SHG}
	LRCCSD	−14.90	−15.50	23.90	28.02	−15.30	−16.88	26.57	40.49
	TDCCSD	−14.94	−15.59	24.20	28.45	−15.47	−17.27	27.35	41.94
	TDOMP2	−15.64	−16.42	30.66	36.26	−15.81	−17.39	35.50	58.38
	LRCC2	−16.69	−17.40	33.80	39.87	−17.16	−19.01	37.72	58.61
	TDCC2	−17.32	−18.13	35.80	41.90	−17.51	−19.17	41.24	66.61
	TDCC2-b	−17.00	−17.79	32.60	38.26	−17.19	−18.81	37.80	61.67

[a]Notation: $\beta_{iii}^{OR} = \beta_{iii}(0; \omega, -\omega)$ and $\beta_{iii}^{SHG} = \beta_{iii}(-2\omega; \omega, \omega)$. The LRCCSD and LRCC2 results for HF are taken from Larsen et al.[50]
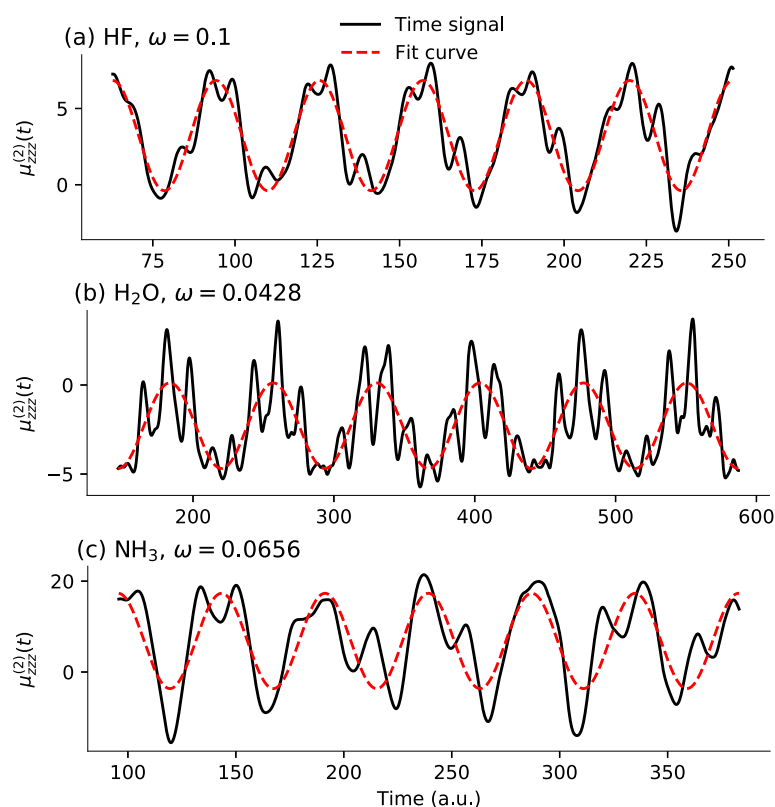
Figure 5. Second-order dipole responses for HF, H_2O, and NH_3 from TDCCSD simulations.

The agreement between RT simulations and response theory is seen to be somewhat worse than for polarizabilities, especially for frequencies closer to the pole of the hyperpolarizability. To a large extent this can be ascribed to the second-order dipole response extracted from the time-dependent simulations not being well described by the sinusoidal form of eq 76, as illustrated in Figure 5.

Analogous observations were done by Ding et al.[49] in the context of RT-TDDFT simulations. Hence, moving on to higher-order nonlinear optical properties cannot generally be expected to provide more than a rough estimate with the present extraction algorithm. As for the polarizabilites mentioned above, we observe that the first hyperpolarizabilities obtained from TDOMP2 simulations are generally closer to TDCCSD and LRCCSD results than those from TDCC2 and LRCC2 theory. The source of the improvement over TDCC2 theory must be the bivariational orbital relaxation, although we stress that the larger differences between TDOMP2 theory and TDCCSD theory, which are particularly pronounced for NH_3, clearly demonstrate the insufficient electron correlation treatment of the former for highly accurate predictions of nonlinear optical properties. The importance of orbital relaxation is corroborated by the TDCC2-b hyperpolarizabilities, which are somewhat closer to the TDOMP2 and TDCCSD results than the TDCC2 ones.

4. CONCLUDING REMARKS

In this work, we have presented a new unified derivation of TDOCC and TDNOCC theories, including the second-order approximations TDOMP2 and TDNOMP2, using exponential orbital-rotation operators and the bivariational Euler−Lagrange

equations. Using five small 10-electron molecules as test cases, we have extracted absorption spectra and frequency-dependent polarizabilities and hyperpolarizabilities from TDOMP2 simulations with weak fields within the electric-dipole approximation and compared the results with those from conventional TDCCSD and TDCC2 simulations. Although the TDOMP2 absorption spectra are almost identical to the TDCC2 spectra, including in the spectral region of core excitations, the TDOMP2 polarizabilities and hyperpolarizabilities are significantly closer to the TDCCSD results than those from TDCC2 simulations, especially for frequencies comfortably away from resonances. Further corroborated by TDCC2-b simulations, our results strongly indicate that fully (bi-)variational orbital relaxation is important for frequency-dependent polarizabilities and hyperpolarizabilities, while nearly irrelevant for absorption spectra.

Combined with the observations by Pathak et al.,[26] who found that TDOMP2 theory outperforms TDCC2 theory for strong-field many-electron dynamics, our results may serve as a motivation for further development of TDOMP2 theory. First of all, a reduced-scaling implementation of TDOMP2 theory, obtained, for example, by exploiting the sparsity of the correlating doubles amplitudes,[64] can provide reasonably accurate results for larger systems and basis sets that are out of reach for today's TDCC implementations. Second, an efficient implementation of OMP2 linear and quadratic response functions is warranted.

■ ASSOCIATED CONTENT

ⓢ Supporting Information

The Supporting Information is available free of charge at https://pubs.acs.org/doi/10.1021/acs.jctc.1c01309.

71

(Supporting information ZIP)

Algebraic expressions for the closed-shell spin-restricted OMP2 method, molecular geometries, electronic ground-state energies and electric-dipole moments, and comparison of TDCC2 absorption spectra with those from the LRCC2 theory in the range 0−930 eV (PDF)

■ AUTHOR INFORMATION

Corresponding Authors

Håkon Emil Kristiansen − *Hylleraas Centre for Quantum Molecular Sciences, Department of Chemistry, University of Oslo, Oslo N-0315, Norway;* ⊙ orcid.org/0000-0001-9884-1024; Email: h.e.kristiansen@kjemi.uio.no

Thomas Bondo Pedersen − *Hylleraas Centre for Quantum Molecular Sciences, Department of Chemistry, University of Oslo, Oslo N-0315, Norway; Centre for Advanced Study at the Norwegian Academy of Science and Letters, Oslo N-0271, Norway;* ⊙ orcid.org/0000-0001-8967-6055; Email: t.b.pedersen@kjemi.uio.no

Authors

Benedicte Sverdrup Ofstad − *Hylleraas Centre for Quantum Molecular Sciences, Department of Chemistry, University of Oslo, Oslo N-0315, Norway*

Eirill Hauge − *Hylleraas Centre for Quantum Molecular Sciences, Department of Chemistry, University of Oslo, Oslo N-0315, Norway; Simula Research Laboratory, Oslo 0164, Norway*

Einar Aurbakken − *Hylleraas Centre for Quantum Molecular Sciences, Department of Chemistry, University of Oslo, Oslo N-0315, Norway*

Øyvind Sigmundson Schøyen − *Department of Physics, University of Oslo, Oslo N-0316, Norway*

Simen Kvaal − *Hylleraas Centre for Quantum Molecular Sciences, Department of Chemistry, University of Oslo, Oslo N-0315, Norway; Centre for Advanced Study at the Norwegian Academy of Science and Letters, Oslo N-0271, Norway;* ⊙ orcid.org/0000-0002-5118-4546

Complete contact information is available at:
https://pubs.acs.org/10.1021/acs.jctc.1c01309

Notes

The authors declare no competing financial interest.

■ REFERENCES

(1) Olsen, J.; Jørgensen, P. Linear and nonlinear response functions for an exact state and for an MCSCF state. *J. Chem. Phys.* **1985**, *82*, 3235−3264.

(2) Li, X.; Govind, N.; Isborn, C.; DePrince, A. E.; Lopata, K. Real-Time Time-Dependent Electronic Structure Theory. *Chem. Rev.* **2020**, *120*, 9951−9993.

(3) Runge, E.; Gross, E. K. U. Density-functional theory for time-dependent systems. *Phys. Rev. Lett.* **1984**, *52*, 997−1000.

(4) van Leeuwen, R. Mapping from densities to potentials in time-dependent density-functional theory. *Phys. Rev. Lett.* **1999**, *82*, 3863−3866.

(5) Ullrich, C. A. *Time-Dependent Density-Functional Theory*; Oxford University Press: Oxford, 2012.

(6) Zanghellini, J.; Kitzler, M.; Fabian, C.; Brabec, T.; Scrinzi, A. An MCTDHF Approach to Multielectron Dynamics in Laser Fields. *Laser Phys.* **2003**, *13*, 1064−1068.

(7) Kato, T.; Kono, H. Time-dependent multiconfiguration theory for electronic dynamics of molecules in an intense laser field. *Chem. Phys. Lett.* **2004**, *392*, 533−540.

(8) *Multidimensional Quantum Dynamics: MCTDH Theory and Applications*; Meyer, H.-D., Gatti, F., Worth, G., Eds.; Wiley: Weinheim, Germany, 2009.

(9) Hochstuhl, D.; Hinz, C. M.; Bonitz, M. Time-dependent multiconfiguration methods for the numerical simulation of photoionization processes of many-electron atoms. *Eur. Phys. J.: Spec. Top.* **2014**, *223*, 177−336.

(10) Sato, T.; Ishikawa, K. L. Time-dependent complete-active-space self-consistent-field method for multielectron dynamics in intense laser fields. *Phys. Rev. A* **2013**, *88*, 023402.

(11) Miyagi, H.; Madsen, L. B. Time-dependent restricted-active-space self-consistent-field theory for laser-driven many-electron dynamics. *Phys. Rev. A* **2013**, *87*, 062511.

(12) Bauch, S.; Sørensen, L. K.; Madsen, L. B. Time-dependent generalized-active-space configuration-interaction approach to photoionization dynamics of atoms and molecules. *Phys. Rev. A* **2014**, *90*, 062508.

(13) Bartlett, R. J.; Musiał, M. Coupled-cluster theory in quantum chemistry. *Rev. Mod. Phys.* **2007**, *79*, 291−352.

(14) Krylov, A. I. Equation-of-Motion Coupled-Cluster Methods for Open-Shell and Electronically Excited Species: The Hitchhiker's Guide to Fock Space. *Annu. Rev. Phys. Chem.* **2008**, *59*, 433−462.

(15) Bartlett, R. J. Coupled-cluster theory and its equation-of-motion extensions. *Wiley Interdiscip. Rev.: Comput. Mol. Sci.* **2012**, *2*, 126−138.

(16) Huber, C.; Klamroth, T. Explicitly time-dependent coupled cluster singles doubles calculations of laser-driven many-electron dynamics. *J. Chem. Phys.* **2011**, *134*, 054113.

(17) Kvaal, S. Ab initio quantum dynamics using coupled-cluster. *J. Chem. Phys.* **2012**, *136*, 194109.

(18) Nascimento, D. R.; DePrince, A. E. Linear Absorption Spectra from Explicitly Time-Dependent Equation-of-Motion Coupled-Cluster Theory. *J. Chem. Theory Comput.* **2016**, *12*, 5834−5840.

(19) Nascimento, D. R.; DePrince, A. E. Simulation of Near-Edge X-ray Absorption Fine Structure with Time-Dependent Equation-of-Motion Coupled-Cluster Theory. *J. Phys. Chem. Lett.* **2017**, *8*, 2951−2957.

(20) Sato, T.; Pathak, H.; Orimo, Y.; Ishikawa, K. L. Communication: Time-dependent optimized coupled-cluster method for multielectron dynamics. *J. Chem. Phys.* **2018**, *148*, 051101.

(21) Pedersen, T. B.; Kvaal, S. Symplectic integration and physical interpretation of time-dependent coupled-cluster theory. *J. Chem. Phys.* **2019**, *150*, 144106.

(22) Nascimento, D. R.; DePrince, A. E. A general time-domain formulation of equation-of-motion coupled-cluster theory for linear spectroscopy. *J. Chem. Phys.* **2019**, *151*, 204107.

(23) Koulias, L. N.; Williams-Young, D. B.; Nascimento, D. R.; Deprince, A. E.; Li, X. Relativistic Real-Time Time-Dependent Equation-of-Motion Coupled-Cluster. *J. Chem. Theory Comput.* **2019**, *15*, 6617−6624.

(24) Park, Y. C.; Perera, A.; Bartlett, R. J. Equation of motion coupled-cluster for core excitation spectra: Two complementary approaches. *J. Chem. Phys.* **2019**, *151*, 164117.

(25) Pathak, H.; Sato, T.; Ishikawa, K. L. Time-dependent optimized coupled-cluster method for multielectron dynamics. II. A coupled electron-pair approximation. *J. Chem. Phys.* **2020**, *152*, 124115.

(26) Pathak, H.; Sato, T.; Ishikawa, K. L. Time-dependent optimized coupled-cluster method for multielectron dynamics. III. A second-order many-body perturbation approximation. *J. Chem. Phys.* **2020**, *153*, 034110.

(27) Pathak, H.; Sato, T.; Ishikawa, K. L. Study of laser-driven multielectron dynamics of Ne atom using time-dependent optimised second-order many-body perturbation theory. *Mol. Phys.* **2020**, *118*, No. e1813910.

(28) Skeidsvoll, A. S.; Balbi, A.; Koch, H. Time-dependent coupled-cluster theory for ultrafast transient-absorption spectroscopy. *Phys. Rev. A* **2020**, *102*, 023115.

(29) Kristiansen, H. E.; Schøyen, Ø. S.; Kvaal, S.; Pedersen, T. B. Numerical stability of time-dependent coupled-cluster methods for many-electron dynamics in intense laser pulses. *J. Chem. Phys.* **2020**, *152*, 071102.

(30) Pedersen, T. B.; Kristiansen, H. E.; Bodenstein, T.; Kvaal, S.; Schøyen, Ø. S. Interpretation of coupled-cluster many-electron dynamics in terms of stationary states. *J. Chem. Theory Comput.* **2021**, *17*, 388−404.

(31) Cooper, B. C.; Koulias, L. N.; Nascimento, D. R.; Li, X.; DePrince, A. E. Short Iterative Lanczos Integration in Time-Dependent Equation-of-Motion Coupled-Cluster Theory. *J. Phys. Chem. A* **2021**, *125*, 5438−5447.

(32) Park, Y. C.; Perera, A.; Bartlett, R. J. Equation of motion coupled-cluster study of core excitation spectra II: Beyond the dipole approximation. *J. Chem. Phys.* **2021**, *155*, 094103.

(33) Skeidsvoll, A. S.; Moitra, T.; Balbi, A.; Paul, A. C.; Coriani, S.; Koch, H. Simulating weak-field attosecond processes with a Lanczos reduced basis approach to time-dependent equation-of-motion coupled-cluster theory. *Phys. Rev. A* **2022**, *105*, 023103.

(34) Hoodbhoy, P.; Negele, J. W. Time-dependent coupled-cluster approximation to nuclear dynamics. I. Application to a solvable model. *Phys. Rev. C* **1978**, *18*, 2380−2394.

(35) Koch, H.; Jørgensen, P. Coupled cluster response functions. *J. Chem. Phys.* **1990**, *93*, 3333−3344.

(36) Pedersen, T. B.; Koch, H. Coupled cluster response functions revisited. *J. Chem. Phys.* **1997**, *106*, 8059−8072.

(37) Pedersen, T. B.; Koch, H.; Hättig, C. Gauge invariant coupled cluster response theory. *J. Chem. Phys.* **1999**, *110*, 8318−8327.

(38) Pedersen, T. B.; Fernández, B.; Koch, H. Gauge invariant coupled cluster response theory using optimized nonorthogonal orbitals. *J. Chem. Phys.* **2001**, *114*, 6983−6993.

(39) Sherrill, C. D.; Krylov, A. I.; Byrd, E. F. C.; Head-Gordon, M. Energies and analytic gradients for a coupled-cluster doubles model using variational Brueckner orbitals: Application to symmetry breaking in O_4^+. *J. Chem. Phys.* **1998**, *109*, 4171−4181.

(40) Krylov, A. I.; Sherrill, C. D.; Byrd, E. F. C.; Head-Gordon, M. Size-consistent wave functions for nondynamical correlation energy: The valence active space optimized orbital coupled-cluster doubles model. *J. Chem. Phys.* **1998**, *109*, 10669−10678.

(41) Köhn, A.; Olsen, J. Orbital-optimized coupled-cluster theory does not reproduce the full configuration-interaction limit. *J. Chem. Phys.* **2005**, *122*, 084116.

(42) Myhre, R. H. Demonstrating that the nonorthogonal orbital optimized coupled cluster model converges to full configuration interaction. *J. Chem. Phys.* **2018**, *148*, 094110.

(43) Bozkaya, U.; Turney, J. M.; Yamaguchi, Y.; Schaefer, H. F.; Sherrill, C. D. Quadratically convergent algorithm for orbital optimization in the orbital-optimized coupled-cluster doubles method and in orbital-optimized second-order Møller-Plesset perturbation theory. *J. Chem. Phys.* **2011**, *135*, 104103.

(44) Arponen, J. Variational principles and linked-cluster exp S expansions for static and dynamic many-body problems. *Ann. Phys.* **1983**, *151*, 311−382.

(45) Christiansen, O.; Koch, H.; Jørgensen, P. The second-order approximate coupled cluster singles and doubles model CC2. *Chem. Phys. Lett.* **1995**, *243*, 409−418.

(46) Kats, D.; Korona, T.; Schütz, M. Local CC2 electronic excitation energies for large molecules with density fitting. *J. Chem. Phys.* **2006**, *125*, 104106.

(47) Repisky, M.; Konecny, L.; Kadek, M.; Komorovsky, S.; Malkin, O. L.; Malkin, V. G.; Ruud, K. Excitation Energies from Real-Time Propagation of the Four-Component Dirac-Kohn-Sham Equation. *J. Chem. Theory Comput.* **2015**, *11*, 980−991.

(48) Goings, J. J.; Li, X. An atomic orbital based real-time time-dependent density functional theory for computing electronic circular dichroism band spectra. *J. Chem. Phys.* **2016**, *144*, 234102.

(49) Ding, F.; Van Kuiken, B. E.; Eichinger, B. E.; Li, X. An efficient method for calculating dynamical hyperpolarizabilities using real-time time-dependent density functional theory. *J. Chem. Phys.* **2013**, *138*, 064104.

(50) Larsen, H.; Olsen, J.; Hättig, C.; Jørgensen, P.; Christiansen, O.; Gauss, J. Polarizabilities and first hyperpolarizabilities of HF, Ne, and BH from full configuration interaction and coupled cluster calculations. *J. Chem. Phys.* **1999**, *111*, 1917−1925.

(51) Dunning, T. H., Jr. Gaussian basis sets for use in correlated molecular calculations. I. The atoms boron through neon and hydrogen. *J. Chem. Phys.* **1989**, *90*, 1007−1023.

(52) Kendall, R. A.; Dunning, T. H., Jr.; Harrison, R. J. Electron affinities of the first-row atoms revisited. Systematic basis sets and wave functions. *J. Chem. Phys.* **1992**, *96*, 6796−6806.

(53) Woon, D. E.; Dunning, T. H., Jr. Gaussian basis sets for use in correlated molecular calculations. IV. Calculation of static electrical response properties. *J. Chem. Phys.* **1994**, *100*, 2975−2988.

(54) Pritchard, B. P.; Altarawy, D.; Didier, B.; Gibson, T. D.; Windus, T. L. New Basis Set Exchange: An Open, Up-to-Date Resource for the Molecular Sciences Community. *J. Chem. Inf. Model.* **2019**, *59*, 4814−4820.

(55) Sun, Q.; Berkelbach, T. C.; Blunt, N. S.; Booth, G. H.; Guo, S.; Li, Z.; Liu, J.; McClain, J. D.; Sayfutyarova, E. R.; Sharma, S.; Wouters, S.; Chan, G. K. L. PySCF: the Python-based simulations of chemistry framework. *Wiley Interdiscip. Rev.: Comput. Mol. Sci.* **2018**, *8*, No. e1340.

(56) Helgaker, T.; Jørgensen, P.; Olsen, J. *Molecular Electronic-Structure Theory*; John Wiley & Sons, 2014.

(57) Aidas, K.; Angeli, C.; Bak, K. L.; Bakken, V.; Bast, R.; Boman, L.; Christiansen, O.; Cimiraglia, R.; Coriani, S.; Dahle, P.; Dalskov, E. K.; Ekström, U.; Enevoldsen, T.; Eriksen, J. J.; Ettenhuber, P.; Fernández, B.; Ferrighi, L.; Fliegl, H.; Frediani, L.; Hald, K.; Halkier, A.; Hättig, C.; Heiberg, H.; Helgaker, T.; Hennum, A. C.; Hettema, H.; Hjertenaes, E.; Høst, S.; Høyvik, I.-M.; Iozzi, M. F.; Jansík, B.; Jensen, H. J. A.; Jonsson, D.; Jørgensen, P.; Kauczor, J.; Kirpekar, S.; Kjaergaard, T.; Klopper, W.; Knecht, S.; Kobayashi, R.; Koch, H.; Kongsted, J.; Krapp, A.; Kristensen, K.; Ligabue, A.; Lutnaes, O. B.; Melo, J. I.; Mikkelsen, K. V.; Myhre, R. H.; Neiss, C.; Nielsen, C. B.; Norman, P.; Olsen, J.; Olsen, J. M. H.; Osted, A.; Packer, M. J.; Pawlowski, F.; Pedersen, T. B.; Provasi, P. F.; Reine, S.; Rinkevicius, Z.; Ruden, T. A.; Ruud, K.; Rybkin, V. V.; Sałek, P.; Samson, C. C. M.; de Merás, A. S.; Saue, T.; Sauer, S. P. A.; Schimmelpfennig, B.; Sneskov, K.; Steindal, A. H.; Sylvester-Hvid, K. O.; Taylor, P. R.; Teale, A. M.; Tellgren, E. I.; Tew, D. P.; Thorvaldsen, A. J.; Thøgersen, L.; Vahtras, O.; Watson, M. A.; Wilson, D. J. D.; Ziolkowski, M.; Ågren, H. The Dalton quantum chemistry program system. *Wiley Interdiscip. Rev.: Comput. Mol. Sci.* **2014**, *4*, 269−284.

(58) Olsen, J. M. H.; Reine, S.; Vahtras, O.; Kjellgren, E.; Reinholdt, P.; Hjorth Dundas, K. O.; Li, X.; Cukras, J.; Ringholm, M.; Hedegård, E. D.; Di Remigio, R.; List, N. H.; Faber, R.; Cabral Tenorio, B. N.; Bast, R.; Pedersen, T. B.; Rinkevicius, Z.; Sauer, S. P. A.; Mikkelsen, K. V.; Kongsted, J.; Coriani, S.; Ruud, K.; Helgaker, T.; Jensen, H. J. A.; Norman, P. Dalton Project: A Python platform for molecular- and

73

electronic-structure simulations of complex systems. *J. Chem. Phys.* **2020**, *152*, 214115.

(59) Hairer, E.; Lubich, C.; Wanner, G. *Geometric Numerical Integration*, 2nd ed.; Springer: Berlin, 2006.

(60) Schreiber, M.; Silva-Junior, M. R.; Sauer, S. P. A.; Thiel, W. Benchmarks for electronically excited states: CASPT2, CC2, CCSD, and CC3. *J. Chem. Phys.* **2008**, *128*, 134110.

(61) Coriani, S.; Christiansen, O.; Fransson, T.; Norman, P. Coupled-cluster response theory for near-edge x-ray-absorption fine structure of atoms and molecules. *Phys. Rev. A* **2012**, *85*, 022507.

(62) Hastie, T.; Tibshirani, R.; Friedman, J. *The Elements of Statistical Learning: Data Mining, Inference, and Prediction*; Springer: New York, NY, 2009; pp 43−99.

(63) Christiansen, O.; Coriani, S.; Gauss, J.; Hättig, C.; Jørgensen, P.; Pawłowski, F.; Rizzo, A. In *Non-Linear Optical Properties of Matter: From Molecules to Condensed Phases*; Papadopoulos, M. G., Sadlej, A. J., Leszczynski, J., Eds.; Springer Netherlands: Dordrecht, 2006; Chapter 2, pp 51−99.

(64) Crawford, T. D.; Kumar, A.; Bazanté, A. P.; Remigio, R. D. Reduced-scaling coupled cluster response theory: Challenges and opportunities. *Wiley Interdiscip. Rev.: Comput. Mol. Sci.* **2019**, *9*, No. e1406.

74

Correction to "Linear and Nonlinear Optical Properties from TDOMP2 Theory"

Håkon Emil Kristiansen,* Benedicte Sverdrup Ofstad, Eirill Hauge, Einar Aurbakken,
Øyvind Sigmundson Schøyen, Simen Kvaal, and Thomas Bondo Pedersen*

Cite This: *J. Chem. Theory Comput.* 2022, 18, 5755−5757

Read Online

ACCESS | Metrics & More | Article Recommendations

An error has been discovered in the equations of motion (EOMs) for the λ_a^i amplitudes of the TDCC2 method, eq 22. The contributions arising from the term

$$\sum_{\mu_2} \lambda_{\mu_2} \langle \Phi_{\mu_2} | [[\tilde{V}, \hat{X}_i^a], \hat{T}_2] | \Phi_0 \rangle$$
$$= -\frac{1}{2} \sum_{jkbc} (\tilde{V}_b^i \lambda_{ac}^{jk} \tau_{jk}^{bc} + \tilde{V}_a^j \lambda_{bc}^{ik} \tau_{jk}^{bc}) \tag{1}$$

of the TDCC2 Hamilton function, eq 21, were erroneously left out. Including these contributions, eq 22 becomes

$$i\dot{\lambda}_a^i = (f_1)_a^i + \sum_b (f_1)_a^b \lambda_b^i - \sum_j (f_1)_j^i \lambda_a^j + \sum_{bj} \lambda_b^j \tilde{v}_{aj}^{ib}$$
$$+ \frac{1}{2} \sum_{bjc} \lambda_{bc}^{ij} \tilde{v}_{aj}^{bc} - \frac{1}{2} \sum_{bjk} \lambda_{ab}^{jk} \tilde{v}_{jk}^{ib}$$
$$+ \sum_{ck} \left(\lambda_b^j \tau_{jk}^{bc} \tilde{v}_{ac}^{ik} - \frac{1}{2} \lambda_b^i \tau_{jk}^{bc} \tilde{v}_{ac}^{jk} - \frac{1}{2} \lambda_a^j \tau_{jk}^{bc} \tilde{v}_{bc}^{ik} \right)$$
$$- \frac{1}{2} \sum_{jkbc} (\tilde{V}_b^i \lambda_{ac}^{jk} \tau_{jk}^{bc} + \tilde{V}_a^j \lambda_{bc}^{ik} \tau_{jk}^{bc}) \tag{2}$$

The missing contributions were also left out in the implementation of the TDCC2 and TDCC2-b methods. We have added the missing contributions to the implementation, which has been verified by comparing expectation values of the electric-dipole operator at nonzero electric-field strengths with those obtained by numerical differentiation (second-order central difference) of total energies. Note that energy derivatives at *nonzero* field strengths are required to detect the error.

The peak positions in the absorption spectra (i.e., the excitation energies) are unaffected by the error since the EOMs for the τ amplitudes are unchanged. The relative intensities deviate from the original results by at most 0.0015, typically much less, for all molecules studied. Errors of this magnitude are not visible in plotted spectra. The maximum error occurs for the water molecule as shown in Figure 1. Hence, the reported TDCC2 and TDCC2-b spectra are practically unaffected.
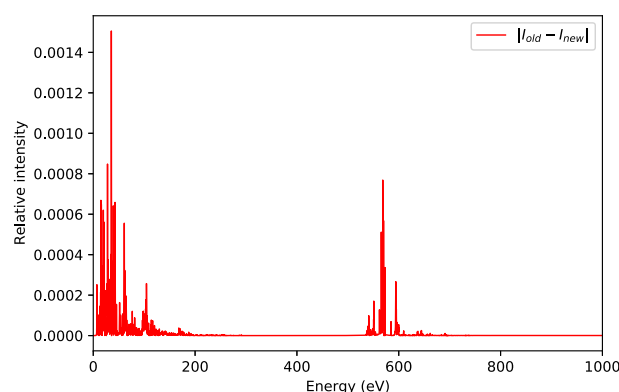
Figure 1. Absolute difference of the TDCC2 absorption spectra of the water molecule before ("old") and after ("new") correcting the EOMs for the λ_a^i amplitudes.

On the other hand, the computed values of the polarizabilities and first hyperpolarizabilities change. In Table 1 and Table 2 we report updated values for the polarizabilities and first hyperpolarizabilities, respectively. We note that the TDCC2 results are now in much better agreement with the LRCC2 results than originally reported. This is also evident in Figure 4 (replacing Figure 4 in the original paper) where we have plotted the dispersion of the isotropic polarizability using the new polarizabilties from TDCC2 and TDCC2-b simulations. Also, in Figure 2 and Figure 3 we have plotted the first-order dipole response functions for the HF molecule from corrected TDCC2 simulations, which corrects the middle panels of Figure 2 and Figure 3 in the original paper, respectively.
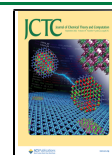
Published: August 25, 2022

Table 1. Polarizabilities (au) of Ne, HF, H_2O, NH_3, and CH_4 Extracted from LRCC2, TDCC2, and TDCC2-b Simulations[a]

		$\omega = 0.1$ au	$\omega = 0.2$ au	$\omega = 0.3$ au	$\omega = 0.4$ au	$\omega = 0.5$ au
Ne	LRCC2*	2.86	2.96	3.18	3.59	4.74
	TDCC2	2.86	2.96	3.18	3.73	5.27
	TDCC2*	2.87	2.98	3.19	3.75	5.29
	TDCC2-b	2.84	2.95	3.16	3.71	5.23
	TDCC2-b*	2.86	2.97	3.18	3.73	5.26

		$\omega = 0.1$ au		$\omega = 0.2$ au		$\omega = 0.3$ au	
		α_{yy}	α_{zz}	α_{yy}	α_{zz}	α_{yy}	α_{zz}
HF	LRCC2*	4.70	6.78	5.20	7.25	7.24	8.29
	TDCC2	4.71	6.78	5.24	7.28	8.47	8.36
	TDCC2*	4.75	6.85	5.28	7.36	8.54	8.45
	TDCC2-b	4.68	6.72	5.20	7.20	8.35	8.27
	TDCC2-b*	4.72	6.79	5.24	7.28	8.42	8.36

		$\omega = 0.0428$ au			$\omega = 0.0656$ au			$\omega = 0.1$ au		
		α_{xx}	α_{yy}	α_{zz}	α_{xx}	α_{yy}	α_{zz}	α_{xx}	α_{yy}	α_{zz}
H_2O	LRCC2*	9.41	10.43	9.63	9.55	10.50	9.71	9.91	10.66	9.92
	TDCC2	9.41	10.43	9.63	9.55	10.50	9.71	9.91	10.67	9.94
	TDCC2*	9.51	10.56	9.74	9.65	10.63	9.83	10.01	10.79	10.06
	TDCC2-b	9.35	10.35	9.55	9.49	10.42	9.63	9.84	10.58	9.86
	TDCC2-b*	9.44	10.47	9.66	9.58	10.54	9.74	9.94	10.71	9.97

		$\omega = 0.0428$ au		$\omega = 0.0656$ au		$\omega = 0.1$ au	
		α_{yy}	α_{zz}	α_{yy}	α_{zz}	α_{yy}	α_{zz}
NH_3	LRCC2*	13.56	15.86	13.67	16.21	13.92	17.15
	TDCC2	13.56	15.86	13.67	16.25	13.93	17.21
	TDCC2*	13.72	16.03	13.83	16.43	14.10	17.40
	TDCC2-b	13.48	15.76	13.59	16.15	13.84	17.09
	TDCC2-b*	13.64	15.93	13.75	16.32	14.01	17.28

		$\omega = 0.0656$ au	$\omega = 0.1$ au	$\omega = 0.2$ au
CH_4	LRCC2*	17.49	17.84	20.08
	TDCC2	17.50	17.85	20.12
	TDCC2*	17.69	18.05	20.34
	TDCC2-b	17.42	17.77	20.02
	TDCC2-b*	17.61	17.96	20.25

[a]The LRCC2 results for Ne and HF are from ref [1], and the LRCC2 results are computed with the Dalton quantum chemistry program (ref [2]). The calculations marked with * refers to the values reported in the original paper.
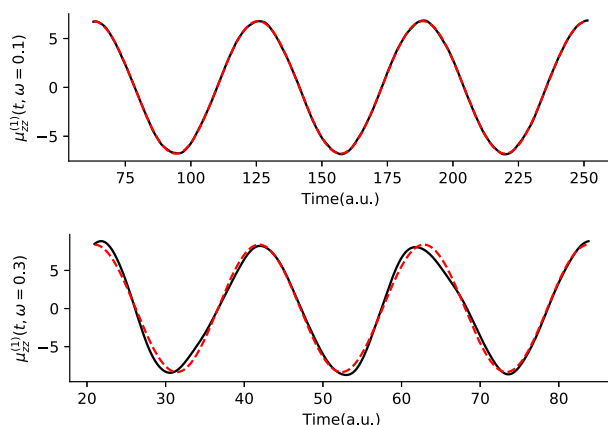

Figure 2. Zz-component of the first-order dipole responses for HF at $\omega = 0.1$ au and $\omega = 0.3$ au from corrected TDCC2 simulations.
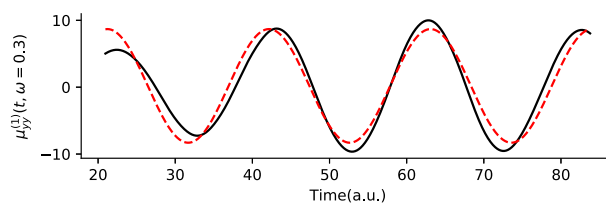

Figure 3. Yy-component of the first-order dipole response for HF at $\omega = 0.3$ au from the corrected TDCC2 simulation.

Table 2. First Hyperpolarizabilities (au) of HF, H$_2$O, and NH$_3$ from TDCCSD, TDOMP2, TDCC2, and TDCC2-b Simulations[a]

		$\omega = 0.1$ au		$\omega = 0.2$ au		$\omega = 0.3$ au	
		β_{zzz}^{OR}	β_{zzz}^{SHG}	β_{zzz}^{OR}	β_{zzz}^{SHG}	β_{zzz}^{OR}	β_{zzz}^{SHG}
HF	LRCC2*	15.52	17.52	18.69	37.67	27.35	−51.78
	TDCC2	15.54	17.53	18.26	34.31	30.57	−60.52
	TDCC2*	16.53	18.63	19.40	36.39	32.11	−61.17
	TDCC2-b	14.73	16.62	17.26	32.34	28.76	−64.06
	TDCC2-b*	15.32	17.26	17.95	33.56	29.76	−64.95

		$\omega = 0.0428$ au		$\omega = 0.0656$ au		$\omega = 0.1$ au	
		β_{zzz}^{OR}	β_{zzz}^{SHG}	β_{zzz}^{OR}	β_{zzz}^{SHG}	β_{zzz}^{OR}	β_{zzz}^{SHG}
H$_2$O	LRCC2*	−12.39	−13.12	−12.87	−14.83	−14.11	−20.76
	TDCC2	−12.42	−13.16	−12.93	−14.83	−14.45	−22.02
	TDCC2*	−13.63	−14.42	−14.17	−16.18	−15.75	−23.70
	TDCC2-b	−11.21	−11.88	−11.69	−13.41	−13.10	−20.08
	TDCC2-b*	−11.89	−12.58	−12.38	−14.15	−13.84	−21.01

		$\omega = 0.0428$ au				$\omega = 0.0656$ au			
		β_{yyy}^{OR}	β_{yyy}^{SHG}	β_{zzz}^{OR}	β_{zzz}^{SHG}	β_{yyy}^{OR}	β_{yyy}^{SHG}	β_{zzz}^{OR}	β_{zzz}^{SHG}
NH$_3$	LRCC2*	−16.69	−17.40	33.80	39.87	−17.16	−19.01	37.72	58.61
	TDCC2	−16.78	−17.58	33.97	39.88	−16.97	−18.59	39.26	63.96
	TDCC2*	−17.32	−18.13	35.80	41.90	−17.51	−19.17	41.24	66.61
	TDCC2-b	−16.59	−17.37	31.53	37.10	−16.77	−18.37	36.62	60.11
	TDCC2-b*	−17.00	−17.79	32.60	38.26	−17.19	−18.81	37.80	61.67

[a]Notation: $\beta_{iii}^{OR} = \beta_{iii}(0; \omega, -\omega)$ and $\beta_{iii}^{SHG} = \beta_{iii}(-2\omega; \omega, \omega)$. The LRCCSD and LRCC2 results for HF are taken from Larsen et al.[1]
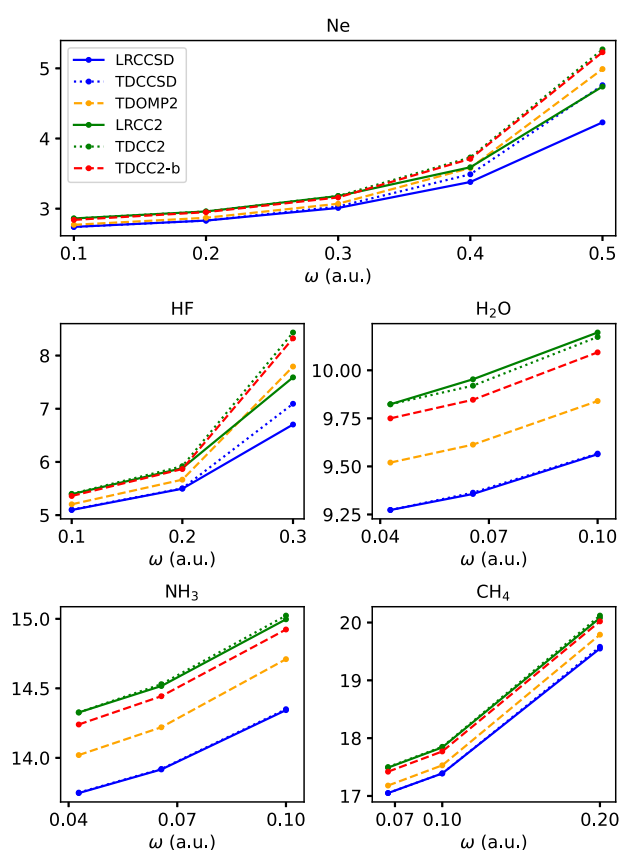

Figure 4. Isotropic polarizabilities extracted from TDCC2, TDOMP2, and TDCCSD simulations and from LRCC2 and LRCCSD calculations.

Finally, we emphasize that the conclusions of the original paper are unaffected by the error.

■ REFERENCES

(1) Larsen, H.; Olsen, J.; Hättig, C.; Jørgensen, P.; Christiansen, O.; Gauss, J. Polarizabilities and first hyperpolarizabilities of HF, Ne, and BH from full configuration interaction and coupled cluster calculations. *J. Chem. Phys.* **1999**, *111*, 1917−1925.

(2) Aidas, K.; Angeli, C.; Bak, K. L.; Bakken, V.; Bast, R.; Boman, L.; Christiansen, O.; Cimiraglia, R.; Coriani, S.; Dahle, P.; Dalskov, E. K.; Ekström, U.; Enevoldsen, T.; Eriksen, J. J.; Ettenhuber, P.; Fernández, B.; Ferrighi, L.; Fliegl, H.; Frediani, L.; Hald, K.; Halkier, A.; Hättig, C.; Heiberg, H.; Helgaker, T.; Hennum, A. C.; Hettema, H.; Hjertenaes, E.; Høst, S.; Høyvik, I.-M.; Iozzi, M. F.; Jansík, B.; Jensen, H. J. A.; Jonsson, D.; Jørgensen, P.; Kauczor, J.; Kirpekar, S.; Kjaergaard, T.; Klopper, W.; Knecht, S.; Kobayashi, R.; Koch, H.; Kongsted, J.; Krapp, A.; Kristensen, K.; Ligabue, A.; Lutnaes, O. B.; Melo, J. I.; Mikkelsen, K. V.; Myhre, R. H.; Neiss, C.; Nielsen, C. B.; Norman, P.; Olsen, J.; Olsen, J. M. H.; Osted, A.; Packer, M. J.; Pawlowski, F.; Pedersen, T. B.; Provasi, P. F.; Reine, S.; Rinkevicius, Z.; Ruden, T. A.; Ruud, K.; Rybkin, V. V.; Sałek, P.; Samson, C. C. M.; Sánchez de Merás, A.; Saue, T.; Sauer, S. P. A.; Schimmelpfennig, B.; Sneskov, K.; Steindal, A. H.; Sylvester-Hvid, K. O.; Taylor, P. R.; Teale, A. M.; Tellgren, E. I.; Tew, D. P.; Thorvaldsen, A. J.; Thøgersen, L.; Vahtras, O.; Watson, M. A.; Wilson, D. J. D.; Ziolkowski, M.; Ågren, H. The Dalton quantum chemistry program system. *Wiley Interdiscip. Rev. Comput. Mol. Sci.* **2014**, *4*, 269−284.

77

Paper II

Adiabatic extraction of nonlinear optical properties from real-time time-dependent electronic-structure theory

II

Adiabatic extraction of nonlinear optical properties from real-time time-dependent electronic-structure theory

View Online   Export Citation   CrossMark

Benedicte Sverdrup Ofstad,[1,a)] (ID) Håkon Emil Kristiansen,[1] (ID) Einar Aurbakken,[1] (ID)
Øyvind Sigmundson Schøyen,[2] (ID) Simen Kvaal,[1] (ID) and Thomas Bondo Pedersen[1,b)] (ID)

AFFILIATIONS

[1] Hylleraas Centre for Quantum Molecular Sciences, Department of Chemistry, University of Oslo, Oslo, Norway
[2] Department of Physics, University of Oslo, Oslo, Norway

[a)] Author to whom correspondence should be addressed: b.s.ofstad@kjemi.uio.no
[b)] Electronic mail: t.b.pedersen@kjemi.uio.no

ABSTRACT

Real-time simulations of laser-driven electron dynamics contain information about molecular optical properties through all orders in response theory. These properties can be extracted by assuming convergence of the power series expansion of induced electric and magnetic multipole moments. However, the accuracy relative to analytical results from response theory quickly deteriorates for higher-order responses due to the presence of high-frequency oscillations in the induced multipole moment in the time domain. This problem has been ascribed to missing higher-order corrections. We here demonstrate that the deviations are caused by nonadiabatic effects arising from the finite-time ramping from zero to full strength of the external laser field. Three different approaches, two using a ramped wave and one using a pulsed wave, for extracting electrical properties from real-time time-dependent electronic-structure simulations are investigated. The standard linear ramp is compared to a quadratic ramp, which is found to yield highly accurate results for polarizabilities, and first and second hyperpolarizabilities, at roughly half the computational cost. Results for the third hyperpolarizability are presented along with a simple, computable measure of reliability.

I. INTRODUCTION

Extraction of frequency-dependent, off-resonance linear and nonlinear optical properties of molecules from real-time time-dependent electronic-structure simulations has been increasingly used[1–18] in place of conventional response theory[19,20] in recent years. One likely reason is that the implementation of response theory becomes increasingly cumbersome with increasing response order, whereas time-dependent methods are relatively straightforward to implement.

While response theory is based on perturbation expansions, real-time approaches where the initial ground-state wave function (or density or density matrix) is propagated in the presence of an external laser field automatically include responses to all orders in perturbation theory. In principle, therefore, optical response properties through *any* order can be extracted from induced multipole moments recorded during the real-time simulation. If the total number of time steps in the wave function propagation can be kept low enough, the real-time approach may become computationally advantageous over the response approach for higher-order nonlinear properties such as the second hyperpolarizability.

The time required for real-time simulations depends on several parameters besides the inherent computational complexity of the equations of motion for the wave function parameters, which generally take the form $\dot{y} = f(y, t)$ where the dot denotes the time derivative. The choice of integrator affects how large a time step may be used without sacrificing accuracy and the number of expensive evaluations of the function $f(y, t)$ per time step. For given choices of electronic-structure model and suitable integrator, however, the key parameter determining both computational effort and
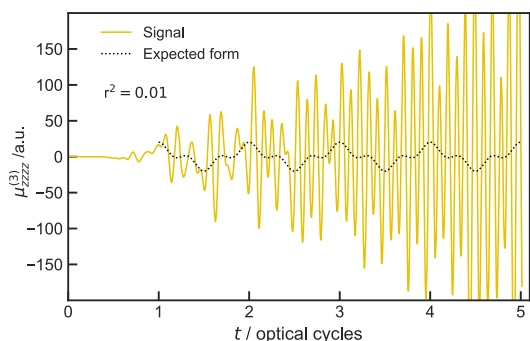
FIG. 1. Comparison of the third-order induced dipole moment extracted from TDCCSD simulations of the Ne atom with a least-squares fitting to the form expected from response theory.

accuracy of the extracted properties is the form used for the external, time-dependent field.

Two general approaches for the extraction of response properties have been proposed recently. While Uemoto *et al.*[14] used a pulsed (i.e., with finite duration) wave, Ding *et al.*[8] used a monochromatic continuous wave ramped from zero to full strength in a finite-time interval to mimic the adiabatic switching-on required by response theory. In both cases, the individual orders of the response of the electronic system are separated by running simulations with different field strengths, followed by curve fitting to extract specific frequency-dependent properties at each order. The accuracy and total simulation time thus intrinsically depend on the duration of the pulsed or continuous wave, including the ramping time for the latter.

In this work, we investigate the convergence of the extracted response properties (polarizabilities, and first and second hyperpolarizabilities) toward the results from response theory with respect to the duration of the pulsed wave (PW). For the ramped continuous wave (RCW) approach, we perform the same convergence study with respect to the adiabatic ramping time and the post-ramp time.

The results reported by Ding *et al.*[8] indicate that linear polarizabilities can be extracted from simulations with errors below ~1%, while the percentwise errors increase by roughly a factor of ten at each nonlinear order for hyperpolarizabilities. The source of these errors is the significant deviation of the higher-order time-domain dipole signals from the form expected from frequency-dependent response theory. Figure 1 shows an example for the Ne atom where we have extracted the third-order induced dipole moment from time-dependent coupled-cluster singles-and-doubles (TDCCSD) simulations with the approach recommended by Ding *et al.*[8] That is, we have used a continuous wave linearly ramped for one optical cycle, followed by wave-function propagation with full field strength for four optical cycles. Evidently, the deviation between the computed dipole and the fitted one is much too big for an accurate determination of the second hyperpolarizability, as also indicated by the coefficient of determination, $r^2 = 0.01$.

Such deviations have been ascribed to higher-order truncation errors,[8] and additional linear ramping time has been shown

to improve the accuracy of hyperpolarizabilities in the context of time-dependent configuration-interaction simulations, both spin-unrestricted and with spin-restriction through the graphical unitary group approach.[12] In this work, we investigate if the deviations can be reduced by switching to a softer adiabatic ramping while maintaining or reducing the total computational cost of the time-dependent simulations.

The remainder of this paper is organized as follows: In Sec. II, we review the RCW and PW methods for extracting up to the third hyperpolarizability and propose an alternative to the linear ramping of Ding *et al.*[8] aimed at mitigating nonadiabatic effects. Test systems and other computational details are provided in Sec. III, followed by presentation and discussion of results in Sec. IV. Finally, concluding remarks are given in Sec. V.

II. THEORY

The electronic dynamics induced by an electromagnetic field is governed by the time-dependent Schrödinger equation

$$i\frac{\partial \Psi(t)}{\partial t} = \hat{H}(t)\Psi(t), \quad \Psi(0) = \Psi_0, \tag{1}$$

where Ψ_0 is the initial condition, here chosen to be the normalized, time-independent ground-state wavefunction. The time-dependent Hamiltonian $\hat{H}(t)$ is given by

$$\hat{H}(t) = \hat{H}_0 + \hat{V}(t), \tag{2}$$

where $\hat{H}_0$ is the molecular electronic Hamiltonian in the clamped-nuclei Born-Oppenheimer approximation, and the matter–field interaction operator $\hat{V}(t)$ is given in the length-gauge electric-dipole approximation as

$$\hat{V}(t) = -\hat{\mu} \cdot E(t). \tag{3}$$

Here, $\hat{\mu}$ is the electric-dipole operator and $E(t)$ is a uniform classical electric field. The time evolution of the electric-dipole moment is obtained from the explicitly time-propagated wavefunction as

$$\mu(t) = \langle \Psi(t)|\hat{\mu}|\Psi(t)\rangle. \tag{4}$$

Provided the external field is sufficiently weak and adiabatically switched on, each Cartesian coordinate of the time-dependent dipole moment $\mu_i(t)$ can be expanded as a power series in the electric field $E_j(t)$. Separating the electric-field component $E_j(t) = E_j F(t)$ into a constant amplitude E_j and a time-dependent function $F(t), |F(t)| \le 1$, we may write[21]

$$\mu_i(t) = \mu_i^0 + \sum_j \mu_{ij}^{(1)}(t)E_j + \sum_{jk} \mu_{ijk}^{(2)}(t)E_jE_k$$
$$+ \sum_{jkl} \mu_{ijkl}^{(3)}(t)E_jE_kE_l$$
$$+ \sum_{jklm} \mu_{ijklm}^{(4)}(t)E_jE_kE_lE_m + \cdots. \tag{5}$$

The time-dependent dipole responses $\mu^{(n)}(t)$ can be written either in the time domain or in the frequency domain.

In the time domain, we may write the dipole responses as the convolutions of time-dependent polarizabilities and hyperpolarizabilities with the field factors $F(t)$,[21]

$$\mu_{ij}^{(1)}(t) = \int_{-\infty}^{\infty} \alpha_{ij}^{(1)}(t - t_1) F(t_1) \, dt_1, \tag{6a}$$

$$\mu_{ijk}^{(2)}(t) = \iint_{-\infty}^{\infty} \alpha_{ijk}^{(2)}(t - t_1, t - t_2) F(t_1) F(t_2) \, dt_1 \, dt_2, \tag{6b}$$

$$\mu_{ijkl}^{(3)}(t) = \iiint_{-\infty}^{\infty} \alpha_{ijkl}^{(3)}(t - t_1, t - t_2, t - t_3) \\ \times F(t_1) F(t_2) F(t_3) \, dt_1 \, dt_2 \, dt_3, \tag{6c}$$

$$\mu_{ijklm}^{(4)}(t) = \iiiint_{-\infty}^{\infty} \alpha_{ijklm}^{(4)}(t - t_1, t - t_2, t - t_3, t - t_4) \\ \times F(t_1) F(t_2) F(t_3) F(t_4) \, dt_1 \, dt_2 \, dt_3 \, dt_4. \tag{6d}$$

By causality, the time-dependent (hyper-)polarizability tensors $\alpha^{(n)}$ vanish when any of the arguments $t - t_n < 0$. In the frequency domain, adopting the conventions of response theory,[19]

$$\mu_{ij}^{(1)}(t) = \int_{-\infty}^{\infty} \alpha_{ij}(-\omega; \omega) \tilde{F}(\omega) e^{-i\omega t} \, d\omega, \tag{7a}$$

$$\mu_{ijk}^{(2)}(t) = \frac{1}{2} \iint_{-\infty}^{\infty} \beta_{ijk}(-\omega^{(2)}; \omega_1, \omega_2) \\ \times \tilde{F}(\omega_1) \tilde{F}(\omega_2) e^{-i(\omega_1 + \omega_2)t} \, d\omega_1 \, d\omega_2, \tag{7b}$$

$$\mu_{ijkl}^{(3)}(t) = \frac{1}{6} \iiint_{-\infty}^{\infty} \gamma_{ijkl}(-\omega^{(3)}; \omega_1, \omega_2, \omega_3) \\ \times \tilde{F}(\omega_1) \tilde{F}(\omega_2) \tilde{F}(\omega_3) e^{-i(\omega_1 + \omega_2 + \omega_3)t} \, d\omega_1 \, d\omega_2 \, d\omega_3, \tag{7c}$$

$$\mu_{ijklm}^{(4)}(t) = \frac{1}{24} \iiiint_{-\infty}^{\infty} \delta_{ijklm}(-\omega^{(4)}; \omega_1, \omega_2, \omega_3, \omega_4) \\ \times \tilde{F}(\omega_1) \tilde{F}(\omega_2) \tilde{F}(\omega_3) \tilde{F}(\omega_4) e^{-i(\omega_1 + \omega_2 + \omega_3 + \omega_4)t} \\ \times d\omega_1 \, d\omega_2 \, d\omega_3 \, d\omega_4, \tag{7d}$$

where $\omega^{(n)} = \omega_1 + \omega_2 + \cdots + \omega_n$ and

$$\tilde{F}(\omega) = \frac{1}{2\pi} \int_{-\infty}^{\infty} F(t) e^{i\omega t} \, dt. \tag{8}$$

Using the notation of Olsen and Jørgensen,[19] the frequency-dependent (hyper-)polarizabilities are the linear and nonlinear response functions,

$$\alpha_{ij}(-\omega; \omega) = -\langle\langle \hat{\mu}_i; \hat{\mu}_j \rangle\rangle_\omega, \tag{9a}$$

$$\beta_{ijk}(-\omega^{(2)}; \omega_1, \omega_2) = \langle\langle \hat{\mu}_i; \hat{\mu}_j, \hat{\mu}_k \rangle\rangle_{\omega_1, \omega_2}, \tag{9b}$$

$$\gamma_{ijkl}(-\omega^{(3)}; \omega_1, \omega_2, \omega_3) = -\langle\langle \hat{\mu}_i; \hat{\mu}_j, \hat{\mu}_k, \hat{\mu}_l \rangle\rangle_{\omega_1, \omega_2, \omega_3}, \tag{9c}$$

$$\delta_{ijklm}(-\omega^{(4)}; \omega_1, \omega_2, \omega_3, \omega_4) = \langle\langle \hat{\mu}_i; \hat{\mu}_j, \hat{\mu}_k, \hat{\mu}_l, \hat{\mu}_m \rangle\rangle_{\omega_1, \omega_2, \omega_3, \omega_4}. \tag{9d}$$

The response functions of the right-hand sides can, in principle, be evaluated analytically with a wide range of quantum chemical methods using response theory,[22] although we are not aware of any implementation beyond cubic response—i.e., beyond the second hyperpolarizability γ_{ijkl}.

With the electric field polarized along a specific axis, say j, the "diagonal" components of the dipole responses, $\mu_{ijj\cdots j}^{(n)}(t)$, can be extracted from $\mu_i(t)$ recorded during simulations using the central difference formulas,

$$\mu_{ij}^{(1)}(t) \approx \frac{8\Delta_i^-(t, E_j) - \Delta_i^-(t, 2E_j)}{12E_j}, \tag{10a}$$

$$\mu_{ijj}^{(2)}(t) \approx \frac{16\Delta_i^+(t, E_j) - \Delta_i^+(t, 2E_j) - 30\mu_i^0}{24E_j^2}, \tag{10b}$$

$$\mu_{ijjj}^{(3)}(t) \approx \frac{-13\Delta_i^-(t, E_j) + 8\Delta_i^-(t, 2E_j) - \Delta_i^-(t, 3E_j)}{48E_j^3}, \tag{10c}$$

$$\mu_{ijjjj}^{(4)}(t) \approx \frac{1}{144E_j^4}\left(-39\Delta_i^+(t, E_j) + 12\Delta_i^+(t, 2E_j) \\ - \Delta_i^+(t, 3E_j) + 56\mu^0\right). \tag{10d}$$

The truncation error is $\mathcal{O}(E_j^4)$ in each case, and

$$\Delta_i^\pm(t, E_j) = \mu_i(t, E_j) \pm \mu_i(t, -E_j), \tag{11}$$

is the sum/difference of the time-dependent dipole moments computed with opposite polarization directions and same field strength E_j. One can now use different choices for $F(t)$ to obtain the frequency-dependent response functions using either the frequency-domain expressions (7) or those in the time-domain (6).

A. Ramped continuous wave approach

As the name suggests, the RCW approach uses a continuous wave, i.e., $F(t) = \cos(\omega t)$. This choice allows us to perform the Fourier transformations of Eq. (7) analytically to obtain

$$\mu_{ij}^{(1)}(t) = \alpha_{ij}(-\omega; \omega) \cos(\omega t), \tag{12a}$$

$$\mu_{ijj}^{(2)}(t) = \frac{1}{4}\left[\beta_{ijj}^{\text{SHG}}(\omega) \cos(2\omega t) + \beta_{ijj}^{\text{OR}}(\omega)\right], \tag{12b}$$

$$\mu_{ijjj}^{(3)}(t) = \frac{1}{24}\left[\gamma_{ijjj}^{\text{THG}}(\omega) \cos(3\omega t) + 3\gamma_{ijjj}^{\text{DFWM}}(\omega) \cos(\omega t)\right], \tag{12c}$$

$$\mu_{ijjjj}^{(4)}(t) = \frac{1}{192}\left[\delta_{ijjjj}^{\text{FHG}}(\omega) \cos(4\omega t) \\ + 4\delta_{ijjjj}^{\text{FSHG}}(\omega) \cos(2\omega t) + 3\delta_{ijjjj}^{\text{HOR}}(\omega)\right], \tag{12d}$$

where the (hyper-)polarizabilities are assumed real, a valid assumption given that $\hat{H}_0$ does not contain static magnetic fields, and

$$\beta_{ijj}^{\text{SHG}}(\omega) = \beta_{ijj}(-2\omega; \omega, \omega), \tag{13a}$$

$$\beta_{ijj}^{\text{OR}}(\omega) = \beta_{ijj}(0; \omega, -\omega), \tag{13b}$$

$$\gamma_{ijjj}^{\text{THG}}(\omega) = \gamma_{ijjj}(-3\omega; \omega, \omega, \omega), \tag{13c}$$

$$\gamma_{ijjj}^{\text{DFWM}}(\omega) = \gamma_{ijjj}(-\omega; \omega, \omega, -\omega), \tag{13d}$$

$$\delta_{ijjjj}^{\text{FHG}}(\omega) = \delta_{ijjj}(-4\omega; \omega, \omega, \omega, \omega), \tag{13e}$$

$$\delta_{ijjjj}^{\text{HSHG}}(\omega) = \delta_{ijjj}(-2\omega; \omega, \omega, \omega, -\omega), \tag{13f}$$

$$\delta_{ijjjj}^{\text{HOR}}(\omega) = \delta_{ijjj}(0; \omega, \omega, -\omega, -\omega). \tag{13g}$$

The superscripts refer to the following nonlinear optical processes: Second harmonic generation (SHG), optical rectification (OR), third harmonic generation (THG), degenerate four-wave mixing
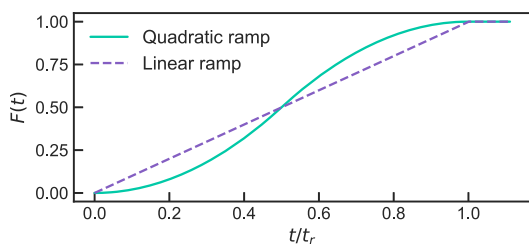
FIG. 2. The time profiles F^{LRCW} and F^{QRCW} with $\omega = 0$.

(DFWM), fourth harmonic generation (FHG), higher-order second harmonic generation (HSHG), and higher-order optical rectification (HOR). With the left-hand sides known from simulations through Eq. (10), Eqs. (12a)–(12d) yield the frequency-dependent (hyper-)polarizabilities by curve fitting.

Frequency-dependent response theory, however, requires the field to be adiabatically switched on.[19] This can be achieved by a smooth modification of the continuous wave such that it is switched-on at $t \to -\infty$ and reaches full strength at $t \to \infty$. Of course, this is impractical and a finite-time ramping of the field from zero to full strength must be applied in a way that minimizes nonadiabatic effects using only post-ramp signals to extract the dipole responses $\mu^{(n)}(t)$. In Ref. 8, the adiabatic switching-on is simulated by a linear ramp lasting for one optical cycle, i.e., a ramping time $t_r = t_c$ where the cycle time is $t_c = \frac{2\pi}{\omega}$. We refer to this approach as the linear RCW (LRCW) approach for which

$$F^{LRCW}(t) = \begin{cases} \dfrac{t}{t_r}\cos(\omega t), & 0 \leq t < t_r, \\ \cos(\omega t), & t_r \leq t \leq t_{tot}. \end{cases} \quad (14)$$

Following the ramping phase, Ding *et al.*[8] propagated the system for a further four optical cycles, giving a total simulation time of $t_{tot} = 5t_c$. We will here investigate the effect of a longer ramping time consisting of n_r optical cycles, $t_r = n_r t_c$. We note that the linear ramp is not continuously differentiable at $t = 0$ and at $t = t_r$.

In addition to extending the ramping time beyond a single optical cycle, we investigate the *quadratic ramp* to achieve a more adiabatic switching on of the electric field. We refer to this approach as the quadratic RCW (QRCW) approach. Specifically,

$$F^{QRCW}(t) = \begin{cases} \dfrac{2t^2}{t_r^2}\cos(\omega t), & 0 \leq t < \dfrac{t_r}{2}, \\ \dfrac{t_r^2 - 2(t - t_r)^2}{t_r^2}\cos(\omega t), & \dfrac{t_r}{2} \leq t < t_r, \\ \cos(\omega t), & t_r \leq t \leq t_{tot}, \end{cases} \quad (15)$$

which is continuously differentiable at both $t = 0$ and $t = t_r$. As illustrated in Fig. 2, the quadratic ramp provides a gentler increase of the electric field than the linear ramp for small t and near $t = t_r$, albeit with a more rapid increase around $t = \frac{t_r}{2}$. A similar sigmoid (Fermi-like) function has been used to obtain electronic ground states by

adiabatically switching on electronic interactions, thus providing an alternative to imaginary-time propagation.[23]

B. Pulsed wave approach

Uemoto *et al.*[14] proposed an alternative approach to the extraction of linear and nonlinear properties from simulations of electron dynamics driven by a laser pulse rather than by a continuous wave. We refer to this approach as the pulsed wave (PW) approach, which starts from the time-domain responses, Eqs. (6a)–(6d). Retardation effects are neglected and the polarization thus is considered local in time, i.e.,

$$\mu^{(n)}(t) = \iint \cdots \int_{-\infty}^{\infty} \alpha^{(n)}(t - t_1, t - t_2, \ldots, t - t_n)$$
$$\times F(t_1)F(t_2)\cdots F(t_n) \, dt_1 \, dt_2 \cdots dt_n$$
$$\approx \alpha^{(n)}(t)F(t)^n, \quad (16)$$

where the Cartesian indices have been omitted for notational convenience. Following Uemoto *et al.*,[14] the time-dependence of the finite laser pulse is described using a trigonometric envelope, which provides a well-defined approximation to the Gaussian envelope typically used in experimental work,[24]

$$F^{PW}(t) = \sin^2\left(\frac{\pi t}{t_{tot}}\right)\cos(\omega t), \qquad 0 \leq t \leq t_{tot}. \quad (17)$$

The finite duration of the laser pulse implies that the frequency distribution is broadened around the carrier frequency ω. This, in turn, implies that $\alpha^{(n)}(t)$ contains (hyper-)polarizabilities in a range of frequencies and, therefore, a filtering procedure must be applied to extract the proper nonlinear response functions in the frequency domain. If the frequency distribution of the laser pulse is sufficiently sharply centered at the carrier frequency—i.e., if the pulse duration is sufficiently long—the linear polarizability dominates the time signal and can be found by a direct fitting of the signal to the time profile of the pulse,

$$\mu_{ij}^{(1)}(t) = \alpha_{ij}(-\omega; \omega)F^{PW}(t). \quad (18)$$

This is essentially the same procedure used for a monochromatic continuous wave [Eq. (12a)] above.

For the hyperpolarizabilities, where more than one frequency component is present in the signal, the individual frequency components are separated by means of a Fourier filtering procedure: $\mu^{(n)}(t)$ is Fourier transformed to the frequency domain to obtain

$$\tilde{\mu}^{(n)}(\omega') = \frac{1}{2\pi}\int_{-\infty}^{\infty}\mu^{(n)}(t)e^{i\omega' t}\,dt, \quad (19)$$

which is subsequently transformed back to the time domain using a suitably chosen frequency window specified as a positive integer multiple k of the carrier frequency ω,

$$\mu^{(n)}(t; k\omega) = \int_{-(k+1)\omega}^{-(k-1)\omega}\tilde{\mu}^{(n)}(\omega')e^{-i\omega' t}\,d\omega'$$
$$+ \int_{(k-1)\omega}^{(k+1)\omega}\tilde{\mu}^{(n)}(\omega')e^{-i\omega' t}\,d\omega'. \quad (20)$$

The same procedure is applied to $F^{\mathrm{PW}}(t)$,

$$F^{\mathrm{PW}}(t; k\omega) = \int_{-(k+1)\omega}^{-(k-1)\omega} \tilde{F}^{\mathrm{PW}}(\omega') e^{-i\omega' t} \, d\omega'$$
$$+ \int_{(k-1)\omega}^{(k+1)\omega} \tilde{F}^{\mathrm{PW}}(\omega') e^{-i\omega' t} \, d\omega'. \tag{21}$$

The frequency-dependent hyperpolarizabilities are then acquired by finding the coefficient needed to fit $\mu^{(n)}(t; k\omega)$ to $[F^{\mathrm{PW}}(t; k\omega)]^n$. Thus, the first hyperpolarizabilities are found by curve fitting according to

$$\mu_{ijj}^{(2)}(t; 0) = \frac{1}{4} \beta_{ijj}^{\mathrm{OR}}(\omega) [F^{\mathrm{PW}}(t; 0)]^2, \tag{22a}$$

$$\mu_{ijj}^{(2)}(t; 2\omega) = \frac{1}{4} \beta_{ijj}^{\mathrm{SHG}}(\omega) [F^{\mathrm{PW}}(t; 2\omega)]^2, \tag{22b}$$

the second hyperpolarizabilities according to

$$\mu_{ijjj}^{(3)}(t; \omega) = \frac{1}{8} \gamma_{ijjj}^{\mathrm{DFWM}}(\omega) [F^{\mathrm{PW}}(t; \omega)]^3, \tag{23a}$$

$$\mu_{ijjj}^{(3)}(t; 3\omega) = \frac{1}{24} \gamma_{ijjj}^{\mathrm{THG}}(\omega) [F^{\mathrm{PW}}(t; 3\omega)]^3, \tag{23b}$$

and the third hyperpolarizabilities according to

$$\mu_{ijjjj}^{(4)}(t; 0) = \frac{1}{64} \delta_{ijjjj}^{\mathrm{HOR}}(\omega) [F^{\mathrm{PW}}(t; 0)]^4, \tag{24a}$$

$$\mu_{ijjjj}^{(4)}(t; 2\omega) = \frac{1}{48} \delta_{ijjjj}^{\mathrm{HSHG}}(\omega) [F^{\mathrm{PW}}(t; 2\omega)]^4, \tag{24b}$$

$$\mu_{ijjjj}^{(4)}(t; 4\omega) = \frac{1}{192} \delta_{ijjjj}^{\mathrm{FHG}}(\omega) [F^{\mathrm{PW}}(t; 4\omega)]^4. \tag{24c}$$

III. COMPUTATIONAL DETAILS

The time-dependent Schrödinger equation (1) is solved approximately using the time-dependent configuration-interaction singles (TDCIS)[25,26] method, the time-dependent coupled-cluster singles-and-doubles (TDCCSD)[27–29] method, the second-order approximate time-dependent coupled-cluster (TDCC2)[17,30] model, and the time-dependent orbital-optimized second-order Møller–Plesset (TDOMP2)[17,31] model. The time-dependent coupled-cluster methods have been used recently to simulate optical properties, including linear absorption spectra,[32–37] transient pump-probe absorption spectra,[38,39] and ionization dynamics and high-harmonic generation.[31,40–44]

For the nonvariational methods, the dipole moment is computed using the inherently real expectation-value functional proposed in Refs. 28 and 45.

We test the RCW and PW approaches using the same ten-electron systems as in Ref. 17, namely, Ne, HF, H_2O, NH_3, and CH_4. The geometries of these molecules can be found in the supplementary material. The d-aug-cc-pVDZ[46] basis set is used for Ne, while the aug-cc-pVDZ[47] basis set is used for the four remaining systems. The basis set definitions are taken from the Basis Set Exchange (BSE).[48] The carrier frequencies are chosen in accord with Ref. 17: Ne: $\omega = 0.1$, HF: $\omega = 0.1$, H_2O: $\omega = 0.0428$, NH_3: $\omega = 0.0428$, and CH_4: $\omega = 0.0656$ a.u. These frequencies come in at less than one third of the first dipole-allowed excitation energy for each system,

enabling properties up to (at least) the third hyperpolarizability to be reliably extracted.

The Hartree–Fock reference orbitals and Hamiltonian integrals are calculated using the Python-based Simulations of Chemistry Framework[49] (PySCF) with the gradient norm convergence threshold set to 10^{-10} a.u.

The ground states are computed using a locally developed closed-shell spin-restricted code,[50] all computed with a residual norm convergence criteria of 10^{-12} a.u. The equations of motion are integrated using the sixth order (three-stage, $s = 3$) symplectic Gauss–Legendre integrator[51] as described in Ref. 28 with a time step of $\Delta t = 0.01$ a.u. and the residual norm convergence criterion set to 10^{-10} a.u. for the implicit equations. The least-squares curve fitting, using the Levenberg–Marquardt algorithm, as implemented in the *optimize* module of SciPy[52] is used to extract the (hyper-)polarizabilities.

The coupled-cluster response data are computed using the Dalton quantum chemistry package[53–59] with the following gradient/residual norm convergence criteria: 10^{-10} a.u. for the Hartree–Fock reference orbitals, 10^{-10} a.u. for the CC ground-state residual norms, and 10^{-8} a.u. for the response equations. The CIS response data are computed using sum-over-states expressions.[19,60]

For all simulations, the electric-field strengths $E = \pm 0.001, \pm 0.002, \pm 0.003$ a.u. are used in order to reduce numerical noise for higher-order properties. The electric-field strengths should be of a magnitude where *both* the errors associated with numerical noise *and* the errors arising from numerical truncation and nonadiabatic effects remain small. Ding *et al.*[8] explored field strengths in the range 0.0005 to 0.005 a.u. and found $E = 0.002$ a.u. to provide the most accurate results. Uemoto *et al.*[14] used field strengths from $E \approx 0.0002$ a.u. to $E \approx 0.002$ a.u. and did not find the PW approach to be sensitive within this range.

IV. RESULTS

A. Time evolution of the nonlinear dipole responses in the RCW approach

The accuracy of the (hyper-)polarizabilities obtained using the RCW approach depends on how closely the time-domain dipole responses $\mu^{(n)}(t)$ *actually* are to their expected forms, expressed by Eqs. (12a)–(12d). Therefore, we start by comparing the signals extracted after linear and quadratic ramping. The motivation for this is twofold: First, we wish to investigate if the deviations previously observed[8] for time signals of nonlinear properties can be alleviated with the closer-to-adiabatic quadratic ramp. Second, we wish to investigate the effect of varying the ramping time $t_r = n_r t_c$ and the propagation time $t_p = n_p t_c$. Their relative importance will be assessed, and the most favorable ratio between n_r and n_p will be determined. When the time parameters are explicitly specified, the approach will be denoted RCW(n_r, n_p). Results obtained with the TDCCSD method will be presented and discussed; analogous results with the TDCC2, TDOMP2, and TDCIS methods are given in the supplementary material.

The systems are ramped using either the linear ramp profile F^{LRCW} [Eq. (14)] or the quadratic ramp profile F^{QRCW} [Eq. (15)]. The ramp duration is increased in increments of one optical cycle, up to a maximum of seven optical cycles ($n_r = 1, 2, \ldots, 7$), followed by four

85

optical cycles of propagation ($n_p = 4$). The second- and third-order time-dependent dipole responses $\mu^{(n)}(t)$, $n = 2, 3$, are collected, and fitted to the expected shapes in Eqs. (12b) and (12c).

The time-domain dipole response $\mu_{zzz}^{(2)}(t)$ for the NH_3 molecule is displayed in Fig. 3. The upper-most panel exhibits the one-cycle ramp, and for each descending panel the number of ramping cycles is increased by one. The function obtained by fitting the analytic form over the range of four cycles post-ramp is displayed in black along with its coefficient of determination, r^2. The function obtained by fitting to one post-ramp cycle is plotted in green.

Ramping with the linear profile, we observe the high-frequency oscillations previously reported in Refs. 8 and 17. The correspondence between the signal and expected form improves significantly as the linear ramping time is increased to two and three optical cycles. Increasing the linear ramp time above three optical cycles only delivers marginal improvements. The simulations conducted using the quadratic ramp, in contrast, appear to behave correctly already at the one-cycle ramp stage. Evidently, the signal can be improved either by switching to the quadratic ramp or by increasing the duration of the linear ramping. The curves fitted using one post-ramp cycle typically have r^2 values slightly above those obtained by fitting to four post-ramp cycles.

The second hyperpolarizability, a much smaller contribution to the total induced dipole moment, is highly sensitive to errors in the time signal. The third-order response signal, $\mu_{zzz}^{(3)}(t)$, features both the high-frequency oscillations observed for the first hyperpolarizability and the increase in amplitude as time progress. The molecule least sensitive to these effects is H_2O, for which results are presented in Figs. 4(a) and 4(b). The molecule most sensitive is CH_4, for which results are presented in Figs. 4(c) and 4(d). The linear one-cycle ramp is clearly inadequate for describing the second hyperpolarizability for both molecules, indicating that even a small amount of nonadiabatic error dramatically reduces the correspondence of the signal with its expected form. Increasing the ramping time to two or three optical cycles greatly improves the signal, but analogously to what was observed for the first hyperpolarizability, increasing beyond three cycles does not improve the signal. Even with increased ramping time, the linear ramp does not provide an accurate description of the third order response signal, yielding at best $r^2 = 0.22$ for CH_4. The quadratic ramp profile fairs notably better, although the high-frequency oscillations and the drift of the amplitude is observed for the CH_4 molecule when a one-cycle ramp is employed—i.e., in contrast to what was observed for the first hyperpolarizability, a one-cycle quadratic ramp appears to be insufficient.
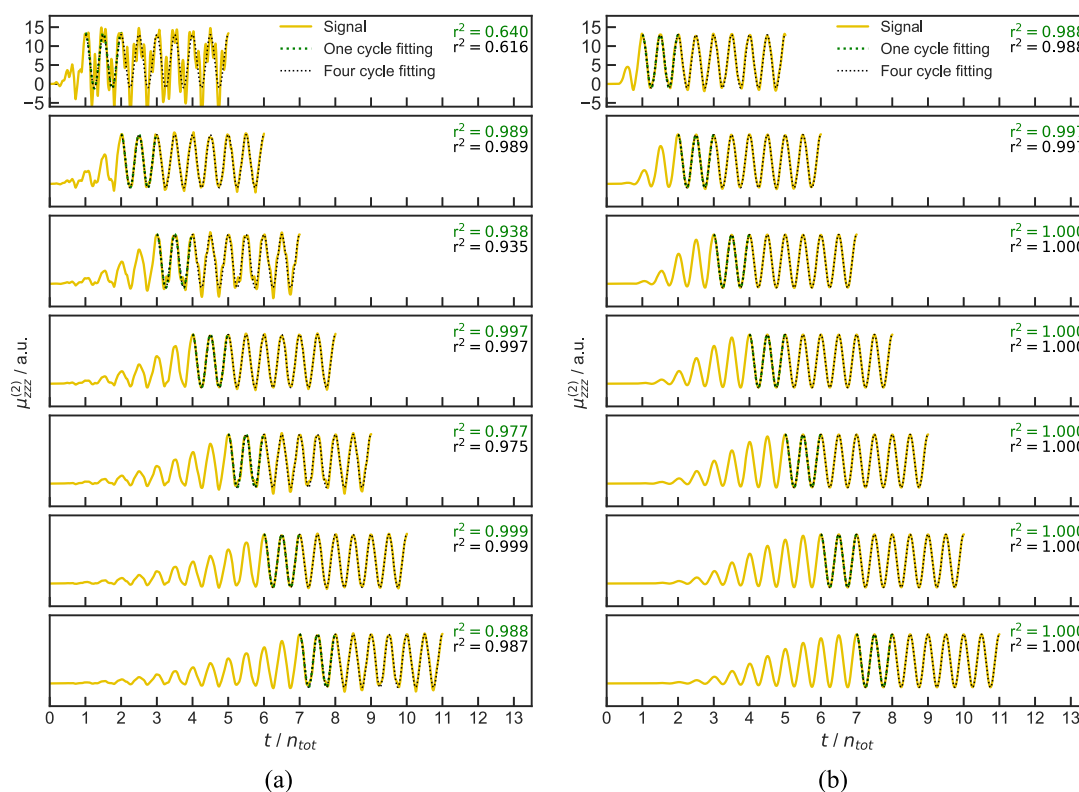
FIG. 3. The second-order dipole response obtained from TDCCSD simulations using, from top to bottom, $n_r = (1, 2, 3, 4, 5, 6, 7)$ linear ramp (a) or quadratic ramp (b) cycles followed by four post-ramp cycles of propagation time for NH_3. The fitting in black is done on all four post-ramp cycles, the fitting in green is done on one post-ramp cycle. All plots are on the same scale.
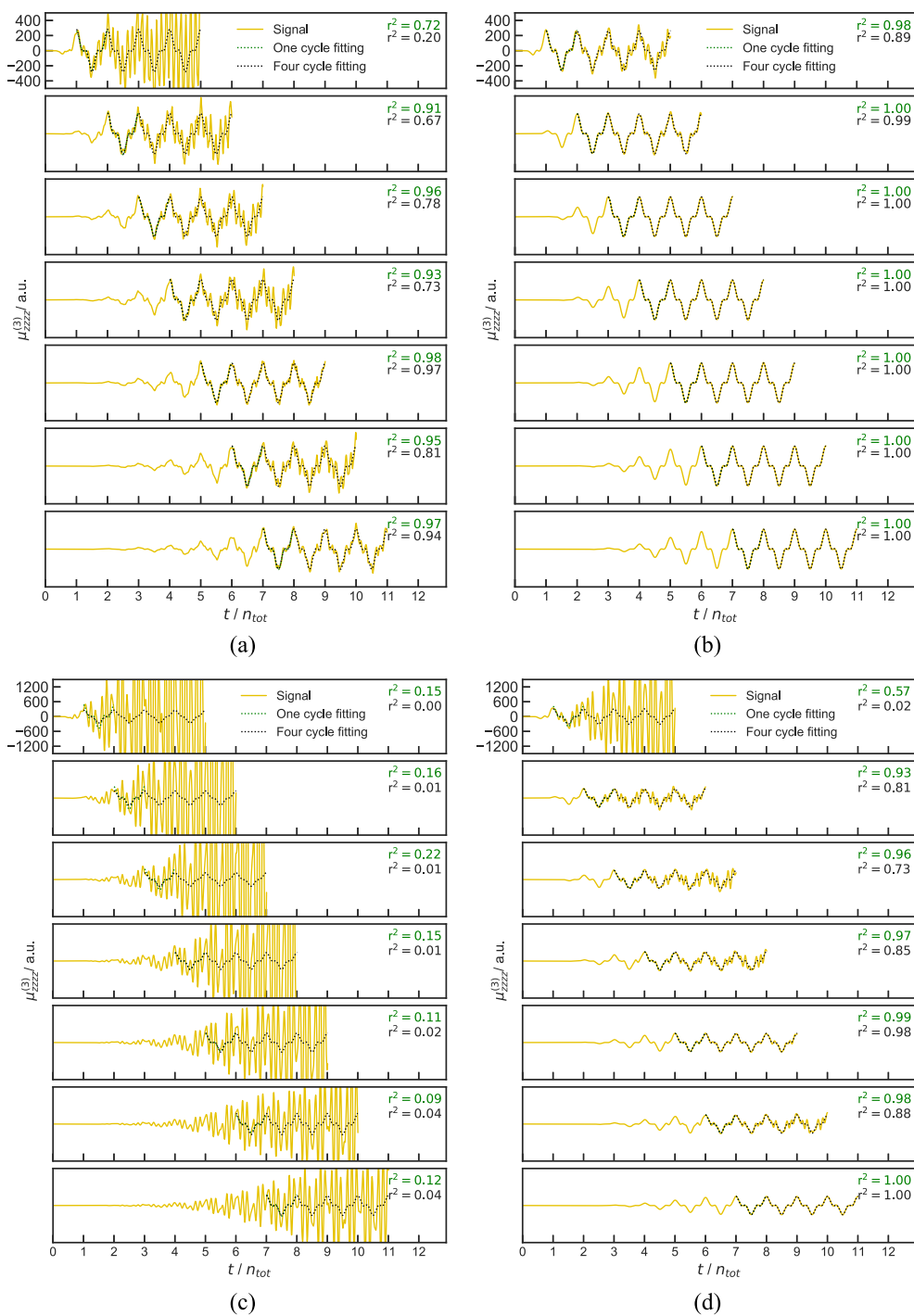
FIG. 4. The third-order dipole response obtained from TDCCSD simulations for (a) H_2O using a linear ramp profile, (b) H_2O using a quadratic ramp profile, (c) CH_4 using a linear ramp profile, and (d) CH_4 using a quadratic ramp profile. From top to bottom panel, $n_r = (1, 2, 3, 4, 5, 6, 7)$ ramp cycles are followed by four post-ramp cycles of propagation. The fitting in black is done on all four post-ramp cycles, the fitting in green is done on one post-ramp cycle. All four plots are on the same scale for each system.
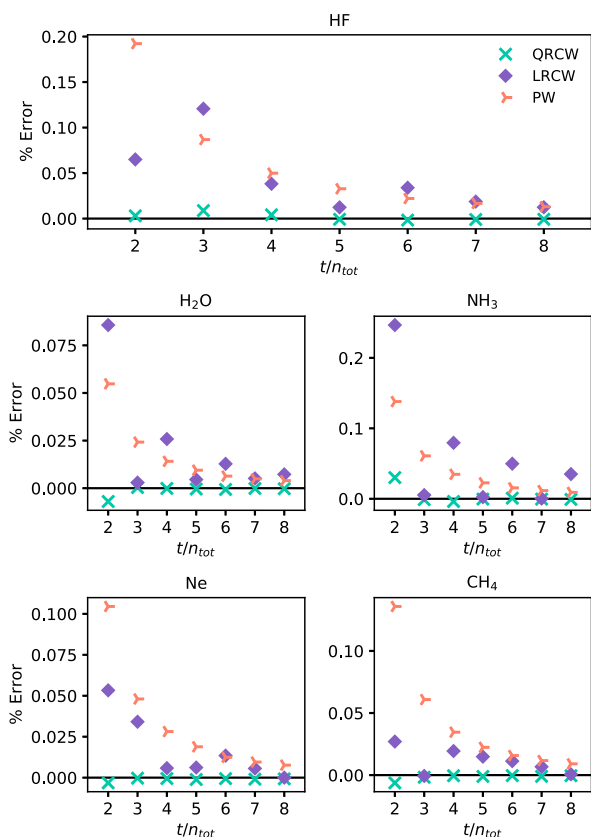
FIG. 5. Convergence toward CCSD linear response results of polarizabilities, α_{zz}, extracted from TDCCSD simulations using the LRCW($n_{tot} - 1, 1$), QRCW($n_{tot} - 1, 1$), and PW(n_{tot}) methods.

FIG. 6. Convergence toward CCSD quadratic response results of first hyperpolarizabilities extracted from TDCCSD simulations using the LRCW($n_{tot} - 1, 1$), QRCW($n_{tot} - 1, 1$), and PW(n_{tot}) methods.

Increasing the number of ramping cycles quickly leads to convergence, giving $r^2 = 0.999\,98$ when seven cycles are used for the CH_4 molecule.

The gradual ramping of the electric-field strength is found to reduce the signal errors indicating that nonadiabatic effects are the main source of error, given that the dipole expansion is not divergent in any order. Furthermore, it is clear that the quadratic ramp aids in reaching an adiabatic description more rapidly than the linear ramp. It is found that fitting the expected function to the signal after only one post-ramp cycle is warranted when the simulation has ramped in a sufficiently adiabatic manner. Based on these observations, we shall compare the RCW method to the PW method using one post-ramp cycle.

B. Polarizability

In the interest of gauging the accuracy of the different approaches, polarizabilities extracted using the LRCW, QRCW, and PW approach are compared to response theory calculations. By assessing the closeness of the real-time approaches to response theory at different total simulation times, $t_{tot} = (n_r + n_p)t_c = n_{tot}t_c$, we

may compare the accuracy achieved by the three approaches at similar computational costs.

The RCW simulations are performed using $n_{tot} = n_r + 1$, i.e., using the LRCW($n_r, 1$) and QRCW($n_r, 1$) methods, in line with the discussion in Sec. IV A. The first-order dipole response is separated from the time signal using the finite difference formula (10) for all approaches. By point-group symmetry, the polarizability tensors of Ne and CH_4 are equal for all Cartesian directions, and only the zz component is computed. For the NH_3 and HF molecules, the xx and yy polarizability components are the same by symmetry, whereas polarizability tensors for all three Cartesian directions are computed for H_2O. The polarizabilities at the CCSD level for the five systems in the zz direction are displayed in Fig. 5. The other unique polarizability components at the CCSD level

TABLE I. First hyperpolarizabilities, β_{zzz}^{SHG}, extracted from TDCCSD simulations using the LRCW(n_r, n_p) and QRCW(n_r, n_p) methods compared with CCSD linear response results.

	HF	H_2O	NH_3
LRCW(1,4)	14.428	−9.683	29.330
QRCW(1,4)	14.372	−9.588	28.022
QRCW(1,1)	14.375	−9.603	27.941
QRCW(2,1)	14.368	−9.590	28.005
QRCW(3,1)	14.371	−9.590	28.027
QRCW(4,1)	14.372	−9.591	28.020
QRCW(5,1)	14.370	−9.591	28.020
Response	14.370	−9.591	28.020
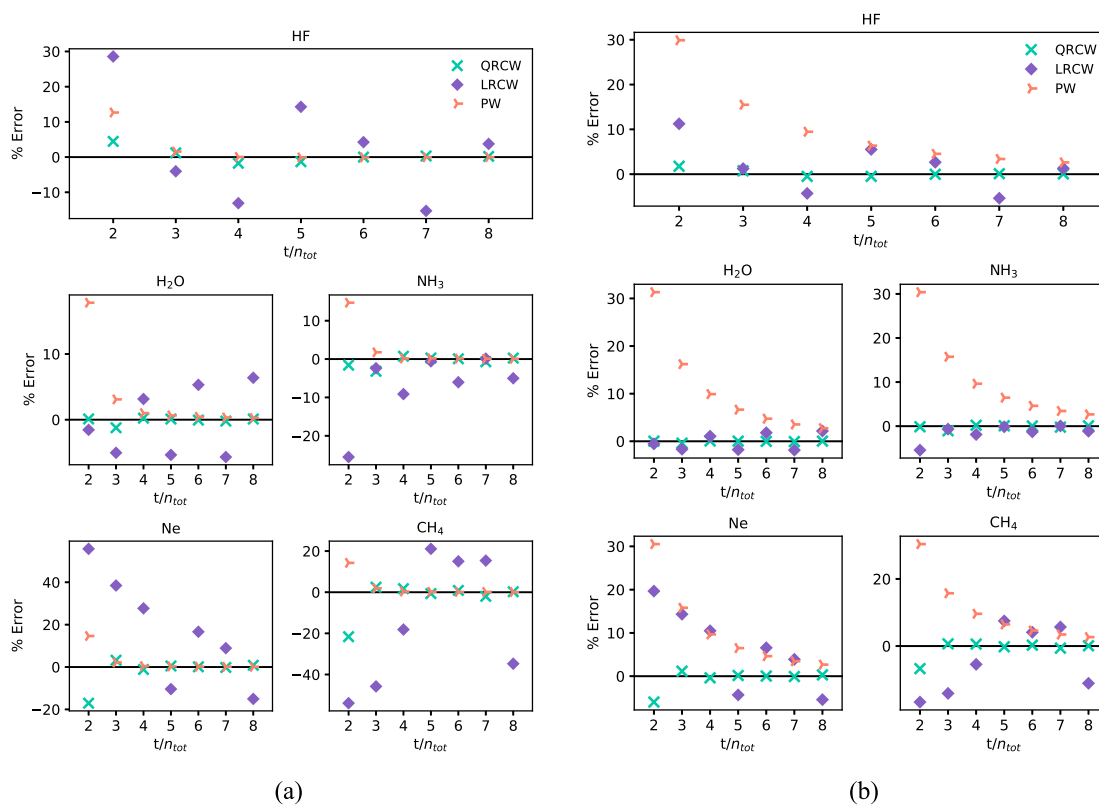
FIG. 7. Convergence toward CCSD cubic response results of second hyperpolarizabilities (a) γ_{zzzz}^{THG} and (b) γ_{zzzz}^{DFWM} extracted from TDCCSD simulations using the LRCW($n_{tot} - 1, 1$), QRCW($n_{tot} - 1, 1$), and PW(n_{tot}) methods.

can be found in the supplementary material along with CC2 level results.

The QRCW approach consistently produces polarizabilities with the highest accuracy, achieving a 0.03% accuracy after the minimum two cycles of total simulation time, $n_r = 1, n_p = 1$. The PW approach requires longer computational time in order to attain polarizabilities of the same accuracy as QRCW, yet it converges

consistently toward the correct value with increasing cycles of simulation time. Albeit with irregular convergence behavior, the LRCW method achieves accuracies comparable to the PW approach as illustrated for the NH_3 and H_2O molecules in Fig. 5.

The errors for the extracted polarizabilities are overall small for all three approaches regardless of ramping. For the shortest ramp length and poorest performing extraction approach, the

TABLE II. The third harmonic generation components $\gamma_{jjjj}^{\text{THG}}$ of the second hyperpolarizabilities of Ne, HF, H$_2$O, NH$_3$, and CH$_4$ extracted from TDCCSD, TDOMP2, TDCC2, and TDCIS simulations compared with results from cubic response theory.

		TDCCSD	TDOMP2	TDCC2	TDCIS		TDCCSD	TDOMP2	TDCC2	TDCIS
HF		$\gamma_{xxxx}^{\text{THG}}$					$\gamma_{zzzz}^{\text{THG}}$			
	PW(3)	−718	−912	−1180	−236		−509	−531	−685	−329
	LRCW(2,1)	−834	−997	−1050	−196		−539	−426	−588	−321
	QRCW(2,1)	−570	−700	−1010	−227		−511	−524	−643	−332
	Response	−625	⋯	−949	−230		−517	⋯	−653	−332
NH$_3$		$\gamma_{yyyy}^{\text{THG}}$					$\gamma_{zzzz}^{\text{THG}}$			
	PW(3)	−1180	−1260	−1380	10.3		−7710	−8930	−9770	−4030
	LRCW(2,1)	−770	−1850	−2010	−470		−8030	−9500	− 11 000	−4310
	QRCW(2,1)	−1260	−1300	−1450	−2.40		−8100	−9070	−9990	−4110
	Response	−1220	⋯	−1420	13.8		−7850	⋯	−9950	−4130
H$_2$O		$\gamma_{xxxx}^{\text{THG}}$					$\gamma_{yyyy}^{\text{THG}}$			
	PW(3)	−1750	−2000	−2320	−796		−546	−562	−653	−14.1
	LRCW(2,1)	−1980	−1930	−2390	−866		−475	− 1040	−766	−174
	QRCW(2,1)	−1820	−2050	−2380	−831		−559	−584	−668	−23.2
	Response	−1800	⋯	−2380	−820		−565	⋯	−675	−13.8
		$\gamma_{zzzz}^{\text{THG}}$								
	PW(3)	−1040	−1150	−1320	−469					
	LRCW(2,1)	−1130	−1050	−1310	−531					
	QRCW(2,1)	−1090	−1180	−1360	−491					
	Response	−1080	⋯	−1360	−483					
Ne		$\gamma_{jjjj}^{\text{THG}}$				CH$_4$	$\gamma_{jjjj}^{\text{THG}}$			
	PW(3)	−119	−129	−148	−61.3		−2670	−2750	−2910	19.2
	LRCW(2,1)	−74.6	−189	−120	−63.5		−3950	−3020	−4140	−720
	QRCW(2,1)	−118	−128	−153	−65.5		−2650	−2800	−2910	2.03
	Response	−122	⋯	−151	−62.8		−2720	⋯	−2960	46.0

polarizability is still correct to 0.25%. This modest error can be reduced to below 0.0009% using the QRCW(7,1) method for all molecules.

C. First hyperpolarizability

The second-order dipole response signal is sensitive to non-adiabatic effects, as seen in Fig. 3. Adiabatic ramping, therefore, is expected to significantly improve accuracy.

Due to symmetry, all the diagonal components of the first hyperpolarizability are zero for the Ne and CH$_4$ molecules. The H$_2$O and the HF molecule exhibit diagonal first hyperpolarizabilities in the zzz-direction, and the NH$_3$ molecule has non-vanishing hyperpolarizabilities in the yyy- and zzz-direction. The β_{zzz}^{SHG} and β_{zzz}^{OR} components extracted from TDCCSD simulations are displayed in Fig. 6. The β_{yyy}^{SHG} and β_{yyy}^{OR} components of NH$_3$ can be found in the supplementary material along with all non-zero diagonal first hyperpolarizabilities at the CC2 level.

The errors of the extracted first hyperpolarizabilities are found to be roughly an order of magnitude greater than for polarizabilities with $n_{\text{tot}} = 2$. Using the LRCW(1,1) method to extract the β_{zzz}^{SHG}

component yields the following % errors: HF 0.33%, H$_2$O 0.33%, and NH$_3$ 2.6%. Using the QRCW(1,1) method reduces these to: HF 0.01%, H$_2$O 0.07%, NH$_3$ 0.2%. We obtain hyperpolarizabilities with the smallest relative errors when applying QRCW(7,1) with accuracies of: HF 0.0006%, H$_2$O 0.001%, NH$_3$ 0.003% for the β_{zzz}^{SHG} component and: HF 0.003%, H$_2$O 0.002%, NH$_3$ 0.005% for the β_{zzz}^{OR} component. With this error reduction the first hyperpolarizability tensors have accuracies comparable to the extracted polarizability tensors.

The PW approach performs surprisingly poorly with regard to extracting the first hyperpolarizabilities as seen in Fig. 6. For the shortest simulation times, some of the errors obtained for the β_{zzz}^{SHG} component are beyond the scale of the plot, especially for the HF molecule. To check convergence, the total propagation time for the HF molecule was increased to PW(20), resulting in a reduction of the error from 0.07% to 0.01% for the β_{zzz}^{OR} component and from −1.8% to 0.29% for the β_{zzz}^{SHG} component. Although improved, the PW(20) results are still of significantly lower accuracy than the RCW(7,1) results, for which the errors are 0.0006% for the β_{zzz}^{OR} component and 0.004% for the β_{zzz}^{SHG} component.

TABLE III. The degenerate four wave mixing component γ_{jjjj}^{DFWM} of the second hyperpolarizabilities of Ne, HF, H_2O, NH_3, and CH_4 extracted from TDCCSD, TDOMP2, TDCC2, and TDCIS simulations compared with results from cubic response theory.

		TDCCSD	TDOMP2	TDCC2	TDCIS		TDCCSD	TDOMP2	TDCC2	TDCIS
HF		γ_{xxxx}^{DFWM}					γ_{zzzz}^{DFWM}			
	PW(3)	−254	−284	−342	−109		−303	−312	−397	−184
	LRCW(2,1)	−326	−360	−397	−134		−354	−334	−424	−219
	QRCW(2,1)	−290	−324	−393	−128		−356	−365	−439	−215
	Response	−298	⋯	−387	−128		−358	⋯	−441	−217
NH_3		γ_{yyyy}^{DFWM}					γ_{zzzz}^{DFWM}			
	PW(3)	−913	−955	−1050	64.2		−4940	−5550	−6100	−2690
	LRCW(2,1)	−948	−1310	−1430	−71.9		−5900	−6540	−7350	−3240
	QRCW(2,1)	−1100	−1140	−1260	73.9		−5930	−6570	−7230	−3190
	Response	−1090	⋯	−1260	78.8		−5870	⋯	−7240	−3200
H_2O		γ_{xxxx}^{DFWM}					γ_{yyyy}^{DFWM}			
	PW(3)	−1260	−1420	−1640	−590		−438	−449	−521	5.67
	LRCW(2,1)	−1550	−1660	−1950	−715		−495	−681	−651	−44.3
	QRCW(2,1)	−1510	−1690	−1950	−706		−522	−538	−621	4.39
	Response	−1510	⋯	−1950	−703		−524	⋯	−623	7.44
		γ_{zzzz}^{DFWM}								
	PW(3)	−803	−877	−1010	−349					
	LRCW(2,1)	−975	−1010	−1180	−431					
	QRCW(2,1)	−963	−1050	−1200	−419					
	Response	−959	⋯	−1200	−417					
Ne		γ_{jjjj}^{DFWM}				CH_4	γ_{jjjj}^{DFWM}			
	PW(3)	−79.3	−84.7	−95.7	−41.8		−1730	−1750	−1870	313
	LRCW(2,1)	−80.6	−114	−105	−51.3		−2330	−2130	−2500	192
	QRCW(2,1)	−93.1	−99.7	−114	−50.4		−2030	−2080	−2200	373
	Response	−94.2	⋯	−114	−49.7		−2050	⋯	−2210	384

The accuracies achieved using the QRCW$(n_r, 1)$ with $n_r = (1, 2, 3, 4, 5)$ are compared to LRCW(1,4) and QRCW(1,4) in Table I. Depending on the demands placed on computational cost and accuracy, it is worth noting that propagating for only two optical cycles ($n_r = n_p = 1$) may be sufficient: The QRCW(1,1) approach produces higher accuracy than the LRCW(1,4) approach.

The errors of the first hyperpolarizabilities presented in this section can be compared with the goodness of fit (r^2) of the signals they were extracted from. Taking NH_3 as an example, increasing n_r from 1 to 7 yields the errors (4.68, 1.08, 1.50, 0.53, 0.93, 0.34, 0.65)% with the LRCW method. As expected, the errors correlate strongly to the coefficient of determination of the signal where they were extracted from; the r^2 value increases as (0.640, 0.989, 0.938, 0.997, 0.977, 0.999, 0.988). This correlation holds true for all molecules, confirming that the r^2 value can be used as a crude indicator of accuracy.

D. Second hyperpolarizability

Accurate extraction of second hyperpolarizabilities is well known to be challenging, showing errors an order of magnitude greater than those observed for the first hyperpolarizabilities.[8] An increase of the r^2 values in the third-order dipole response signal will thus substantially increase trust in second hyperpolarizabilities extracted from real-time simulations.

The errors of the γ_{zzzz}^{THG} components as functions of simulation time are compared for the different approaches in Fig. 7(a) at the CCSD level. Results for the other Cartesian components can be found in the supplementary material, including results obtained from simulations at other levels of theory.

Starting with two cycles of simulation time, the LRCW(1,1) approach produces γ_{zzzz}^{THG} results with errors that vary greatly between the systems, spanning from −1.5% for H_2O to +56% for Ne. Increasing the ramping time to seven optical cycles [LRCW(7,1)] does not reduce the errors which now range from −34% for CH_4 to −16% for Ne. The lacking improvement highlights the convergence issues of the LRCW approach, as is clearly visible in the CH_4 and H_2O panels of Fig. 7(a). The poor convergence is accompanied by dipole response signals $\mu_{zzz}^{(3)}(t)$ that do not show the expected form. For example, the coefficient of determination for CH_4 ranges from $r^2 = 0.09$ to $r^2 = 0.22$ as the number of ramping cycles is increased.
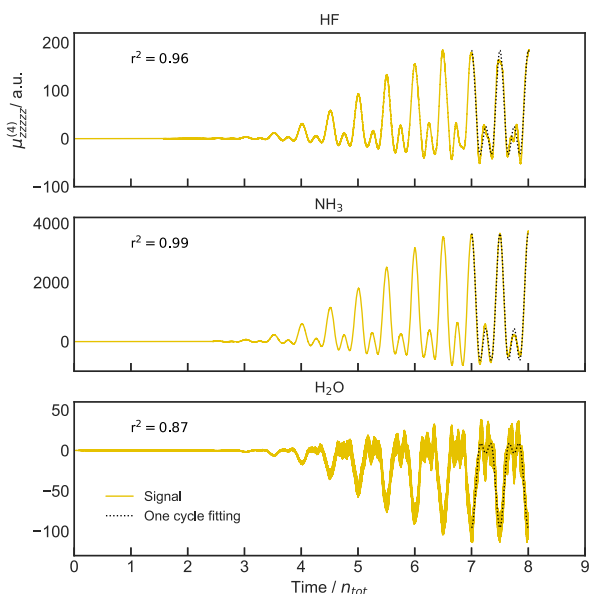
FIG. 8. The fourth-order dipole response functions obtained from TDCCSD simulations for the HF, NH$_3$, and H$_2$O molecules using QRCW(7,1).

TABLE IV. The third hyperpolarizabilities δ_{zzzzz} extracted from TDCCSD simulations with QRCW(2,1), QRCW(7,1), PW(3), and PW(8).

	$\delta^{\mathrm{FHG}}_{zzzzz}$	$\delta^{\mathrm{HSHG}}_{zzzzz}$	$\delta^{\mathrm{HOR}}_{zzzzz}$
HF			
QRCW(2,1)	10 636	3 863	2 726
QRCW(7,1)	11 948	3 808	2 705
PW(3)	14 795	3 082	2 641
PW(8)	12 512	3 699	2 724
NH$_3$			
QRCW(2,1)	324 317	76 998	56 012
QRCW(7,1)	231 482	81 326	53 906
PW(3)	244 356	62 355	52 571
PW(8)	240 228	74 587	54 103
H$_2$O			
QRCW(2,1)	−5 067	−2 271	−1 694
QRCW(7,1)	−4 520	−2 208	−1 662
PW(3)	−4 452	−1 748	−1 608
PW(8)	−4 536	−2 129	−1 665

The PW(2) approach produces $\gamma^{\mathrm{THG}}_{zzzz}$ with small intersystem variations in error; the smallest error is 13% for HF, the largest 17.8% for H$_2$O. The properties also converge in a systematic fashion with increasing simulation time. At the maximum simulation time, the PW(8) method is able to attain errors as small as −0.02% for HF and no larger than −0.25% for H$_2$O.

The QRCW approach produces $\gamma^{\mathrm{THG}}_{zzzz}$ results with the smallest errors. The improvement over the other approaches is most striking when only a few optical cycles of simulation time are used. With QRCW (1,1), one gets $\gamma^{\mathrm{THG}}_{zzzz}$ results with errors smaller than 1.6% for HF, H$_2$O, and NH$_3$ and somewhat higher errors for Ne and CH$_4$. Including an extra ramping cycle, the QRCW(2,1) method reduces the errors of Ne from −17% to 3% and of CH$_4$ from −21% to 2.0%. Hence, the QRCW(2,1) method stands out as a possible compromise between computational cost and accuracy. The most accurate $\gamma^{\mathrm{THG}}_{zzzz}$ results are acquired using the QRCW(7,1) method, achieving accuracies with errors below 0.8% for all systems. However, the lowest error obtained for $\gamma^{\mathrm{THG}}_{zzzz}$ is still a 1000-fold greater than that found for the polarizabilities and $\beta^{\mathrm{OR}}_{zzzz}$, showing that some loss of accuracy must be expected for higher-order responses.

The extracted $\gamma^{\mathrm{DFWM}}_{zzzz}$ results [Fig. 7(b)] behave similarly to $\gamma^{\mathrm{THG}}_{zzzz}$. The errors are generally large when two cycles of simulation time is used, 20% for LRCW(1,1), 31% for PW(2), and −6.7% for QRCW(1,1). Increasing the simulation time quickly leads to very accurate results when using the QRCW approach, less so for the PW approach, and the LRCW approach continues to perform irregularly as a function of simulation time. The main difference between the $\gamma^{\mathrm{DFWM}}_{zzzz}$ and the $\gamma^{\mathrm{THG}}_{zzzz}$ results lies in the slower convergence with increasing simulation time for the PW approach. The inferior performance of PW for $\gamma^{\mathrm{DFWM}}_{zzzz}$ resembles the poorer performance found for β^{SHG}. The $\gamma^{\mathrm{DFWM}}_{zzzz}$ results are accurate to within 0.3% for all systems when using the QRCW(7,1) approach.

Also, for the second hyperpolarizability, we find a relation between r^2 values of the fit with the errors observed, confirming that r^2 values close to 1 are needed for a reliable extraction. The results obtained with the TDCCSD, TDOMP2, TDCC2, and TDCIS methods for $\gamma^{\mathrm{THG}}_{xxxx}$, $\gamma^{\mathrm{THG}}_{yyyy}$, and $\gamma^{\mathrm{THG}}_{zzzz}$ after a total simulation time of three optical cycles are shown in Table II. The $\gamma^{\mathrm{DFWM}}_{xxxx}$, $\gamma^{\mathrm{DFWM}}_{yyyy}$, and $\gamma^{\mathrm{DFWM}}_{zzzz}$ results are shown in Table III. In general, we observe that the QRCW(2,1) approach yields more accurate second hyperpolarizabilities than the LRCW(2,1) and PW(3) approaches regardless of the electronic-structure method used. We note in passing that, in agreement with the observations made in Ref. 17, the TDOMP2 method yields optical properties that fall between those of the TDCC2 and TDCCSD methods. Although there is no response data available for the OMP2 method, we may assume that the TDOMP2 values reported with the QRCW approach is correct to within 1% based on the accuracies observed for the TDCCSD, TDCC2, and TDCIS methods.

As expected,[61] the simulations at the TDCIS level provides optical properties vastly different from the other three methods due to lack of electron correlation. Since the fourth-order dipole signal is very weak, separation by numerical differentiation is more challenging. Although the optimal choice of the electric-field strength is beyond the scope of this paper, we remark that increasing the electric-field strength from $E = 0.001$ to $E = 0.004$ seems to reduce the error of the numerical differentiation for the TDCIS method.

E. Third hyperpolarizability

The RCW and PW approaches can straightforwardly be extended to evaluate higher order properties, here exemplified with third hyperpolarizabilities. An example of extracting fourth hyperpolarizabilities can be found in the supplementary material.

To the best of our knowledge, there are no implemented analytic response functions available for third hyperpolarizabilities.

Instead, we will use the r^2 value of the fit to the fourth-order dipole response function $\mu^{(4)}(t)$ to gauge the accuracy of the extracted third hyperpolarizabilities. Figure 8 shows $\mu_{zzzzz}^{(4)}(t)$ calculated at the TDCCSD level of theory along with the associated curve fitting using the QRCW(7,1) method. The fitted curves have r^2 values ranging from 0.87 to 0.99, indicating that only the third hyperpolarizability results for NH$_3$ ($r^2 = 0.99$) and HF ($r^2 = 0.96$) are fully reliable while the results for H$_2$O are decent estimates.

The third hyperpolarizabilities for HF, NH$_3$, and H$_2$O are given in in Table IV. The discrepancies between the PW and RCW approaches are modest, typically on the order of 3% for the $\delta_{zzzzz}^{\text{FHG}}$ and 0.5% for the $\delta_{zzzzz}^{\text{HSHG}}$ when simulating for a total of eight optical cycles. Increasing the total simulation time (i.e., increasing n_r in the case of the QRCW approach) is likely to improve the accuracy further, in analogy to the convergence behavior observed for the lower-order responses above.

V. CONCLUDING REMARKS

We have compared three approaches to the extraction of linear and nonlinear optical properties from electron dynamics simulations with respect to accuracy relative to results from response theory and computational effort. The LRCW and QRCW approaches are based on a monochromatic continuous wave perturbation ramped from zero to full strength linearly and quadratically, while the PW approach uses Fourier filtering to extract properties at a given frequency from signals recorded during the interaction of electrons with a finite laser pulse. All three approaches rely on numerical (finite-difference) differentiation to separate different orders of response in the time domain, followed by curve fitting to obtain the property of interest at a given frequency.

Showing irregular convergence behavior toward response results as the ramping time is increased, the LRCW approach is difficult to apply reliably for higher-order nonlinear responses. Using a single optical cycle for ramping is found to be insufficient. On the other hand, we find that the post-ramp simulation time can be reduced to a single cycle without incurring an accuracy penalty The QRCW approach, proposed in this work, is a clear improvement due to reduced nonadiabatic effects. Although the convergence behavior remains somewhat irregular, errors observed for linear and nonlinear response properties are significantly reduced. Our tests indicate that the QRCW approach yields highly accurate linear and quadratic response properties with simulation times as short as two optical cycles, one cycle for ramping and one post-ramp cycle for extracting the response property of interest from wave-function simulations. An additional ramp cycle should be added to reliably extract cubic response properties, however. The QRCW approach thus yields significantly improved accuracy at about half the computational cost of the LRCW approach.

We find that the coefficient of determination (r^2) obtained for the curve fitting can be used as an indicator of accuracy *in lieu* of analytical results from response theory. In all cases studied in this work, the r^2 value can be improved by increasing the ramping time of the QRCW approach.

The PW approach offers an alternative to QRCW. The PW approach shows monotonous but typically rather slow convergence toward response results with respect to simulation time. For comparable accuracy, the PW approach typically requires much longer simulation times than the QRCW approach, which we recommend for reliable and efficient extraction of linear and nonlinear response properties.

While our tests are based on TDCC and TDCIS methods, we expect that our conclusions remain valid also for other electronic-structure methods, hopefully including time-dependent density-functional theory which has yet to be tested.

SUPPLEMENTARY MATERIAL

The HF, H$_2$O, NH$_3$, and CH$_4$ geometries used throughout this article can be found in Sec. I of the supplementary material. The procedure for finding the fifth-order hyperpolarizabilities and example calculations for the HF molecule are found in Sec. II. Tables displaying polarizabilities, first hyperpolarizabilities, and second hyperpolarizabilities extracted using QRCW(7,1), LRCW(7,1), and PW(8) for all unique diagonal directions at the CC2, OMP2, CIS, and CCSD levels of theory are available in Sec. III. Finally, figures displaying the relative errors of the polarizabilities, first hyperpolarizabilities, and second hyperpolarizabilities as functions of $n_{\text{tot}} = (2, 3, 4, 5, 6, 7, 8)$ at the CC2 and CCSD levels of theory for all diagonal directions are available in Sec. IV.

ACKNOWLEDGMENTS

AUTHOR DECLARATIONS

Conflict of Interest

The authors have no conflicts to disclose.

Author Contributions

Benedicte Sverdrup Ofstad: Conceptualization (equal); Formal analysis (lead); Investigation (lead); Software (equal); Validation (lead); Visualization (lead); Writing – original draft (lead). **Håkon Emil Kristiansen**: Formal analysis (supporting); Software (equal); Writing – original draft (supporting). **Einar Aurbakken**: Software (equal); Writing – original draft (supporting). **Øyvind Sigmundson Schøyen**: Software (equal); Writing – original draft (supporting). **Simen Kvaal**: Funding acquisition (equal); Software (equal); Visualization (supporting); Writing – review & editing (equal). **Thomas Bondo Pedersen**: Conceptualization (equal); Funding acquisition (equal); Software (equal); Supervision (lead); Writing – original draft (equal); Writing – review & editing (equal).

DATA AVAILABILITY

The data that support the findings of this study are available from the corresponding author upon reasonable request.

REFERENCES

[1] K. Yabana and G. F. Bertsch, "Time-dependent local-density approximation in real time," Phys. Rev. B **54**, 4484–4487 (1996).

[2] A. Tsolakidis, D. Sánchez-Portal, and R. M. Martin, "Calculation of the optical response of atomic clusters using time-dependent density functional theory and local orbitals," Phys. Rev. B **66**, 235416 (2002).

[3] K. Yabana, T. Nakatsukasa, J.-I. Iwata, and G. F. Bertsch, "Real-time, real-space implementation of the linear response time-dependent density-functional theory," Phys. Status Solidi B **243**, 1121–1138 (2006).

[4] F. Wang, C. Y. Yam, G. Chen, and K. Fan, "Density matrix based time-dependent density functional theory and the solution of its linear response in real time domain," J. Chem. Phys. **126**, 134104 (2007).

[5] F. Wang, C. Y. Yam, and G. Chen, "Time-dependent density-functional theory/localized density matrix method for dynamic hyperpolarizability," J. Chem. Phys. **126**, 244102 (2007).

[6] Y. Takimoto, F. D. Vila, and J. J. Rehr, "Real-time time-dependent density functional theory approach for frequency-dependent nonlinear optical response in photonic molecules," J. Chem. Phys. **127**, 154114 (2007).

[7] V. A. Goncharov and K. Varga, "Real-space, real-time calculation of dynamic hyperpolarizabilities," J. Chem. Phys. **137**, 094111 (2012).

[8] F. Ding, B. E. Van Kuiken, B. E. Eichinger, and X. Li, "An efficient method for calculating dynamical hyperpolarizabilities using real-time time-dependent density functional theory," J. Chem. Phys. **138**, 064104 (2013).

[9] M. Yamaguchi and K. Nobusada, "Large hyperpolarizabilities of the second harmonic generation induced by nonuniform optical near fields," J. Phys. Chem. C **120**, 23748–23755 (2016).

[10] L. Konecny, M. Kadek, S. Komorovsky, O. L. Malkina, K. Ruud, and M. Repisky, "Acceleration of relativistic electron dynamics by means of X_2C transformation: Application to the calculation of nonlinear optical properties," J. Chem. Theory Comput. **12**, 5823–5833 (2016).

[11] T. Yatsui, M. Yamaguchi, and K. Nobusada, "Nano-scale chemical reactions based on non-uniform optical near-fields and their applications," Prog. Quantum Electron. **55**, 166–194 (2017).

[12] P. J. Lestrange, M. R. Hoffmann, and X. Li, "Time-dependent configuration interaction using the graphical unitary group approach: Nonlinear electric properties," in *Advances in Quantum Chemistry, Novel Electronic Structure Theory: General Innovations and Strongly Correlated Systems*, edited by P. E. Hoggan (Academic Press, 2018), Vol. 76, pp. 295–313.

[13] J. J. Goings, P. J. Lestrange, and X. Li, "Real-time time-dependent electronic structure theory," Wiley Interdiscip. Rev.: Comput. Mol. Sci. **8**, e1341 (2018).

[14] M. Uemoto, Y. Kuwabara, S. A. Sato, and K. Yabana, "Nonlinear polarization evolution using time-dependent density functional theory," J. Chem. Phys. **150**, 094101 (2019).

[15] X. Li, N. Govind, C. Isborn, A. E. DePrince, and K. Lopata, "Real-time time-dependent electronic structure theory," Chem. Rev. **120**, 9951–9993 (2020).

[16] A. Baiardi, "Electron dynamics with the time-dependent density matrix renormalization group," J. Chem. Theory Comput. **17**, 3320–3334 (2021).

[17] H. E. Kristiansen, B. S. Ofstad, E. Hauge, E. Aurbakken, Ø. S. Schøyen, S. Kvaal, and T. B. Pedersen, "Linear and nonlinear optical properties from TDOMP2 theory," J. Chem. Theory Comput. **18**, 3687–3702 (2022).

[18] H. E. Kristiansen, B. S. Ofstad, E. Hauge, E. Aurbakken, Ø. S. Schøyen, S. Kvaal, and T. B. Pedersen, "Correction to "linear and nonlinear optical properties from TDOMP2 theory,"" J. Chem. Theory Comput. **18**, 5755–5757 (2022).

[19] J. Olsen and P. Jørgensen, "Linear and nonlinear response functions for an exact state and for an MCSCF state," J. Chem. Phys. **82**, 3235–3264 (1985).

[20] O. Christiansen, P. Jørgensen, and C. Hättig, "Response functions from Fourier component variational perturbation theory applied to a time-averaged quasienergy," Int. J. Quantum Chem. **68**, 1–52 (1998).

[21] P. N. Butcher and D. Cotter, *The Elements of Nonlinear Optics*, Cambridge Studies in Modern Optics (Cambridge University Press, Cambridge, 1990).

[22] T. Helgaker, S. Coriani, P. Jørgensen, K. Kristensen, J. Olsen, and K. Ruud, "Recent advances in wave function-based methods of molecular-property calculations," Chem. Rev. **112**, 543–631 (2012).

[23] S. Hermanns, K. Balzer, and M. Bonitz, "The non-equilibrium Green function approach to inhomogeneous quantum many-body systems using the generalized Kadanoff–Baym ansatz," Phys. Scr. **T151**, 014036 (2012).

[24] I. Barth and C. Lasser, "Trigonometric pulse envelopes for laser-induced quantum dynamics," J. Phys. B: At., Mol. Opt. Phys. **42**, 235101 (2009).

[25] J. B. Foresman, M. Head-Gordon, J. A. Pople, and M. J. Frisch, "Toward a systematic molecular orbital theory for excited states," J. Phys. Chem. **96**, 135–149 (1992).

[26] T. Klamroth, "Laser-driven electron transfer through metal-insulator-metal contacts: Time-dependent configuration interaction singles calculations for a jellium model," Phys. Rev. B **68**, 245421 (2003).

[27] C. Huber and T. Klamroth, "Explicitly time-dependent coupled cluster singles doubles calculations of laser-driven many-electron dynamics," J. Chem. Phys. **134**, 054113 (2011).

[28] T. B. Pedersen and S. Kvaal, "Symplectic integration and physical interpretation of time-dependent coupled-cluster theory," J. Chem. Phys. **150**, 144106 (2019).

[29] T. B. Pedersen, H. E. Kristiansen, T. Bodenstein, S. Kvaal, and Ø. S. Schøyen, "Interpretation of coupled-cluster many-electron dynamics in terms of stationary states," J. Chem. Theory Comput. **17**, 388–404 (2021).

[30] O. Christiansen, H. Koch, and P. Jørgensen, "The second-order approximate coupled cluster singles and doubles model CC2," Chem. Phys. Lett. **243**, 409–418 (1995).

[31] H. Pathak, T. Sato, and K. L. Ishikawa, "Time-dependent optimized coupled-cluster method for multielectron dynamics. III. A second-order many-body perturbation approximation," J. Chem. Phys. **153**, 034110 (2020).

[32] D. R. Nascimento and A. E. DePrince, "Linear absorption spectra from explicitly time-dependent equation-of-motion coupled-cluster theory," J. Chem. Theory Comput. **12**, 5834–5840 (2016).

[33] D. R. Nascimento and A. E. DePrince, "Simulation of near-edge x-ray absorption fine structure with time-dependent equation-of-motion coupled-cluster theory," J. Phys. Chem. Lett. **8**, 2951–2957 (2017).

[34] Y. C. Park, A. Perera, and R. J. Bartlett, "Equation of motion coupled-cluster for core excitation spectra: Two complementary approaches," J. Chem. Phys. **151**, 164117 (2019).

[35] L. N. Koulias, D. B. Williams-Young, D. R. Nascimento, A. E. DePrince, and X. Li, "Relativistic real-time time-dependent equation-of-motion coupled-cluster," J. Chem. Theory Comput. **15**, 6617–6624 (2019).

[36] B. C. Cooper, L. N. Koulias, D. R. Nascimento, X. Li, and A. E. DePrince, "Short iterative lanczos integration in time-dependent equation-of-motion coupled-cluster theory," J. Phys. Chem. A **125**, 5438–5447 (2021).

[37] Y. C. Park, A. Perera, and R. J. Bartlett, "Equation of motion coupled-cluster study of core excitation spectra II: Beyond the dipole approximation," J. Chem. Phys. **155**, 094103 (2021).

[38] A. S. Skeidsvoll, A. Balbi, and H. Koch, "Time-dependent coupled-cluster theory for ultrafast transient-absorption spectroscopy," Phys. Rev. A **102**, 023115 (2020).

[39] A. S. Skeidsvoll, T. Moitra, A. Balbi, A. C. Paul, S. Coriani, and H. Koch, "Simulating weak-field attosecond processes with a Lanczos reduced basis approach to time-dependent equation-of-motion coupled-cluster theory," Phys. Rev. A **105**, 023103 (2022).

[40] E. Luppi and M. Head-Gordon, "Computation of high-harmonic generation spectra of H_2 and N_2 in intense laser pulses using quantum chemistry methods and time-dependent density functional theory," Mol. Phys. **110**, 909–923 (2012).

[41] T. Sato, H. Pathak, Y. Orimo, and K. L. Ishikawa, "Communication: Time-dependent optimized coupled-cluster method for multielectron dynamics," J. Chem. Phys. **148**, 051101 (2018).

[42] H. Pathak, T. Sato, and K. L. Ishikawa, "Time-dependent optimized coupled-cluster method for multielectron dynamics. II. A coupled electron-pair approximation," J. Chem. Phys. **152**, 124115 (2020).

[43] H. Pathak, T. Sato, and K. L. Ishikawa, "Study of laser-driven multielectron dynamics of Ne atom using time-dependent optimised second-order many-body perturbation theory," Mol. Phys. **118**, e1813910 (2020).

94

[44] H. Pathak, T. Sato, and K. L. Ishikawa, "Time-dependent optimized coupled-cluster method for multielectron dynamics. IV. Approximate consideration of the triple excitation amplitudes," J. Chem. Phys. **154**, 234104 (2021).

[45] T. B. Pedersen and H. Koch, "Coupled cluster response functions revisited," J. Chem. Phys. **106**, 8059–8072 (1997).

[46] D. E. Woon and T. H. Dunning, "Gaussian basis sets for use in correlated molecular calculations. IV. Calculation of static electrical response properties," J. Chem. Phys. **100**, 2975–2988 (1994).

[47] R. A. Kendall, T. H. Dunning, and R. J. Harrison, "Electron affinities of the first-row atoms revisited. Systematic basis sets and wave functions," J. Chem. Phys. **96**, 6796–6806 (1992).

[48] B. P. Pritchard, D. Altarawy, B. Didier, T. D. Gibson, and T. L. Windus, "New basis set Exchange: An open, up-to-date resource for the molecular sciences community," J. Chem. Inf. Model. **59**, 4814–4820 (2019).

[49] Q. Sun, T. C. Berkelbach, N. S. Blunt, G. H. Booth, S. Guo, Z. Li, J. Liu, J. D. McClain, E. R. Sayfutyarova, S. Sharma, S. Wouters, and G. K. L. Chan, "PySCF: The python-based simulations of chemistry framework," Wiley Interdiscip. Rev.: Comput. Mol. Sci. **8**, e1340 (2018).

[50] E. Aurbakken, H. E. Kristiansen, S. Kvaal, B. S. Ofstad, T. B. Pedersen, Ø. S. Schøyen, "HyQD," 04 February 2023, URL: https://github.com/HyQD.

[51] E. Hairer, G. Wanner, and C. Lubich, *Geometric Numerical Integration*, Springer Series in Computational Mathematics Vol. 31, 2nd ed. (Springer, Berlin, Heidelberg, 2006).

[52] P. Virtanen, R. Gommers, T. E. Oliphant, M. Haberland, T. Reddy, D. Cournapeau, E. Burovski, P. Peterson, W. Weckesser, J. Bright, S. J. van der Walt, M. Brett, J. Wilson, K. J. Millman, N. Mayorov, A. R. J. Nelson, E. Jones, R. Kern, E. Larson, C. J. Carey, İ. Polat, Y. Feng, E. W. Moore, J. VanderPlas, D. Laxalde, J. Perktold, R. Cimrman, I. Henriksen, E. A. Quintero, C. R. Harris, A. M. Archibald, A. H. Ribeiro, F. Pedregosa, P. van Mulbregt, and SciPy 1.0 Contributors, "SciPy 1.0: Fundamental algorithms for scientific computing in Python," Nat. Methods **17**, 261–272 (2020).

[53] K. Aidas, C. Angeli, K. L. Bak, V. Bakken, R. Bast, L. Boman, O. Christiansen, R. Cimiraglia, S. Coriani, P. Dahle, E. K. Dalskov, U. Ekström, T. Enevoldsen, J. J. Eriksen, B. Ettenhuber, B. Fernández, L. Ferrighi, H. Fliegl, L. Frediani, K. Hald, A. Halkier, C. Hättig, H. Heiberg, T. Helgaker, A. C. Hennum, H. Hettema, E. Hjertenaes, S. Høst, I.-M. Høyvik, M. F. Iozzi, B. Jansík, H. J. A. Jensen, D. Jonsson, P. Jørgensen, J. Kauczor, S. Kirpekar, T. Kjaergaard, W. Klopper, S. Knecht, R. Kobayashi, H. Koch, J. Kongsted, A. Krapp, K. Kristensen, A. Ligabue, O. B. Lutnaes, J. I. Melo, K. V. Mikkelsen, R. H. Myhre, C. Neiss, C. B. Nielsen, P. Norman, J. Olsen, J. M. H. Olsen, A. Osted, M. J. Packer, F. Pawlowski, T. B. Pedersen, P. F. Provasi, S. Reine, Z. Rinkevicius, T. A. Ruden, K. Ruud, V. V. Rybkin, P. Sałek, C. C. M. Samson, A. S. de Merás, T. Saue, S. P. A. Sauer, B. Schimmelpfennig, K. Sneskov, A. H. Steindal, K. O. Sylvester-Hvid, P. R. Taylor, A. M. Teale, E. I. Tellgren, D. P. Tew, A. J. Thorvaldsen, L. Thøgersen, O. Vahtras, M. A. Watson, D. J. D. Wilson, M. Ziolkowski, and H. Ågren, "The Dalton quantum chemistry program system," Wiley Interdiscip. Rev.: Comput. Mol. Sci. **4**, 269–284 (2014).

[54] J. M. H. Olsen, S. Reine, O. Vahtras, E. Kjellgren, P. Reinholdt, K. O. Hjorth Dundas, X. Li, J. Cukras, M. Ringholm, E. D. Hedegård, R. Di Remigio, N. H. List, R. Faber, B. N. Cabral Tenorio, R. Bast, T. B. Pedersen, Z. Rinkevicius, S. P. A. Sauer, K. V. Mikkelsen, J. Kongsted, S. Coriani, K. Ruud, T. Helgaker, H. J. A. Jensen, and P. Norman, "Dalton project: A Python platform for molecular- and electronic-structure simulations of complex systems," J. Chem. Phys. **152**, 214115 (2020).

[55] H. Koch, A. Sánchez de Merás, T. Helgaker, and O. Christiansen, "The integral-direct coupled cluster singles and doubles model," J. Chem. Phys. **104**, 4157–4165 (1996).

[56] A. Halkier, H. Koch, O. Christiansen, P. Jørgensen, and T. Helgaker, "First-order one-electron properties in the integral-direct coupled cluster singles and doubles model," J. Chem. Phys. **107**, 849–866 (1997).

[57] O. Christiansen, A. Halkier, H. Koch, P. Jørgensen, and T. Helgaker, "Integral-direct coupled cluster calculations of frequency-dependent polarizabilities, transition probabilities, and excited-state properties," J. Chem. Phys. **108**, 2801–2816 (1998).

[58] C. Hättig, O. Christiansen, H. Koch, and P. Jørgensen, "Frequency-dependent first hyperpolarizabilities using coupled cluster quadratic response theory," Chem. Phys. Lett. **269**, 428–434 (1997).

[59] C. Hättig, O. Christiansen, and P. Jørgensen, "Frequency-dependent second hyperpolarizabilities using coupled cluster cubic response theory," Chem. Phys. Lett. **282**, 139–146 (1998).

[60] B. J. Orr and J. F. Ward, "Perturbation theory of the non-linear optical polarization of an isolated system," Mol. Phys. **20**, 513–526 (1971).

[61] H. Larsen, J. Olsen, C. Hättig, P. Jørgensen, O. Christiansen, and J. Gauss, "Polarizabilities and first hyperpolarizabilities of HF, Ne, and BH from full configuration interaction and coupled cluster calculations," J. Chem. Phys. **111**, 1917–1925 (1999).

Paper III

Magnetic optical activity from real-time simulations

III

Magnetic Optical Rotation from Real-Time Simulations in Finite Magnetic Fields

Benedicte Sverdrup Ofstad,[1, a)] Meilani Wibowo-Teale,[2] Håkon Emil Kristiansen,[1] Einar Aurbakken,[1] Marios Petros Kitsaras,[3] Øyvind Sigmundson Schøyen,[4] Eirill Hauge,[1, 5] Tom J. P. Irons,[2] Simen Kvaal,[1] Stella Stopkowicz,[1, 3] Andrew M. Wibowo-Teale,[1, 2] and Thomas Bondo Pedersen[1, b)]

[1)] *Hylleraas Centre for Quantum Molecular Sciences, Department of Chemistry, University of Oslo, Norway*

[2)] *School of Chemistry, University of Nottingham, University Park, Nottingham NG7 2RD, United Kingdom*

[3)] *University of Saarland, Physical and Theoretical Chemistry, Campus B2.2, 66123, Saarbruecken, Germany*

[4)] *Department of Physics, University of Oslo, Norway*

[5)] *Department of Numerical Analysis and Scientific Computing, Simula Research Laboratory, 0164 Oslo, Norway*

We present a numerical approach to magnetic optical rotation based on real-time time-dependent electronic-structure theory. Not relying on perturbation expansions in the magnetic-field strength, the formulation allows us to test the range of validity of the linear relation between the rotation angle per unit path length and the magnetic-field strength that was established empirically by Verdet 160 years ago. Results obtained from time-dependent coupled-cluster and time-dependent current density-functional theory are presented for the closed-shell molecules H_2, HF, and CO in magnetic fields up to $55\,kT$ at standard temperature and pressure conditions. We find that Verdet's linearity remains valid up to roughly 10–$20\,kT$, above which significant deviations from linearity are observed. Among the three current density-functional approximations tested in this work, the current-dependent Tao-Perdew-Staroverov–Scuseria hybrid functional performs the best in comparison with time-dependent coupled-cluster singles and doubles results for the magnetic optical rotation.

I. INTRODUCTION

Nonperturbative approaches to matter-field interactions have found increasing use in electronic-structure theory over the past decades. Not only do such approaches allow one to overcome the inherent limitations of perturbation theory—weak field strengths, adiabatic switching-on of the fields, (lack of) convergence of the perturbation series—they also pave the way for fundamental discoveries, such as the paramagnetic bonding mechanism in strong magnetic fields[1] or the quantum-dynamical mechanism underpinning high-harmonic generation.[2]

Using atom-centered Gaussian basis sets, quantum-chemical studies of electronic ground and bound excited states in strong magnetic fields up to about one atomic unit $(1\,B_0 = m_e E_h / e\hbar \approx 235\,052\,T)$ are often motivated by the astrophysical search for heavier atoms and even complex polyatomic molecules in, e.g., the atmosphere of magnetic white dwarfs.[3] Such calculations require some modifications of existing implementations of commonly used electronic-structure theories such as Hartree–Fock theory,[4–7] full configuration-interaction (FCI) theory,[1] and coupled-cluster (CC) theory.[8–11] In the case of density-functional theory (DFT), however, a more fundamental change is required since the density-

functional approximation must depend on the current density in addition to the electron density to be applicable to electrons in a static uniform magnetic field.[12–17] As an added benefit, the resulting current density-functional theory (CDFT)[15] is applicable also at low magnetic-field strengths, thus potentially improving upon results obtained from conventional DFT for, e.g., nuclear magnetic resonance shielding constants.

Similarly, real-time time-dependent electronic-structure theory[18,19] allows one to simulate laser-induced quantum dynamics without invoking perturbation theory. This is particularly important for the simulation of time-resolved spectroscopies where a pump laser is used to create a non-stationary electronic wave packet, which is then probed by a second laser pulse applied at variable delays relative to the pump laser. With attosecond laser pulses, it thus becomes possible to observe and manipulate ultrafast electronic motion, opening a new field of chemistry—attochemistry.[20,21] Moreover, by carefully choosing laser-pulse parameters such as shape, electric-field strength, and carrier frequency, it becomes possible to extract complete linear absorption spectra, including bound core as well as valence excitations, and low-order nonlinear optical properties from a single or a few simulations.[19]

By combining the nonperturbative treatment of static uniform magnetic fields with real-time time-dependent electronic-structure theory of laser-driven multi-electron dynamics we get access to magnetic-field-induced, frequency-dependent molecular properties such as mag-

[a)] Electronic mail: b.s.ofstad@kjemi.uio.no
[b)] Electronic mail: t.b.pedersen@kjemi.uio.no

netic optical rotation (MOR). Also named the Faraday effect after its discoverer,[22] MOR is the rotation of the polarization plane of linearly polarized light passing through a transparent medium in the presence of a magnetic field with nonzero component along the propagation direction of the light beam. While phenomenologically similar,[23] MOR differs from natural optical rotation by being observable for chiral and achiral molecules alike.

The Faraday effect, which was of pivotal importance for the development of Maxwell's electromagnetic theory,[24] is today exploited in a large number of technological applications, including fiber-optic current sensors,[25] satellite communication systems,[26] and measurement of interstellar and intergalactic magnetic fields.[27] Consequently, much research effort remains invested in the development of high-MOR materials.[28] The foundation of these applications is the linear relationship, discovered through a series of thorough experiments by Verdet,[29,30] between the rotation angle θ per unit path length ℓ and the magnetic-field strength B along the propagation direction of the light: $\theta/\ell = VB$. The constant of proportionality, the Verdet constant V, was found by Verdet to depend on the frequency of the light and to be characteristic of each type of molecule such that V for a given solution can be obtained by summation over the contributions from each solute and solvent molecule.[29–32] Verdet's linear law is commonly used to measure the strength of magnetic fields generated by, e.g., laser-driven micro coils.[33] As an example, Nakamura *et al.*[34] recently reported a "record indoor magnetic field of 1200 T", which was measured using MOR with the underlying assumption that the Verdet constant is essentially independent of the magnetic field strength, even for such a strong field. It is, therefore, of interest to investigate the range of validity of Verdet's linear relationship using a nonperturbative approach.

Based on Verdet's observations, a quantum-mechanical account of the microscopic origin of MOR can be approximately reduced to the response of a single molecule to a static uniform magnetic field and a time-dependent uniform electric field.[23,35,36] Accordingly, Parkinson and Oddershede formulated the Verdet constant in terms of a mixed magnetoelectric quadratic response function, i.e., a third-order mixed perturbation theory, linear in the magnetic field and quadratic in the electric field.[37] The response-function approach has been used to compute Verdet constants at the CC level of theory by Coriani et al.[38–40]

Avoiding the perturbation expansion in the magnetic-field strength, we will in this work investigate the range of validity of the linear relationship between θ/l and B using real-time time-dependent coupled-cluster (TDCC) theory[41] and real-time time-dependent current density-functional theory (TDCDFT).[42] This allows, for the first time, a direct comparison of electron dynamics simulations at the TDCDFT and TDCC levels of theory. Moreover, by using real-time simulations instead of perturbation theory for the interaction with the radiation field,

the present work constitutes the initial steps towards simulations of highly nonlinear processes such as high-harmonic generation and ionization in the presence of a finite magnetic field.

This paper is organized as follows. The general quantum-mechanical theory of MOR is outlined in Sec. II along with a description of how real-time time-dependent electronic-structure simulations may be utilized to compute θ/l without perturbation expansion in B. In Sec. III we validate our magnetic-field-dependent implementation of various TDCC theories by comparing linear absorption spectra from simulations at finite B with those obtained from equation-of-motion excitation-energy coupled-cluster (EOM-EE-CC) theory,[9] followed by presentation and discussion of MOR results obtained from TDCDFT and TDCC simulations. Finally, Sec. IV contains our concluding remarks.

II. THEORY

A. Magnetic optical rotation

The polarization plane of linearly polarized light propagating parallel to a static uniform magnetic field through a sample of molecules is rotated by an angle θ_r, given by[23,35,36]

$$\frac{\theta_r}{\ell} = \frac{1}{3}C\omega \sum_{ijk} \epsilon_{ijk} \text{Im}\left[\alpha_{ij}^{(k)}(-\omega;\omega)\right], \qquad (1)$$

where ℓ is the path length, ω is the angular frequency of the light, $\alpha_{ij}^{(k)}(-\omega;\omega)$ is the Cartesian ij component of the molecular polarizability tensor in the presence of the magnetic field along axis k, and ϵ_{ijk} denotes the Levi–Civita symbol. The subscript r signifies that the sample of molecules are randomly oriented. The constant C is given by

$$C = \frac{1}{2c}\left(\frac{2\pi\mathcal{N}}{4\pi\epsilon_0}\right), \qquad (2)$$

where $\mathcal{N}$ is the number density, c is the speed of light, and ϵ_0 is the vacuum permittivity.

For weak magnetic fields, the polarizability α_{ij}^k may be expanded to first order in the magnetic-field strength B, leading to the conventional formula

$$\frac{\theta_r}{\ell} = V(\omega)B, \qquad (3)$$

where $V(\omega)$ is the Verdet constant, which can be expressed in terms of frequency-dependent quadratic response functions.[37–40,43] Avoiding the expansion in B, we instead work treat the magnetic field nonperturbatively and thus enable the calculation of MOR at any magnetic-field strength.

As the magnetic-field strength grows, however, the ori-

enting effect of the magnetic field becomes increasingly important.[44] In lieu of a rigorous averaging procedure, we also compute the MOR assuming that all molecules of the sample are found in the energetically most favorable geometry and orientation relative to the magnetic field. For the case of fixed orientation, denoted with the subscript o, we use the following expression for the MOR per unit path length,

$$\frac{\theta_o}{\ell} = C\omega\mathrm{Im}\left[\alpha_{xy}^{(z)}(-\omega;\omega)\right], \tag{4}$$

where the magnetic field vector is chosen parallel to the z-axis.

We now turn to the problem of extracting the complex frequency-dependent polarizability from simulations of laser-driven electron dynamics in the presence of a static uniform magnetic field. We note in passing that the polarizability tensor could equally well be computed from frequency-dependent linear response theory[45] in the presence of a finite magnetic field but, to our knowledge, no such implementation has been reported for neither CC theory nor CDFT.

B. Electron dynamics in a finite magnetic field

We consider a nonrelativistic atomic or molecular system with N electrons exposed to a static uniform magnetic field $\boldsymbol{B}$ and a time-dependent radiation field with the electric and magnetic fields $\boldsymbol{\mathcal{E}}(\boldsymbol{r},t)$ and $\boldsymbol{\mathcal{B}}(\boldsymbol{r},t)$. Although vibrational effects must be taken into account for highly accurate calculations of the MOR,[38,43,46] we will only consider electronic contributions in this work. Within the clamped-nuclei Born-Oppenheimer approximation, the electronic minimal-coupling Hamiltonian can be written as (we use atomic units throughout)

$$\hat{H}(t) = \sum_{i=1}^{N}\left\{\frac{1}{2}\hat{\pi}_i^2(\boldsymbol{r}_i,t) + \hat{\boldsymbol{S}}_i\cdot[\boldsymbol{B}+\boldsymbol{\mathcal{B}}(\boldsymbol{r}_i,t)]\right\} + W_{\mathrm{en}} + W_{\mathrm{ee}}, \tag{5}$$

where W_{en} is the electronic-nuclear Coulomb attraction, W_{ee} is the electronic-electronic Coulomb repulsion, and $\hat{\boldsymbol{S}}_i$ and $\boldsymbol{r}_i$ are the spin and position operators, respective, of electron i. The constant nuclear repulsion energy is excluded for convenience and the kinetic momentum operator,

$$\hat{\boldsymbol{\pi}}(\boldsymbol{r},t) = \hat{\boldsymbol{p}} + \boldsymbol{A}(\boldsymbol{r}) + \boldsymbol{\mathcal{A}}(\boldsymbol{r},t), \tag{6}$$

differs from the canonical momentum operator $\hat{\boldsymbol{p}} = -\mathrm{i}\boldsymbol{\nabla}$ by including the time-dependent electromagnetic vector potential $\boldsymbol{\mathcal{A}}(\boldsymbol{r},t)$ and the static magnetic vector potential

$$\boldsymbol{A}(\boldsymbol{r}) = \frac{1}{2}\boldsymbol{B}\times(\boldsymbol{r}-\boldsymbol{O}), \tag{7}$$

where $\boldsymbol{O}$ is the magnetic gauge origin. The Coulomb gauge condition is chosen for the electromagnetic vector potential and the scalar potential vanishes such that the source-free electric and magnetic fields are given by

$$\boldsymbol{\mathcal{E}}(\boldsymbol{r},t) = -\partial_t\boldsymbol{\mathcal{A}}(\boldsymbol{r},t), \qquad \boldsymbol{\mathcal{B}}(\boldsymbol{r},t) = \boldsymbol{\nabla}\times\boldsymbol{\mathcal{A}}(\boldsymbol{r},t). \tag{8}$$

The Hamiltonian can be recast as

$$\hat{H}(t) = \hat{H}_0 + \hat{V}(t), \tag{9}$$

where the time-independent Hamiltonian

$$\hat{H}_0 = \sum_{i=1}^{N}\left(\frac{1}{2}(\hat{\boldsymbol{p}}_i + \boldsymbol{A}(\boldsymbol{r}_i))^2 + \hat{\boldsymbol{S}}_i\cdot\boldsymbol{B}\right) + W_{\mathrm{en}} + W_{\mathrm{ee}}, \tag{10}$$

describes the electronic system interacting with the static uniform magnetic field $\boldsymbol{B}$, and

$$\hat{V}(t) = \sum_{i=1}^{N}\left([\hat{\boldsymbol{p}}_i + \boldsymbol{A}(\boldsymbol{r}_i)]\cdot\boldsymbol{\mathcal{A}}(\boldsymbol{r}_i,t) + \hat{\boldsymbol{S}}_i\cdot\boldsymbol{\mathcal{B}}(\boldsymbol{r}_i,t)\right.$$
$$\left. + \frac{1}{2}\boldsymbol{\mathcal{A}}^2(\boldsymbol{r}_i,t)\right), \tag{11}$$

describes the interaction with the time-dependent radiation field. Unless $\boldsymbol{B}$ and $\boldsymbol{\mathcal{E}}(\boldsymbol{r},t)$ are parallel, the dependence on the static uniform magnetic field cannot be isolated in the energy operator $\hat{H}_0$ but appears in the time-dependent interaction operator as well.

The time-dependent Schrödinger equation reads

$$\mathrm{i}\partial_t\Psi(t) = \hat{H}(t)\Psi(t), \qquad \Psi(0) = \Psi_0, \tag{12}$$

where Ψ_0 is the wave function of the initial electronic state before the radiation field is switched on. We choose Ψ_0 to be the magnetic field-dependent ground-state wave function ψ_0 with energy E_0,

$$\hat{H}_0\psi_0 = E_0\psi_0. \tag{13}$$

This equation can be solved approximately using recent implementations of quantum-chemical methods such as Hartree–Fock theory,[4] coupled-cluster theory,[8] and current density-functional theory.[15] With finite-dimensional, isotropic Gaussian-type orbital basis sets, magnetic gauge-origin invariance can be maintained by multiplying each basis function with a magnetic field-dependent phase factor to obtain the so-called London atomic orbitals (LAOs).[47] This approach works well for ground and excited states in magnetic fields up to about $1\,\mathrm{B}_0$, whereas anisotropic Gaussians or high angular momenta are required for even stronger magnetic fields.[48,49]

The interaction operator of Eq. (11) can be substantially simplified by assuming the electric-dipole approximation, $\boldsymbol{\mathcal{A}}(\boldsymbol{r},t) \approx \boldsymbol{\mathcal{A}}(\boldsymbol{0},t) \equiv \boldsymbol{\mathcal{A}}(t)$, which is valid for radiation wavelengths well beyond the "size" of the atomic or molecular system. In the context of MOR, we are interested in the transparent spectral region of the molecules

studied, i.e., in energies below the first excitation energy, and the conditions for using the electric-dipole approximation thus are satisfied. A simple gauge transformation then yields the usual length-gauge dipole interaction operator,

$$\hat{V}(t) = \sum_{i=1}^{N} \hat{\boldsymbol{r}}_i \cdot \boldsymbol{\mathcal{E}}(t), \tag{14}$$

where $\boldsymbol{\mathcal{E}}(t) = -\partial_t \boldsymbol{\mathcal{A}}(t)$. Thus, within the electric-dipole approximation, the interaction operator is independent of the static uniform magnetic field. The electric-dipole interaction operator is assumed in the following sections where we briefly summarize the TDCC and TDCDFT approaches to the simulation of laser-driven electron dynamics in a static uniform magnetic field.

C. Time-dependent electronic-structure theory

1. Time-dependent coupled-cluster theory

Providing systematically improvable ground- and excited-state energies and properties, the CC hierarchy of wave-function approximations[50–56] is arguably the most successful wave function-based approach to the calculation of atomic and molecular electronic structure. At least for systems with a nondegenerate ground state dominated by a single Slater determinant, CC calculations—especially with the "Gold Standard" of quantum chemistry, the CC singles and doubles with perturbative triples (CCSD(T))[57] model—are generally more reliable than and can serve as benchmarks for affordable density-functional approximations within DFT.

In the past decade, CC theory for ground[8,11] and excited[9,11] states has been developed for molecules in finite magnetic fields, i.e., for Hamiltonians of the form given in Eq. (10). Compared with a conventional field-free implementation of CC theory,[50,51] the main complications arising from the finite magnetic field are that the molecular orbitals and cluster amplitudes necessarily become complex and that the dependence on the magnetic gauge-origin must be eliminated. As mentioned above, the latter can be elegantly handled by using LAO basis functions[4] and suitably modified integral-evaluation algorithms.[4,58,59] The complex orbitals, however, reduce the permutational symmetries of the one- and two-electron integrals. As long as these permutational-symmetry reductions are properly taken into account, a conventional CC implementation can be rather straightforwardly turned into a magnetic-field implementation by switching from real to complex arithmetic. Similarly, an implementation of TDCC theory[41] only requires complex arithmetic in the ground-state CC functions, and may thus be used without modifications to simulate electron dynamics in finite magnetic fields provided that the reduced integral permutation symmetry is properly handled.

In this work we use two different classes of TDCC theory. In the first class, the single reference determinant is chosen to be the Hartree–Fock ground-state Slater determinant obtained from the magnetic Hamiltonian given in Eq. (10). The TDCC singles-and-doubles (TDCCSD)[60] model and its second-order approximation, the TDCC2 model,[61,62] belong to this class. In the second class, the single reference determinant is built from time-dependent spin orbitals which are bivariationally optimized alongside the cluster amplitudes. The orbital relaxation is constrained to conserve orthonormality in orbital-optimized TDCC (TDOCC) theory,[63,64] whereas nonorthogonal orbital-optimized TDCC (TDNOCC) theory[65,66] requires biorthonormal orbitals. In both cases, the orbital relaxation makes the singles cluster operators redundant.[63–66] Here we use the TDNOCCD model,[65,67] which includes doubles amplitudes only, and the time-dependent orbital-optimized second-order Møller-Plesset (TDOMP2) method,[62,68] which is a second-order approximation analogous to TDCC2 theory. The TDCCSD and TDNOCCD methods exhibit a computational scaling of $\mathcal{O}(K^6)$ with respect to the number of basis functions K, while the TDCC2 and TDOMP2 models scale as $\mathcal{O}(K^5)$.

2. Time-dependent current density functional theory

The density-functional theory (DFT) is extended to take into account the effect of an external magnetic field by including a dependence on both the charge density ρ and the paramagnetic component of the induced current density $\mathbf{j}_p$ in the universal density functional $F[\rho, \mathbf{j}_p]$. It was shown in Refs. 14, 17 that the Vignale–Rasolt formulation[12,13] of current-DFT (CDFT) can be treated in a similar manner to Lieb's formulation[69] of conventional DFT.

A non-perturbative treatment of an external magnetic field in the Kohn–Sham CDFT scheme can be set up by using LAOs (see Refs. 13, 15, 16 for details of the resulting Kohn-Sham equations). A central challenge in CDFT calculations is then to define the exchange–correlation functional $E_{xc}[\rho, \mathbf{j}_p]$, which now also depends on both the charge- and paramagnetic current densities. It has been shown that the accuracy of CDFT calculations using vorticity-based corrections to local density approximation (LDA) and generalised gradient approximation (GGA) levels is poor[15,70,71]. However, introducing an explicit current dependence at the meta-GGA level via a modification of the kinetic energy density as suggested by Dobson[72] and later used by Becke[73] and Bates and Furche[74] as

$$\tau(\mathbf{r}) \rightarrow \tilde{\tau}(\mathbf{r}) = \sum_i^{occ} [\nabla \varphi_i(\mathbf{r})]^* \cdot [\nabla \varphi_i(\mathbf{r})] - \frac{|\mathbf{j}_p(\mathbf{r})|^2}{\rho(\mathbf{r})}, \tag{15}$$

leads to a well-defined and properly bounded iso-orbital indicator when it is applied to the Tao-Perdew-

Staroverov–Scuseria (TPSS) functional[75], which in this work is denoted as cTPSS. Two variants of hybrid cTPSS functionals, denoted as cTPSSh and cTPSSrsh, have been introduced to dynamic CDFT in Ref. [42].

The cTPSSh functional includes a mixture of 10% orbital-dependent exchange and 90% cTPSS exchange functionals for the exchange contribution and 100% of the cTPSS correlation contribution. The cTPSSrsh functional similarly consists of a 100% cTPSS correlation functional, and a range-separated TPSS-like exchange functional defined in Ref. [76]. In this work we will use the cTPSS, cTPSSh, and cTPSSrsh functionals for computing the magnetic optical activity and compare their performance relative to the TDCC models above.

D.   Extracting dynamic properties

Depending on the shape of the time-dependent electric field, the induced dipole moment computed as an expectation value of the electric-dipole operator at each time step during a simulation can be used to extract properties such as absorption spectra and polarizabilities. We first consider the generation of linear absorption spectra, which we will later use to validate the TDCC implementations by comparison with spectra computed through time-independent EOM-EE-CC[9,54,77] theory. We then describe the extraction procedure used to obtain complex polarizabilities, which are subsequently combined to yield the MOR. For notational convenience, we do not use the superscript k to denote the direction of the magnetic field in this section.

1.   Absorption spectra

In order to extract excitation energies and intensities using time-dependent electronic-structure theory, the external electric field $\boldsymbol{\mathcal{E}}(t)$ in Eq. (14) is chosen as a δ-pulse at $t = 0$, $\boldsymbol{\mathcal{E}}(t) = \mathcal{E}\boldsymbol{u}\delta(t)$ where $\mathcal{E}$ is the field strength, $\boldsymbol{u}$ is the (linear) unit polarization vector, and $\delta(t)$ is the Dirac delta function. Completely localized in time, this pulse is infinitely broad in the frequency domain and, therefore, excites the electronic system from the ground state into all electric-dipole allowed excited states. If the field strength is sufficiently weak, nonlinear processes such as multiphoton transitions and transitions among excited states are negligible, resulting in a linear absorption spectrum.

The δ-pulse is approximated as a box function,

$$\boldsymbol{\mathcal{E}}(t) = \begin{cases} \mathcal{E}\boldsymbol{u} & 0 \leq t \leq \Delta t, \\ 0 & \text{else,} \end{cases} \qquad (16)$$

where Δt is the time step of the simulation—i.e., the field is on during the first time step only. The absorption spectrum is given by

$$S(\omega) = \frac{4\pi\omega}{3c}\mathrm{Im}\sum_i \mu_i(\omega), \qquad (17)$$

where $\mu_i(\omega)$ is obtained as the discrete Fourier transform, computed with the normalized fast Fourier transform (FFT) of the time-dependent dipole moment induced along Cartesian axis i by a δ-pulse polarized along the same axis,

$$\mu_i(\omega) = \mathrm{FFT}[(\mu_i(t) - \mu_i^{(0)})\mathrm{e}^{-\gamma t}]/\mathcal{E}, \qquad (18)$$

where $\mu_i^{(0)}$ is the permanent ground-state dipole moment, and $\mu_i(t)$ is the dipole moment computed at time t. The damping factor $\exp(-\gamma t)$ is applied to avoid artifacts from the periodic FFT procedure and the parameter $\gamma > 0$ can be interpreted as a common (inverse) lifetime of the excited states, causing Lorentzian shapes of the absorption lines. In general, the calculation of the linear absorption spectrum thus requires three independent simulations, one for each Cartesian direction. To ensure satisfactory resolution in the resulting spectra, the duration of the simulations need to be relatively long, typically with total simulation times exceeding 1000 a.u.

2.   Complex polarizabilities

The frequency-dependent polarizability $\alpha_{ij}(-\omega;\omega)$ can be extracted from simulations using the ramped continuous wave approach of Ding $et\ al.$[78] with the quadratic ramp proposed by Ofstad $et\ al.$[79] to suppress nonadiabatic effects. In the present case, however, it must be recalled that the polarizability is complex in the presence of the magnetic field.

With linear polarization vector $\boldsymbol{u}$ and field strength $\mathcal{E}$, the electric field takes the form[79]

$$\boldsymbol{\mathcal{E}}(t) = \begin{cases} \frac{2t^2}{t_{n_r}^2}\mathcal{E}\boldsymbol{u}\sin(\omega t) & 0 \leq t < \frac{t_{n_r}}{2}, \\ \frac{t_{n_r}^2 - 2(t-t_{n_r})^2}{t_{n_r}^2}\mathcal{E}\boldsymbol{u}\sin(\omega t) & \frac{t_{n_r}}{2} \leq t < t_{n_r}, \\ \mathcal{E}\boldsymbol{u}\sin(\omega t) & t_{n_r} \leq t \leq t_{\mathrm{tot}}, \end{cases} \quad (19)$$

where t_{n_r} is the ramping time expressed as a multiple n_r of optical cycles,

$$t_{n_r} = n_r\frac{2\pi}{\omega}, \qquad (20)$$

after which the electric field remains a full-strength, monochromatic continuous wave until the simulation concludes at $t = t_{\mathrm{tot}}$.

For sufficiently weak electric-field strengths, the Cartesian component i of the electric dipole moment computed at times $t_{n_r} \leq t \leq t_{\mathrm{tot}}$ can be expanded as

$$\mu_i(t) = \mu_i^{(0)} + \sum_j \alpha_{ij}(t)\mathcal{E}_j + \cdots, \qquad (21)$$

where

$$\alpha_{ij}(t) = \mathrm{Re}\left[\alpha_{ij}(-\omega;\omega)\right]\sin(\omega t)$$
$$+ \mathrm{Im}\left[\alpha_{ij}(-\omega;\omega)\right]\cos(\omega t). \quad (22)$$

The time-domain polarizability $\alpha_{ij}(t)$ is computed by a four-point finite difference formula, followed by a fitting procedure to obtain the frequency-domain polarizability $\alpha_{ij}(-\omega;\omega)$ as described in Refs. 78 and 79.

III. RESULTS

A. Absorption Spectra

We have implemented the TDCC models discussed above in the open-source HYQD software[80] using the QUEST program[81] to generate optimized Hartree–Fock orbitals and Hamiltonian integrals in LAO basis to ensure magnetic gauge-origin invariance.[4] We validate our implementation of TDCCSD theory by comparing absorption spectra obtained from δ-pulse simulations with spectra computed by the time-independent finite magnetic field EOM-EE-CCSD model[9] with the same LAO basis. The TDCCSD dipole moment is computed using the inherently real expectation-value functional proposed in Refs. 60 and 82, and the electric-field strength is $\mathcal{E} = 0.001$ a.u. While the excitation energies are identical with the two approaches, the intensities may differ when the number of electrons surpasses two. The approaches were nonetheless found to coincide quite well, with only slight deviations observed between EOM-EE-CCSD, TDCC and linear-response CC (LRCC)[10]. Although the time-dependent approach generates the full absorption spectrum, including core-valence excitations, we only compare low-lying transitions to avoid full diagonalization of the EOM-EE-CC matrix. The finite magnetic field EOM-EE-CCSD calculations are performed using the QCUMBRE software[83] together with an interface to the CFOUR program package,[84,85] which provides the Hartree–Fock ground-state solution using the MINT integral package.[86] The EOM-EE-CCSD transition dipole moments are calculated with the expectation value approach.[77]

Absorption spectra are computed for H_2, He, Be, and LiH at the magnetic-field strength $0.2\,B_0$ directed along the y-axis, perpendicular to the bond axis for the diatomic molecules. The geometries of H_2 and LiH are optimized in the magnetic field at the cTPSS level of theory with the aug-cc-pVDZ[87–90] basis set using QUEST.[44,81] The resulting bond lengths are $1.39106\,a_0$ for H_2 and $2.96117\,a_0$ for LiH.

For the EOM-EE-CCSD calculations, a convergence threshold of 10^{-7} is used for the Hartree–Fock densities and CC amplitudes, while a looser threshold of 10^{-6} (10^{-5}) is used for the right-hand (left-hand) side EOM vectors. For the TDCCSD simulations, a convergence threshold of 10^{-12} for the energy-gradient norm is used

for the Hartree–Fock ground state optimization, while the CCSD ground-state amplitudes are converged to a residual norm of 10^{-12}. The TDCCSD equations of motion are integrated using sixth order (three-stage, $s = 3$) symplectic Gauss-Legendre integrator[60,91] with time step $\Delta t = 0.01$ a.u. and residual norm convergence criterion 10^{-10} for the implicit equations. The total simulation time is 1500 a.u. for He and H_2, 2000 a.u. for Be, and 1000 a.u. for LiH.

Figure 1 displays the absorption spectra of the four systems obtained from the TDCCSD and EOM-EE-CCSD approaches with the aug-cc-pVTZ[87–90] basis set and a damping factor with $\gamma = 0.004$. The excitation energies are equivalent to within the resolution of the FFT (approximately 0.004 a.u. for He and H_2, and 0.003 a.u. for Be and LiH) for all systems. For the two-electron systems, the intensities also agree, while minor deviations are observed for Be and LiH, as expected.

Corresponding absorption plots obtained from TDCC2 and EOM-EE-CC2/ EOM-EE-CCSD approaches can be found in the Supplementary material. No implementations of excitation energies for the OMP2 and NOCCD methods are available (only a pilot implementation of linear response theory was reported in Ref. 65), and, hence, no validation is possible for these methods.

B. Magnetic Optical Activity

1. Computational details

Magnetic optical activity calculations are performed for twenty magnetic-field strengths in the range 0 T to 55 000 T by extracting the imaginary part of the polarizability as described in Sec. II D. The field strength of the time-dependent electric field is chosen to be $\mathcal{E} = 0.001$ a.u., which is small enough to warrant the dipole expansion in Eq. (21). We consider two cases: The orientation of the molecule is either taken to be independent of the direction of the magnetic field—i.e., the molecules of the sample are assumed to be randomly oriented—and the MOR is computed according to Eq. (1), or the molecule is taken to be *fixed* at the energetically most favorable orientation with respect to the magnetic-field direction and Eq. (4) is used. To determine the most favorable orientation, the Hartree–Fock/aug-cc-pVDZ ground-state bond lengths were computed at both the perpendicular and parallel orientation for each molecule. The ground-state energy difference as a function of the magnetic-field strength is displayed in Figure 2. For H_2 and HF, the parallel orientation with respect to the magnetic field direction is the most energetically favorable, while the perpendicular orientation is found to be most favorable for CO. All three molecules are closed-shell diamagnetic molecules, and the difference in orientation stems from differences in the terms quadratic in the magnetic field—the diamagnetic terms—contained in Eq. (10). The optimized bond lengths for
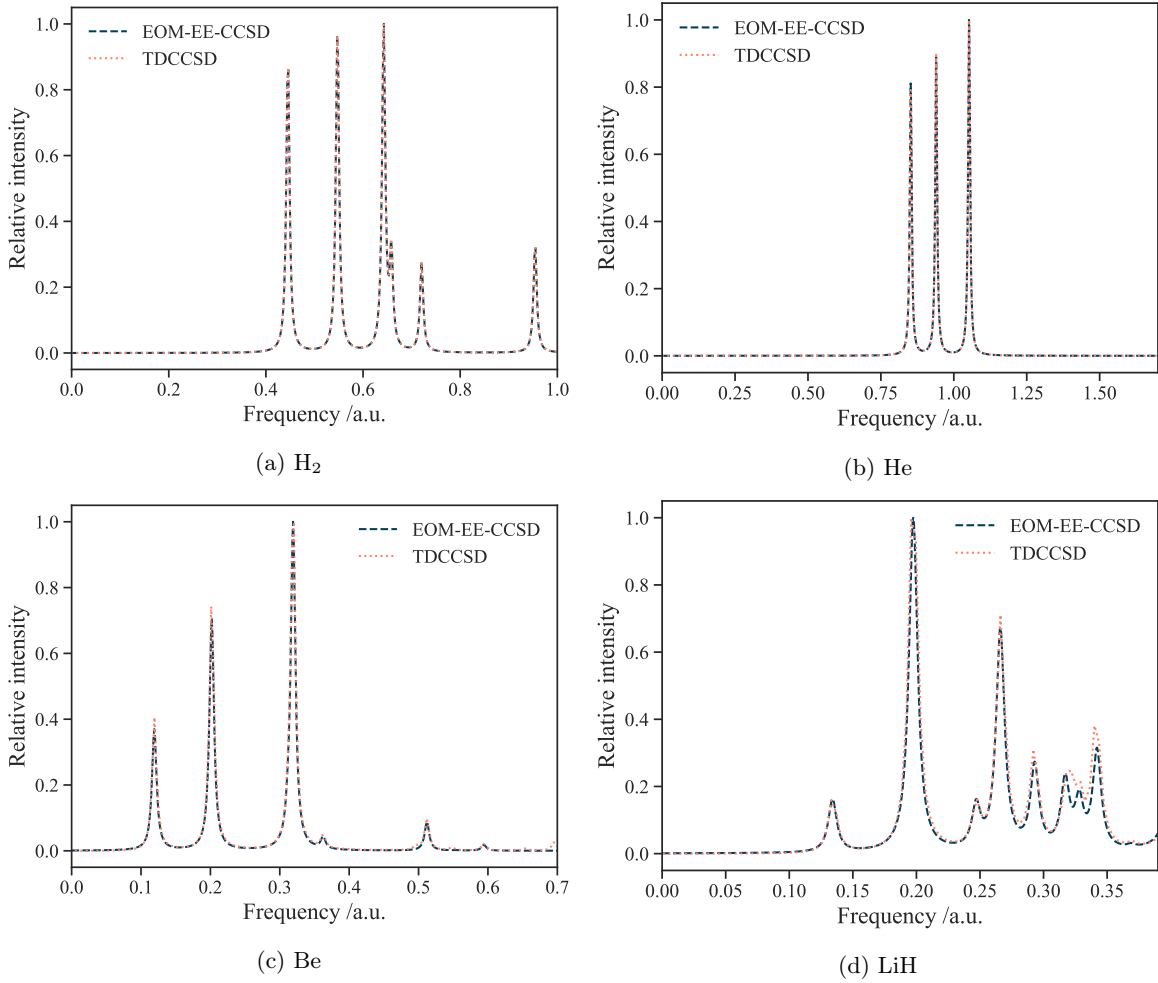
(a) H$_2$

(b) He

(c) Be

(d) LiH

FIG. 1: Overlay of absorption spectra generated by TDCCSD and EOM-EE-CCSD at the magnetic-field strength $0.2\,B_0$ (perpendicular to the internuclear axis for the diatomic molecules) with the aug-cc-pVTZ basis set.

the three molecules can be found in the Supplementary Information.

When evaluating Eq. (1) and Eq. (4), the ideal gas approximation is employed at standard temperature ($0\,°C$) and pressure ($1\,atm$). Note that we do *not* use $1\,bar$ as the standard pressure in order to enable comparison with previous work.[38–40] The number density thus is $\mathcal{N} = 2.68678 \times 10^{25}\,m^{-3} = 3.98140 \times 10^{-6}\,a_0^{-3}$, and

$$C = 2.53048 \times 10^{27}\,\frac{J\,s}{C^2\,m^3} = 9.12748 \times 10^{-8}\,\frac{\hbar}{e^2\,a_0^3}. \quad (23)$$

(With standard pressure $1\,bar$, one obtains instead $C = 9.00812 \times 10^{-8}\,\hbar/e^2 a_0^3$.) We compute the MOR for the H$_2$ molecule at $\omega = 0.08284\,a.u.$ ($\lambda = 550\,nm$), while $\omega = 0.11391\,a.u.$ ($\lambda = 400\,nm$) is used for the CO and HF molecules in accordance with the experimental work of Ingersoll and Lebenberg.[92]

For the randomly oriented case, simulations are car-ried out with experimental field-free bond lengths: $1.4\,a_0$ for H$_2$, $2.132\,a_0$ for CO, and $1.7328\,a_0$ for HF. For the fixed orientation case, the bond lengths of H$_2$, CO, and HF are optimized for each magnetic-field strength at the cTPSS/aug-cc-pVDZ level of theory with the magnetic field vector parallel (H$_2$ and HF) or perpendicular (CO) to the bond axis.

We compute the MOR from TDHF, TDCC2, TD-CCSD, TDOMP2, and TDNOCCD simulations with the HyQD software.[80] Apart from using a stricter residual norm convergence criteria of 10^{-12} for the implicit equations of the Gauss-Legendre integrator, the same convergence thresholds are applied for the MOR calculations as those specified in Sec. III A The TDCDFT simulations are performed with the current–dependent exchange–correlation functionals cTPSS, cTPSSh, and cTPSSrsh as described in Ref. 42. The density is propagated using the Magnus 2 propagator[93] with a modest time step of $0.1\,a.u.$, which has been shown to yield a good balance
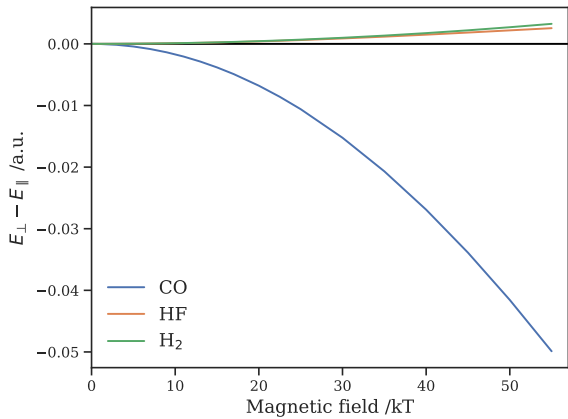
FIG. 2: The Hartree–Fock/aug-cc-pVDZ ground-state energy difference between perpendicular and parallel molecular orientation with respect to the magnetic field direction as a function of field strength. The horizontal black line marks zero energy difference.

TABLE I: The Verdet constant (in 10^{-7} a.u.) extracted from simulations. Experimental values are taken from Ref. 92.

	H_2	HF	CO
ω/a.u.	0.08284	0.11391	0.11391
TDHF	0.248	0.202	0.687
TDCC2	0.246	0.358	0.906
TDCCSD	0.245	0.304	0.884
TDOMP2	0.247	0.329	0.972
TDNOCCD	-	0.274	0.876
cTPSS	0.303	0.416	0.987
cTPSSh	0.235	0.288	0.761
cTPSSrsh	0.160	0.202	0.512
Exp.	0.251	-	0.895

between accuracy and efficiency for computing absorption spectra in the presence of a magnetic field.[42] The TDCDFT simulations are performed with the QUEST code.[81] For all calculations, the aug-cc-pVDZ basis set is employed, and it should be noted that the basis set limit has not been reached.[39] Moreover, the CC expansion lacks triple excitations, which are important for high accuracy,[40] and rovibrational effects are not taken into account. Consequently, the simulations presented here cannot be expected to reproduce or predict experimental results with very high accuracy.

2. Verdet constants

We determine Verdet constants by fitting the MOR data for randomly oriented samples to a fifth-order polynomial in the magnetic-field strength, identifying $V(\omega)$ as the coefficient of the linear term. The results are listed in Table I along with the experimental results of Ingersoll and Lebenberg.[92]

While electron correlation effects are important for HF and CO, their impact is less pronounced in the case of H_2. The wave function methods that take electron correlation into account yield Verdet constant which agree with experimental values (for H_2 and CO) to within 2–10%, which is reasonable considering the lack of higher-order correlation effects[40] and vibrational contributions,[94] in addition to the relatively small basis set. With errors ranging from 6% to 38%, the TDCDFT model with the cTPSSrsh functional exhibit comparatively large errors, especially considering that the TDHF results remain below 24%.

Computations conducted using quadratic response theory[39,43] should yield identical Verdet constants, although

slight variations may arise, for example, due to numerical errors from the finite-difference calculations involved in the linear-response-function extraction.[78,79] Parkinson et al.[43] computed Verdet constants for the three molecules at the Hartree–Fock level (i.e., the random phase approximation). They used a somewhat larger basis set than aug-cc-pVDZ, albeit without the LAO phase factors, and obtained Verdet constants of 0.232×10^{-7} a.u. for H_2, 0.219×10^{-7} a.u. for HF, and 0.702×10^{-7} a.u. for CO, in fair agreement with our TDHF results in Table I. Coriani et al.[39] computed the Verdet constant for HF at the CCSD level with the same basis set to be 0.3038×10^{-7} a.u., which is within 0.03% of our result (0.3037×10^{-7} a.u.). This confirms that our MOR procedure indeed reproduces quadratic response theory at low magnetic-field strengths.

3. TDCC results at finite magnetic field

Figure 3 shows the MOR obtained from wave function-based simulations of H_2, HF, and CO as a function of magnetic-field strength, with the dashed lines representing the values predicted from Eq. (3) using the Verdet constants reported in Table I. Results for randomly oriented molecules are shown in the left-hand panels, while those for oriented molecules are shown in the right-hand panels. There are significant deviations from linearity for both oriented and randomly oriented samples, as we shall discuss in more detail below.

The two uppermost panels of Fig. 3 show the MOR of H_2 obtained from TDHF, TDCC2, TDCCSD, and TDOMP2 simulations. Since the H_2 molecule is a two-electron system, the TDCCSD and TDNOCCD methods are equivalent. As also observed for the Verdet constants above, electron correlation effects are not highly important for the MOR of H_2 at the range of magnetic-field strengths considered here. The effect of orientation—which includes varying bond lengths—is significant, with θ_r roughly 28% greater than θ_o.

FIG. 3: The magnetic optical rotation of H_2, HF, and CO as a function of the magnetic-field strength computed with wave function methods. The panels on the left display the MOR for the randomly oriented molecules, while the panels on the right display the MOR for the fixed orientation relative to the magnetic field vector (parallel for H_2 and HF systems, perpendicular for CO). The dashed lines are obtained from the Verdet constants in Table I.

For both HF and CO, however, correlation effects are crucial, confirming previous observations based on quadratic response theory by Parkinson *et al.*[43] and Coriani *et al.*[40] While the TDCCSD and TDNOCCD results agree for CO, the optimization of the time-dependent orbitals in the TDNOCCD method give rise to a significant change compared with the static orbitals of TDCCSD theory for the HF molecule. This observation also applies to the second-order approximations TDCC2 and TDOMP2, where we also note that TDOMP2 results are closer to the TDCCSD ones than those obtained from TDCC2 theory for HF. However, this is not at all the case for CO. The latter is in agreement with magnetic field-free polarizability and hyperpolarizability results reported by Kristiansen *et al.*[62] It is, however, not possible to conclude which of the TDNOCCD and TDCCSD methods is superior based on the present results, as it requires a more careful study of convergence with respect to higher-order excitations beyond doubles. We will, therefore, compare TDCDFT results with the MOR obtained from both the TDCCSD and TDNOCCD methods.

It is noteworthy that the MOR is almost identical for oriented and randomly oriented HF, whereas a significant orientation effect is observed for the CO molecule. While one might speculate that the "oriented" contribution, Eq. (4), dominates the averaging in Eq. (1) for HF, it turns out to be caused by the change in bond length obtained in the magnetic-field dependent geometry optimization.

4. TDCDFT results at finite magnetic field

Figure 4 shows the MOR obtained from TDCDFT simulations of H_2, HF, and CO as a function of magnetic-field strength with the dashed lines representing the predicted values using Eq. (3) with the Verdet constants reported in Table I. Results for randomly oriented and oriented molecules are shown in the left- and right-hand panels, respectively, and the TDHF, TDCCSD, and TDNOCCD results are reproduced here for comparison. For the TDCDFT results, we also observe significant deviations from linearity as the magnetic-field strength increases.

It has been shown in previous studies[42,76] that the current-dependent DFT functionals (cTPSS, cTPSSh, and cTPSSrsh) improve the accuracy of calculations of chemical properties of molecules such as the isotropic NMR shielding constants and the absorption spectra of molecules in magnetic fields. These three functionals have previously been applied to the calculation of isotropic NMR shielding constants,[76] and it was shown that the cTPSSh and cTPSSrsh functionals have no significant improvements compared with the cTPSS functional. The cTPSSrsh functional has, however, been found to better describe excited states compared to cTPSS and cTPSSh in the magnetic field-free case.[42] In this study, we observe that the cTPSSh functional generally produces MOR values that are somewhat closer to TDCCSD/TDNOCD results than the cTPSS functional. Moreover, the cTPSSh functional outperforms the TDHF method for HF and CO, but not for H_2. The MOR values computed using the cTPSSh functional fall in between the cTPSS and cTPSSrsh results, which are over- and under-estimates of the MOR, respectively. The poor performance of the cTPSSrsh functional is somewhat surprising considering that range separation is known to improve the description of nonlinear properties.[95,96] The cTPSSrsh functional incorporates a large fraction of the current-independent PBE functional, which might contribute to the quite poor performance in finite magnetic fields. When the magnetic field is set to zero, the cTPSSrsh functional yields ground state energies and dipole moments comparable to cTPSSh, both of which outperform the cTPSS functional. Nevertheless, we can see that in general, the TDCDFT results show a similar trend to TDCC results. Furthermore, the TDCDFT calculations have a relatively low computational cost, which scales as $O(K^3)$, where K is the number of basis functions – compared with the computational scaling of TDCCSD and TDNOCCD, $O(K^6)$, or TDCC2 and TDOMP2, $O(K^5)$.

5. Deviation from Verdet's linear law

As noted above, it is evident from Figs. 3 and 4 that Verdet's linear relation between the MOR and the magnetic-field strength only holds for sufficiently small magnetic-field strengths. While this is not surprising, considering that the observations of Verdet can be accounted for by first-order perturbation theory, it is not straightforward to uniquely define a field strength at which linearity is broken. In this work, we will define the "breaking point" as the magnetic-field strength at which the fifth-order polynomial function fitted to the nonperturbative MOR deviates from the value predicted from the Verdet constants, defined as the linear coefficient of this polynomial function, by a given percentage.

The magnetic-field strengths at which 3% and 5% deviations are observed can be found in Table II. With random orientation, the breaking point roughly lies somewhere between 10 and 20 kT ($0.04–0.09\,B_0$), 2–3 orders of magnitude above the strongest sustainable static magnetic-field strength produced on Earth with a high-temperature superconducting magnet, namely 45.5 T ($2\times10^{-4}\,B_0$).[97] At 45.5 T, the TDCCSD and TDNOCCD results deviate from linearity by about 0.9% for H_2 and CO and by about 0.09% for HF (with random orientation). Even at the short-lived record field strength of 1.2 kT generated by electromagnetic flux-compression,[34] the deviation from linearity remains low. At worst, the deviation is slightly above 1% for the cases studied here. This compares well with the deviation (of the Verdet constant) estimated to be around 1% by Nakamura *et al.*[34] Our results thus indicate that Verdet's law can be safely
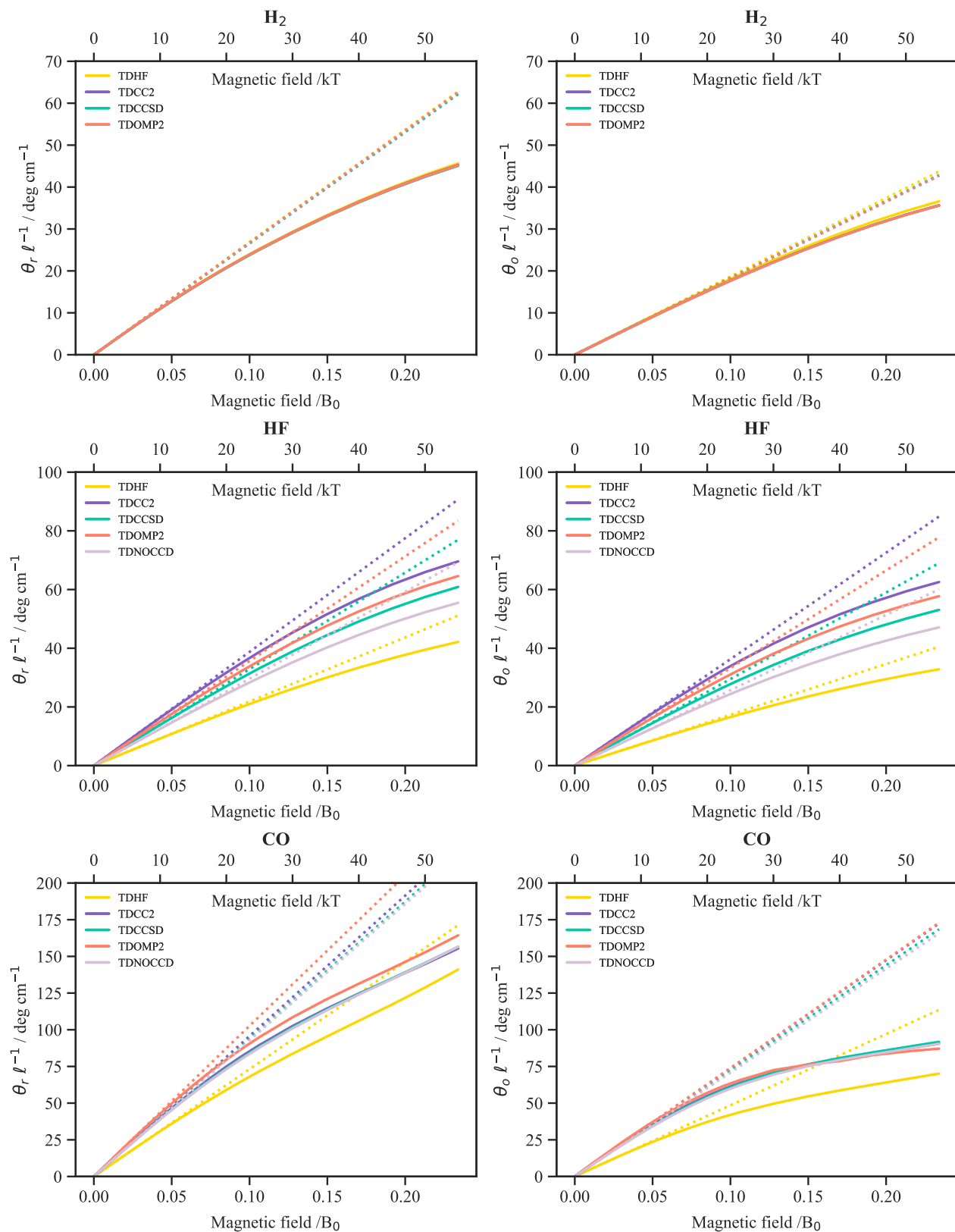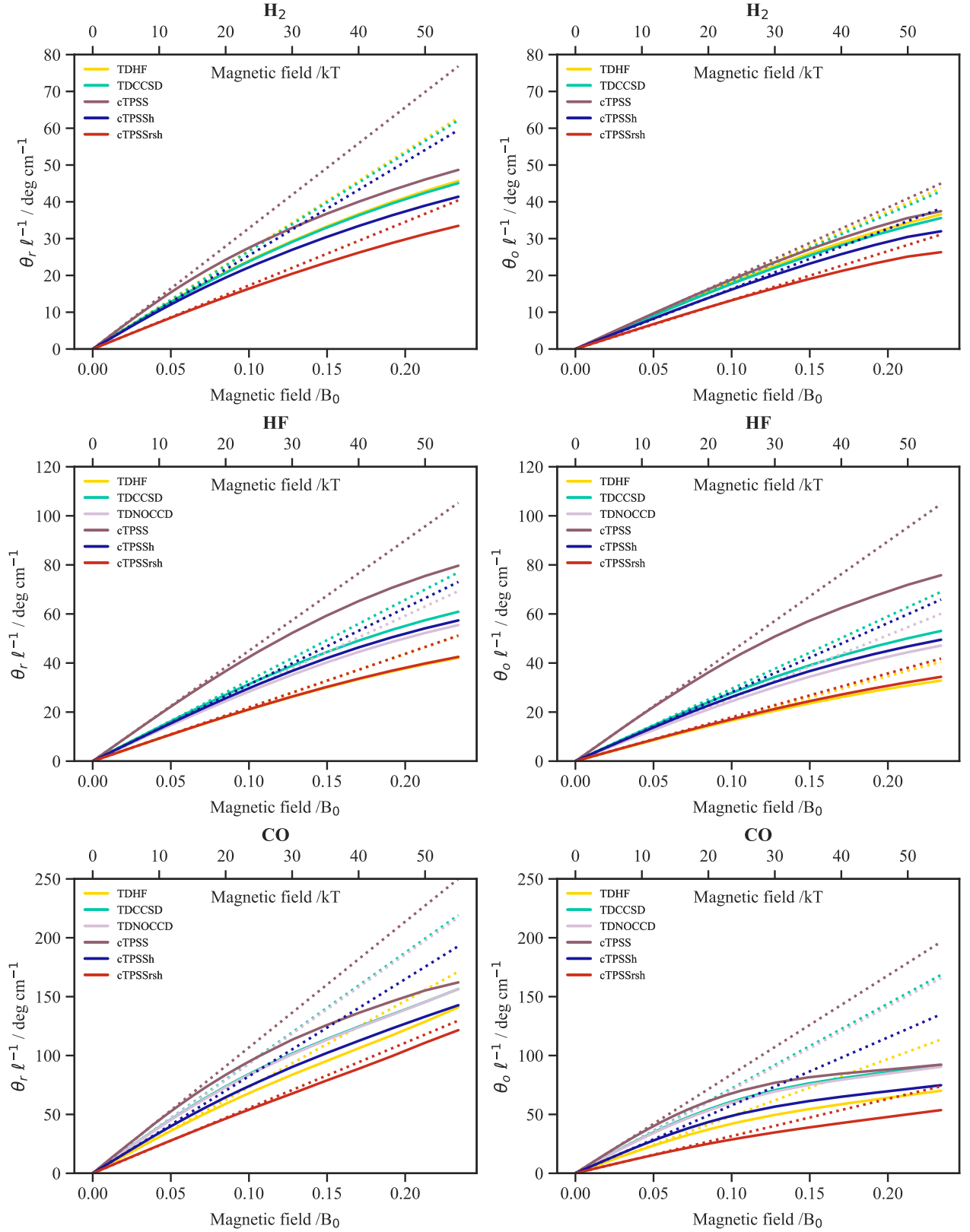
FIG. 4: The magnetic optical rotation of H_2, HF, and CO as a function of the magnetic-field strength computed with TDCDFT and the TDHF, TDCCSD, and TDNOCCD methods. The panels on the left display the MOR for the randomly oriented molecules, while the panels on the right display the MOR for the fixed orientation relative to the magnetic field vector (parallel for H_2 and HF systems, perpendicular for CO). The dashed lines are obtained from the Verdet constants in Table I.

TABLE II: The magnetic-field strength (in kT) at which the nonperturbative MOR deviates from Verdet's law by a chosen percentage.

		Random		Fixed	
		3%	5%	3%	5%
H_2	TDHF	9.03	13.1	22.1	28.5
	TDCC2	9.14	13.2	21.9	28.2
	TDCCSD	9.25	13.3	21.6	27.8
	TDOMP2	9.03	13.0	21.9	28.2
	cTPSS	6.39	9.69	27.1	32.3
	cTPSSh	7.76	11.5	29.1	34.0
	cTPSSrsh	16.2	22.6	31.2	36.2
HF	TDHF	20.3	26.4	18.7	24.4
	TDCC2	17.1	22.1	15.4	20.0
	TDCCSD	18.7	24.0	16.2	21.3
	TDOMP2	17.5	22.6	15.1	19.5
	TDNOCCD	19.3	24.7	18.3	23.2
	cTPSS	16.9	21.4	15.2	19.3
	cTPSSh	18.1	23.3	13.3	18.6
	cTPSSrsh	21.2	27.4	18.2	24.4
CO	TDHF	14.9	19.0	11.6	14.2
	TDCC2	12.4	15.4	10.7	12.9
	TDCCSD	12.8	16.0	11.0	13.3
	TDOMP2	11.5	14.5	10.2	11.4
	TDNOCCD	12.7	15.9	11.0	13.3
	cTPSS	13.7	16.2	9.86	11.9
	cTPSSh	11.0	14.6	11.1	13.4
	cTPSSrsh	24.9	33.3	13.9	17.0

applied for the range of magnetic-field strengths that can be produced in current experimental setups, but one must be careful if or when even stronger fields can be generated.

IV. CONCLUDING REMARKS

We have in this work presented the first implementation of TDCC theory for the study of laser-driven multielectron dynamics in finite magnetic fields. The implementation is validated by comparing linear absorption spectra obtained from simulations with those obtained from time-independent EOM-EE-CC theory. The implementation supports both static and dynamic reference determinants with the orbitals expanded in London atomic orbitals to ensure magnetic gauge-origin invariance.

The new implementation is applied to the calculation of magnetic optical rotation at finite magnetic-field strengths, demonstrating that Verdet's linear relationship is valid up to field strengths of roughly 10–20 kT $(0.04$–$0.09 \, B_0)$. A deviation from linearity below 1% is found at 45.5 T, which is the strongest sustainable static

magnetic field ever produced by a superconducting magnet on Earth. Our results may also serve as reference for future implementations of linear response theory[45] in the presence of finite magnetic fields.

We have also compared the TDCC magnetic optical rotations with those obtained from TDCDFT simulations using the current-dependent cTPSS, cTPSSh, and cTPSSrsh density-functional approximations. With TD-CCSD and TDNOCCD results as benchmark, we find that the best-performing functional is cTPSSh. The cTPSS functional tends to overestimate the rotation while the cTPSSrsh functional tends to underestimate it.

SUPPLEMENTARY MATERIAL

The supplementary material contains cTPSS/aug-cc-pVDZ equilibrium bond lengths of H_2, HF, and CO placed in a magnetic field parallel or perpendicular to the bond axis with field strengths ranging from 1 T to 55 kT. The overlayed absorption spectra generated from TDCC2 simulations and from time-independent EOM-EE-CC2 calculations can also be found in the supplementary material.

ACKNOWLEDGMENT

DATA AVAILABILITY STATEMENT

The data that support the findings of this study are available from the corresponding author upon reasonable request.

[1] K. K. Lange, E. I. Tellgren, M. R. Hoffmann, and T. Helgaker, "A Paramagnetic Bonding Mechanism for Diatomics in Strong Magnetic Fields," Science **337**, 327–331 (2012).

[2] M. Lewenstein, P. Balcou, M. Y. Ivanov, A. L'Huillier, and P. B. Corkum, "Theory of high-harmonic generation by low-frequency laser fields," Phys. Rev. A **49**, 2117–2132 (1994).

[3] M. A. Hollands, S. Stopkowicz, M. P. Kitsaras, F. Hampe, S. Blaschke, and J. J. Hermes, "A DZ white dwarf with a 30 MG magnetic field," Mon. Notices Royal Astron. Soc. **520**, 3560–3575 (2023).

[4] E. I. Tellgren, A. Soncini, and T. Helgaker, "Nonperturbative *ab initio* calculations in strong magnetic fields using London orbitals," J. Chem. Phys. **129**, 154114 (2008).

[5] S. Sen, K. K. Lange, and E. I. Tellgren, "Excited States of Molecules in Strong Uniform and Nonuniform Magnetic Fields," J. Chem. Theory Comput. **15**, 3974–3990 (2019).

[6] S. Sun, D. Williams-Young, and X. Li, "An ab Initio Linear Response Method for Computing Magnetic Circular Dichroism Spectra with Nonperturbative Treatment of Magnetic Field," J. Chem. Theory Comput. **15**, 3162–3169 (2019).

[7] S. Sun, D. B. Williams-Young, T. F. Stetina, and X. Li, "Generalized Hartree–Fock with Nonperturbative Treatment of Strong Magnetic Fields: Application to Molecular Spin Phase Transitions," J. Chem. Theory Comput. **15**, 348–356 (2019).

[8] S. Stopkowicz, J. Gauss, K. K. Lange, E. I. Tellgren, and T. Helgaker, "Coupled-cluster theory for atoms and molecules in strong magnetic fields," J. Chem. Phys. **143**, 074110 (2015).

[9] F. Hampe and S. Stopkowicz, "Equation-of-motion coupled-cluster methods for atoms and molecules in strong magnetic fields," J. Chem. Phys. **146**, 154105 (2017).

[10] F. Hampe and S. Stopkowicz, "Transition-Dipole Moments for Electronic Excitations in Strong Magnetic Fields Using Equation-of-Motion and Linear Response Coupled-Cluster Theory," J. Chem. Theory Comput. **15**, 4036–4043 (2019).

[11] F. Hampe, N. Gross, and S. Stopkowicz, "Full triples contribution in coupled-cluster and equation-of-motion coupled-cluster methods for atoms and molecules in strong magnetic fields," Phys. Chem. Chem. Phys. **22**, 23522–23529 (2020).

[12] G. Vignale and M. Rasolt, "Density-functional theory in strong magnetic fields," Phys. Rev. Lett. **59**, 2360–2363 (1987).

[13] G. Vignale and M. Rasolt, "Current- and spin-density-functional theory for inhomogeneous electronic systems in strong magnetic fields," Phys. Rev. B **37**, 10685–10696 (1988).

[14] E. I. Tellgren, S. Kvaal, E. Sagvolden, U. Ekström, A. M. Teale, and T. Helgaker, "Choice of basic variables in current-density-functional theory," Phys. Rev. A **86**, 062506 (2012).

[15] E. I. Tellgren, A. M. Teale, J. W. Furness, K. K. Lange, U. Ekström, and T. Helgaker, "Non-perturbative calculation of molecular magnetic properties within current-density functional theory," J. Chem. Phys. **140**, 034101 (2014).

[16] J. W. Furness, J. Verbeke, E. I. Tellgren, S. Stopkowicz, U. Ekström, T. Helgaker, and A. M. Teale, "Current Density Functional Theory Using Meta-Generalized Gradient Exchange-Correlation Functionals," J. Chem. Theory Comput. **11**, 4169–4181 (2015).

[17] S. Kvaal, A. Laestadius, E. Tellgren, and T. Helgaker, "Lower Semicontinuity of the Universal Functional in Paramagnetic Current–Density Functional Theory," J. Phys. Chem. Lett. **12**, 1421–1425 (2021).

[18] J. J. Goings, P. J. Lestrange, and X. Li, "Real-time time-dependent electronic structure theory," WIREs Comput. Mol. Sci. **8**, e1341 (2018).

[19] X. Li, N. Govind, C. Isborn, A. E. DePrince, and K. Lopata, "Real-Time Time-Dependent Electronic Structure Theory," Chem. Rev. **120**, 9951–9993 (2020).

[20] M. Nisoli, P. Decleva, F. Calegari, A. Palacios, and F. Martín, "Attosecond Electron Dynamics in Molecules," Chem. Rev. **117**, 10760–10825 (2017).

[21] A. Palacios and F. Martín, "The quantum chemistry of attosecond molecular science," WIREs Comput. Mol. Sci. **10**, e1430 (2020).

[22] M. Faraday, "I. Experimental researches in electricity.—Nineteenth series," Philos. Trans. R. Soc. London **136**, 1–20 (1846).

[23] A. D. Buckingham and P. J. Stephens, "Magnetic Optical Activity," Ann. Rev. Phys. Chem. **17**, 399–432 (1966).

[24] O. Knudsen, "The Faraday Effect and Physical Theory, 1845-1873," Arch. Hist. Exact Sci. **15**, 235–281 (1976).

[25] R. Hui and M. O'Sullivan, "Fiber-based optical metrology and spectroscopy techniques," in Fiber-Optic Measurement Techniques, edited by R. Hui and M. O'Sullivan (Academic Press, Boston, MA, 2023) 2nd ed., pp. 557–649.

[26] T. Iida and H. Wakana, "Communications Satellite Systems," in Encyclopedia of Physical Science and Technology, edited by R. A. Meyers (Academic Press, New York, 2003) 3rd ed., pp. 375–408.

[27] J. L. Han, "Observing Interstellar and Intergalactic Magnetic Fields," Annu. Rev. Astron. Astrophys. **55**, 111–157 (2017).

[28] K. J. Carothers, R. A. Norwood, and J. Pyun, "High Verdet Constant Materials for Magneto-Optical Faraday Rotation: A Review," Chem. Mater. **34**, 2531–2544 (2022).

[29] E. Verdet, "Recherches sur les propriétés optiques développées dans les corps transparents par l'action du magnétisme," Ann. Chim. Phys. 3e Sér. **41**, 370–412 (1854).

[30] E. Verdet, "Recherches sur les propriétés optiques développées dans les corps transparents par l'action du magnétisme," Ann. Chim. Phys. 3e Sér. **43**, 37–44 (1855).

[31] E. Verdet, "Recherches sur les propriétés optiques développées dans les corps transparents par l'action du magnétisme," Ann. Chim. Phys. 3e Sér. **52**, 129–163 (1858).

[32] E. Verdet, "Recherches sur les propriétés optiques développées dans les corps transparents par l'action du magnétisme. de la dispersion des plans de polarisations des rayons de diverses couleurs"," Ann. Chim. Phys. 3e Sér. **69**, 415–491 (1863).

[33] H. Morita and S. Fujioka, "Generation, measurement, and modeling of strong magnetic fields generated by laser-driven micro coils," Rev. Mod. Plasma Phys. **7**, 13 (2023).

[34] D. Nakamura, A. Ikeda, H. Sawabe, Y. H. Matsuda, and S. Takeyama, "Record indoor magnetic field of 1200 T generated by electromagnetic flux-compression," Rev. Sci. Instrum. **89**, 095106 (2018).

[35] R. Serber, "The Theory of the Faraday Effect in Molecules," Phys. Rev. **41**, 489–506 (1932).

[36] L. D. Barron, Molecular Light Scattering and Optical Activity, 2nd ed. (Cambridge University Press, Cambridge, 2004).

[37] W. A. Parkinson and J. Oddershede, "Response function analysis of magnetic optical rotation," Int. J. Quantum Chem. **64**, 599–605 (1997).

[38] S. Coriani, C. Hättig, P. Jørgensen, A. Halkier, and A. Rizzo, "Coupled cluster calculations of Verdet constants," Chem. Phys. Lett. **281**, 445–451 (1997).

[39] S. Coriani, C. Hättig, P. Jørgensen, and T. Helgaker, "Gauge-origin independent magneto-optical activity within coupled cluster response theory," J. Chem. Phys. **113**, 3561–3572 (2000).

[40] S. Coriani, P. Jørgensen, O. Christiansen, and J. Gauss, "Triple excitation effects in coupled cluster calculations of Verdet constants," Chem. Phys. Lett. **330**, 463–470 (2000).

[41] B. S. Ofstad, E. Aurbakken, Ø. S. Schøyen, H. E. Kristiansen, S. Kvaal, and T. B. Pedersen, "Time-dependent coupled-cluster theory," WIREs Comput. Mol. Sci. **13**, e1666 (2023).

[42] M. Wibowo, T. J. P. Irons, and A. M. Teale, "Modeling Ultrafast Electron Dynamics in Strong Magnetic Fields Using Real-Time Time-Dependent Electronic Structure Methods," J. Chem. Theory Comput. **17**, 2137–2165 (2021).

[43] W. A. Parkinson, S. P. A. Sauer, J. Oddershede, and D. M. Bishop, "Calculation of the Verdet constants for H_2, N_2, CO, and FH," J. Chem. Phys. **98**, 487–495 (1993).

[44] T. J. P. Irons, G. David, and A. M. Teale, "Optimizing Molecular Geometries in Strong Magnetic Fields," J. Chem. Theory Comput. **17**, 2166–2185 (2021).

[45] J. Olsen and P. Jørgensen, "Linear and nonlinear response functions for an exact state and for an MCSCF state," J. Chem. Phys. **82**, 3235–3264 (1985).

[46] D. M. Bishop and S. M. Cybulski, "Magnetic optical rotation in H2 and D2," J. Chem. Phys. **93**, 590–599 (1990).

[47] F. London, "Théorie quantique des courants interatomiques dans les combinaisons aromatiques," J. Phys. Radium **8**, 397–409 (1937).

[48] P. Schmelcher and L. S. Cederbaum, "Molecules in strong magnetic fields: Properties of atomic orbitals," Phys. Rev. A **37**, 672–681 (1988).

[49]S. Lehtola, M. Dimitrova, and D. Sundholm, "Fully numerical electronic structure calculations on diatomic molecules in weak to strong magnetic fields," Mol. Phys. **118**, e1597989 (2020).

[50]T. Helgaker, P. Jørgensen, and J. Olsen, *Molecular Electronic-Structure Theory* (John Wiley & Sons, Chichester, 2000).

[51]T. D. Crawford and H. F. Schaefer III, "An Introduction to Coupled Cluster Theory for Computational Chemists," in *Reviews in Computational Chemistry*, Vol. 14, edited by K. B. Lipkowitz and D. B. Boyd (John Wiley & Sons, New York, 2000) pp. 33–136.

[52]R. J. Bartlett and M. Musiał, "Coupled-cluster theory in quantum chemistry," Rev. Mod. Phys. **79**, 291–352 (2007).

[53]I. Shavitt and R. J. Bartlett, *Many-Body Methods in Chemistry and Physics. MBPT and Coupled-Cluster Theory* (Cambridge University Press, New York, 2009).

[54]A. I. Krylov, "Equation-of-Motion Coupled-Cluster Methods for Open-Shell and Electronically Excited Species: The Hitchhiker's Guide to Fock Space," Annu. Rev. Phys. Chem. **59**, 433–462 (2008).

[55]K. Sneskov and O. Christiansen, "Excited state coupled cluster methods," WIREs Comput. Mol. Sci. **2**, 566–584 (2012).

[56]T. Helgaker, S. Coriani, P. Jørgensen, K. Kristensen, J. Olsen, and K. Ruud, "Recent Advances in Wave Function-Based Methods of Molecular-Property Calculations," Chem. Rev. **112**, 543–631 (2012).

[57]K. Raghavachari, G. W. Trucks, J. A. Pople, and M. Head-Gordon, "A fifth-order perturbation comparison of electron correlation theories," Chem. Phys. Lett. **157**, 479–483 (1989).

[58]E. I. Tellgren, S. S. Reine, and T. Helgaker, "Analytical GIAO and hybrid-basis integral derivatives: application to geometry optimization of molecules in strong magnetic fields," Phys. Chem. Chem. Phys. **14**, 9492–9499 (2012).

[59]T. J. P. Irons, J. Zemen, and A. M. Teale, "Efficient Calculation of Molecular Integrals over London Atomic Orbitals," J. Chem. Theory Comput. **13**, 3636–3649 (2017).

[60]T. B. Pedersen and S. Kvaal, "Symplectic integration and physical interpretation of time-dependent coupled-cluster theory," J. Chem. Phys. **150**, 144106 (2019).

[61]O. Christiansen, H. Koch, and P. Jørgensen, "The second-order approximate coupled cluster singles and doubles model CC2," Chem. Phys. Lett. **243**, 409–418 (1995).

[62]H. E. Kristiansen, B. S. Ofstad, E. Hauge, E. Aurbakken, Ø. S. Schøyen, S. Kvaal, and T. B. Pedersen, "Linear and Nonlinear Optical Properties from TDOMP2 Theory," J. Chem. Theory Comput. **18**, 3687–3702 (2022).

[63]T. B. Pedersen, H. Koch, and C. Hättig, "Gauge invariant coupled cluster response theory," J. Chem. Phys. **110**, 8318–8327 (1999).

[64]T. Sato, H. Pathak, Y. Orimo, and K. L. Ishikawa, "Communication: Time-dependent optimized coupled-cluster method for multielectron dynamics," J. Chem. Phys. **148**, 051101 (2018).

[65]T. B. Pedersen, B. Fernández, and H. Koch, "Gauge invariant coupled cluster response theory using optimized nonorthogonal orbitals," J. Chem. Phys. **114**, 6983–6993 (2001).

[66]S. Kvaal, "Ab initio quantum dynamics using coupled-cluster," J. Chem. Phys. **136**, 194109 (2012).

[67]H. E. Kristiansen, Ø. S. Schøyen, S. Kvaal, and T. B. Pedersen, "Numerical stability of time-dependent coupled-cluster methods for many-electron dynamics in intense laser pulses," J. Chem. Phys. **152**, 071102 (2020).

[68]H. Pathak, T. Sato, and K. L. Ishikawa, "Time-dependent optimized coupled-cluster method for multielectron dynamics. III. A second-order many-body perturbation approximation," J. Chem. Phys. **153**, 034110 (2020).

[69]E. H. Lieb, "Density functionals for Coulomb systems," Int. J. Quantum Chem. **24**, 243–277 (1983).

[70]A. M. Lee, N. C. Handy, and S. M. Colwell, "The density functional calculation of nuclear shielding constants using London atomic orbitals," J. Chem. Phys. **103**, 10095–10109 (1995).

[71]W. Zhu and S. B. Trickey, "Exact density functionals for two-electron systems in an external magnetic field," J. Chem. Phys. **125**, 094317 (2006).

[72]J. F. Dobson, "Alternative expressions for the fermi hole curvature," J. Chem. Phys. **98**, 8870–8872 (1993).

[73]A. D. Becke, "Current-density dependent exchange-correlation functionals," Can. J. Chem. **74**, 995–997 (1996).

[74]J. E. Bates and F. Furche, "Harnessing the meta-generalized gradient approximation for time-dependent density functional theory," J. Chem. Phys. **137**, 164105 (2012).

[75]J. Tao, J. P. Perdew, V. N. Staroverov, and G. E. Scuseria, "Climbing the density functional ladder: Nonempirical meta–generalized gradient approximation designed for molecules and solids," Phys. Rev. Lett. **91**, 146401 (2003).

[76]T. J. P. Irons, L. Spence, G. David, B. T. Speake, T. Helgaker, and A. M. Teale, "Analyzing Magnetically Induced Currents in Molecular Systems Using Current-Density-Functional Theory," J. Phys. Chem. A **124**, 1321–1333 (2020).

[77]J. F. Stanton and R. J. Bartlett, "The equation of motion coupled-cluster method. A systematic biorthogonal approach to molecular excitation energies, transition probabilities, and excited state properties," J. Chem. Phys. **98**, 7029–7039 (1993).

[78]F. Ding, B. E. Van Kuiken, B. E. Eichinger, and X. Li, "An efficient method for calculating dynamical hyperpolarizabilities using real-time time-dependent density functional theory," J. Chem. Phys. **138**, 064104 (2013).

[79]B. S. Ofstad, H. E. Kristiansen, E. Aurbakken, Ø. S. Schøyen, S. Kvaal, and T. B. Pedersen, "Adiabatic extraction of nonlinear optical properties from real-time time-dependent electronic-structure theory," J. Chem. Phys. **158**, 154102 (2023).

[80]Aurbakken, E. and Fredly, K. H. and Kristiansen, H. E. and Kvaal, S. and Myhre, R. H. and Ofstad, B. S. and Pedersen, T. B. and Schøyen, Ø. S. and Sutterud, H. and Winther-Larsen, S. G., "HyQD: Hylleraas Quantum Dynamics," (2023-02-04), URL: https://github.com/HyQD.

[81]QUEST, "QUEST, a rapid development platform for QUantum Electronic-Structure Techniques," (2022), URL: https://quest.codes.

[82]T. B. Pedersen and H. Koch, "Coupled cluster response functions revisited," J. Chem. Phys. **106**, 8059–8072 (1997).

[83]F. Hampe, S. Stopkowicz, N. Gross, M.-P. Kitsaras, L. Grazioli, S. Blaschke, P. Yergün, and L. Monzel, "QCUMBRE, quantum chemical utility enabling magnetic-field dependent investigations benefitting from rigorous electron-correlation treatment," (2023).

[84]J. F. Stanton, J. Gauss, L. Cheng, M. E. Harding, D. A. Matthews, and P. G. Szalay, "CFOUR, Coupled-Cluster techniques for Computational Chemistry, a quantum-chemical program package," With contributions from A. Asthana, A.A. Auer, R.J. Bartlett, U. Benedikt, C. Berger, D.E. Bernholdt, S. Blaschke, Y. J. Bomble, S. Burger, O. Christiansen, D. Datta, F. Engel, R. Faber, J. Greiner, M. Heckert, O. Heun, M. Hilgenberg, C. Huber, T.-C. Jagau, D. Jonsson, J. Jusélius, T. Kirsch, M.-P. Kitsaras, K. Klein, G.M. Kopper, W.J. Lauderdale, F. Lipparini, J. Liu, T. Metzroth, L.A. Mück, D.P. O'Neill, T. Nottoli, J. Oswald, D.R. Price, E. Prochnow, C. Puzzarini, K. Ruud, F. Schiffmann, W. Schwalbach, C. Simmons, S. Stopkowicz, A. Tajti, T. Uhlirova, J. Vázquez, F. Wang, J.D. Watts, P. Yergün, C. Zhang, XZheng, and the integral packages MOLECULE (J. Almlöf and P.R. Taylor), PROPS (P.R. Taylor), ABACUS (T. Helgaker, H.J. Aa. Jensen, P. Jørgensen, and J. Olsen), and ECP routines by A. V. Mitin and C. van Wüllen. For the current version, see http://www.cfour.de.

[85]D. A. Matthews, L. Cheng, M. E. Harding, F. Lipparini, S. Stopkowicz, T.-C. Jagau, P. G. Szalay, J. Gauss, and J. F. Stanton, "Coupled-cluster techniques for computational chemistry: The CFOUR program package," J. Chem. Phys. **152**, 214108 (2020).

[86]J. Gauss, F. Lipparini, S. Burger, S. Blaschke, M. Kitsaras, and S. Stopkowicz, "MINT, Mainz INTegral package," (2015-2021), Johannes Gutenberg-Universität Mainz, unpublished.

[87] T. H. Dunning, "Gaussian basis sets for use in correlated molecular calculations. I. The atoms boron through neon and hydrogen," J. Chem. Phys. **90**, 1007–1023 (1989).

[88] R. A. Kendall, T. H. Dunning, and R. J. Harrison, "Electron affinities of the first-row atoms revisited. Systematic basis sets and wave functions," J. Chem. Phys. **96**, 6796–6806 (1992).

[89] D. E. Woon and T. H. Dunning, "Gaussian basis sets for use in correlated molecular calculations. iv. calculation of static electrical response properties," J. Chem. Phys. **100**, 2975–2988 (1994).

[90] B. P. Prascher, D. E. Woon, K. A. Peterson, T. H. Dunning, and A. K. Wilson, "Gaussian basis sets for use in correlated molecular calculations. vii. valence, core-valence, and scalar relativistic basis sets for li, be, na, and mg," Theor. Chem. Acc. **128**, 69–82 (2011).

[91] E. Hairer, G. Wanner, and C. Lubich, *Geometric Numerical Integration*, 2nd ed. (Springer, Berlin, Heidelberg, 2006).

[92] L. R. Ingersoll and D. H. Lebenberg, "Faraday Effect in Gases and Vapors. II," J. Opt. Soc. Am. **46**, 538–542 (1956).

[93] S. Blanes and F. Casas, *A Concise Introduction to Geometric Numerical Integration* (CRC press: Boca Raton, 2016).

[94] B. C. Mort and J. Autschbach, "Vibrational corrections to magneto-optical rotation — A computational study," J. Phys. Chem. A **111**, 5563–5571 (2007).

[95] A. J. Garza, G. E. Scuseria, S. B. Khan, and A. M. Asiri, "Assessment of long-range corrected functionals for the prediction of non-linear optical properties of organic materials," Chem. Phys. Lett. **575**, 122–125 (2013).

[96] M. Chołuj, J. Kozłowska, and W. Bartkowiak, "Benchmarking DFT methods on linear and nonlinear electric properties of spatially confined molecules," Int. J. Quantum Chem. **118**, e25666 (2018).

[97] S. Hahn, K. Kim, K. Kim, X. Hu, T. Painter, I. Dixon, S. Kim, K. R. Bhattarai, S. Noguchi, J. Jaroszynski, and D. C. Larbalestier, "45.5-tesla direct-current magnetic field generated with a high-temperature superconducting magnet," Nature **570**, 496–499 (2019).

Paper IV

Transient spectroscopy from time-dependent electronic-structure theory without multipole expansions

IV

Paper V

Time-dependent coupled-cluster theory

V

ADVANCED REVIEW

Time-dependent coupled-cluster theory

Benedicte Sverdrup Ofstad[1] [iD] | Einar Aurbakken[1] [iD] |
Øyvind Sigmundson Schøyen[2] [iD] | Håkon Emil Kristiansen[1] [iD] | Simen Kvaal[1] [iD] |
Thomas Bondo Pedersen[1] [iD]

[1]Hylleraas Centre for Quantum Molecular Sciences, Department of Chemistry, University of Oslo, Oslo, Norway

[2]Department of Physics, University of Oslo, Oslo, Norway

Correspondence
Thomas Bondo Pedersen, Hylleraas Centre for Quantum Molecular Sciences, Department of Chemistry, University of Oslo, Oslo, Norway.
Email: t.b.pedersen@kjemi.uio.no

Funding information
Centre for Advanced Study in Oslo; Norges Forskningsråd, Grant/Award Number: 262695

Edited by: Sandra Luber, Associate Editor

Abstract

Recent years have witnessed an increasing interest in time-dependent coupled-cluster (TDCC) theory for simulating laser-driven electronic dynamics in atoms and molecules, and for simulating molecular vibrational dynamics. Starting from the time-dependent bivariational principle, we review different flavors of single-reference TDCC theory with either orthonormal static, orthonormal time-dependent, or biorthonormal time-dependent spin orbitals. The time-dependent extension of equation-of-motion coupled-cluster theory is also discussed, along with the applications of TDCC methods to the calculation of linear absorption spectra, linear and low-order nonlinear response functions, highly nonlinear high harmonic generation spectra and ionization dynamics. In addition, the role of TDCC theory in finite-temperature many-body quantum mechanics is briefly described along with a few other application areas.

This article is categorized under:

    Electronic Structure Theory > Ab Initio Electronic Structure Methods
    Theoretical and Physical Chemistry > Spectroscopy
    Software > Simulation Methods

KEYWORDS

attosecond dynamics, coupled-cluster theory, laser-driven electron dynamics, transient spectroscopy, vibrational coupled-cluster

1 | INTRODUCTION

The objective of time-dependent molecular electronic structure theory[1,2] is to solve the time-dependent Schrödinger equation (TDSE),

$$\left(\mathrm{i}\partial_t - \widehat{H}(t)\right)|\Psi(t)\rangle = 0, \qquad |\Psi(0)\rangle = |\Psi_0\rangle, \tag{1}$$

where the Hamiltonian, $\widehat{H}(t) = \widehat{H}_0 + \widehat{V}(t)$, contains the time-independent, clamped-nuclei Born–Oppenheimer electronic Hamiltonian,[3,4] $\widehat{H}_0$, and an explicitly time-dependent operator, $\widehat{V}(t)$, representing the interaction of the electrons with external driving forces, usually electromagnetic fields. Atomic units will be used throughout this review unless explicitly stated otherwise. With the appropriate initial state, $|\Psi_0\rangle$, the TDSE thus allows simulation of electronic dynamics directly corresponding to experimental setups.

However, within the clamped-nuclei approximation, time-dependent electronic structure theory can only be expected to yield reliable dynamics on time scales short enough that nuclear motion can be neglected—typically, up to a few femtoseconds. An important example is the charge migration across the nuclear framework initiated by ionization.[5] For longer time scales, the nonadiabatic coupling of electronic and nuclear motion must be taken into account using, for example, semiclassical methods based on the Ehrenfest theorem[6,7] or, if feasible, fully quantum-mechanical methods like the time-dependent Feshbach close-coupling method.[8] An obvious application of time-dependent electronic structure theory thus is the simulation of processes induced by attosecond laser pulses,[9] including attosecond transient absorption spectroscopy.[10] However, the broad spectral range of attosecond laser pulses combined with relatively high intensities almost invariably induce ionization processes, placing heavy demands on the electronic structure method and basis sets, which must accurately capture both bound states and the electronic continuum. The most accurate approach is to solve the TDSE using mesh-based methods in both space and time such as, for example, the finite element discrete variable representation [FEDVR].[11] Although not without limitations, a less computationally demanding approach is based on density-functional theory in combination with scattering states expanded in B-splines.[9,12]

Direct simulation of experiments is not the only valuable application of the TDSE; for example, energies and in principle also the associated stationary-state wave functions of $\widehat{H}_0$ can be extracted from simulations *without* external driving forces simply by starting in a nonstationary state.[13] With judicious but artificial choices of the interaction operator $\widehat{V}(t)$, the TDSE can also be used as an alternative to perturbation theory for the calculation of molecular optical properties and spectra. A weak electric-field kick applied to the electronic ground state, for example, yields linear absorption spectra from the induced electric-dipole moment. The spectra automatically include all electric-dipole allowed transitions, both valence and core excitations, from a single simulation or a few simulations, depending on symmetry and whether the spectrum is simulated for an aligned or randomly oriented sample.[2] This approach avoids diagonalization of large matrices and is potentially advantageous for systems with a high density of states where a large number of eigenvalues would be needed in traditional time-independent methods. Linear and low-order nonlinear optical properties—polarizabilities and hyperpolarizabilities—can be extracted from induced electric and magnetic moments using either a ramped continuous wave[14] or a pulsed wave[15] to perturb the ground-state wave function. Only a few, relatively short simulations are required.

The main computational obstacles for methods aimed at solving the TDSE are the long simulation times required to achieve sufficient resolution in Fourier analyses of the recorded signals and the small time steps required to capture high-frequency components in the wave function. Since electron correlation effects must be accounted for, it is no surprise that the most widely used electronic-structure method for electronic dynamics simulations is time-dependent density-functional theory (TDDFT),[16–18] often called real-time (RT) TDDFT to clearly distinguish it from perturbation-based density response theory in the frequency domain. Similar to ground-state calculations, the TDDFT approach often strikes a reasonable balance between computational effort and accuracy.

For higher accuracy, one must turn to methods that parameterize the wave function explicitly. Since electronic excited states are often multi-configurational, high-accuracy simulations of electronic dynamics have been dominated by the multi-configurational time-dependent Hartree–Fock (MCTDHF) method[19–23] or the closely related complete,[24] restricted,[25,26] and generalized[27] active space self-consistent field methods. These methods suffer from the *curse of dimensionality*, making coupled-cluster (CC)[28–31] approximations attractive alternatives with their more benign polynomial scaling, at least for simulating electronic processes where the time-dependent wave function is dominated by a single, generally time-dependent, electron configuration.

Time-dependent CC (TDCC) theory was first formulated by Monkhorst[32] in 1977, albeit not with the purpose of studying electronic dynamics. Rather, Monkhorst[32] and later Dalgaard and Monkhorst[33] applied perturbation theory to the TDCC equations and derived expressions for linear response properties such as the frequency-dependent electric-dipole polarizability, identifying excitation energies—the poles of the linear response function—as the eigenvalues of a non-hermitian matrix. The non-hermiticity implies that the eigenvalues are not necessarily real and, indeed, Takahashi and Paldus[34] observed complex eigenvalues in their orthogonally spin-adapted TDCC approach to excitation energies. However, they only obtained complex excitation energies with a (quoting Takahashi and Paldus[34]) "very poor (in fact almost meaningless) CC representation for the ground state" of strongly correlated systems. Complex excitation energies would be potentially disastrous for a TDCC description of electronic dynamics,[35] but we note that Thomas et al.[36] have recently argued that complex eigenvalues should be rare except in the context of conical intersections.[37–39]

Like time-independent CC theory,[40–43] TDCC theory without perturbation expansions has its roots in nuclear physics.[44–46] While Monkhorst's TDCC formulation was based on a fixed reference determinant, Hoodbhoy and Negele[44,45] allowed the underlying spin orbitals to be time-dependent, determined by time-dependent Hartree–Fock theory. (We will

use the terms spin orbital and orbital interchangeably.) Note, however, that Pigg et al.[46] used static orbitals in the most recent application of TDCC theory to nucleon dynamics. Later, in analogy to MCTDHF theory, the time evolution of the orbitals was formulated with full coupling to the evolution of the correlating cluster amplitudes.[47–49] Shortly after the publication of Hoodbhoy and Negele's first article,[44] Schönhammer and Gunnarsson[50] applied TDCC theory to compute the spectral weight function from the phase factor of the TDCC wave function for prediction of core-level spectra of atomic and molecular adsorbates. The next application of TDCC theory was also to a solid-state problem. In 1985, Sebastian[51] used TDCC theory to simulate scattering of high-energy cations from surfaces, computing the probability of neutralization through a one-electron charge-transfer process. Sebastian proposed a conventional expression for the TDCC expectation-value functional which, for truncated cluster operators, does not fulfill the Hellmann–Feynman theorem.[52,53]

A CC expectation-value functional that fulfills the Hellmann–Feynman theorem is a key result of Arponen's bivariational formulation[54] and of the equivalent constrained optimization approach of Helgaker and Jørgensen.[55,56] This expectation-value functional quickly became the standard choice and was used by Bishop and Emary in their TDCC study of a two-level system in a quantized electromagnetic field.[35]

The remainder of this review is organized as follows. We start in Section 2 with a brief summary of traditional perturbative approaches to TDCC theory with emphasis on concepts that are important for the time-dependent bivariational theory presented in Section 3. In Section 4, we describe the time-dependent extension of equation-of-motion CC theory, which is equivalent to TDCC theory in the limit of untruncated cluster operators, while Section 5 reviews TDCC theory applied to molecular vibrational dynamics. Finally, Section 6 briefly reviews a few other application areas where TDCC theory plays a role, and Section 7 contains our concluding remarks.

2 | PERTURBATION-BASED APPROACHES

Besides the early applications to dynamical systems mentioned above, TDCC theory has mainly been used as a starting point for the calculation of frequency-dependent response properties in molecular electronic-structure theory.[57] Inspired by Helgaker and Jørgensen's[55,56] constrained optimization (Lagrangian) approach to static properties as energy derivatives and by Olsen and Jørgensen's[58] time-dependent variational formulation of response theory, Koch and Jørgensen[59] generalized the perturbation-based TDCC approach of Monkhorst[32] and Dalgaard and Monkhorst[33] to formulate a general CC response theory. Equivalent to the bivariational theory of the "normal" TDCC method of Arponen,[54] the starting point is *independent Ansätze* for the wave function and its conjugate

$$|\Psi(t)\rangle = e^{\widehat{T}(t)}|\Phi_0\rangle e^{\tau_0(t)}, \tag{2}$$

$$\langle\widetilde{\Psi}(t)| = e^{-\tau_0(t)}\langle\Phi_0|\left(1+\widehat{\Lambda}(t)\right)e^{-\widehat{T}(t)}, \tag{3}$$

where the normalized reference Slater determinant, $|\Phi_0\rangle$, is time-independent and usually taken to be the Hartree–Fock ground-state determinant. The cluster operators $\widehat{T}(t)$ and $\widehat{\Lambda}(t)$ for an N-electron system are parameterized by time-dependent amplitudes $\tau(t)$ and $\lambda(t)$,

$$\widehat{T}(t) = \sum_\mu \tau_\mu(t)\widehat{X}_\mu, \quad \widehat{\Lambda}(t) = \sum_\mu \lambda_\mu(t)\widehat{Y}_\mu, \tag{4}$$

where the summations are over all possible excitations out of the reference determinant: $\widehat{X}$ and $\widehat{Y}$ denote excitation and de-excitation operators such that

$$\left\langle\widetilde{\Phi}_\mu|\Phi_\nu\right\rangle = \left\langle\Phi_0|\widehat{Y}_\mu\widehat{X}_\nu|\Phi_0\right\rangle = \delta_{\mu\nu}. \tag{5}$$

Note that the excitation and de-excitation operators separately commute: $\left[\widehat{X}_\mu,\widehat{X}_\nu\right] = \left[\widehat{Y}_\mu,\widehat{Y}_\nu\right] = 0$. While the phase amplitude, $\tau_0(t)$, plays no role in CC response theory as formulated by Koch and Jørgensen, it becomes important in the interpretation of TDCC dynamics.[60,61]

Truncation of the cluster operators after single excitations yields the TDCC singles (TDCCS) model, after singles and doubles yields the TDCC singles and doubles (TDCCSD) model, and so on. If the cluster operators are not truncated, TDCC theory becomes equivalent to the formally exact time-dependent full configuration interaction (TDFCI) theory, albeit with a wave function which is not normalized. Regardless of truncation, the TDCC wave functions instead satisfy the (intermediate) normalization conditions

$$e^{-\tau_0(t)}\langle\Phi_0|\Psi(t)\rangle = 1, \quad \left\langle\widetilde{\Psi}(t)|\Psi(t)\right\rangle = 1. \tag{6}$$

The equations of motion for the amplitudes are derived by inserting $|\Psi(t)\rangle$ and $\langle\widetilde{\Psi}(t)|$ into the TDSE and its conjugate, respectively, followed by projection onto the excited determinants, yielding[59]

$$i\dot{\tau}_\mu(t) = \left\langle\widetilde{\Phi}_\mu|e^{-\widehat{T}(t)}\widehat{H}(t)e^{\widehat{T}(t)}|\Phi_0\right\rangle, \tag{7}$$

$$i\dot{\lambda}_\mu(t) = -\left\langle\widetilde{\Psi}(t)\left|\left[\widehat{H}(t),\widehat{X}_\mu\right]\right|\Psi(t)\right\rangle, \tag{8}$$

where, as usual, the "dot" denotes the time derivative. The phase amplitude is determined by

$$i\dot{\tau}_0(t) = \left\langle\Phi_0|e^{-\widehat{T}(t)}\widehat{H}(t)e^{\widehat{T}(t)}|\Phi_0\right\rangle. \tag{9}$$

Assuming that the electronic system is initially in its ground state and that the driving forces are adiabatically switched-on and weak, the amplitudes are expanded in orders of the perturbation, leading to equations that must be solved order-by-order. Rather than solving the equations in the time domain, it is assumed that the Fourier transforms of the interaction operator, $\widehat{V}(t)$, and of the nth order, $n \geq 1$ amplitudes exist, such that the amplitude equations can be transformed to the frequency domain and solved at the frequencies of interest.

The expectation value of an operator $\widehat{A}$ takes the form originally suggested by Arponen[54]

$$\left\langle\widehat{A}\right\rangle(t) = \left\langle\widetilde{\Psi}(t)|\widehat{A}|\Psi(t)\right\rangle, \tag{10}$$

which satisfies the time-dependent Hellmann–Feynman theorem.[62-64] Note that the expectation value does not depend on the phase amplitude $\tau_0(t)$. Expanding the expectation value in orders of the perturbation then leads to an identification of linear, quadratic, cubic, etc. response functions. If, for example, $\widehat{V}(t)$ represents the interaction of the electrons with an electric field in the electric-dipole approximation, the response functions are (apart from a sign) the electric-dipole polarizability and hyperpolarizabilities. Excitation energies and transition moments are identified from the poles and residues of the response functions. If the interaction operator is further assumed periodic in time such that its Fourier series converges, equivalent expressions for the CC response functions can be conveniently derived as derivatives of the cycle-averaged quasienergy Lagrangian.[57,65]

Solving the TDSE with the ground state as the initial condition is thus the starting point for CC response theory. In principle, the perturbative solutions obtained in the frequency domain can be transformed back to the time domain but this would require a dense grid of frequencies and is never done in practice. Hence, in effect, CC response theory is a time-independent method. Another time-independent approach is equation-of-motion CC (EOM-CC) theory,[30,66-70] where excited states are written explicitly as linear excitation operators acting on the CC ground-state wave function. This is a fundamentally different approach from CC response theory where explicit expressions for excited-state wave functions are neither needed nor assumed. Still, the excitation energies obtained from CC response theory are identical to those obtained from EOM-CC theory: The same non-hermitian eigenvalue problem arises in both theories. Transition moments and response functions differ, however, and only those obtained from (truncated) CC response theory are properly size consistent.[71,72] Both CC response theory and EOM-CC theory converge to the full configuration interaction (FCI) limit when no truncation of the cluster (and linear excitation) operators are introduced. A formulation of response theory starting from a time-dependent EOM-CC *Ansatz* has been given by Coriani et al.[73]

For truncated cluster operators, the expectation-value functional (10) leads to broken symmetry properties of the CC response functions under complex conjugation. This issue, which results in spurious origin-dependence of some optical properties, is rather easily fixed by using only the real part of Equation (10), as suggested by Pedersen and Koch.[74] Alternatively, one can enforce the proper symmetries on the response functions a posteriori.[65] Another issue of truncated TDCC theory is gauge dependence.[74–77] In order to resolve this, the orbitals must be dynamical variables and Pedersen, Koch and coworkers proposed the time-dependent orbital-optimized CC (TDOCC) model[47] and later the time-dependent nonorthogonal orbital-optimized CC (TDNOCC) model,[48] which were formulated as response theories. Never implemented in a production-level code, the TDOCC and TDNOCC models have not been extensively used or tested, but they have gained importance for studying laser-driven electronic dynamics through Kvaal's formulation of orbital-adaptive time-dependent coupled-cluster (OATDCC) theory,[49] which is an adaptation of the basic idea of MCTDHF theory. The OATDCC model is equivalent to TDNOCC theory if the underlying time-dependent orbital space is not split into active and external subspaces. For dynamics, it is advantageous to start from the bivariational approach of Arponen.[54]

3 | ELECTRONIC DYNAMICS WITH BIVARIATIONAL CC THEORIES

While computationally demanding, RT TDCC theory offers clear advantages over perturbation-based approaches. Explicitly time-dependent simulations contain responses to all orders and, therefore, are able to describe highly nonlinear optical phenomena in a time-resolved manner. Furthermore, experimental parameters like pulse shape and pulse duration can be embedded directly into the simulation. The TDCC methods can accordingly serve as a theoretical complement to the increasingly topical field of experimental attosecond science. For certain use cases, such as the calculation of near-edge x-ray absorption spectra, TDCC simulations may even prove to be computationally competitive.

The first application of TDCC theory to simulate laser-driven molecular electronic dynamics was presented in 2011 by Huber and Klamroth[78] who used the semiclassical electric-dipole approximation, truncated the cluster operator $\widehat{T}(t)$ after double excitations to obtain the TDCCSD model, and propagated only the τ amplitudes according to Equation (7). Consequently, induced electric-dipole moments could not be computed from Equation (10) and Huber and Klamroth instead resorted to an approximation using the configuration interaction singles-and-doubles expression, leading to relatively large errors in excitation energies. More detrimental to the prospects of TDCC theory of laser-driven electronic dynamics, Huber and Klamroth found that the TDCCSD method became numerically unstable in strong external fields and with increasing basis set quality.

3.1 | The bivariational formalism

Arponen's bivariational principle[54] naturally leads to the expectation-value functional (10) which satisfies the Hellmann–Feynman theorem, both in the time-independent and in the time-dependent case. In the FCI limit, Arponen's *extended* CC formulation is equivalent to the Lagrangian approach of Helgaker and Jørgensen,[55,56] as discussed in detail by Kvaal.[79]

The starting point is the bivariational action functional[54]

$$S\left[\widetilde{\Psi}, \Psi\right] = \int_0^T \mathcal{L} \mathrm{d}t, \tag{11}$$

with the Lagrangian

$$\mathcal{L} = \left\langle \widetilde{\Psi}(t) | \mathrm{i}\partial_t - \widehat{H}(t) | \Psi(t) \right\rangle = \mathrm{i}\left\langle \widetilde{\Psi}(t) | \dot{\Psi}(t) \right\rangle - \mathcal{H}(t), \tag{12}$$

where the Hamilton function is

$$\mathcal{H}(t) = \left\langle \widetilde{\Psi}(t) | \widehat{H}(t) | \Psi(t) \right\rangle. \tag{13}$$

The ket and bra, $|\Psi(t)\rangle$ and $\langle\widetilde{\Psi}(t)|$, are independent approximations to the exact wave function and its conjugate, respectively. Under the condition that the bivariational action functional is complex analytic, requiring $\mathcal{S}$ be stationary with respect to variations in the bra and in the ket leads to the TDSE and its conjugate:

$$i\,|\,\dot{\Psi}(t)\rangle = \frac{\partial\mathscr{H}}{\partial\langle\widetilde{\Psi}(t)\,|}, \tag{14}$$

$$i\langle\dot{\widetilde{\Psi}}(t)\,| = -\frac{\partial\mathscr{H}}{\partial\,|\,\Psi(t)\rangle}. \tag{15}$$

These equations guarantee that the normalization condition

$$\left\langle\widetilde{\Psi}(t)|\Psi(t)\right\rangle = 1, \tag{16}$$

is conserved. Evidently, Equations (14) and (15) are complex symplectic generalizations of the classical Hamiltonian equations[80] with the ket and bra functions as canonical variables. This connection with classical Hamiltonian mechanics has been extensively explored by Arponen and coworkers[81–84] (see also Ref. [64]) and suggests that $|\Psi(t)\rangle$ and $\langle\widetilde{\Psi}(t)|$ *together* represent the quantum state of the system.

This observation led Pedersen and Kvaal[60] to propose the two-component state vector

$$|\,S\rangle\rangle = \frac{1}{\sqrt{2}}\begin{pmatrix}|\Psi\rangle\\ |\widetilde{\Psi}\rangle\end{pmatrix}, \tag{17}$$

and the *indefinite* inner product

$$\begin{aligned}\langle\langle S_1|S_2\rangle\rangle &= \frac{1}{2}\left(\langle\widetilde{\Psi}_1|\ \langle\Psi_1|\right)\begin{pmatrix}|\Psi_2\rangle\\ |\widetilde{\Psi}_2\rangle\end{pmatrix}\\ &= \frac{1}{2}\left\langle\widetilde{\Psi}_1|\Psi_2\right\rangle + \frac{1}{2}\left\langle\widetilde{\Psi}_2|\Psi_1\right\rangle^*,\end{aligned} \tag{18}$$

which induces the expectation-value functional

$$\left\langle\widehat{A}\right\rangle = \frac{1}{2}\left\langle\widetilde{\Psi}|\widehat{A}|\Psi\right\rangle + \frac{1}{2}\left\langle\widetilde{\Psi}|\widehat{A}^\dagger|\Psi\right\rangle^*. \tag{19}$$

This form still satisfies the Hellmann–Feynman theorem and naturally leads to the correct symmetries in response functions.[64,74] For hermitian operators, the expectation-value functional (19) equals the real part of Equation (10).

Using z to denote the vector of *all* wave function variables, the Lagrangian becomes a function of z, $\dot{z}$, and time t, $\mathscr{L} = \mathscr{L}(z,\dot{z},t)$, and the stationarity condition becomes the Euler–Lagrange equations

$$\frac{\mathrm{d}}{\mathrm{d}t}\frac{\partial\mathscr{L}}{\partial\dot{z}_\mu} = \frac{\partial\mathscr{L}}{\partial z_\mu}, \tag{20}$$

which may offer a simpler derivation of the equations of motion for the chosen approximate parameterization.

3.2 | Formulations of TDCC theory with static or time-dependent orbitals

The *Ansätze* for the ket and bra states take the general form

$$|\Psi(t)\rangle = e^{\widehat{T}(t)} |\Phi_0(t)\rangle e^{\tau_0(t)}, \tag{21}$$

$$\langle\widetilde{\Psi}(t)| = e^{-\tau_0(t)} \langle\widetilde{\Phi}_0(t)| \left(\lambda_0(t) + \widehat{\Lambda}(t)\right) e^{-\widehat{T}(t)}, \tag{22}$$

such that, with $\lambda_0 = 1$, the state vector (17) is normalized with respect to the indefinite inner product (18), $\langle\langle S(t)|S(t)\rangle\rangle = \text{Re}(\lambda_0(t))$. The phase amplitude τ_0 is canonically conjugate to λ_0.

In the conventional TDCC theory for an N-electron system, $|\Phi_0(t)\rangle = |\Phi_0\rangle$ is chosen to be the time-independent field-free Hartree–Fock ground-state determinant and $\langle\widetilde{\Phi}_0(t)| = \langle\Phi_0|$. The underlying spin orbitals are orthonormal and the cluster operator $\widehat{T}(t)$ $(\widehat{\Lambda}(t))$ contains from single to n-tuple, $1 \leq n \leq N$, excitation (de-excitation) operators with respect to the Hartree–Fock determinant. The cluster operators are parameterized by the amplitudes $\tau(t)$ and $\lambda(t)$, one amplitude per excitation and de-excitation, as in Equation (4). If $n = N$, conventional TDCC theory is equivalent to the formally exact TDFCI theory, although the intermediate normalization $\exp(-\tau_0(t))\langle\Phi_0|\Psi(t)\rangle = 1$ may cause severe numerical instabilities (see below for details). The amplitude equations of motion are given by Equations (7) and (8).

In time-dependent nonorthogonal orbital-optimized CC (TDNOCC) theory,[48] all determinants contributing to $|\Psi(t)\rangle$ and $\langle\widetilde{\Psi}(t)|$ are time-dependent variational parameters. The underlying spin orbitals constitute a biorthonormal set, $\langle\widetilde{\phi}_p(t)|\phi_q(t)\rangle = \delta_{pq}$. Single excitations (de-excitations) are redundant when the orbitals are time-dependent[48,49] and, consequently, they are removed from $\widehat{T}(t)$ $(\widehat{\Lambda}(t))$ in TDNOCC theory.

Inspired by MCTDHF theory, orbital-adaptive TDCC (OATDCC)[49] theory adds the concept of active orbital space to TDNOCC theory. The cluster operators are restricted to a subset of the orbital space, which is optimized along with its orthogonal complement throughout the dynamics. This approach is very important for describing ionization dynamics.

With time-dependent orbitals, the amplitude equations of motion become[49]

$$i\dot{\tau}_\mu = \left\langle \widetilde{\Phi}_\mu | e^{-\widehat{T}} \left(\widehat{H} - i\widehat{D}_0\right) e^{\widehat{T}} | \Phi_0 \right\rangle, \tag{23}$$

$$-i\dot{\lambda}_\mu = \left\langle \widetilde{\Psi} | \left[\widehat{H} - i\widehat{D}_0, \widehat{X}_\mu\right] | \Psi \right\rangle, \tag{24}$$

where $\mu \geq 0$, $\widehat{X}_\mu$ is an excitation operator such that $|\Phi_\mu\rangle = \widehat{X}_\mu |\Phi_0\rangle$, $\widehat{X}_0 = 1$, and $\langle\widetilde{\Phi}_\mu|\Phi_\nu\rangle = \delta_{\mu\nu}$. Since $\dot{\lambda}_0 = 0$, normalization with respect to the indefinite inner product is conserved and $\lambda_0 = 1$ is a natural choice. The time-dependence of the orbitals gives rise to the operator

$$\widehat{D}_0 = \sum_{pq} <\widetilde{\phi}_p|\dot{\phi}_q> \widehat{a}_p^\dagger \widehat{a}_q, \tag{25}$$

where the creation and annihilation operators, which satisfy the usual fermionic anticommutator relations, refer to the biorthonormal orbitals. With time-dependent orbitals, the τ and λ amplitude equations become coupled and must be solved simultaneously.

If all orbitals are chosen active, we may write[49]

$$|\dot{\phi}_q\rangle = \sum_p |\varphi_p\rangle \eta_q^p, \quad \langle\dot{\widetilde{\phi}}_p| = -\sum_q \eta_q^p \langle\widetilde{\phi}_q|. \tag{26}$$

The nonvanishing components of η_q^p are determined by the linear equations

$$i\sum_{bj} A_{aj}^{ib}\eta_b^j = R_a^i, \tag{27}$$

$$-i\sum_{bj} A_{bi}^{ja}\eta_j^b = R_i^a, \tag{28}$$

where the right-hand sides depend on the correlated one- and two-electron effective density matrices, thus coupling the orbital evolution to the correlating amplitudes. For explicit expressions for the right-hand sides, we refer to Equations (30a) and (30b) of Ref. [49]. The matrix elements A_{aj}^{ib} are given by

$$A_{aj}^{ib} = \delta_a^b \rho_j^i - \delta_j^i \rho_a^b, \tag{29}$$

where ρ is the one-electron effective density matrix. In order for Equations (27) and (28) to be well-determined, the matrix $\mathbf{A} = \left[A_{aj}^{ib} \right]$ must remain nonsingular at any time t. While this cannot be mathematically guaranteed, the singularity has not been reported in any publication to date.

Constraining the spin orbitals to be orthonormal throughout the dynamics, $\langle \widetilde{\phi}_p(t) | = \langle \phi_p(t) |$, TDNOCC theory turns into time-dependent orbital-optimized CC (TDOCC) theory.[47,85] The Lagrangian is forced to be real, $\mathscr{L} \leftarrow \mathrm{Re}(\mathscr{L})$, and the two orbital equations of motion (26) are then related by complex conjugation, with the right-hand side of the orbital equation of motion given in Equation (23) of Ref. [85]. As in OATDCC theory, the orbital space can be split into active and inactive subspaces in TDOCC theory,[85] facilitating simulations of highly nonlinear optical phenomena such as ionization.

The TDOCC, TDNOCC, and OATDCC theories thus are very closely related and, unlike TDCC theory based on static orbitals, they all provide gauge invariant results regardless of the truncation level of the cluster operators. As demonstrated by Köhn and Olsen,[86] however, TDOCC theory does *not* reproduce TDFCI results in the limit of untruncated cluster operators when $N > 2$. While this unfortunate feature was long believed to apply to TDNOCC theory, too, Myhre[87] recently showed that the correct limit can be obtained in TDNOCC theory for any N. On the other hand, the benchmark studies of Sato and coworkers[85,88–90] indicate that the deviation of TDOCC results from TDFCI results is often negligible, at least for strong-field dynamics, see Section 3.5 below.

3.3 | Numerical integration

Collecting the bivariational parameters in a single vector z, the equations of motion can be written in the form of a complex ordinary differential equation (ODE),

$$\dot{z}(t) = f(z, t), \quad z(0) = z_0. \tag{30}$$

A wealth of numerical integrators for ODEs have been developed, addressing numerical issues such as conservation of symplectic structure and stiffness, see, for example, the authorative treatise by Hairer, Lubich, and Wanner.[91]

Starting with the work of Huber and Klamroth,[78] a popular integrator for TDCC theory has been the explicit fourth-order Runge–Kutta (RK4) algorithm. Its popularity can most likely be traced to two properties: It is very simple to implement and requires exactly four evaluations of the function f per time step, making computational time easily predictable. The RK4 integrator, however, is not symplectic and may thus break physically important conservation laws. Pedersen and Kvaal[60] instead proposed to use the symplectic s-stage Gauss–Legendre integrator[91] (which is of even order $2s$, $s = 1, 2, 3, \ldots$) and showed that this yields long-time conservation of energy close to machine precision and that, depending on the time-step size and on the initial guess employed for the iterative solution of the implicit equations, may yield *fewer f*-evaluations per time step than the RK4 integrator for $s \leq 3$.

More recently, Wang, Peyton, and Crawford[92] investigated modified Runge–Kutta integrators with adaptive time step, which increases stability when the parameters oscillate rapidly and allows larger time steps when they do not. Remarkably, stability and accuracy is maintained also in conjunction with single-precision arithmetic, which allows highly efficient calculations on graphical processing units. The combination of larger time steps when possible and single-precision arithmetic leads to significant acceleration (more than an order of magnitude). Note, however, that Wang, Peyton, and Crawford used the frozen core approximation, thus excluding the highest frequencies from the amplitude oscillations. The high energies associated with core excitations and with ionization dynamics, in particular, introduce stiffness in the TDCC equations and Sato et al.[85] proposed to use an exponential Runge–Kutta integrator to handle this.

3.4 | Bivariational interpretation

The definitions of the state vector (17) and of the indefinite inner product (18) provide the foundation for analysis of the electronic dynamics in close analogy with conventional quantum mechanics. Autocorrelation functions (ACFs)—overlaps of the quantum state with itself at different times—contain important information about the dynamics. The early application of TDCC theory to core-level excitations of adsorbates by Schönhammer and Gunnarsson[50] is an interesting example that does not involve an external driving force.

Pedersen and Kvaal[60] defined the ACF as

$$A(t',t) = \langle\langle S(t')|S(t)\rangle\rangle$$
$$= \frac{1}{2}\left\langle\widetilde{\Psi}(t')|\Psi(t)\right\rangle + \frac{1}{2}\left\langle\widetilde{\Psi}(t)|\Psi(t')\right\rangle^*, \tag{31}$$

and demonstrated that the total energies of the stationary states contributing to the electronic dynamics can be extracted from it by Fourier transformation when t' is taken to be the switch-off time of an external laser pulse. It should be stressed that the phase amplitude $\tau_0(t)$ is important for a correct calculation of the ACF. The work of Pedersen and Kvaal[60] was restricted to conventional TDCC theory with static orbitals, since the calculation of overlaps between time-dependent Slater determinants exhibits factorial scaling, hampering the practical application of ACFs in TDCC theories with time-dependent orbitals.

Not only the energies of participating stationary states, but also their populations during the dynamics can be computed using the indefinite inner product. Pedersen et al.[61] introduced the (two-component) operator,

$$\widehat{P}_I = \begin{pmatrix} |\Psi_I\rangle\langle\widetilde{\Psi}_I| & 0 \\ 0 & |\widetilde{\Psi}_I\rangle\langle\Psi_I| \end{pmatrix}, \tag{32}$$

projecting onto stationary state I. Here, $|\Psi_I\rangle$ and $\langle\widetilde{\Psi}_I|$ are the right and left wave functions of state I from EOM-CC theory (see below for the precise definition). The projection operator (32) is hermitian with respect to the indefinite inner product (18) and the population of state I at time t thus becomes

$$p_I(t) = \left\langle\left\langle S(t)|\widehat{P}_I|S(t)\right\rangle\right\rangle$$
$$= \mathrm{Re}\left(\left\langle\widetilde{\Psi}(t)|\Psi_I\right\rangle\left\langle\widetilde{\Psi}_I|\Psi(t)\right\rangle\right). \tag{33}$$

While inherently real, the populations are neither bounded below by 0 nor above by 1. Like ACFs, stationary-state populations are considerably more challenging to compute with time-dependent orbitals than with conventional static orbitals, and Pedersen et al.[61] only presented results for the latter. Pedersen et al. also proposed a projection operator based on CC linear response theory, which led to populations that are practically indistinguishable from those obtained with the EOM-CC projector in most cases. It was found, however, that the linear-response projector may lead to spurious high-frequency oscillations in the populations and it was recommended to mainly use the EOM-CC projector.

As an example, Figure 1 shows the final TDCCSD populations of stationary states below the ionization energy for the LiH molecule after interaction with a short, chirped laser pulse with carrier frequency resonant with the transition from the $^1\Sigma^+$ ground state to the lowest-lying electric-dipole allowed $^1\Pi$ state. The final populations are plotted as functions of the laser chirp rate b. It is interesting to note that the greatest population of the resonant $^1\Pi$ state is achieved by a slight up-chirp, whereas a slightly larger down-chirp leads to virtually no population of the same state. These effects are caused by transitions among excited states that are nonlinear optical processes from the viewpoint of response theory. As illustrated in Ref. [61], such nonlinear processes, including quenched Rabi oscillations between excited sates, can be tracked by recording populations. In the FCI limit, the populations are strictly conserved in the absence of external driving forces but may show slight drifts and low-amplitude oscillations with truncated cluster operators. The TDCCSD populations agree well with TDFCI populations provided all states participating in the dynamics are well described at the EOM-CCSD level of theory.
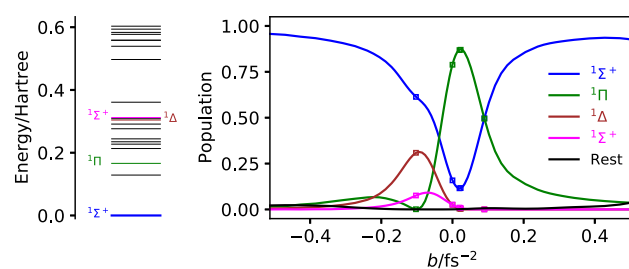
FIGURE 1 Controlling the ratio of CCSD energy level populations for LiH by altering the chirp rate of a laser pulse. The squares mark reference populations from TDFCI simulations. The aug-cc-pVDZ basis set was used. (Reprinted from Ref. [61]. Copyright ©2020. T. B. Pedersen, H. E. Kristiansen, T. Bodenstein, S. Kvaal, and Ø. S. Schøyen. Published by American Chemical Society.)

3.5 | Strong-field and ionization dynamics

The TDCC theory with static orbitals has an inherent instability. If an intense, resonant laser pulse is applied to the TDCC ground state of a system dominated by the Hartree–Fock ground-state determinant, the ground state is rapidly depleted and the state of the system thus becomes essentially orthogonal to the Hartree–Fock determinant. Yet, by construction, the intermediate normalization condition $\exp(-\tau_0(t))\langle\Phi_0|\Psi(t)\rangle = 1$ must hold at any time t. This causes violent behavior of the amplitudes. Indeed, Pedersen and Kvaal[60] found that even with untruncated cluster operators, TDCC theory fails when the resonant laser pulse is strong enough. This implies, for example, that Rabi oscillations between the ground state and an excited state are practically impossible to describe within static-reference TDCC theory.

Choosing the time-dependent Brueckner determinant—the single determinant with the greatest overlap with the TDFCI wave function at any time t—as reference determinant, one would expect the intermediate normalization condition to place much less severe demands on the amplitudes, at least when the Brueckner weight is sufficiently close to 1. Kristiansen et al.[93] showed that the time-dependent reference determinant in TDNOCC theory (equal to OATDCC theory without splitting of the orbital space) is, in fact, an excellent approximation to the Brueckner determinant and that, therefore, TDNOCC theory shows improved numerical stability compared with static-reference TDCC theory. An example is given in Figure 2, which shows the weight of the reference determinant in TDNOCCD and TDCCSD simulations of the Be atom exposed to an intense near-resonant laser pulse, comparing with the weight of the time-dependent Brueckner determinant and of the Hartree–Fock ground-state determinant in TDFCI simulations. Also shown are the norms of the doubles amplitudes. The weight of the reference determinant is defined by,[93]

$$W = |\langle\langle R(t)|S(t)\rangle\rangle|^2, \tag{34}$$

where

$$|R(t)\rangle\rangle = \frac{1}{\sqrt{2}}\begin{pmatrix}|\Phi_0(t)\rangle \\ |\widetilde{\Phi}_0(t)\rangle\end{pmatrix}, \tag{35}$$

is the two-component state vector representing the reference determinant, either time-dependent for TDNOCC, OATDCC, and TDOCC theory or the static Hartree–Fock determinant for conventional TDCC theory. The extreme behavior of the amplitudes in TDCCSD theory is clearly correlated with low Hartree–Fock weights and enhanced stability is obtained in TDNOCCD theory (labeled OATDCCD theory in Figure 2) where the reference determinant is an excellent approximation to the Brueckner determinant. Instabilities may still occur in TDNOCCD theory,[93] however, and an absolutely stable TDCC theory likely requires a multireference *Ansatz* with time-dependent orbitals.

For a physically correct description of electronic dynamics with nonvanishing ionization probability, including high-harmonic generation (HHG), the underlying basis set used to expand the time-dependent spin orbitals must support the electronic continuum. In the TDOCC approach of Sato et al.,[85] a FEDVR is used along with absorbing
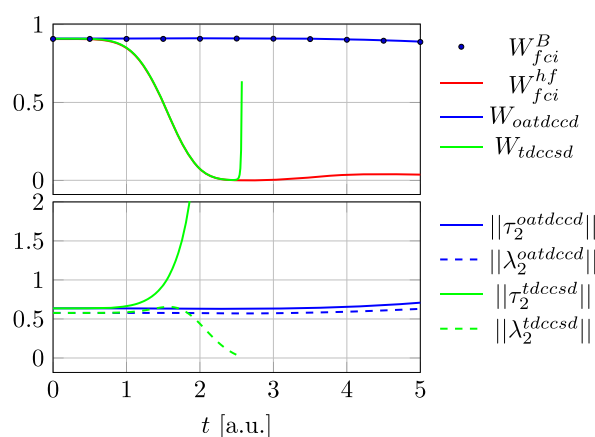
FIGURE 2 TDCCSD, OATDCCD, and TDFCI simulations of Be with the cc-pVDZ basis exposed to a laser pulse with peak electric-field strength 1 a.u. and carrier frequency $\omega = 0.2068175$ a.u. (Reprinted from Ref. [93] with the permission of AIP Publishing.)

boundary conditions and splitting of the spin-orbital space into active and inactive subspaces. The main goal of Sato et al.[85] was to simulate HHG processes induced by a few-cycles, near-infrared (800 nm) laser pulse for atoms, including estimation of one- and two-electron ionization probabilities. To keep the computational cost reasonably low, the core electrons were frozen.

The HHG spectra were computed from the absolute square of the Fourier transform of the induced dipole acceleration, while Sato et al. estimated one- and two-electron ionization probabilities as the probabilities of finding one or two electrons outside a sphere of radius 20 a.u. around the nucleus. Examples are given in Figures 3 and 4 for ionization probabilities and HHG spectra, respectively, where results from TDOCCD and TDOCCDT simulations are compared with time-dependent complete active space self-consistent field (TDCASSCF) results which, with the same orbital-space splitting, can be regarded as TDFCI benchmark results. Both HHG spectra and ionization probabilities show considerable electron correlation effects and triple excitations must be included in the TDOCC treatment to get results close to the TDFCI limit. Note, however, that even without triple excitations, the TDOCCD model yields very significant improvements over the uncorrelated Hartree–Fock method.

Sato and coworkers have since 2018 published several studies of ionization and HHG processes with less computationally demanding CC-like approximations based on the FEDVR. The simplest time-dependent orbital-optimized coupled-electron pair (TDOCEPA0)[88] approximation, which can be viewed as a linearization of the TDOCCD method, was shown to yield results roughly on par with the parent TDOCCD theory at low and intermediate laser intensities, while the effects of electron correlation are somewhat overestimated at higher intensities. Although the TDOCEPA0 approximation carries the same formal computational complexity, $O(N^6)$, as the parent TDOCCD method, the linearization leads to significant computational simplifications, including halving the number of equations to be propagated due to the symmetry $\lambda^*(t) = \tau(t)$.

Further reductions in computational time was obtained with the time-dependent orbital-optimized second-order Møller–Plesset (TDOMP2)[88] model, where only terms through second order in the fluctuation potential are retained in the TDOCCD Hamilton function $\mathcal{H}$, leading to an approximation scaling as $O(N^5)$. The TDOMP2 model is related to the time-dependent second-order CC model, TDCC2,[94] replacing single-excitation amplitudes by orbital rotations. The TDOMP2 method tends to overestimate electron-correlation effects at a wide range of intensities, but strikes a reasonable balance between accuracy and efficiency. Pathak, Sato, and Ishikawa[95] also computed TDOMP2 results with those obtained with a variant of TDCC2 theory where the single-excitation amplitudes are included alongside orbital optimization. It was found that the TDOMP2 method yields superior HHG spectra compared with the TDCC2-like method proposed by Pathak, Sato, and Ishikawa.[95] Compared with higher-level theories, it was concluded that the accuracy of the TDOMP2 model is moderate.

Recently, Pathak, Sato, and Ishikawa[90] also introduced the TDOCCDT(4) method, which includes triple-excitation corrections through fourth order in the Hamilton function and shows a computational complexity of $O(N^7)$, intermediate between the TDOCCD ($O(N^6)$) and full TDOCCDT ($O(N^8)$) models. Test calculations on the Ne and Ar atoms indicate that the TDOCCDT(4) method gives results almost indistinguishable from the full TDOCCDT model and the TDCASSCF model for HHG spectra and one- and two-electron ionization probabilities.
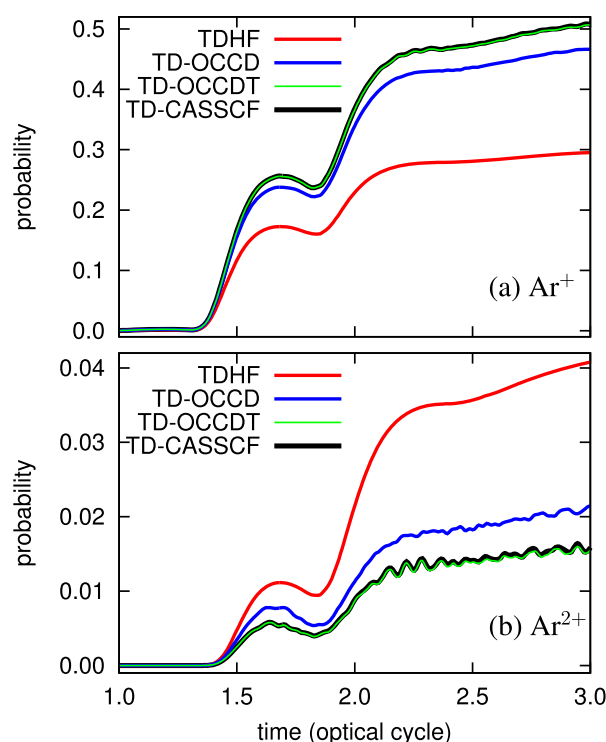
FIGURE 3 The probabilities, as a function of time, of finding one (a) and two (b) electrons outside a sphere of radius $R_0 = 20$ a.u. Comparison of the results of TDHF, TD-OCCD, TD-OCCDT, and TD-CASSCF methods. (Reprinted from Ref. [85] with the permission of AIP Publishing).
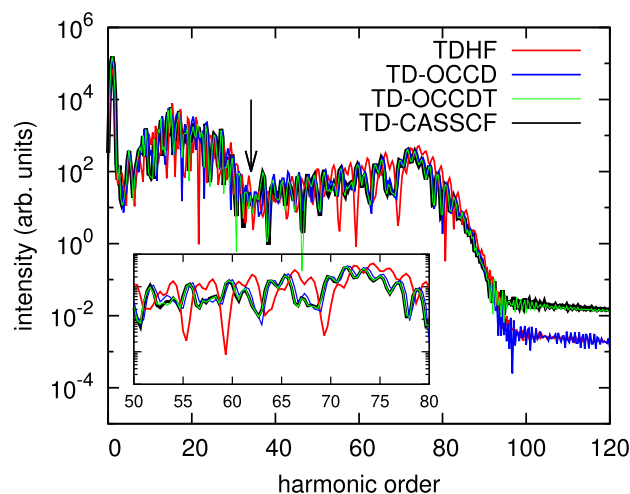
FIGURE 4 The HHG spectra of Ar exposed to a laser pulse with a wavelength of 800 nm and an intensity of 6×10^{14} W/cm^2. Comparison of the results of TDHF, TD-OCCD, TD-OCCDT, and TD-CASSCF methods. The inset shows a close-up of the spectra from 50th to 80th harmonic order. (Reprinted from Ref. [85] with the permission of AIP Publishing.)

3.6 | Linear and low-order nonlinear optical properties

Transient absorption spectroscopy[10] is an important application of time-dependent electronic-structure theory, yielding time-resolved spectra containing much richer information than conventional steady-state spectroscopy. Skeidsvoll, Balbi, and Koch[96] adapted the theory of transient absorption by Wu et al.[10] to bivariational TDCC theory and presented simulations of transient core-level spectra of the LiH and LiF molecules at the TDCCSD level of

theory. Using a resonant valence-exciting pump pulse followed by a core-exciting probe pulse, Skeidsvoll, Balbi, and Koch observed oscillations of intensities with the pump-probe delay caused by interference in the wavepacket generated by the pump pulse. Using a static reference determinant, ionization dynamics is out of reach and, therefore, only weak lasers were studied. In fact, the wavepacket generated by the pump laser is overwhelmingly dominated by the electronic ground state: the LiF ground-state population was found to be roughly 99.5% in Ref. [61]. Consequently, the pump-probe spectra were dominated by features ascribable to ground-to-excited state transitions, that is, essentially linear absorption spectra.

Conventional linear absorption spectra can be extracted from simulations, too. A molecule, initially in its ground state, is exposed to a weak electric-field kick—a weak delta-function shaped laser pulse—which induces transitions from the ground state to *all* excited states that can be populated within the electric-dipole selection rules. For sufficiently weak fields, multiphoton transitions are virtually absent. Moreover, the excited-state populations are so small that transitions between them are virtually absent, too, yielding a linear absorption spectrum. The absorption cross section may then be obtained from the Fourier transform of the induced electric-dipole moment. The great advantage of this approach to linear absorption spectra is that the *entire* spectrum, including the high-frequency core-valence transitions, is obtained from 1 to 3 simulations, one for each polarization direction to emulate random orientation of the sample relative to the propagation direction of the laser. The main challenge is the very long simulation times required to achieve sufficient resolution of the simulated spectrum. The simulation time can be reduced by about a factor 5 using Padé approximants for the Fourier transformation.[97]

Kristiansen et al.[98] used linear absorption spectra, including core excitations, generated from the dipole moment induced by an electric-field kick to validate their implementation of the TDCC2 model[94] by comparing with results from linear response theory. They also presented a derivation of the equations of motion for the TDOMP2 and TDNOMP2 (where the spin orbitals are required to be biorthonormal instead of orthonormal) models based on exponentially parameterized orbital rotations and the Euler–Lagrange Equation (20), and found that, despite the full orbital relaxation included in the TDOMP2 model, no significant improvement over TDCC2 spectra was obtained in the core region of the spectrum.

However, for frequency-dependent polarizabilities and hyperpolarizabilities extracted from TDCC2, TDCCSD, and TDOMP2 simulations with ramped monochromatic continuous-wave lasers as suggested by Ding et al.,[14] Kristiansen et al.[98] found that TDOMP2 theory outperforms the TDCC2 model, producing linear and nonlinear response functions much closer to the full TDCCSD results. While the linear absorption spectra were in perfect agreement with results from linear response theory (to within the resolution of the Fourier transformation), the TDCC2 and TDCCSD polarizabilities and hyperpolarizabilities were found to deviate slightly. These deviations are most likely caused by the nonperturbative nature of TDCC simulations and by nonadiabatic effects not being entirely removed by the single-cycle ramping.

4 | ELECTRONIC DYNAMICS WITH EOM-CC THEORY

With a finite basis, the eigenfunctions of the time-independent Hamiltonian $\widehat{H}_0$ of the many-electron systemparticle-system—the stationary states—can in principle be used to expand the time-dependent wave function because the continuum (for which normalizable eigenfunctions do not exist) becomes discretized. Starting from the EOM-CC *Ansätze*[30,66–70] for the left and right eigenfunctions of the similarity-transformed Hamiltonian, one may formulate an alternative theory, based on the eigenstate superposition approach, which converges to the correct FCI limit but provides different results than TDCC theory with truncated cluster operators. This idea was used by Kjønstad and Koch[99] to recast the Born–Huang approximation[4] to the fully coupled time-dependent electronic-nuclear wavefunction of a molecular system in the framework of CC theory.

4.1 | Equation-of-motion coupled-cluster theory

In EOM-CC theory,[30,66–70] the time-independent excited states are *parameterized* on top of the CC ground state as

$$| \Psi_I \rangle = \widehat{R}_I e^{\widehat{T}} | \Phi_0 \rangle, \tag{36}$$

147

$$\langle \widetilde{\Psi}_I | = \langle \Phi_0 | \widehat{L}_I e^{-\widehat{T}}, \tag{37}$$

where $\widehat{T}$ is the time-independent cluster operator of the ground-state CC wavefunction and $|\Phi_0\rangle$ is a static reference determinant, typically the Hartree–Fock ground-state determinant. The linear excitation and de-excitation operators $\widehat{R}_I$ and $\widehat{L}_I$, respectively, are defined by

$$\widehat{R}_I = {}^I r_0 \widehat{I} + \sum_{ai}^I r_i^a \widehat{a}_a^\dagger \widehat{a}_i + \frac{1}{4} \sum_{abij}^I r_{ij}^{ab} \widehat{a}_a^\dagger \widehat{a}_i \widehat{a}_b^\dagger \widehat{a}_j + \cdots, \tag{38}$$

$$\widehat{L}_I = {}^I l_0 \widehat{I} + \sum_{ai}^I l_a^i \widehat{a}_i^\dagger \widehat{a}_a + \frac{1}{4} \sum_{abij}^I l_{ab}^{ij} \widehat{a}_j^\dagger \widehat{a}_b \widehat{a}_i^\dagger \widehat{a}_a + \cdots. \tag{39}$$

The coefficients of $\widehat{L}_I$ and $\widehat{R}_I$ are collected in the left and right eigenvectors of the field-free similarity transformed Hamiltonian $\overline{H} = \exp\left(-\widehat{T}\right) \widehat{H}_0 \exp\left(\widehat{T}\right)$,

$$\overline{H}R = RE, \tag{40}$$

$$L\overline{H} = EL, \tag{41}$$

$$\overline{H}_{\mu\nu} = \left\langle \Phi_\mu | \overline{\widehat{H}} | \Phi_\nu \right\rangle, \tag{42}$$

where $E = \text{diag}(E_I)$ contains the energies of the ground and excited states, and the columns of R and the rows of L define the right and left eigenvectors, respectively, such that the biorthonormality condition

$$\left\langle \widetilde{\Psi}_I | \Psi_J \right\rangle = L_I R_J = \delta_{IJ}, \tag{43}$$

is fulfilled (L_I is the Ith row of L and R_J the Jth column of R).

4.2 | Time-dependent equation-of-motion coupled-cluster theory

The most direct formulation of time-dependent EOM-CC (TD-EOM-CC) theory is to expand the time-dependent bra and ket wavefunctions in the basis of field-free EOM-CC states

$$|\Psi(t)\rangle = \sum_I |\Psi_I\rangle C_I(t), \tag{44}$$

$$\langle \widetilde{\Psi}(t)| = \sum_I \widetilde{C}_I(t) \langle \widetilde{\Psi}_I |. \tag{45}$$

Equations of motion for the time-dependent expansion coefficients $\widetilde{C}_I(t)$ and $C_I(t)$ can either be obtained from the time-dependent bivariational principle or by requiring that the time-dependent Schrödinger equation holds for the left and right wavefunctions, that is,

$$\text{i} | \dot{\Psi}(t) \rangle = \widehat{H}(t) | \Psi(t) \rangle, \tag{46}$$

$$-\text{i} \langle \dot{\widetilde{\Psi}}(t) | = \langle \widetilde{\Psi}(t) | \widehat{H}(t). \tag{47}$$

Insertion of the *Ansätze* (44) and (45) into the TDSE and projecting onto the EOM-CC ket (bra) state yields

$$i\dot{C}_I(t) = \sum_J H_{IJ}(t) C_J(t), \tag{48}$$

$$-i\dot{\widetilde{C}}_J(t) = \sum_I \widetilde{C}_I(t) H_{IJ}(t), \tag{49}$$

where $H_{IJ}(t)$ are the matrix elements of the Hamiltonian $\widehat{H}(t)$ in the EOM-CC basis,

$$H_{IJ}(t) = \left\langle \widetilde{\Psi}_I | \widehat{H}(t) | \Psi_J \right\rangle = \left\langle \Phi_0 | \widehat{L}_I \overline{H}(t) \widehat{R}_J | \Phi_0 \right\rangle. \tag{50}$$

When the time-dependent expansion coefficients have been determined, the expectation value of an arbitrary operator $\widehat{\Omega}$ is given by

$$\left\langle \widetilde{\Psi}(t) | \widehat{\Omega} | \Psi(t) \right\rangle = \sum_{IJ} \widetilde{C}_I(t) \Omega_{IJ} C_J(t), \tag{51}$$

in accordance with the Hellmann–Feynman theorem. The matrix elements Ω_{IJ} are defined as in Equation (50). Note that since $\langle \widetilde{\Psi}(t) |$ and $| \Psi(t) \rangle$ are not Hermitian conjugates, the expectation value of $\widehat{\Omega}$ is generally complex valued. Of course, the indefinite inner product, Equation (18), could also be used here to obtain real values for hermitian operators.

For a time-dependent Hamiltonian on the form $\widehat{H}(t) = \widehat{H}_0 + \widehat{V}(t)$, the matrix elements of the Hamiltonian can be written as

$$H_{IJ}(t) = E_I \delta_{IJ} + V_{IJ}(t), \tag{52}$$

where the matrix elements $V_{IJ}(t)$ constitute a non-hermitian matrix with elements defined as in Equation (50). This approach has been used by different groups to study explicitly time-dependent optical processes within the EOM-CC framework with $\widehat{V}(t) = -\widehat{\mu} \cdot F(t)$, where $\widehat{\mu}$ is the electric-dipole operator and $F(t)$ is the spatially uniform electric field of the laser.

For example, Sonk, Caricato, and Schlegel[100] studied the optical response of butadiene to short, intense laser pulses while Luppi and Head-Gordon[101] used the method to compute HHG spectra of H_2 and N_2. In both articles, the transition dipole matrix $D_{IJ} = \left\langle \widetilde{\Psi}_I | \widehat{\mu} | \Psi_J \right\rangle$ was symmetrized according to

$$D_{IJ} \leftarrow \frac{1}{2} \left(D_{IJ} + D_{JI}^* \right), \tag{53}$$

because the authors were worried that the non-hermitian transiton dipole matrix in Equation (52) could lead to dynamics that do not conserve the norm of the wavefunction. However, if the left and right TDSE are satisfied, it follows that

$$\frac{d}{dt} \left\langle \widetilde{\Psi}(t) | \Psi(t) \right\rangle = 0. \tag{54}$$

Hence, the biorthonormality of the left and right wavefunctions *is* conserved, provided that $\left\langle \widetilde{\Psi}(t_0) | \Psi(t_0) \right\rangle = 1$. Note that with symmetrization (and real energies), the Hamiltonian matrix (52) becomes hermitian and the left and right expansion coefficients become complex conjugates, $\widetilde{C}_I(t) = C_I^*(t)$.

With the symmetrization (53), which was also used in Ref. [61] for test purposes (albeit with transition dipole moments from CC response theory rather than EOM-CC theory), the left and right expansion coefficients are related by complex conjugation. In a recent publication,[102] Skeidsvoll et al. used the TD-EOM-CCSD method *without* symmetrization to simulate weak-field attosecond processes in small molecules—that is, distinct left and right expansion

coefficients were retained. Core-level pump-probe spectra of LiH and LiF were compared with TDCCSD results from Ref. [96] and found to be in good agreement.

The TD-EOM-CCSD approach can be much more efficient than the TDCCSD method if the participating states can be limited by a careful selection procedure,[102] but the main computational drawback of the approach is the full diagonalization of the Hamiltonian required for completely general quantum dynamics simulations. It is generally hard to predict a priori how many and which states are required to describe a given dynamical process and a prohibitively large number of states may be needed. Skeidsvoll et al.[102] used an asymmetric band Lanczos algorithm combined with state selection criteria based on transition strengths and frequencies to successfully limit the number of participating states, including high-lying core-excited states using core-valence separation.[103,104]

Another alternative is to avoid the diagonalization problem entirely by propagating directly in a determinant basis. While this effectively removes all issues related to diagonalization of large matrices—such as stability, selection of states, and large memory usage—the computational complexity is moved to the time propagation, exactly as in TDCC theory albeit with the benefit of linear parameterization. This would be especially disadvantageous in simulating transient absorption spectroscopy, since the ability to analytically propagate the wavefunction after the pulses are switched off is removed, exactly as in TDCC theory. Still, this *may* be an attractive approach in cases where one is interested in broad frequency ranges and large number of states.

4.3 | Time-dependent formulation of linear absorption spectra

As far as we know, propagation in the determinant basis has only been done for linear absorption spectra.[105–111] The starting point is the line-shape function obtained from Fermi's Golden Rule,[112] which results from solving the TDSE to first order in time-dependent perturbation theory with the ground-state wavefunction as initial condition and using the rotating wave approximation (i.e., only ground-to-excited state one-photon transitions are included). The line-shape function thus implicitly assumes weak-field perturbations. Adapting to EOM-CC states and assuming the electric-dipole approximation for the semiclassical matter-field interaction, Fermi's Golden Rule for the line-shape function can be written as[107]

$$\mathcal{I}^{\alpha}(\omega) = \sum_I \left\langle \widetilde{\Psi}_0 | \widehat{\mu}^{\alpha} | \Psi_I \right\rangle \left\langle \widetilde{\Psi}_I | \widehat{\mu}^{\alpha} | \Psi_0 \right\rangle \mathscr{L}(\omega; \omega_I, \gamma), \tag{55}$$

where $\alpha \in \{x, y, z\}$, $\omega_I = E_I - E_0$, and we have assumed a Lorentzian line shape with fixed lifetime $1/\gamma$ for all excited states:

$$\mathscr{L}(\omega; \omega_I, \gamma) = \frac{1}{\pi} \frac{\gamma}{(\omega - \omega_I)^2 + \gamma^2}, \quad \gamma > 0. \tag{56}$$

Here, we follow Nascimento and DePrince[107] and include the ground state in the summation over states I. The ground state was *not* included in the work of Park, Perera, and Bartlett.[109] Note that the line-shape function may be complex in EOM-CC theory; had we used the indefinite inner product instead, only the real part of this expression would be used.

Using that $\mathscr{L}(\omega; \omega_I, \gamma)$ is the Fourier transform of $\exp(i\omega_I t - \gamma|t|)$, the line-shape function can be rewritten as

$$\mathcal{I}^{\alpha}(\omega) = \int_{-\infty}^{\infty} \left\langle \widetilde{M}^{\alpha}(0) | e^{i(\widehat{H}_0 - E_0)t} | M^{\alpha}(0) \right\rangle e^{-\gamma|t|} e^{-i\omega t} dt, \tag{57}$$

where the right and left dipole functions are defined as

$$| M^{\alpha}(0) \rangle = \widehat{\mu}^{\alpha} | \Psi_0 \rangle, \tag{58}$$

$$\langle \widetilde{M}^{\alpha}(0) | = \langle \widetilde{\Psi}_0 | \widehat{\mu}^{\alpha}. \tag{59}$$

The line-shape function (57) thus may be evaluated by Fourier transformation of either of the dipole ACFs

$$\left\langle \widetilde{M}^{\alpha}(0) | M^{\alpha}(-t) \right\rangle \ \text{ or } \ \left\langle \widetilde{M}^{\alpha}(t) | M^{\alpha}(0) \right\rangle, \tag{60}$$

after multiplication by the damping factor $\exp(-\gamma|t|)$. Here,

$$| M^{\alpha}(-t) \rangle = e^{i\left(\widehat{H}_0 - E_0\right)t} | M^{\alpha}(0) \rangle, \tag{61}$$

$$\langle \widetilde{M}^{\alpha}(t) | = \langle \widetilde{M}^{\alpha}(0) | e^{i\left(\widehat{H}_0 - E_0\right)t}. \tag{62}$$

Only one of these propagations need to be performed to compute the dipole ACF. While DePrince and coworkers[105–107,111] used a projection procedure for the TDSE for either $| M^{\alpha}(-t) \rangle$ or $\langle \widetilde{M}^{\alpha}(t) |$, Park, Perera, and Bartlett[109] used the evolution of the dipole operators in the Heisenberg picture. Formally, at least, the two approaches are equivalent. The absorption spectrum is then obtained from

$$S(\omega) = \frac{2\omega}{3} \sum_{\alpha} \text{Re}(I^{\alpha}(\omega)). \tag{63}$$

Since this approach does not require explicit diagonalization of the similarity transformed Hamiltonian, it provides a direct route to the study of core excitation spectra[106,109] and has been generalized to include scalar relativistic effects at the exact two-component (X2C) level with a fifth-order Douglas–Kroll–Hess Hamiltonian.[109] Scalar relativistic effects including spin-orbit coupling at the X2C level was explicitly addressed in Ref. [108], where Koulias et al. illustrated both frequency shift, activation of spin-forbidden transitions, and energy splitting of the $^2P_{1/2}$ and $^2P_{3/2}$ states in atoms and cations of the alkali and alkaline earth metal groups.

It should be noted that the methodology outlined above is not restricted to the electric-dipole approximation and can be generalized to account for beyond-dipole effects.[107,110] Examples are shown in Figures 5 and 6, where the method was applied to compute linear absorption and isotropic electronic circular dichroism spectra in substituted oxiranes. Park, Perera, and Bartlett[110] reported an implementation which included higher-order multipole functions corresponding to full second-order oscillator strengths, simulating the $3p \rightarrow 4d$ quadrupole-allowed transition in the pre K-edge region of Ti^{4+} and $TiCl_4$. This study also includes scalar relativistic effects.

Since the computational cost of these methods is dominated by the time integration and since long simulation times are required to achieve sufficient resolution in the Fourier transform of the ACF, some effort has been spent on algorithms designed to accelerate the simulations. Nascimento and DePrince[106] used Padé approximants of the Fourier
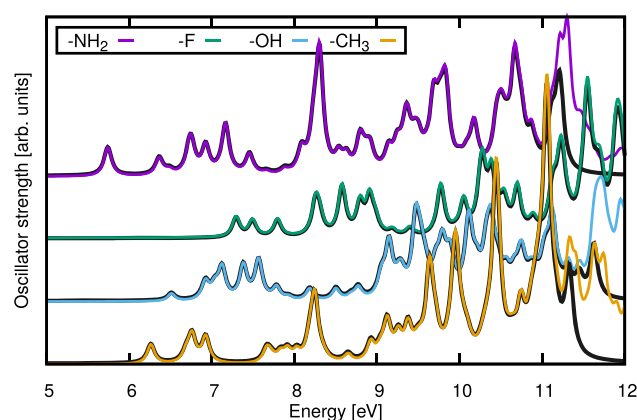
FIGURE 5 Linear absorption spectra for substituted oxiranes computed at the TD-EOM-CC2/aug-cc-pVDZ level of theory. The solid black lines correspond to artificially broadened stick spectra obtained from standard, frequency-domain EOM-CC2 computations. The labels —NH$_2$, —F, —OH, and —CH$_3$ represent the oxirane substituents. (Reprinted from Ref. [107] with the permission of AIP Publishing.)
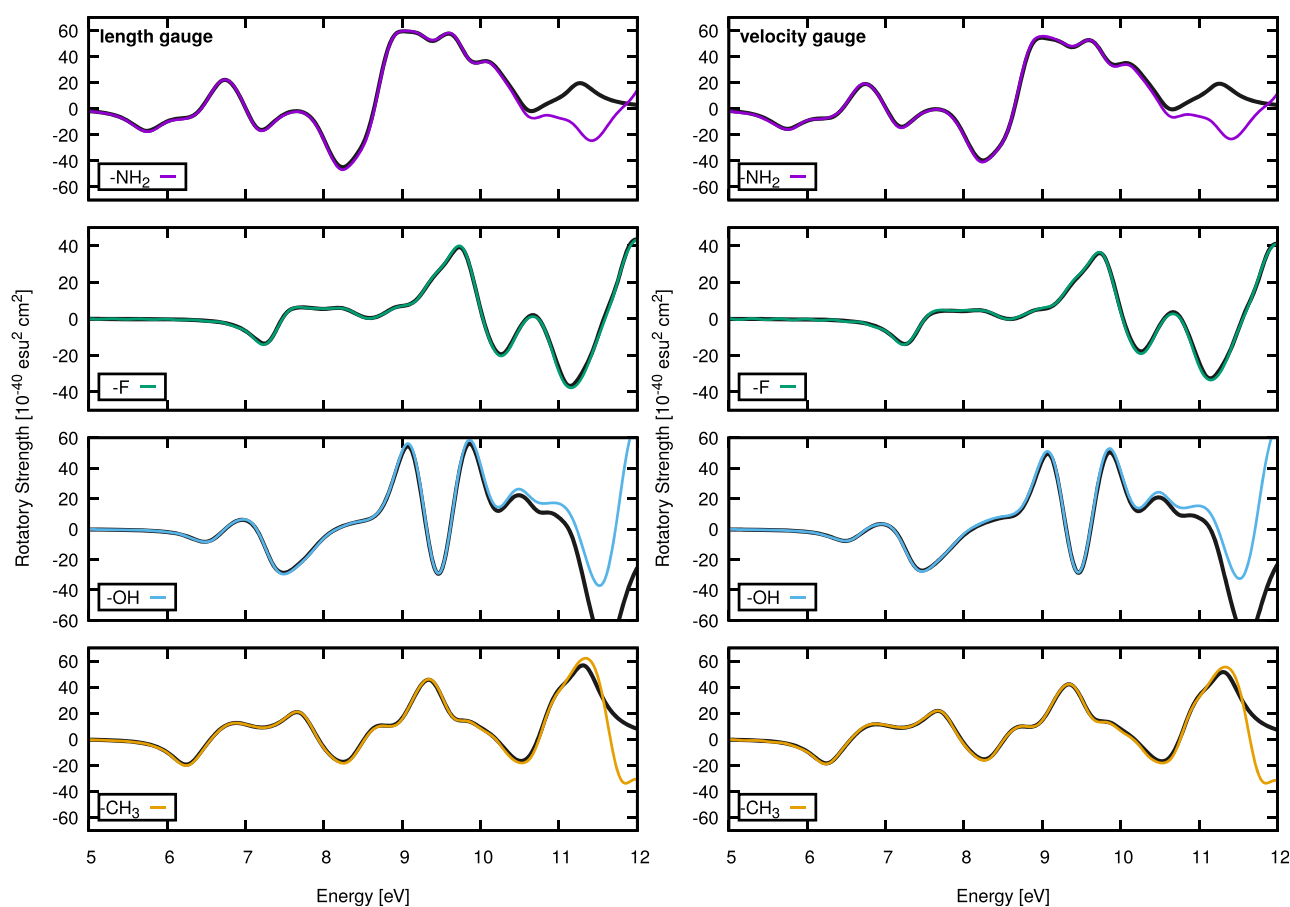
FIGURE 6 Electronic circular dichroism spectra for the substituted oxiranes computed at the EOM-CC2/aug-cc-pVDZ level of theory in the length (left panels) and velocity (right panels) gauges. Colored lines correspond to TD-EOM-CC2-derived data, while the solid black lines are frequency-domain spectra obtained by artificially broadening the corresponding stick spectra. (Reprinted from Ref. [107] with the permission of AIP Publishing.)

transform, achieving an order of magnitude speedup with small or no errors in the linear absorption spectrum. Later, however, Cooper et al.[111] reported that the Padé approximants may give faulty results in dense spectral regions. The same group later reported an implementation using a short iterative Lanczos (SIL) integration scheme.[111] This method utilized the fact that the main computational cost in the time propagation is the evaluation of the right hand side of the TDSE, which amount to a matrix vector product $\overline{H}C$. In the SIL approach, a tridiagonal approximation $\overline{H}_k$ to the Hamiltonian matrix is constructed and used to propagate a moment vector within a Krylov subspace of dimension k. Due to the simple Hamiltonian form, they used the matrix representation of $\exp(i\overline{H}_k dt)$ directly in the time propagation. The approximate Hamiltonian and the corresponding Krylov subspace must be regenerated regularly, but still the authors report up to an order of magnitude speedup relative to the RK4 integrator. Although they used an algorithm designed for hermitian matrices, it was shown that the SIL method generates frequency spectra with mostly negligible differences from those generated with the RK4 integrator.

5 | TIME-DEPENDENT VIBRATIONAL COUPLED-CLUSTER THEORY

Vibrational coupled-cluster (VCC) theory refers to the application of CC theory to the nuclear Schrödinger equation in the adiabatic Born–Oppenheimer approximation. There are two distinct flavors of VCC theory: First, a basis-free method based on bosonic CC theory[54,113–115] was developed into sophisticated VCC theory by Banik, Pal, and Prasad[116] and Faucheaux and Hirata,[117] who coined the acronym XVCC. The second approach is the modal approach to VCC

theory, simply termed VCC, developed by Christiansen.[118,119] RT propagation has been developed in both flavors. Indeed, in the XVCC case, this is where it started.

5.1 | Bosonic VCC theory: XVCC

The bosonic VCC theory starts with the harmonic approximation, writing the nuclear Hamiltonian as an M-dimensional harmonic oscillator plus anharmonic perturbations. Each of the M modes have associated harmonic-oscillator ladder operators $\widehat{a}_n^\dagger$ satisfying

$$\left[\widehat{a}_m, \widehat{a}_n^\dagger\right] = \delta_{m,n}, \quad 1 \leq m, n \leq M, \tag{64}$$

with joint vacuum $|0\rangle$, that is, the ground state of the M-dimensional harmonic oscillator. The XVCC nuclear wavefunction is given by

$$|\Psi_{\text{XVCC}}\rangle = e^{\widehat{S}} |0\rangle, \tag{65}$$

with the untruncated cluster operator $\widehat{S}$ defined by

$$\widehat{S} = \sum_{m=1}^{M} \sigma_m \widehat{a}_m^\dagger + \sum_{m,n=1}^{M} \sigma_{m,n} \widehat{a}_m^\dagger \widehat{a}_n^\dagger + \cdots. \tag{66}$$

The shown terms up to second order define the SUB2 approximation, while higher-order approximations, denoted SUBN, truncate $\widehat{S}$ at the Nth order. The theory now proceeds as in traditional CC theory. It is to be remarked, that the SUB2 approximation generates a wavefunction which is a squeezed state, that is, a general complex-valued Gaussian.

In Ref. [120], Prasad introduced TDCC theory for the study of Franck–Condon spectra, that is, the nuclear transition probabilities to the various vibrational eigenstates upon (instantaneous) excitation from the nuclear ground state at the equilibrium geometry to an excited electronic surface. This seems to be the first application of CC theory to the vibrational Schrödinger equation, and at the same time it is an early application of TDCC theory. Notable here is that only the ket ($|\Psi\rangle$) is propagated in time, since the transition probability is obtained in terms of an ACF only dependent on this ket. Prasad presented an application to a two-dimensional (2D) model system previously studied by Heller using frozen Gaussians,[121,122] pointing out similarities and differences. For example, the TDCC treatment in the SUB2 approximation is roughly equivalent to the thawed Gaussian approximation. In a follow-up study, Sastry and Prasad[123] applied the above methodology to the Beswick–Jortner model[124] of photodissociation of the form ABC → AB + C.

In Ref. [125], Latha and Prasad studied the possibility of using TDCC theory to describe nonadiabatic dynamics on conically intersecting potential-energy surfaces. In addition to treating multiple electronic surfaces, the basis is made time dependent using a time-dependent self-consistent field (TDSCF) procedure. Although a very simple model system was employed, the findings were encouraging. In particular, spurious peaks in the ACF arising from TDSCF theory alone were strongly alleviated by the CC couplings.

5.2 | Modal VCC theory

In the VCC theory developed by Christiansen,[118,119] the exponential *Ansatz* is applied to the vibrational Schrödinger equation for nuclear motion. Formally, the theory can be described as standard single-reference CC theory with multiple species of *distinguishable particles*, called modes. The starting point is the vibrational self-consistent field (VSCF) procedure,[119] which approximates the nuclear wavefunction as a Hartree product of M functions $\phi_0^m(q_m)$ called *modals*, where $m = 1, \cdots, M$. Similar to the Hartree–Fock procedure, VSCF also produces excited Hartree products,

$$\Phi_s(\mathbf{q}) = \prod_{m=1}^{M} \phi_{s^m}^m(q_m), \tag{67}$$

where $s = (s^1, \cdots, s^M)$ enumerates the modals, and where $\mathbf{q} = (q_1, \cdots, q_m)$ are the nuclear coordinates. A certain arbitrariness exists in the choice of the mode coordinates q_m. The VSCF ground state Hartree product $\Phi_0(\mathbf{q})$ and the excited products form the many-mode Hilbert space basis. A second-quantization formalism can be set up which in a natural manner defines the exponential ansatz for the vibrational Schrödinger equation. Each modal $\phi_{s^m}^m$ is associated with a creation operator $\widehat{a}_{s^m}^{\dagger,m}$, satisfying

$$\left[\widehat{a}_{s^m}^m, \widehat{a}_{s'^{m'}}^{\dagger,m'} \right] = \delta_{m,m'} \delta_{s^m,s'^{m'}}. \tag{68}$$

A general cluster operator reads $\widehat{T} = \sum_\mu \tau_\mu \widehat{X}_\mu$, with μ being a generic index enumerating the various m-mode simultaneous excitations, up to M simultaneous excitations. For example, a single-mode cluster operator reads

$$\widehat{T}_1 = \sum_{m=1}^{M} \sum_{s^m}^{A^m} \tau_{s^m}^m \widehat{a}_{s^m}^{\dagger,m} \widehat{a}_0^m, \tag{69}$$

where A^m is the number of modals for mode m, while a two-mode cluster operator reads

$$\widehat{T}_2 = \sum_{m=1}^{M} \sum_{m'=m+1}^{M} \sum_{s^m}^{A^m} \sum_{s^{m'}}^{A^{m'}} \tau_{s^m,s^{m'}}^{m,m'} \widehat{a}_{s^m}^{\dagger,m} \widehat{a}_{s^{m'}}^{\dagger,m'} \widehat{a}_0^{m'} \widehat{a}_0^m. \tag{70}$$

The cluster operator is usually truncated at a number n of simultaneous mode excitations, denoted the VCC[n] approximation.[118]

Apart from the qualitative differences arising from having multiple distinguishable particle species, the Hamiltonian in VCC theory is also qualitatively different, since the *particles* are now modes, and there are, in principle, arbitrarily many such particles interacting at the same time. In particular, the Baker–Campbell–Hausdorff expansion does not truncate for VCC for the exact Born–Oppenheimer potential-energy surface. The Hamiltonian is typically truncated at a maximum number of interacting modals (e.g., using a sum-of-products approximation).

The Christiansen group has also developed RT time-dependent VCC (TDVCC) theory using the bivariational framework in Section 3. In Ref. [126], Hansen et al. introduced the TDVCC formalism, along with an analysis of the separability of the bra and ket wavefunctions as well as the corresponding extensivity of expectation values. The authors also considered imaginary-time propagation for locating the ground-state solution. These theoretical results are also highly relevant for electronic-structure TDCC theory. The authors present an implementation of the TDVCC[2] method, using the Dormand–Prince 8(5,3) explicit Runge–Kutta method with adaptive step size control, see Ref. [127], Section II.5.

In order to verify their implementation and analysis, the authors tested their TDVCC[2] code on the 2D Hénon–Heiles potential, as well as calculations on the water and formaldehyde molecules, using approximate potentials on a sum-over-products format coupling at most two modes per term, generated using Gaussian process regression.[128] One interesting finding is that round-off errors in the asymptotic region of imaginary-time propagation can, even for such an accurate Runge–Kutta integrator, lead to slightly incorrect exponential decay rates, thereby predicting slightly wrong excitation energies. The authors also studied the integration of a system driven by an explicitly time-dependent laser pulse.

In a follow-up study,[129] an automated implementation of the full hierarchy of TCVCC[n] approximations was presented. Again, the Dormand–Prince 8(5,3) method was the chosen integrator for the numerical studies. The authors note that even though the integrator is not symplectic, it is sufficiently accurate so that there are no stability or non-conservation problems often associated with explicit Runge–Kutta methods.[91]

The authors performed several detailed numerical experiments, demonstrating the convergence to the vibrational FCI (VFCI) limit for a 5-mode system (formaldehyde). An extended truncation scheme inspired by single-reference based multireference theory[130] is also introduced, called VCC[$k$ext$n$], where a single mode is chosen to have $n-k$ more

excitations than the VCC[k] truncation scheme. The convergence toward the VFCI limit was demonstrated to be enhanced when a single mode dominated the dynamics.

The authors also discussed ACFs in detail with respect to their separability properties for separated noninteracting systems, singling out the ACF defined by $A(t',t) = \langle \widetilde{\Psi}(t') | \Psi(t) \rangle$ as being the only one producing physically reasonable values (i.e., with absolute values smaller than 1). The ACF $B(t',t) = \langle \widetilde{\Psi}(t) | \Psi(t') \rangle^*$ was observed to have significantly unphysical values. It is interesting to compare this with the ACF used by Pedersen and Kvaal,[60] Equation (31), which is the average of A and B. In the work of Pedersen and Kvaal, no unphysical values were observed for $B(t',t)$ unless the integration of the equations of motion failed due to ground-state depletion (in which case also $A(t',t)$ becomes ill-behaved). The third ACF studied was based on the relation $\langle \Psi(0) | \Psi(t) \rangle = \langle \Psi(t/2)^* | \Psi(t/2) \rangle$, valid in standard hermitian dynamics for a real $\Psi(0)$ and a real Hamiltonian. However, the authors found severely unphysical behavior of this ACF. Finally, we mention that the authors applied their implementation to a larger system, studying the intramolecular vibrational-energy redistribution of the imidazole molecule (with 21 modes) using an accurate many-term potential-energy surface.

In a related study, Hansen, Madsen, and Christiansen[131] implemented the full time-dependent *extended* CC method of Arponen,[54] that is, the TDEVCC method. Although unfeasible for larger systems than, say, $M = 6$ modes, the TDEVCC method utilizes a double exponential *Ansatz* for the bra and ket vectors, implying full multiplicative separability and corresponding separability of expectation values. The authors observed that for ground-state energy calculations, EVCC theory does not offer a significant improvement over "plain" VCC theory, especially taking the computational cost into consideration. This is a finding consistent with the conventional wisdom in electronic-structure theory.[132] However, the authors noted that for *time-dependent* calculations, TDEVCC[k] performs in general much better than TDVCC[k] with regards to the closeness of both the bra and the ket to the TDVFCI limit and accuracy of expectation values. Both ACFs of type A and B are correctly separable with TDEVCC[k].

The Christiansen group has also developed and implemented a VCC analogue of orbital-adaptive TDCC[49] (cf., Section 3), called time-dependent modal VCC (TDMVCC) theory. In Ref. [133], Madsen et al. presented an advanced implementation of orbital-adaptive theory with very promising results, including the apparent cure of exploding amplitude norms in TDVCC[n] calculations for the water potential-energy surface. This corroborates findings by Kristiansen et al.,[93] who applied TDNOCC theory to electronic systems.

6 | OTHER APPLICATION AREAS

6.1 | Finite-temperature theory

Development of viable computational tools for the study of many-body quantum systems, especially in the condensed phase, at finite temperature is an active research area, see, for example, Refs. [134–137] for recent work within density-functional theory. The earliest efforts to cast quantum mechanics in a thermodynamical framework were based on the close resemblance of the statistical partition function and the quantum-mechanical evolution operator with imaginary time. The Matsubara formalism[138] for Green's functions in quantum-field theory is a notable example of this connection. However, when the time has been rotated to the imaginary-time axis, the dynamics are lost. To circumvent this problem there are several techniques to re-introduce real time, for example, thermofield dynamics and the Keldysh formalism.[139,140]

The first to explore CC theory in a finite-temperature setting were Altenbokum and coworkers.[115,141] They used a density-matrix formulation with the Bloch equation replacing the Schrödinger equation. This, however, requires the knowledge of the full spectrum of the Hamiltonian thus quickly making the solution prohibitive. Several years later the thermal cluster cumulant (TCC) method was developed by Sanyal, Mandal, and Mukherjee as an extension of the thermofield dynamics with the CC method, requiring a thermal formulation of Wick's theorem.[142,143] This resulted in a method resembling the cumulant expansion from statistical mechanics, and bypassed the need to know the full spectrum of the Hamiltonian. In a series of articles this method was studied and applied to an anharmonic oscillator and to the Lipkin model of nuclear physics.[142–146]

In 2018, White and Chan[147] started from an explicitly time-dependent formulation of CC theory and replaced time by an imaginary time. This replaced the time-dependent formulation with a temperature-dependent formalism, dubbed the finite-temperature coupled-cluster (FTCC) method, and was further studied in 2020.[148] Their formulation of FTCC theory is slightly different from the TCC model by Sanyal, Mandal, and Mukherjee,[142] but the methods are equivalent and lead to the same set of equations.

At the same time, Hummel[149] developed an imaginary-time time-dependent truncated CC method for the application to systems at finite temperature. The truncation scheme is the direct-ring coupled-cluster doubles (drCCD) method (i.e., the direct random-phase approximation) and leads to much more cost-effective equations than the FTCC formalism at the price of reduced accuracy.

Following shortly after these publications, Harsha, Henderson, and Scuseria[150] developed an imaginary-time TDCC method for finite-temperature systems from the thermofield dynamics formalism. Results from this method were published already in an earlier work comparing with a thermal configuration-interaction method.[151]

By including dynamics the study of non-equilibirium systems becomes possible. White and Chan[152] utilized the Keldysh formalism to extend the imaginary-time formalism to include a real component for RT dynamics.[140] This method was dubbed the Keldysh coupled-cluster (Keldysh-CC) method. Up to this point all time-dependence and temperature-dependence was kept in the cluster amplitudes. However, in 2021 Peng et al.[153] extended the Keldysh-CC method to include orbital rotations. They formulated the Keldysh-OCC method as an extension of the TDOCC method[85] to finite-temperature systems.

6.2 | Sub-system embedding

Kowalski and Bauman[154] have developed the sub-system embedding sub-algebra CC formalism, which is a generalization of the complete active space CC (CASCC) formalism of Piecuch, Adamowicz, and coworkers.[130,155] The excitations that stay completely in the CAS is an example of a sub-system embedding sub-algebra. In Ref. [154], the formalism is extended to the TDSE. Moreover, a CASCC generalization of unitary CC (UCC) is studied, including variational formulations of the dynamical equations of motion. The UCC method is one of the main contenders for quantum advantage on noisy intermediate-scale quantum (NISQ) devices.[156]

6.3 | Green's function methods

In coupled-cluster Green's function (CCGF) theory,[157] the goal is to compute a quantum mechanical Green's function by means of CC theory. For example, the one-body retarded Green's function defined by

$$G_{pq}^-(t_2 - t_1) = -i\theta(t_2 - t_1)\left\langle \Psi_0 \middle| \left\{ \widehat{a}_p(t_2), \widehat{a}_q^\dagger(t_1) \right\} \middle| \Psi_0 \right\rangle, \tag{71}$$

is a causal propagator that expresses the amplitude of electron/hole propagation from time t_1 to a later time t_2. Here, $\widehat{a}_p(t) = e^{iHt}\widehat{a}_p e^{-iHt}$ is the Heisenberg representation of $\widehat{a}_p$ and θ is the Heaviside step function. Intuitively, G^- contains information about causal single-particle processes in a quantum system starting out in the ground state, and can be used to compute a host of properties.[158] The Green's function is closely related to the ACFs described elsewhere in this review.

In CCGF theory, the bivariational approximations for $|\Psi_0\rangle$ and $\langle\Psi_0|$ constitute the starting point, see Section 3. Conventionally, a momentum-space representation of G^- is sought and approximated using many-body perturbaton theory. In recent work, however, RT propagation methods for $|\Psi_0\rangle$ in conjunction with a cumulant approximation[159] (i.e., exponential *Ansatz*) was explored.

In Refs. [160, 161], Rehr, Vila and coworkers used RT propagation within EOM-CC theory, obtaining a non-perturbative expression for the cumulant appearing in G^- in terms of the solution to a set of coupled first-order, nonlinear differential equations. The primary aim was to study x-ray absorption spectra of molecular systems, and it was shown that the nonlinear terms of the cumulant expansion yields significant improvements over the traditional linear approximation. In Ref. [162], the approach is further extended and applied to the core-hole spectral function for small molecular systems.

7 | CONCLUDING REMARKS

While still in its infancy, TDCC theory is emerging as a versatile tool in computational molecular science. As one might perhaps expect from its unquestionable status as *the* high-accuracy method in time-independent quantum chemistry, it

156

can provide high accuracy relative to TDFCI theory for electronic and vibrational quantum dynamics. With time-dependent orbitals and sufficient flexibility in the basis set used to expand these orbitals, TDCC theory has the potential to make decisive contributions to the understanding of molecular processes on the timescale of the electron—the attosecond timescale—where not only bound states, but also the electronic continuum must be taken into account. With relatively little development effort (since no response equations need to be implemented), TDCC theory can be used to compute full linear absorption spectra, including core-level excitations. Linear and low-order nonlinear response functions may be extracted from relatively short simulations. With proper use of Arponen's bivariational formulation, essentially all information that can be extracted from hermitian quantum dynamics can also be extracted from TDCC simulations despite the non-hermitian formulation.

Several challenges need to be overcome, however. The computational cost of TDCC theories is very high compared with the most widely used method, TDDFT, and two issues need to be addressed. First, the computational complexity or at least the prefactor of the evaluation of the function f in Equation (30) must be reduced. A general algorithm for this is significantly more challenging to formulate than reduced-scaling algorithms for the ground state, since different external driving forces may produce dramatically different responses in the wavefunction. For weak driving fields, for example, it is (very) small changes in the cluster amplitudes that produce the oscillations of interest, making screening procedures difficult to implement with full controllability of the accuracy, whereas strong fields can produce wavefunctions with very wide spatial distribution.

Second, the *number* of f-evaluations must be kept at a minimum, requiring careful selection of the numerical integrator and improved signal processing. Another major challenge, which is shared by all electronic quantum dynamics methods, is the representation of the electronic continuum. Ideally, one would wish to have the accuracy of mesh-based approaches like FEDVR at the cost of Gaussian-based electronic-structure theory.

Third, nuclear motion needs to be included to reliably extend simulation times beyond a few femtoseconds. This can be approached with either classical or quantum nuclear motion but will eventually require a time-dependent multireference CC wavefunction to describe, for example, a photo-induced chemical reaction.

AUTHOR CONTRIBUTIONS

Benedicte Sverdrup Ofstad: Conceptualization (supporting); investigation (equal); writing – original draft (equal). **Einar Aurbakken:** Conceptualization (supporting); investigation (equal); writing – original draft (equal). **Øyvind Sigmundson Schøyen:** Conceptualization (supporting); investigation (equal); writing – original draft (equal). **Håkon Emil Kristiansen:** Conceptualization (supporting); investigation (equal); writing – original draft (equal). **Simen Kvaal:** Conceptualization (lead); funding acquisition (lead); investigation (lead); supervision (lead); writing – original draft (equal). **Thomas Bondo Pedersen:** Conceptualization (lead); funding acquisition (lead); investigation (lead); supervision (lead); writing – original draft (equal).

FUNDING INFORMATION

CONFLICT OF INTEREST STATEMENT

The authors have declared no conflicts of interest for this article.

DATA AVAILABILITY STATEMENT

Data sharing is not applicable to this article as no new data were created or analyzed in this study.

ORCID

Benedicte Sverdrup Ofstad https://orcid.org/0000-0002-6495-2049
Einar Aurbakken https://orcid.org/0009-0000-4571-032X
Øyvind Sigmundson Schøyen https://orcid.org/0000-0002-2049-3696
Håkon Emil Kristiansen https://orcid.org/0000-0001-9884-1024
Simen Kvaal https://orcid.org/0000-0002-5118-4546
Thomas Bondo Pedersen https://orcid.org/0000-0001-8967-6055

RELATED WIREs ARTICLES

Real-time time-dependent electronic structure theory

REFERENCES

1. Goings JJ, Lestrange PJ, Li X. Real-time time-dependent electronic structure theory. WIREs Comput Mol Sci. 2018;8:e1341.
2. Li X, Govind N, Isborn C, DePrince AE III, Lopata K. Real-time time-dependent electronic structure theory. Chem Rev. 2020;120:9951–93.
3. Born M, Oppenheimer R. Zur Quantentheorie der Molekeln. Ann Phys. 1927;389:457–84.
4. Born M, Huang K. Dynamical theory of crystal lattices. Oxford: Clarendon Press; 1954.
5. Cederbaum LS, Zobeley J. Ultrafast charge migration by electron correlation. Chem Phys Lett. 1999;307:205–10.
6. Ehrenfest P. Bemerkung über die angenäherte Gültigkeit der klassischen Mechanik innerhalb der Quantenmechanik. Z Phys. 1927;45:455–7.
7. Vacher M, Bearpark MJ, Robb MA. Direct methods for non-adiabatic dynamics: connecting the single-set variational multi-configuration Gaussian (vMCG) and Ehrenfest perspectives. Theor Chem Acc. 2016;135:187.
8. Palacios A, Sanz-Vicario JL, Martín F. Theoretical methods for attosecond electron and nuclear dynamics: applications to the H_2 molecule. J Phys B. 2015;48:242001.
9. Nisoli M, Decleva P, Calegari F, Palacios A, Martín F. Attosecond electron dynamics in molecules. Chem Rev. 2017;117:10760–825.
10. Wu M, Chen S, Camp S, Schafer KJ, Gaarde MB. Theory of strong-field attosecond transient absorption. J Phys B. 2016;49:062003.
11. Rescigno TN, McCurdy CW. Numerical grid methods for quantum-mechanical scattering problems. Phys Rev A. 2000;62:032706.
12. Bachau H, Cormier E, Decleva P, Hansen JE, Martín F. Applications of B-splines in atomic and molecular physics. Rep Prog Phys. 2001;64:1815–943.
13. Feit MD, Fleck JA, Steiger A. Solution of the Schrödinger equation by a spectral method. J Comput Phys. 1982;47:412–33.
14. Ding F, Van Kuiken BE, Eichinger BE, Li X. An efficient method for calculating dynamical hyperpolarizabilities using real-time time-dependent density functional theory. J Chem Phys. 2013;138:064104.
15. Uemoto M, Kuwabara Y, Sato SA, Yabana K. Nonlinear polarization evolution using time-dependent density functional theory. J Chem Phys. 2019;150:094101.
16. Runge E, Gross EKU. Density-functional theory for time-dependent systems. Phys Rev Lett. 1984;52:997–1000.
17. van Leeuwen R. Mapping from densities to potentials in time-dependent density-functional theory. Phys Rev Lett. 1999;82:3863–6.
18. Ullrich CA. Time-dependent density-functional theory. Oxford: Oxford University Press; 2012.
19. Zanghellini J, Kitzler M, Fabian C, Brabec T, Scrinzi A. An MCTDHF approach to multielectron dynamics in laser fields. Laser Phys. 2003;13:1064–8.
20. Kato T, Kono H. Time-dependent multiconfiguration theory for electronic dynamics of molecules in an intense laser field. Chem Phys Lett. 2004;392:533–40.
21. Nest MM, Klamroth T, Saalfrank P. The multiconfiguration time-dependent Hartree–Fock method for quantum chemical calculations. J Chem Phys. 2005;122:124102.
22. Alon OE, Streltsov AI, Cederbaum LS. Unified view on multiconfigurational time propagation for systems consisting of identical particles. J Chem Phys. 2007;127:154103.
23. Meyer H-D, Gatti F, Worth G, editors. Multidimensional quantum dynamics: MCTDH theory and applications. Weinheim, Germany: Wiley; 2009.
24. Sato T, Ishikawa KL. Time-dependent complete-active-space self-consistent-field method for multielectron dynamics in intense laser fields. Phys Rev A. 2013;88:023402.
25. Miyagi H, Madsen LB. Time-dependent restricted-active-space self-consistent-field theory for laser-driven many-electron dynamics. Phys Rev A. 2013;87:062511.
26. Hochstuhl D, Hinz CM, Bonitz M. Time-dependent multiconfiguration methods for the numerical simulation of photoionization processes of many-electron atoms. Eur Phys J Spec Top. 2014;223:177–336.
27. Bauch S, Sørensen LK, Madsen LB. Time-dependent generalized-active-space configuration-interaction approach to photoionization dynamics of atoms and molecules. Phys Rev A. 2014;90:062508.
28. Crawford TD, Schaefer HF III. An introduction to coupled cluster theory for computational chemists. In: Lipkowitz KB, Boyd DB, editors. Reviews in computational chemistry. Volume 14. New York: John Wiley and Sons, Ltd; 2000. p. 33–136.
29. Bartlett RJ, Musiał M. Coupled-cluster theory in quantum chemistry. Rev Mod Phys. 2007;79:291–352.
30. Shavitt I, Bartlett RJ. Many-body methods in chemistry and physics. MBPT and coupled-cluster theory. New York: Cambridge University Press; 2009.
31. Helgaker T, Jørgensen P, Olsen J. Molecular electronic-structure theory. Chichester: Wiley; 2000.
32. Monkhorst HJ. Calculation of properties with the coupled-cluster method. Int J Quantum Chem. 1977;12:421–32.
33. Dalgaard E, Monkhorst HJ. Some aspects of the time-dependent coupled-cluster approach to dynamic response functions. Phys Rev A. 1983;28:1217–22.
34. Takahashi M, Paldus J. Time-dependent coupled cluster approach: excitation energy calculation using an orthogonally spin-adapted formalism. J Chem Phys. 1986;85:1486–501.
35. Bishop RF, Emary C. Time evolution of the rabi hamiltonian from the unexcited vacuum. J Phys A. 2001;34:5635–51.

36. Thomas S, Hampe F, Stopkowicz S, Gauss J. Complex ground-state and excitation energies in coupled-cluster theory. Mol Phys. 2021; 119:e1968056.

37. Hättig C. Structure optimizations for excited states with correlated second-order methods: CC2 and ADC(2). Adv Quantum Chem. 2005;50:37–60.

38. Köhn A, Tajti A. Can coupled-cluster theory treat conical intersections? J Chem Phys. 2007;127:044105.

39. Kjønstad EF, Myhre RH, Martínez TJ, Koch H. Crossing conditions in coupled cluster theory. J Chem Phys. 2017;147:164105.

40. Coester F. Bound states of a many-particle system. Nucl Phys. 1958;7:421–4.

41. Coester F, Kümmel H. Short-range correlations in nuclear wave functions. Nucl Phys. 1960;17:477–85.

42. Čížek J. On the correlation problem in atomic and molecular systems. Calculation of Wavefunction components in Ursell-type expansion using quantum-field theoretical methods. J Chem Phys. 1966;45:4256–66.

43. Čížek J, Paldus J. Correlation problems in atomic and molecular systems III. Rederivation of the coupled-pair many-electron theory using the traditional quantum chemical methods. Int J Quantum Chem. 1971;5:359–79.

44. Hoodbhoy P, Negele JW. Time-dependent coupled-cluster approximation to nuclear dynamics. I. Application to a solvable model. Phys Rev C. 1978;18:2380–94.

45. Hoodbhoy P, Negele JW. Time-dependent coupled-cluster approximation to nuclear dynamics. II. General formulation. Phys Rev C. 1979;19:1971–82.

46. Pigg D, Hagen G, Nam H, Papenbrock T. Time-dependent coupled-cluster method for atomic nuclei. Phys Rev C. 2012;86:014308.

47. Pedersen TB, Koch H, Hättig C. Gauge invariant coupled cluster response theory. J Chem Phys. 1999;110:8318–27.

48. Pedersen TB, Fernández B, Koch H. Gauge invariant coupled cluster response theory using optimized nonorthogonal orbitals. J Chem Phys. 2001;114:6983–93.

49. Kvaal S. Ab initio quantum dynamics using coupled-cluster. J Chem Phys. 2012;136:194109.

50. Schönhammer K, Gunnarsson O. Time-dependent approach to the calculation of spectral functions. Phys Rev B. 1978;18: 6606–14.

51. Sebastian KL. Correlation effects in ion neutralization scattering with the use of a time-dependent coupled-cluster approach. Phys Rev B. 1985;31:6976–87.

52. Hellmann H. Einführung in die Quantenchemie. Leipzig: Franz Deuticke; 1937.

53. Feynman RP. Forces in molecules. Phys Rev. 1939;56:340–3.

54. Arponen J. Variational principles and linked-cluster exp S expansions for static and dynamic many-body problems. Ann Phys. 1983; 151:311–82.

55. Helgaker T, Jørgensen P. Analytical calculation of geometrical derivatives in molecular electronic structure theory. Adv Quantum Chem. 1988;19:183–245.

56. Helgaker T, Jørgensen P. Configuration-interaction energy derivatives in a fully variational formulation. Theor Chim Acta. 1989;75: 111–27.

57. Helgaker T, Coriani S, Jørgensen P, Kristensen K, Olsen J, Ruud K. Recent advances in wave function-based methods of molecular-property calculations. Chem Rev. 2012;112:543–631.

58. Olsen J, Jørgensen P. Linear and nonlinear response functions for an exact state and for an mcscf state. J Chem Phys. 1985;82:3235–64.

59. Koch H, Jørgensen P. Coupled cluster response functions. J Chem Phys. 1990;93:3333–44.

60. Pedersen TB, Kvaal S. Symplectic integration and physical interpretation of time-dependent coupled-cluster theory. J Chem Phys. 2019; 150:144106.

61. Pedersen TB, Kristiansen HE, Bodenstein T, Kvaal S, Schøyen ØS. Interpretation of coupled-cluster many-electron dynamics in terms of stationary states. J Chem Theory Comput. 2021;17:388–404.

62. Hayes EF, Parr RG. Time-dependent Hellmann-Feynman theorems. J Chem Phys. 1965;43:1831–2.

63. Epstein ST. Time-dependent Hellmann-Feynman theorems for variational wavefunctions. J Chem Phys. 1966;45:384.

64. Pedersen TB, Koch H. On the time-dependent Lagrangian approach in quantum chemistry. J Chem Phys. 1998;108:5194–204.

65. Christiansen O, Jørgensen P, Hättig C. Response functions from Fourier component variational perturbation theory applied to a time-averaged quasienergy. Int J Quantum Chem. 1998;68:1–52.

66. Emrich K. An extension of the coupled cluster formalism to excited states (I). Nucl Phys A. 1981;351:379–96.

67. Stanton JF, Bartlett RJ. The equation of motion coupled-cluster method. A systematic biorthogonal approach to molecular excitation energies, transition probabilities, and excited state properties. J Chem Phys. 1993;98:7029–39.

68. Comeau DC, Bartlett RJ. The equation-of-motion coupled-cluster method. Applications to open- and closed-shell reference states. Chem Phys Lett. 1993;207:414–23.

69. Rico RJ, Head-Gordon M. Single-reference theories of molecular excited states with single and double substitutions. Chem Phys Lett. 1993;213:224–32.

70. Izsák R. Single-reference coupled cluster methods for computing excitation energies in large molecules: the efficiency and accuracy of approximations. WIREs Comput Mol Sci. 2019;10:e1445.

71. Koch H, Kobayashi R, Sanchez de Merás A, Jørgensen P. Calculation of size-intensive transition moments from the coupled cluster singles and doubles linear response function. J Chem Phys. 1994;100:4393–400.

72. Nanda KD, Krylov AI, Gauss J. The pole structure of the dynamical polarizability tensor in equation-of-motion coupled-cluster theory. J Chem Phys. 2018;149:141101.

73. Coriani S, Pawłowski F, Olsen J, Jørgensen P. Molecular response properties in equation of motion coupled cluster theory: a time-dependent perspective. J Chem Phys. 2016;144:024102.

74. Pedersen TB, Koch H. Coupled cluster response functions revisited. J Chem Phys. 1997;106:8059–72.

75. Pedersen TB, Koch H. Gauge invariance of the coupled cluster oscillator strength. Chem Phys Lett. 1998;293:251–60.

76. Pedersen TB, Koch H, Ruud K. Coupled cluster response calculation of natural chiroptical spectra. J Chem Phys. 1999;110:2883–92.

77. Pedersen TB, Koch H, Boman L, Sánchez de Merás AMJ. Origin invariant calculation of optical rotation without recourse to London orbitals. Chem Phys Lett. 2004;393:319–26.

78. Huber C, Klamroth T. Explicitly time-dependent coupled cluster singles doubles calculations of laser-driven many-electron dynamics. Chem Phys. 2011;134:054113.

79. Kvaal S. Variational formulations of the coupled-cluster method in quantum chemistry. Mol Phys. 2013;111:1100–8.

80. Goldstein H. Classical mechanics. 2nd ed. Reading, Massachusetts: Addison-Wesley; 1980.

81. Arponen JS, Bishop RF, Pajanne E. Extended coupled-cluster method. I. Generalized coherent bosonization as a mapping of quantum theory into classical Hamiltonian mechanics. Phys Rev A. 1987;36:2519–38.

82. Arponen JS, Bishop RF, Pajanne E. Extended coupled-cluster method. II. Excited states and generalized random-phase approximation. Phys Rev A. 1987;36:2539–49.

83. Arponen JS. Independent-cluster methods as mappings of quantum theory into classical mechanics. Theor Chim Acta. 1991;80:149–79.

84. Arponen J. Constrained Hamiltonian approach to the phase space of the coupled cluster method. Phys Rev A. 1997;55:2686–700.

85. Sato T, Pathak H, Orimo Y, Ishikawa KL. Time-dependent optimized coupled-cluster method for multielectron dynamics. J Chem Phys. 2018;148:051101.

86. Köhn A, Olsen J. Orbital-optimized coupled-cluster theory does not reproduce the full configuration-interaction limit. J Chem Phys. 2005;122:084116.

87. Myhre RH. Demonstrating that the nonorthogonal orbital optimized coupled cluster model converges to full configuration interaction. J Chem Phys. 2018;148:094110.

88. Pathak H, Sato T, Ishikawa KL. Time-dependent optimized coupled-cluster method for multielectron dynamics. II. A coupled electron-pair approximation. J Chem Phys. 2020;152:124115.

89. Pathak H, Sato T, Ishikawa KL. Time-dependent optimized coupled-cluster method for multielectron dynamics. III. A second-order many-body perturbation approximation. J Chem Phys. 2020;153:034110.

90. Pathak H, Sato T, Ishikawa KL. Time-dependent optimized coupled-cluster method for multielectron dynamics. IV. Approximate consideration of the triple excitation amplitudes. J Chem Phys. 2021;154:234104.

91. Hairer E, Lubich C, Wanner G. Geometric numerical integration. Berlin: Springer; 2006.

92. Wang Z, Peyton BG, Crawford TD. Accelerating real-time coupled cluster methods with single-precision arithmetic and adaptive numerical integration. J Chem Theory Comput. 2022;18:5479–91.

93. Kristiansen HE, Schøyen ØS, Kvaal S, Pedersen TB. Numerical stability of time-dependent coupled-cluster methods for many-electron dynamics in intense laser pulses. J Chem Phys. 2020;152:071102.

94. Christiansen O, Koch H, Jørgensen P. The second-order approximate coupled cluster singles and doubles model CC2. Chem Phys Lett. 1995;243:409–18.

95. Pathak H, Sato T, Ishikawa KL. Study of laser-driven multielectron dynamics of Ne atom using time-dependent optimised second-order many-body perturbation theory. Mol Phys. 2020;118:e1813910.

96. Skeidsvoll AS, Balbi A, Koch H. Time-dependent coupled-cluster theory for ultrafast transient-absorption spectroscopy. Phys Rev A. 2020;102:023115.

97. Bruner A, Lamaster D, Lopata K. Accelerated broadband spectra using transition dipole decomposition and Padé approximants. J Chem Theory Comput. 2016;12:3741–50.

98. Kristiansen HE, Ofstad BS, Hauge E, Aurbakken E, Schøyen ØS, Kvaal S, et al. Linear and nonlinear optical properties from TDOMP2 theory. J Chem Theory Comput. 2022;18:3687–702.

99. Kjønstad EF, Koch H. Biorthonormal formalism for nonadiabatic coupled cluster dynamics. J Chem Theory Comput. 2021;17:127–38.

100. Sonk JA, Caricato M, Schlegel HB. TD-CI simulation of the electronic optical response of molecules in intense fields: comparison of RPA, CIS, CIS(D), and EOM-CCSD. J Phys Chem A. 2011;115:4678–90.

101. Luppi E, Head-Gordon M. Computation of high-harmonic generation spectra of H_2 and N_2 in intense laser pulses using quantum chemistry methods and time-dependent density functional theory. Mol Phys. 2012;110:909–23.

102. Skeidsvoll AS, Moitra T, Balbi A, Paul AC, Coriani S, Koch H. Simulating weak-field attosecond processes with a Lanczos reduced basis approach to time-dependent equation-of-motion coupled-cluster theory. Phys Rev A. 2022;105:023103.

103. Coriani S, Koch H. X-ray absorption spectra and core-ionization potentials within a core-valence separated coupled cluster framework. J Chem Phys. 2015;143:181103.

104. Tenorio BNC, Moitra T, Nascimento MAC, Rocha AB, Coriani S. Molecular inner-shell photoabsorption/photoionization cross sections at core-valence-separated coupled cluster level: theory and examples. J Chem Phys. 2019;150:224104.

105. Nascimento DR, DePrince AE. Linear absorption spectra from explicitly time-dependent equation-of-motion coupled-cluster theory. J Chem Theory Comput. 2016;12:5834–40.

106. Nascimento DR, DePrince AE. Simulation of near-edge x-ray absorption fine structure with time-dependent equation-of-motion coupled-cluster theory. J Phys Chem Lett. 2017;8:2951–7.

107. Nascimento DR, DePrince AE. A general time-domain formulation of equation-of-motion coupled-cluster theory for linear spectroscopy. J Chem Phys. 2019;151:204107.

108. Koulias LN, Williams-Young DB, Nascimento DR, DePrince AE, Li X. Relativistic real-time time-dependent equation-of-motion coupled-cluster. J Chem Theory Comput. 2019;15:6617–24.

109. Park YC, Perera A, Bartlett RJ. Equation of motion coupled-cluster for core excitation spectra: two complementary approaches. J Chem Phys. 2019;151:164117.

110. Park YC, Perera A, Bartlett RJ. Equation of motion coupled-cluster study of core excitation spectra II: beyond the dipole approximation. J Chem Phys. 2021;155:094103.

111. Cooper BC, Koulias LN, Nascimento DR, Li X, DePrince AE. Short iterative Lanczos integration in time-dependent equation-of-motion coupled-cluster theory. J Phys Chem A. 2021;125:5438–47.

112. Merzbacher E. Quantum mechanics. 2nd ed. New York: Wiley; 1970.

113. Arponen J, Pajanne E. Electron liquid in the collective description. V. Exp S approximation for the homogeneous electron gas. J Phys C. 1982;15:2665–81.

114. Hsue C-S, Chern JL. Two-step approach to one-dimensional anharmonic oscillators. Phys Rev D. 1984;29:643–7.

115. Kaulfuss UB, Altenbokum M. Anharmonic oscillator as a test of the coupled-cluster method. Phys Rev D. 1986;33:3658–64.

116. Banik S, Pal S, Prasad MD. Calculation of dipole transition matrix elements and expectation values by vibrational coupled cluster method. J Chem Theory Comput. 2010;6:3198–204.

117. Faucheaux JA, Hirata S. Higher-order diagrammatic vibrational coupled-cluster theory. J Chem Phys. 2015;143:134105.

118. Christiansen O. Vibrational coupled cluster theory. J Chem Phys. 2004;120:2149–59.

119. Christiansen O. A second quantization formulation of multimode dynamics. J Chem Phys. 2004;120:2140–8.

120. Prasad M. Time-dependent coupled cluster method: a new approach to the calculation of molecular absorption spectra. J Chem Phys. 1988;88:7005–10.

121. Heller EJ. Time-dependent approach to semiclassical dynamics. J Chem Phys. 1975;62:1544–55.

122. Heller EJ. Frozen Gaussians: a very simple semiclassical approximation. J Chem Phys. 1981;75:2923–31.

123. Sastry GM, Prasad MD. The time-dependent coupled cluster approach to molecular photodissociation dynamics. Chem Phys Lett. 1994;228:213–8.

124. Beswick JA, Jortner J. Absorption lineshapes for the photodissociation of polyatomic molecules. Chem Phys. 1977;24:1–11.

125. Latha GS, Prasad MD. Time-dependent coupled cluster approach to multimode vibronic dynamics. J Chem Phys. 1996;105:2972–7.

126. Hansen MB, Madsen NK, Zoccante A, Christiansen O. Time-dependent vibrational coupled cluster theory: theory and implementation at the two-mode coupling level. J Chem Phys. 2019;151:154116.

127. Hairer E, Nørsett S, Wanner G. Solving ordinary differential equations I, (Springer Series in Computational Mathematics). Vol 8. Berlin Heidelberg, Berlin, Heidelberg: Springer; 1993.

128. Schmitz G, Artiukhin DG, Christiansen O. Approximate high mode coupling potentials using Gaussian process regression and adaptive density guided sampling. J Chem Phys. 2019;150:131102.

129. Madsen NK, Jensen AB, Hansen MB, Christiansen O. A general implementation of time-dependent vibrational coupled-cluster theory. J Chem Phys. 2020;153:234109.

130. Piecuch P, Oliphant N, Adamowicz L. A state-selective multireference coupled- cluster theory employing the single-reference formalism. J Chem Phys. 1993;99:1875–900.

131. Hansen MB, Madsen NK, Christiansen O. Extended vibrational coupled cluster: stationary states and dynamics. J Chem Phys. 2020;153:044133.

132. Evangelista FA. Alternative single-reference coupled cluster approaches for multireference problems: the simpler, the better. J Chem Phys. 2011;134:224102.

133. Madsen NK, Hansen MB, Christiansen O, Zoccante A. Time-dependent vibrational coupled cluster with variationally optimized time-dependent basis sets. J Chem Phys. 2020;153:174108.

134. Eschrig H. T>0 ensemble-state density functional theory via Legendre transform. Phys Rev B. 2010;82:205120.

135. Pittalis S, Proetto CR, Floris A, Sanna A, Bersier C, Burke K, et al. Exact conditions in finite-temperature density-functional theory. Phys Rev Lett. 2011;107:163001.

136. Cytter Y, Rabani E, Neuhauser D, Baer R. Stochastic density functional theory at finite temperatures. Phys Rev B. 2018;97:115207.

137. Karasiev VV, Dufty JW, Trickey SB. Nonempirical semilocal free-energy density functional for matter under extreme conditions. Phys Rev Lett. 2018;120:076401.

138. Matsubara T. A new approach to quantum-statistical mechanics. Prog Theor Phys. 1955;14:351–78.

139. Das A. Finite temperature field theory. Singapore: World Scientific; 1997.

140. Stefanucci G, van Leeuwen R. Nonequilibrium many-body theory of quantum systems: a modern introduction. 1st ed. Cambridge: Cambridge University Press; 2013.

141. Altenbokum M, Emrich K, Kümmel H, Zabolitzky JG. A temperature dependent coupled cluster method. In: Vashishta P, Kalia RK, Bishop RF, editors. Condensed matter theories. Boston, MA: Springer; 1987. p. 389–96.

142. Sanyal G, Mandal SH, Mukherjee D. Thermal averaging in quantum many-body systems: a non-perturbative thermal cluster cumulant approach. Chem Phys Lett. 1992;192:55–61.

143. Sanyal G, Mandal SH, Guha S, Mukherjee D. Systematic nonperturbative approach for thermal averages in quantum many-body systems: the thermal-cluster-cumulant method. Phys Rev E. 1993;48:3373–89.

144. Mandal SH, Ghosh R, Mukherjee D. A non-perturbative cumulant expansion method for the grand partition function of quantum systems. Chem Phys Lett. 2001;335:281–8.

145. Mandal SH, Ghosh R, Sanyal G, Mukherjee D. A non-perturbative path-integral based thermal cluster expansion approach for grand partition function of quantum systems. Chem Phys Lett. 2002;352:63–9.

146. Mandal SH, Ghosh R, Sanyal G, Mukherjee D. A finite-temperature generalisation of the coupled cluster method: a non-perturbative access to grand partition functions. Int J Mod Phys B. 2003;17:5367–77.

147. White AF, Chan GK-L. A time-dependent formulation of coupled-cluster theory for many-fermion systems at finite temperature. J Chem Theory Comput. 2018;14:5690–700.

148. White AF, Kin-Lic Chan G. Finite-temperature coupled cluster: efficient implementation and application to prototypical systems. J Chem Phys. 2020;152:224104.

149. Hummel F. Finite temperature coupled cluster theories for extended systems. J Chem Theory Comput. 2018;14:6505–14.

150. Harsha G, Henderson TM, Scuseria GE. Thermofield theory for finite-temperature coupled cluster. J Chem Theory Comput. 2019;15:6127–36.

151. Harsha G, Henderson TM, Scuseria GE. Thermofield theory for finite-temperature quantum chemistry. J Chem Phys. 2019;150:154109.

152. White AF, Chan GK-L. Time-dependent coupled cluster theory on the keldysh contour for nonequilibrium systems. J Chem Theory Comput. 2019;15:6137–53.

153. Peng R, White AF, Zhai H, Kin-Lic Chan G. Conservation laws in coupled cluster dynamics at finite temperature. J Chem Phys. 2021;155:044103.

154. Kowalski K, Bauman NP. Sub-system quantum dynamics using coupled cluster downfolding techniques. J Chem Phys. 2020;152:244127.

155. Ivanov VV, Lyakh DI, Adamowicz L. Multireference state-specific coupled-cluster methods. State-of-the-art and perspectives. Phys Chem Chem Phys. 2009;11:2355–70.

156. Cao Y, Romero J, Olson JP, Degroote M, Johnson PD, Kieferová M, et al. Quantum chemistry in the age of quantum computing. Chem Rev. 2019;119:10856–915.

157. Peng B, Bauman NP, Gulania S, Kowalski K. Chapter two—Coupled cluster Green's function: past, present, and future. In: Dixon DA, editor. Annual reports in computational chemistry. Volume 17. Amsterdam: Elsevier; 2021. p. 23–53.

158. Mattuck RD. A guide to Feynman diagrams in the many-body problem. 2nd ed. New York: Dover Books on Physics and Chemistry (Dover Publications); 1992.

159. Kas JJ, Rehr JJ, Reining L. Cumulant expansion of the retarded one-electron green function. Phys Rev B. 2014;90:085112.

160. Rehr JJ, Vila FD, Kas JJ, Hirshberg NY, Kowalski K, Peng B. Equation of motion coupled-cluster cumulant approach for intrinsic losses in x-ray spectra. J Chem Phys. 2020;152:174113.

161. Vila FD, Rehr JJ, Kas JJ, Kowalski K, Peng B. Real-time coupled-cluster approach for the Cumulant Green's Function. J Chem Theory Comput. 2020;16:6983–92.

162. Vila FD, Kowalski K, Peng B, Kas JJ, Rehr JJ. Real-time equation-of-motion CCSD Cumulant Green's Function. J Chem Theory Comput. 2022;18:1799–807.